Universidade de Aveiro Departamento de Química
Ano 2019

Javier Fernando Montero Bullón

Identificação de modificações nitroxidativas em fosfolípidos utilizando espectrometria de massa

MS analytical strategies for identifying nitroxidative modifications in phospholipids

Universidade de Aveiro Departamento de Química
Ano 2019

Javier Fernando Montero Bullón

Identificação de modificações nitroxidativas em fosfolípidos utilizando espectrometria de massa

MS analytical strategies for identifying nitroxidative modifications in phospholipids

Tese apresentada à Universidade de Aveiro para cumprimento dos requisitos necessários à obtenção do grau de Doutor em Bioquímica, realizada sob a orientação científica do Doutor Pedro Miguel Dimas Neves Domingues, Professor Auxiliar com Agregação do Departamento de Química da Universidade de Aveiro, e da Doutora Maria do Rosário Gonçalves dos Reis Marques Domingues, Professora Associada com Agregação do Departamento de Química da Universidade de Aveiro.

I dedicate this work to my family and friends for their unconditional support.

o júri

presidente

Doutor Fernando Joaquim Fernandes Tavares Rocha
Professor Catedrático da Universidade de Aveiro

vogais

Doutora Dolores Pérez-Sala Gonzalo
Investigadora Coordenadora do Consejo Superior de Investigaciones Científicas

Doutora Maria Fedorova
Investigadora Principal da University of Leipzig

Doutor Henrique Manuel Paixão dos Santos Girão
Investigador Auxiliar da Universidade de Coimbra

Doutor Pedro Miguel Dimas Neves Domingues
Professor Auxiliar com Agregação da Universidade de Aveiro (Orientador/Supervisor)

agradecimentos

Thanks to Professor Pedro Domingues and Professor Rosário Domingues for the guidance during this work, for the shared knowledge, for their availability and patience, and for their unconditional encouragement.
I equally thank all of the coauthors of the articles for their contribution.
I thank John Wilkins and Mologic Ltd. for receiving me in the company, located in Bedford (UK). I also thank Isabel Pinto for the support in the laboratory and the good moments shared.
I thank Professor Corinne Spickett and Professor Andrew Pitt for receiving me in their laboratoy, located in Aston University, in Birmingham (UK). I also thank their students Catarina Afonso and Bebiana Sousa for the support in the laboratory and the good moments shared.
I thank Doctor Maria Fedorova and Professor Ralf Hoffman for receiving me in their laboratory, located in the Center for Biotechnology and Biomedicine, in Leipzig (Germany). I also thank Giulia Coliva, Juan Camilo Rojas Echeverri and Mike Lange for the support in the laboratory and the good moments shared.
I thank Professor Friedrich Altmann and his group, that guided me through my first steps in the field of mass spectrometry, in their laboratory in the University of Natural Resources and Life Sciences, in Vienna (Austria).
I thank my colleagues from the MASSTRPLAN project for their amazing teamwork and for the joint learning, as well as for all the precious moments along these three years. I also thank all the principal investigators and Debbie Toomeoks, that have made possible MASSTRPLAN, and specially to its coordinator Corinne Spickett. I thank to my colleagues of the Mass Spectrometry Center in the University of Aveiro, for their help and for the nice work atmosphere in the laboratory. I thank Doctor Cristina Barros for her help in the laboratory and with the mass spectrometers.
Thanks are due to the research unit of Química Orgânica, Produtos Naturais e Agroalimentares (QOPNA) in Universidade de Aveiro (FCT Grant UID/QUI/00062/2013) and to Rede Nacional de Espectrometria de Massa (REDE/1504/REM/2005), and I acknowledge the European program Marie-Sklodowska Curie Actions (HORIZON2020) for the funding of this work and the Ph.D. scholarship through the MASSTRPLAN project (number 675132).

palavras-chave

Espécies reativas de nitrogénio, RNS, stress nitroxidativo, ácidos gordos nitrados, NO_2FA, nitroxidação, fosfolipídos nitroxidados, lipidómica, LC-MS, MS/MS, cardiolipina, aductos, nitro-fosfolípido, modificação pós-translacional, nitroalquilação, lipoxidação, fosfolipidoma, perfil lipídico, análise de alto rendimento, enfarte do miocárdio, caquexia, exercício

resumo

Os lípidos nitroxidados são moléculas bioativas que desempenham funções importantes em condições fisiológicas e fisiopatológicas. Estes lípidos nitroxidados são formados *in vivo* pela reação de lípidos com espécies reativas de nitrogénio (RNS), em condições de stress nitroxidativo. Os ácidos gordos nitrados (NO_2FAs) são os lipídos nitroxidados mais estudados. Os NO_2FAs já foram caracterizados *in vitro*, e têm sido detetados *in vivo*, em tecidos e biofluidos. Estas moléculas têm sido associadas a funções biológicas relevantes, mediando atividades anti-inflamatórias, antioxidantes, vasculoprotetoras, anti-hiperglicémicas, antitumorais e citoprotetoras. Um dos principais mecanismos relacionados com estas atividades é a interação covalente dos NO_2FAs com proteínas. Os fosfolípidos nitroxidados foram recentemente identificados *in vivo*, nomeadamente as fosfatidilcolinas e as fosfatidiletanolaminas. No entanto, este campo de investigação permanece pouco explorado, apesar de os primeiros estudos indicarem que os fosfolipídos nitroxidados também possuem atividade biológica significativa. Além disso, a capacidade dos fosfolipídos nitroxidados formarem aductos covalentes com peptídeos ou proteínas ainda não foi reportada.

Assim, o principal objetivo do trabalho desenvolvido nesta tese de doutoramento foi o desenvolvimento da análise de fosfolipídos nitroxidados e seus aductos covalentes com proteínas utilizando a espectrometria de massa (MS) e modelos *in vitro* para a geração de novas espécies. Além disso, foi estudado o impacto do stress nitroxidativo *in vivo* no lipidoma por análise cromatografia liquída associada à MS (LC-MS) e e espectrometria de massa tandem (MS/MS). Os resultados foram correlacionados com condições patológicas em estdo,i.e., o enfarte agudo do miocárdio e a caquexia induzida por cancro.

Assim, neste trabalho, foram utilizadas plataformas de LC-MS e MS/MS de última geração para a análise de fosfolipídos nitroxidados. Foram desenvolvidos ensaios *in vitro* para caracterizar, pela primeira vez, espécies de cardiolipina nitroxidada bem como aductos entre nitro-fosfolipídos e péptidos representando potenciais alvos em proteínas. Foram identificadas dez modificações nitroxidativas diferentes para a cardiolipina, utilizando a LC-MS e MS/MS utilizando diversos critérios tais como o seu comportamento cromatográfico, medições exatas de massa e as vias de fragmentação em MS/MS. A adição entre nitro-fosfolipídios e a glutationa foi demonstrada, como confirmado pela análise MS/MS dos aductos usando diferentes espectrómetros de massa. O estudo de amostras biológicas ondeé esperada a presença de stress nitroxidativo, nomeadamente, enfarte do miocárdio e caquexia, foi realizado através da análise lipidómica com LC-MS e MS/MS. Esses estudos revelaram um forte impacto do stress nitroxidativo no fenótipo lipídico, que permitiu a diferenciação entre o estado saudável e patológico. Também foi possível

identificar espécies moleculares que respondem ao início e progressão da doença, como os fosfolipídos contendo ácidos gordos poliinsaturados, plasmalogénios e cardiolipinas em caso de enfarte do miocárdio, ou as cardiolipinas e fosfatidilserinas na caquexia.

Em conclusão, estes resultados contribuem para o desenvolvimento da estudo do efeito do stress nitroxidativo no lipidoma em diversas condiçoes fisiológicas e patológicas e constituem um banco de dados e protocolos para a implementação da deteção *in vivo* de novos fosfolipídios nitroxidados e seus adutos com proteínas. Adicionalmente, a caracterização do lipidoma em amostras biológicas sob stress nitroxidativo supõe uma referência para detetar fosfolípidos nitroxidizados *in vivo* e fornece uma perspetiva das mudanças que ocorrem no lipidoma, em situações clínicas relacionadas com o stress nitroxidativo. Estes resultados são também úteis para investigações futuras e uma contribuição importante para a discussão da relevância clínica de alteração do lipidoma e sua modelação em situações de stress nitroxidativo. No geral, este trabalho constitui avanço na análise e compreensão do efeito do stress nitroxidativo nos lípidos e no lipidoma, e devido ao seu potencial significado biológico, do seu possível valor em diagnóstico e em terapêutica.

keywords

RNS, nitroxidative stress, nitrated fatty acids, NO_2FA, nitroxidation, nitroxidized phospholipids, lipidomic, LC-MS, MS/MS, cardiolipin, nitro-phospholipid, adducts, post-translational modification, nitroalkylation, lipoxidation, phospholipidome, lipid profile, high-throughput analysis, myocardial infarction, cachexia, exercise

abstract

Nitroxidized lipids are recognized as important bioactive molecules in physiological and pathophysiological conditions. They are generated *in vivo* by the reaction of lipids with reactive nitrogen species (RNS) under nitroxidative stress conditions. Nitrated fatty acids (NO_2FAs) are the most studied nitroxidized lipids. NO_2FAs were well-characterized *in vitro* and detected *in vivo*, in tissues and biofluids. They are associated with relevant biological roles, such as mediating anti-inflammatory, antioxidant, vasculoprotective, anti-hyperglycemic, antitumoral and cytoprotective activities. One of the main mechanisms for these activities is the covalent interaction of NO_2FAs with proteins. Nitroxidized phospholipids were recently identified *in vivo*, namely in phosphatidylcholines and phosphatidylethanolamines. However, this subject remains largely unaddressed, although the first studies indicate that nitroxidized phospholipids also own significant biological activity. Moreover, the ability of nitroxidized phospholipids to form covalent adducts with peptides or proteins is not yet reported.

Thus, the main goal of the work developed in this PhD thesis has been to contribute for the advancement of mass spectrometry (MS)-based analysis of nitroxidized phospholipids and their covalent adducts with proteins, by using *in vitro* models for the generation of new species. Also, the impact of nitroxidative stress *in vivo* lipidome has was studied by using liquid chromatography (LC)-MS and tandem mass spectrometry (MS/MS) analysis. The data obtained using these approaches were then correlated with the studied pathological conditions, i.e., acute myocardial infarction and cancer-induced cachexia.

In this work, state-of-the-art LC-MS and MS/MS platforms were used analysing nitroxidized phospholipids. *In vitro* assays were used to characterize for the first time nitroxidized species of cardiolipin, and adducts between nitro-phospholipids and peptides representing potential targets in proteins. Up to ten different nitroxidative modifications were identified for cardiolipin by LC-MS and MS/MS, by using their chromatographic behaviour, exact mass measurements and MS/MS fragmentation pathways. Adduction between nitro-phospholipids and glutathione was demonstrated, as confirmed by MS/MS analysis of the adducts using different MS instruments. Analysis of biological samples where nitroxidative stress was expected to occur, namely myocardial infarction and cachexia, was performed by HILIC-LC-MS and MS/MS lipidomics. These studies revealed a strong impact in the lipidic phenotype that allowed to classify between health and disease status. It also allowed to point out molecular species responsive to onset and progress of the disease, as PUFA-containing phospholipids, plasmalogens, and cardiolipins in myocardial infarction, or cardiolipins and phosphatidylserines in cachexia.

In conclusion, these results contribute to the study of the effect of nitroxidative stress in the lipidome in different ways. They provide a database and protocols for implementation of *in vivo* detection of new nitroxidized phospholipids and their adducts with proteins. The profiling of the lipidome in biological samples under nitroxidative stress constitutes a reference to undertaking the challenge of detecting nitroxidized phospholipid *in vivo* and provided a perspective of the changes occurring in lipidome in clinical situations related to nitroxidative stress. These results are also useful to direct future investigation and contribute for the discussion on the clinical relevance of the modulation of the lipidome in health and disease. Overall, this work provides a step forward in the MS-based analysis and understanding of the effect of nitroxidative stress in lipids and the lipidome, and its potential biological significance, diagnostic value and therapeutic utility.

Publications and communications

The results presented in this thesis already originated three publications in international scientific journals with referee, plus two more manuscripts that are under revision or to be submitted, as well as posters and oral communications in national and international meetings.

Scientific articles in peer-reviewed international journals

- Montero-Bullon, J.-F., Melo, T., Domingues, M. R. & Domingues, P. Characterization of Nitrophospholipid-Peptide Covalent Adducts by Electrospray Tandem Mass Spectrometry: A First Screening Analysis Using Different Instrumental Platforms. *Eur. J. Lipid Sci. Technol.* 120, 1800101 (2018).

- Melo, T., Montero-Bullón, J.-F., Domingues, P. & Domingues, M. R. Discovery of bioactive nitrated lipids and nitro-lipid-protein adducts using mass spectrometry-based approaches. *Redox Biol.* 101106 (2019). doi:10.1016/j.redox.2019.101106.

- Montero-Bullon, J.-F., Melo, T., Rosário M Domingues, M. & Domingues, P. Liquid chromatography/tandem mass spectrometry characterization of nitroso, nitrated and nitroxidized cardiolipin products. *Free Radic. Biol. Med.* (2019). doi:10.1016/j.freeradbiomed.2019.05.009

- Javier-Fernando Montero-Bullon, Tânia Melo, Rita Ferreira, Ana Isabel Padrão, Paula A. Oliveira, M Rosário M Domingues, Pedro Domingues. Exercise training counteracts urothelial carcinoma-induced alterations in skeletal muscle mitochondria phospholipidome in an animal model. Under revision in Scientific Reports journal.

- Javier-Fernando Montero-Bullon, Tânia Melo, Tania Martins-Marques, Henrique Girão, M. Rosário M. Domingues, Pedro Domingues. Adaptation of myocardial phospholipidome during acute myocardial infarction and ischemia-reperfusion in an *ex vivo* rat model. To be submitted.

Posters

- Javier-Fernando Montero-Bullon, Tânia Melo, Tania Martins-Marques, Henrique Girão, M. Rosário M. Domingues, Pedro Domingues. “Alteration of phospholipidome profile in the heart of an animal model of acute myocardial infarction”. Abstract: https://doi.org/10.1016/j.freeradbiomed.2017.04.214. Joint OCC World Congress 2017 and Annual SFRR-E Conference: METABOLIC STRESS AND REDOX REGULATION. Berlin (Germany). June 21st-23rd, 2017.

- Javier Fernando Montero Bullón, Tania Melo, M. Rosário M. Domingues, Pedro Domingues. "Mass spectrometry characterization of nitrated cardiolipin". ANALÍTICA 2018, 9th Meeting of the Analytical Chemistry Division. Porto (Portugal). March 26th-27th, 2018.

- Javier Fernando Montero Bullón, Tânia Melo, M. Rosário M. Domingues, Pedro Domingues. 2018. “Study of Covalent Adduction of Nitrated Phospholipids to Peptides Using Tandem Mass Spectrometry in Different Instruments.” Free Radical Biology and Medicine 120 (May). Abstract: https://doi.org/10.1016/J.FREERADBIOMED.2018.04.399. SFRR – International Biennial Meeting. Lisbon (Portugal). June 4th-7th, 2018. 1.

- Javier Fernando Montero Bullón, Tânia Melo, M. Rosário M. Domingues, Pedro Domingues. "Characterization of nitro, nitroso, and isomers of nitroxidized cardiolipin by LC-MS/MS". FEBS Advanced Lecture Course 2018: Redoxomic Technologies and their Application in Health and Disease. Spetses Island (Greece). September 17th-23rd, 2018.

Oral communications

- Phospholipidome alterations associated to myocardial infarction. 7th Workshop in Lipidomics. University of Aveiro. Campus Universitarion de Santiago, 3810-13, Aveiro (Portugal). February 28th, 2018

- Poster pitch: “Characterization of nitro, nitroso, and isomers of nitroxidized cardiolipin by LC-MS/MS". FEBS Advanced Lecture Course 2018: Redoxomic Technologies and their Application in Health and Disease. Spetses Hotel, Spetses Island (Greece). September 17th-23rd, 2018.

- Oral presentation in the conference Advances in the Study of Lipid and Protein Oxidation: From Methods to Targets. Ghent University, Het pand ,Ghent, Oost-Vlaanderen 9000 (Belgium). March 13th-15th, 2019.

Table of contents

List of figures and schemes

CHAPTER 1

CHAPTER 2

CHAPTER 3

CHAPTER 4

CHAPTER 5

List of tables

CHAPTER 1

CHAPTER 2

CHAPTER 4

CHAPTER 5

Abbreviations

RNS	Reactive nitrogen species
ROS	Reactive oxygen species
FA	Fatty acid
NO_2FA	Nitrated fatty acid
SA	Stearic acid
POA	Palmitoleic acid
OA	Oleic acid
LA	Linoleic acid
LNA	Linolenic acid
AA	Arachidonic acid
EPA	Eicosapentaenoic Acid
DHA	Docosahexaenoic acid
PL	Phospholipid
PC	Phosphatidylcholine
PE	Phosphatidylethanolamine
PS	Phosphatidylserine
PI	Phosphatidylinositol
AG	Acylglycerides
TAG	Triacylglycerides
DAG	Diacylglycerides
MAG	Monoacylglycerides
CE	Cholesteryl ester
EI	Electron ionization
ECNICI	Electron capture negative ion chemical ionization

ESI	Electrospray ionization
MALDI	Matrix-assisted laser desorption/ionization
APCI	Atmospheric pressure chemical ionization
MRM	Multiple reaction monitoring
HPLC	High-performance liquid chromatography
NO_2BF_4	Nitronium tetrafluoroborate
SIN-1	Morpholinosynonimine
P-NAP	2,3,5,6-tetramethyl-4-(methylnitrosoamino)phenol
BME	Beta-mercaptoethanol
HEK	Human embryonic kidney cells

CHAPTER 1. Introduction

General introduction

Nitroxidation is a chemical modification that occurs by reaction of reactive nitrogen species (RNS) in a biological condition called nitroxidative stress[1]. *In vivo*, nitroxidative stress modifies proteins, nucleic acids, and lipids[2–6]. RNS, together with reactive oxygen species (ROS), are of significant relevance for biological redox reactions in physiological and pathophysiological processes. RNS are remarkably produced during inflammation, and other well-known sources of RNS are vascular tissue homeostasis, digestion, and exogenous chemicals.

Lipids are biomolecules that are susceptible to reaction with RNS. Unsaturated fatty acids (FAs), free or esterified in phospholipids (PL), acylglycerides (AG), and cholesteryl esters (CEs) have been reported as targets of RNS. MS-based approaches have been used for characterization of nitroxidized lipids, by simplified *in vitro* models mimicking its endogenous production and eventually *in vivo* including information about the biological abundance of these species in healthy and pathological circumstances. Nowadays, nitrated fatty acids (NO_2FAs) are the best-studied species between nitroxidized lipids. They are also known as nitroalkenes, as long as they contain double bonds. Besides, MS approaches have also been important to study covalent adduction of NO_2FAs to proteins, in a lipoxidation reaction. From these studies, it has been established that this is the main mechanism for the beneficial effects of the formation of nitroxidized lipids, responsible for anti-inflammatory, antioxidant, vasculoprotective, anti-hyperglycemic, antitumoral and cytoprotective effects.

Nitroxidation of PLs has only recently been characterized and also detected *in vivo*[7,8], but knowledge is limited and does not include their interaction with proteins. Nitro-PLs have equally shown beneficial physiological effects[9], but more studies are needed in this field. In the following sections, it is introduced how nitroxidative stress occurs from a biochemical point of view. It also details the modifications induced in lipids and their occurrence, including their adduction to proteins, disclosed by mass spectrometry studies. Finally, it reports the biological significance of this kind of molecules.

1.1. The chemistry behind nitroxidative stress

RNS occur in both physiological and pathophysiological situations. Nitric oxide ($NO^{\cdot}$) is one of the most abundant RNS found *in vivo* and precursor of other RNS. It is produced enzymatically with L-arginine as substrate, by a family of enzymes called nitric oxide synthases (NOS). There are three isoforms, being two of these constitutively expressed,

the endothelial NOS (NOS1 or eNOS), that is located membrane-bound in Golgi and caveolae of the membrane in endothelial cells, and the neuronal NOS (NOS3 or nNOS), that is present in the cytosol of central and peripheral neurons[10,11]. Endothelial NOS generate concentrations of $NO^{\cdot}$ in the cardiovascular tissue with a regulating effect, and neuronal NOS produces $NO^{\cdot}$ as a neurotransmitter in the nervous system[11]. A third isoform, inducible NOS (NOS2 or iNOS) is cytosolic and regulated at the transcriptional and post-transcriptional level in cytokine-activated leukocytes during inflammation and defensive cytotoxicity by oxidative burst[10–13]. The physiological concentration of $NO^{\cdot}$ is considered to range from a basal state of 20 nM up to 2 uM[14], being the enzymatic production of $NO^{\cdot}$ by eNOS and nNOS more constant, while the activity of iNOS is considered a key player regarding *in vivo* overproduction of $NO^{\cdot}$, as it occurs due to cellular synthesis by macrophages after LPS-activation[15]. $NO^{\cdot}$ is a lipophilic radical that spreads through the hydrophobic or, to a lesser extent, the aqueous medium, crossing membranes to the extracellular medium and other cells[16]. $NO^{\cdot}$ can reach an order of hundreds of microns of diffusion in physiological media and blood, as calculated from its aqueous diffusion coefficient and its half-life, and as observed in macrophages cultures, where $NO^{\cdot}$ diffused up to 500um away after being produced[17]. However, it is likely that $NO^{\cdot}$ is chemically intercepted earlier *in vivo* (Figure 1A).

Due to its low second-order rate constant of reaction and its concentration, $NO^{\cdot}$ does not initiate free radical reactions itself[14,18] but propagates nitroxidative stress through interaction with other radical intermediates as ROS[14], aminoacyls[19] or lipid peroxyls[20]. $NO^{\cdot}$ is prone to react with superoxide radical anion ($O_2^{-\cdot}$), simultaneously released in activated leukocytes or from other sources as electron transport chain, producing peroxynitrite ($ONOO^-$)[21]. $ONOO^-$ isomerization to nitrate can be considered a terminating step of nitroxidation[14]. However, $ONOO^-$ reacts predominantly through a strong oxidizing activity via one or two electrons withdrawal[21–23]. $ONOO^-$ can react via its reduction to nitrite but downstream reactivity is mainly associated with its dissociation at neutral pH to radicals $NO_2^{\cdot}$ and $OH^{\cdot}$[22]. $NO_2^{\cdot}$ is also produced by the autoxidation of $NO^{\cdot}$, a reaction facilitated in hydrophobic environment[24]. $NO_2^{\cdot}$ is a radical initiator of nitration playing an important role in the nitroxidation of molecules, such as unsaturated lipids. The reaction of $NO^{\cdot}$ with $NO_2^{\cdot}$ originates N_2O_3, which is a strong nitrosating agent[25]. Other *in vivo* source of RNS is the oxidation of nitrite to $NO_2^{\cdot}$ by one electron acceptor species, or to NO_2^+ by two electron acceptor species. For instance, nitrite is transformed into NO_2 by metalloenzymes as iron-containing myeloperoxidase and horseradish peroxidase[26], or by copper-containing superoxide dismutase[27], in the presence of hydrogen peroxide with the transition metal as

a catalyst. Nitryl chloride (NO_2Cl) is derived from the reaction of myeloperoxidase-generated hypochlorous acid (HOCl) with nitrites and originates a powerful electrophilic nitrating agent, the nitronium ion (NO_2^+)[28,29]. Remarkably, the ingestion of nitrates and nitrites in food exposed to acidic conditions in the digestive tract (pH >4) yields species as $NO^{\cdot}$, NO^+, $NO_2^{\cdot}$ or N_2O_3[30]. The pH, but also molecules such as CO_2 or O_2, can play a role in the generation of RNS (Figure 1B). Finally, RNS such as nitrogen oxides, can also be uptaken from exogenous sources, namely cigarette smoke, and atmospheric pollutants.

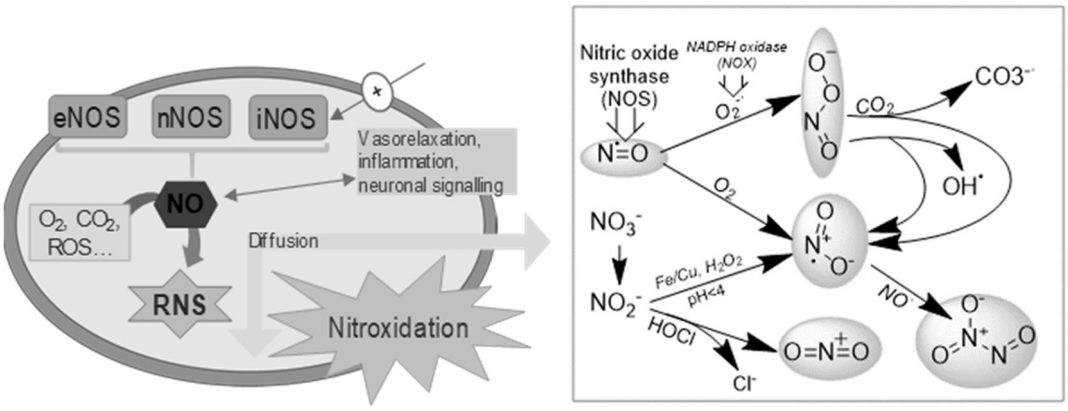

A) B)

Figure 1: A) Schematic representation of the endogenous process of nitroxidation B) Generation and interconversion of RNS.

RNS and ROS species possess a high oxidant potential to attack biomolecules[18]. RNS species can be reactive by abstracting electrons from another molecule, by subtracting radical hydrogen from weak X-H bonds, or by addition to a double bond via homolytic cleavage and capture of one electron, as it is the case in unsaturated FAs. Alternative reactions can occur via electrophilic attack by species such as NO_2^+ or NO^+[25]. Addition of RNS to biomolecules is a well-studied process, as well as its implication in cellular processes, as reviewed in [31,32]. Protein modification by RNS, via nitration/nitrosation of side chains of amino acids, have been widely reported. Sulfhydryl group of exposed cysteines react with $NO^{\cdot}$ to generate a nitrosothiol residue (S-nitrosylation of proteins), with important biological relevance[33]. The 3-nitrotyrosine modification is considered a marker of nitroxidative stress in proteins and of cell damage[18]. RNS and ROS can diffuse and accumulate in hydrophobic environments and react with lipids[14,24]. Nitroxidized species of lipids have been detected *in vitro* and *in vivo* as products of reaction with RNS, and these species are recognized as important signaling molecules[34].

The addition of a nitro group $NO_2^{\cdot}$ to an unsaturated fatty acyl chain is the most prominent reaction towards the formation of NO_2FAs[5,35] (Figure 2). They can be formed via the abstraction by $NO_2^{\cdot}$ of one π electron from a double bond of unsaturated FAs forming a nitroalkyl radical. Following, the loss of a hydrogen atom frequently occurs, originating nitro-allyl or nitro-vinyl derivatives. However, if the nitro group is lost, isomerization of the double bond to trans configuration occurs[36]. The addition of oxygen or concomitant ROS also occurs frequently, leading to the combination with oxidation moieties[37]. The successive attack of other RNS can also occur, as it is the case when $NO_2^{\cdot}$ binds via the oxygen[2], forming an unstable nitro-nitrite ester compound (also called oxonitro[38]). When the nitration of FA is initiated by nitronium ion, NO_2^+, there is an electrophilic addition over the double bond which generates a carbocation that undergoes a loss of hydrogen in the adjacent carbon, re-establishing the double bond with an added nitro moiety[36]. NO_2FAs can derive towards secondary species as by the addition of H_2O over the double bond yielding vicinal nitrohydroxy species[2], or as by the isomerization to nitrosohydroxy derivative[39]. An orthogonal nitroxidation pathway is the reaction of peroxidation products with $NO^{\cdot}$ generating NO_2FAs as demonstrated for *in vitro* models of liposomes and low-density protein oxidation[20,40,41], and similarly in reactions of lipid hydroperoxides with N_2O_4[42] or HNO_2[41]. NO_2FAs can be decomposed and release $NO^{\cdot}$, which seems to be an important signaling mechanism *in vivo*[39,43–45]. The instability of NO_2FAs is higher in the aqueous phase and under moderated acidity. The mechanism proposed is the isomerization to nitrosohydroxy derivative [39] or to nitrite ester[43], and release of $NO^{\cdot}$ by homolytic cleavage. In both cases, it is formed a hydroxy- derivative of the FA. Figure 2A and Figure 2B summarize the common reaction pathways and products of nitroxidation, respectively.

Nitroxidative stress can also modify esterified forms of FAs in PLs, AGs, and CEs, that have been already detected in different studies[7,8,46–48]. It is not well-known if the nitroxidation occurs in the free FAs, that are subsequently incorporated in the esterified form, or if the RNS can attack the esterified fatty acyl chain.

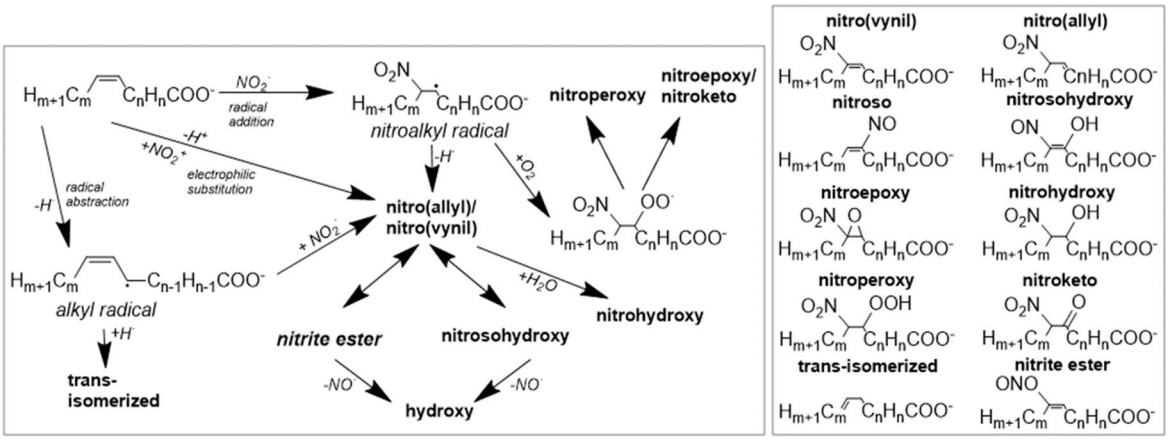

A) B)

Figure 2: A) Most common reaction pathways for the reaction between $NO_2^{\cdot}$ and unsaturated fatty acids. B) Nitroxidative modification observed in FAs.

Oxidation, nitrosation and nitration reactions usually happen in parallel, and their proportion can vary with the ratio between the concentration of $NO^{\cdot}$ and other ROS, principally the superoxide anion[25]. In the presence of the $NO^{\cdot}$ radical, the oxidation process due to ROS is initially enhanced, showing a Gaussian maximum at 1:1 in $NO^{\cdot}$:$O_2^{\cdot-}$ ratio, but accompanied by increasing nitration. A higher concentration of $NO^{\cdot}$ will hamper the oxidation, giving place to a phase of nitrosation via N_2O_3[25]. More recently, an *in silico* work has shed more light on this scenario by modeling the whole reactions network using the experimental data of kinetic constants for the different reactions and species involved[49].

Some studies *in vitro* have provided additional information about the reactivity of RNS versus different fatty acyl chains. Different regioisomers can be formed, and some seem to be more stable than others. For example, five out of the eight possible arachidonic acids (AA) nitro- regioisomers were predominantly observed: 9/11/12/14/15-nitro-AA[50], suggesting a tendency of higher reactivity in highest positions[35,50], and a similar trend was reported for other polyunsaturated FAs as docosahexaenoic acid (DHA) with a predominance of 11/13/14/16/17/19/20-nitro-DHA[50]. In another study, the addition of the nitro group on carbon 9 of linoleic acid (LA) and carbon 11 of AA were reported as the most abundant regioisomers of these FAs[51]. *In vivo*, some regioisomers also appear favored, as in the case of oleic acid (OA) where the addition on the carbon in position 10 seems more abundant than on the carbon in position 9[52]. Experiments have also shown that conjugated double bonds in conjugated linoleic acid (CLA), are more susceptible to nitration, in comparison with non-conjugated double bonds of other FAs[53].

An important feature of nitroxidized lipids is its reactivity with proteins, to form covalent adducts. This process has emerged as the main mechanism associated with the biological function of NO_2FAs. This adduction is currently considered a post-translational modification of lipoxidation type, affecting the function and stability rather than having a deleterious effect[54,55]. The reaction has been generically called nitroalkylation and implies a Michael addition-type reaction, with loss of the double bond of the fatty acyl chain. The double bond is necessary for the reaction and NO_2FAs without double bonds, called nitroalkanes, lack of reactivity since they are not electrophilic[56]. The reaction targets the nucleophilic sites of proteins. It seems that the nitroxidized fatty acyl chains are exposed towards the interphase of hydrophobic/hydrophilic compartments where they get in contact with proteins[57]. The high electronegativity of the nitro group over an unsaturated fatty acid generates an important positive charge density in the methylenic carbon, adjacent to the modification. A reactive carbocation is formed this way, aided by delocalization of the π electrons over the C-N bond and N-O bond, with the oxygen retaining the negative charge, in the form of a nitronate intermediate[58]. Nucleophilic amino acids readily attack this carbocation forming a new linkage through a pair of electrons from the imidazole group of histidine, the amine group of lysine, the guanidine group of arginine or the thiol group of cysteine. Following this reaction, a rearrangement occurs through proton addition over the methylenic carbon bond to the nitrogen, and the N-O bond modified gets re-established to a nitro group, as depicted in Figure 3. Adduction to proteins of nitrated fatty acyl chains in esterified forms by a similar mechanism remains unstudied.

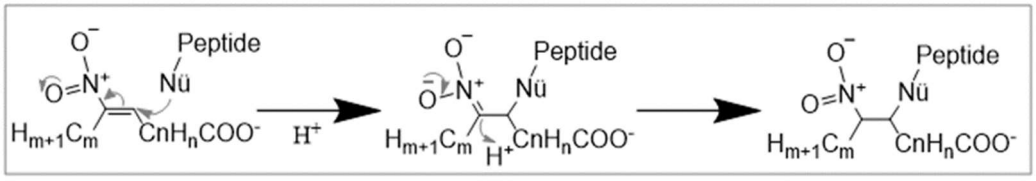

Figure 3: Mechanism of reaction for the covalent adduction of NO_2FAs to nucleophilic aminoacids in peptides and proteins.

1.2. Mass spectrometry analysis of nitroxidized lipids and their covalent adduct with peptides/proteins

Mass spectrometry, especially when coupled with liquid chromatography (LC), is the main analytical methodology for the characterization and monitoring of nitroxidized lipids *in vitro* and biological samples (Figure 4). It has significant advantages in the detection of these modified lipids of low concentration *in vivo*, e.g., in plasma where NO_2-FAs occurs in the

picomolar range[23], and also for *de novo* characterization, that is usually based on *in vitro* assays for simplicity (Figure 4).

LC-MS allows to precisely identify the chemical modification of nitroxidized lipid derivatives, based on mass/charge value shift, on chromatographic behavior and added tandem MS analysis relying on the fragmentation pattern as a structural fingerprint. Nowadays, MS analysis has become a comprehensive high-throughput approach[59–61], with outstanding sensitivity and accuracy. Several LC-MS and LC-MS/MS approaches were established for the detection of nitroxidized lipids. Most of the published works dealing with *in vivo* detection and quantification of nitroxidized lipids have employed targeted MS approaches, mainly multiple reaction monitoring (MRM), and when standards are used in known amounts, e.g., isotopically labeled standards titrated by chemoluminescence[62], absolute quantification is possible as performed for NO_2FAs[52,53,62–69]. Untargeted approaches have also been successfully used[7,8,70].

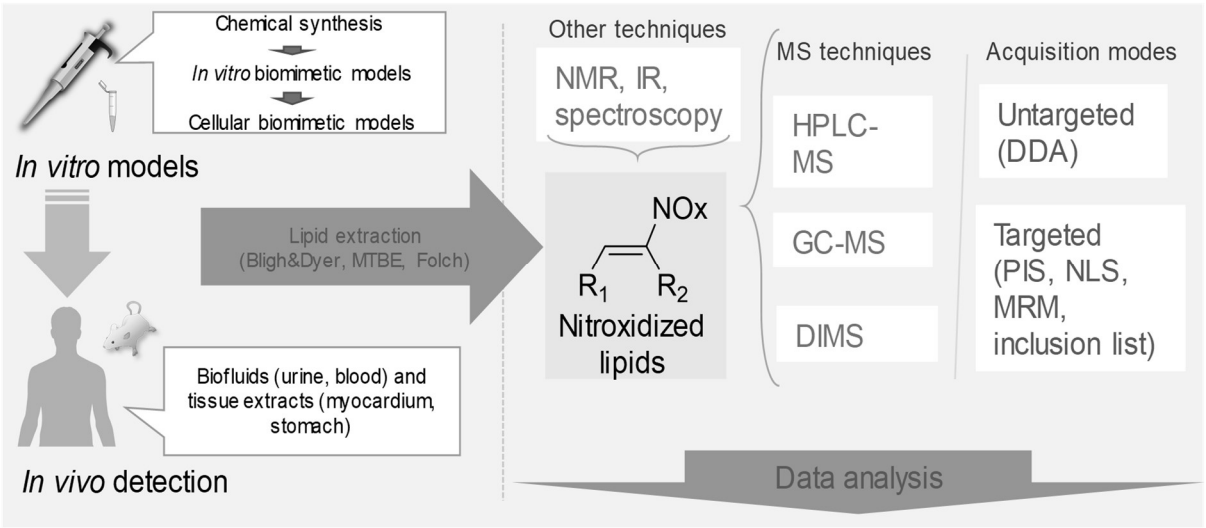

Figure 4: Analytical workflow for the study of nitroxidized lipids based on mass spectrometry.

LC-MS-based approaches have also been used to study adducts of nitroxidized lipids with peptides or proteins. Targeted and untargeted approaches have been used for *in vivo* detection as reviewed in [34,54], but absolute quantitative information of natural occurrence has only been reported for glutathione[71]. In this case, proteomics and lipidomics protocols have been adapted as preparative steps (digestion, electrophoresis, immunoassays) and have a specific contribution to the method. *In vitro* assays have also been very important as a previous step for detection in biological matrixes.

1.2.1 MS characterization of nitroxidized lipids

Different instrumental platforms have been employed to characterize a vast number of nitroxidized lipids. Regarding ionization sources, electron ionization (EI)[67] or electron capture negative ion chemical ionization (ECNICI)[23,38,52,67,68] were initially used to identify NO_2FAs. Both require volatile thermostable analytes as it is achieved by derivatizing fatty acids by esterification with a methyl group or others as pentafluorobenzyl (PFB), and it has been conveniently coupled to gas chromatography. EI generates positively charged molecular ions $[M]^+$ [67]. ECNICI is used in the negative mode, generating $[M-H]^-$ ions, and was used to quantify nitro-OA and nitro-LA in plasma, coupled with GC[23,52,68]. More recent studies use electrospray ionization mass spectrometry (ESI-MS) for detection of NO_2FAs[50,53,64–66,69,72,73], as well as allowing the analysis of esterified derivatives[7,8,38,46,48,70,74]. ESI-MS analysis of nitroxidized FAs have been mainly done in negative ion mode, originating $[M-H]^-$ molecular ions. ESI-MS of nitro-FAs in the positive ion mode has also been able using lithium cations to generate the corresponding $[M+Li]^+$ cations[50]. Esters of cholesterol with NO_2FAs has also been studied in the positive mode, ionized as ammonium adducts[48,74]. Regarding nitroxidized PLs analysis by ESI-MS, very recent work has identified nitro, nitroso and nitroxidized derivatives of phosphatidylcholines (PCs), phosphatidylethanolamines (PEs) and phosphatidylserines (PSs). The analysis was done in both positive and negative modes with the ionization efficiency depending on the polar head[7,8,38,70]. Nitroxidized PCs were detected as $[M+H]^+$ in positive mode, and as acetate adducts, $[M+Ac]^-$ ions, in negative mode[7,8], while PSs and PEs were studied as $[M+H]^+$ and $[M-H]^-$ molecular ions[7,8,38,70]. Nitroxidized AGs have been analyzed in positive mode by ESI but also atmospheric pressure chemical ionization (APCI), as ammonium adducts, $[M+NH_4]^+$ ions[46].

Nitroxidative modifications are first identified in MS data, by the mass shift in the molecular ions compared with the non-modified lipid. The most common case is the formation of nitrated lipids, with a typical mass shift of +45 Da[52,62,67,68,75]. Other modifications were also reported as a mass shift of +29 Da in the case of nitroso derivatives[50], a mass shift of +61 Da for the addition of NO_2 plus one oxygen[50,65] or +63 Da, when the double bond is lost[35,38,62,65,76]. Similar mass shifts have been observed for fatty acids esterified in PLs, AGs or CEs[7,8,38,46,47,70,74].

Further confirmation of the structure of each nitroxidized derivative is achieved by the analysis of tandem MS data, pinpointing the typical fragmentation pathways and the

reporter ions for each type of modification. This information can be exploited for targeted analysis approaches. These approaches have been conveniently used for quantitative works by GC-MS/MS[23,52,63,68] and LC-MS/MS[53,62,64–67,69], including kinetic studies of nitroxidation[50]. The MS/MS spectra from NO_2-FAs$^-$ as $[M-H]^-$ and $[M+Li]^+$ molecular ions show a characteristic neutral loss of 47 Daltons corresponding to the loss of HNO_2, while the characteristic product ion NO_2^- is observed at m/z 46. Nitroso derivatives can be identified by the typical neutral loss of HNO of 31Da[50]. These typical fragmentations also appear for combinations of multiple modifications[50,77] (Table 1). Cleavages in the hydrocarbon chain in the vicinity of the modification are also observed and allow to identify the position of the nitro group for different regioisomers as 9- and 10-NO_2-OA and the four regioisomers of nitro-LA[72], the predominant regioisomers of CLA [53], and AA and DHA[50].

In PLs, the loss of 47 Da for nitration in PCs, PEs, PSs[7,8,70] and 31 Da for nitroso groups[8,70] were also observed. The MS^2 spectra in negative ion mode of nitroxidized PL also showed the modified carboxylate anions. These fragment ions allow localizing the modification on one of the FAs[78]. In positive mode, information on the fatty acyl chain can be obtained when a fatty acid or ketene neutral loss occurs[7]. Fragment ions arising from the cleavage in the hydrocarbon chain in the vicinity of the modification are not easily observed in MS^2, but an MS^3 analysis of the modified fatty acyl chains can allow this observation, that can help to discern between isomeric structures, as done for free FAs[7].

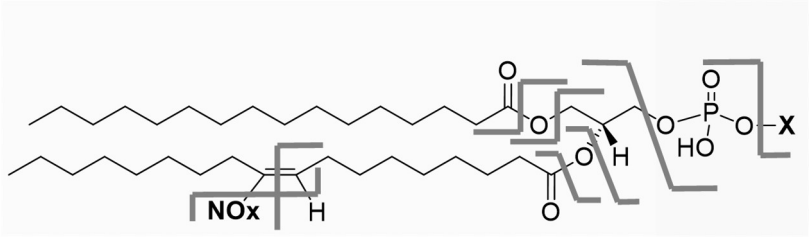

Figure 5: Schematic representation of typical fragmentation pathways that allow identifying nitroxidized phospholipids based on tandem MS. Adapted from [7].

In the case of nitroxidized triacylglycerides (TAGs), it has been described the typical fragmentation of ammonium adducts, that yields a neutral loss of 47 Da for nitrated forms. The neutral loss of the different fatty acyl chains, including the modified one, with the formation of monoacylglyceride (MAG) and diacylglyceride (DAG) ions, was also observed[46]. This feature was used for the MRM screening of nitrated TAGs based on the loss of 346 units, corresponding to ammonium adduct of nitro- stearic acid (SA). Also, an

MS^3 scan of the protonated DAG ions from MS^2 allowed to identify the monoglyceride and acylium ions, revealing the modified fatty acyl chain[46]. Remarkably, the authors of this work assigned the isomerism for the three possible esterified positions of the glycerol backbone with the fatty acyl chains, based on the intensities of the fragment ions corresponding to the neutral loss of sn1/sn2/sn3 fatty acyl chains, as deduced from standards. This was based on the observation that the neutral loss from sn1 and sn3 positions to form DAG cations are more intense in comparison to sn2[46].

Table 1: Summary of MS and MS^2 features of nitroxidized lipids

Modification	**Mass Shift (Da)**	**MS^2 fragments** PI: product ion /NL: neutral loss	**Substrate**	**Ref.**
$(NO_2)_x$	+ $(45)_x$	PI: 46 NL: 47	Fatty acids	50,62,63,67,72
			Phospholipids	7,8,38
			Triacylglycerides	46
			Cholesteryl ester	48,74
$(NO)_x$	+ $(29)_x$	NL: 31	Fatty acids	50
			Phospholipids	8
$(NO)_x$+$(O)_y$	+ $(29)_x$ +$(16)_y$	NL: 18 / 31	Fatty acids	50
			Phospholipids	8
$(NO_2)_x$+$(O)_y$	+ $(45)_x$+$(16)_y$	PI: 46 NL: 47 / 18	Fatty acids	38,50,65
			Phospholipids	8,38
(NO_2)+(H_2O)	+ 63	NL: 47 / 18	Fatty acids	35,38,62,65,76
			Phospholipids	38
$(NO_2)_x$+$(NO)_y$	+ $(45)_x$+$(29)_y$	PI: 46 NL: 47 / 31	Fatty acids	38,50
			Phospholipids	8

Coupling GC and LC to the MS analysis allows increased sensibility and separation of isomers (functional and positional) for their identification. Gas chromatography (GC) coupled to MS is a well-established method for the analysis of FAs and profiling *in vivo* [79–81] and has been successfully applied to NO_2FAs, for quantification purposes[52,63,67,68]. It allows resolving regioisomers, like in the case of 9/10-nitro-OAs[38,52,67,68] or nitro-regioisomers of LA[67]. Nevertheless, most of the works nowadays use LC-MS approaches since the use of reversed phases allows to separate free FAs depending on the length and

unsaturation of the chain, and also partially discriminate oxidized forms of FAs[55]. Works on NO_2FAs have shown that C18-LC-MS were able to resolve the two nitro-OA and four nitro-LA possible regioisomers[38,64,67,72], as well as nitrohydroxy-OA isomers[38,65]. PLs with esterified nitroxidized FAs have been analyzed by HILIC, without separation regarding the nitroxidative modification because of the predominance of polar head-based retention[7,8]. C5-LC-MS discriminated between functional isomers as nitro and nitrosohydroxy, but not regioisomers[8]. C18 columns have also been employed for LC-MS experiments to separate partially nitrated TAGs [46].

1.2.2 *In vitro* models of lipid nitroxidation

Nitroxidized lipids have been obtained and characterized by *in vitro* approaches (Table 2) as reviewed in [82]. The chemical synthesis of pure standards is based on a modified Henry reaction (nitroaldol addition) that allows synthesizing regiospecific pure NO_2FAs[83–86]. This allowed the characterization of several regioisomers by LC-MS/MS, such as the case of nitro-OA with the nitro group in carbon 9 or 10 and nitro-LA with the nitro group in carbon 9, 10, 12 or 13[72]. Another semisynthetic method called nitroselenation was used to obtain nitro-FAs in equimolar quantities of all the regioisomers[38,67,87], by transferring a nitro group from a nitro-alkyl phenyl selenide moiety previously synthesized[88], a method chosen to obtain nitro-OA and nitro-LA used in most of the studies of their biological roles and metabolism. However, these synthetic methods are complex and time-consuming and do not generate a great variety of species at once.

Other synthetic approaches, such as nitronium tetrafluoroborate (NO_2BF_4) in chloroform, has been extensively used for the nitroxidation of FAs [43,48,51,75] and PLs[7,8,70]. It generates a broad mixture of nitroxidized lipids, that includes different modifications and their different isomers. However, it has the advantage of being a very simple synthetic method. Recently, a total of 42 oxidized and nitroxidized species of OA, LA, AA and DHA, and CLA were identified using this nitration reagent[50]. Combinations of multiple additions of nitro, nitroso, hydroxyl groups, and other oxidation moieties were identified[50]. NO_2BF_4 reaction has also been recently used to obtain a wide array of nitroxidized PLs, more particularly with PCs, PEs, and PSs[7,8,70]. The reaction with nitrite in acidic pH has also been used since it represents possible endogenous nitroxidation during digestion and was applied to FAs [53,62,75,89], TAGs standards [46], or natural lipid extracts from heart and liver tissue [53]. This approach yields mainly nitro- and nitrohydroxy- products. Mimetic gastric digestion of TAGs from olives oil with lipases and acidic pH in the presence of nitrites, produced nitrated OA,

LA, and CLA[73]. Peroxynitrite infused in lipid solutions also provided the formation of nitrated LA[62] and CLA[53,90]. However, the treatment of lysed erythrocytes with sodium peroxynitrite leads mostly to oxidation of OA[23]. Alternatively, mimicking closer the biological condition, peroxynitrite can be generated *in situ* by photo-induction over 2,3,5,6-tetramethyl-4-(methylnitrosoamino)phenol (P-NAP) reagent, that allowed to produce different combinations of nitro-, nitroso- and hydroxy- modifications in diverse mono and polyunsaturated FAs[50]. NO_2 bubbling in hexane was also used as a biomimetic membrane-like nitroxidation, generating nitro-, nitrohydroxy-, nitroepoxy- and oxonitro- derivatives of OA, nitro-AA, nitro-LA [51], nitro CLA[53] and nitro-, nitrohydroxy- and nitroepoxy- derivatives of POPS [38]. Also, a N_2O_3 solution in hexane was used producing nitro- derivatives of LA and AA [51]. Nitro- derivatives were also produced by the reaction of nitrate and OA in dimethylformamide[68]. Finally, another biomimetic system, based on myeloperoxidase and $NaNO_2$, was tested in (9*Z*,11*E*)-CLA, (10*E*,12*Z*)-CLA, and LA, and showed to be an effective method of fatty acid nitration[53].

The induction of nitroxidative stress *in vitro* with cellular models has also been performed. Although the identification becomes more complex, these studies provide a perspective closer to physiology. Nitroxidative stress was induced in cardiomyocytes cultures using nitroxidizing agent morpholinosynonimine (SIN-1), and nitro- and nitrohydroxy- modification in OA and polyunsaturated FAs were identified[50]. Adipocytes cell cultures, supplemented with nitro-OA, showed the typical products derived from its catabolism and how these NO_2FAs products were incorporated in TAGs[46]. Nitro- derivatives of SA, OA, CLA, and LA were supplemented to adipocytes showing beta-oxidation products[47]. Also, saturation and desaturation of NO_2FAs were detected [47], as reported previously in human embryonic kidney (HEK) cells[56]. It was also studied the incorporation of these products in MAGs, DAGs, TAGs, PLs including PEs, PCs and phosphatidylinositols (PIs), and CEs[47]. Remarkably, the distribution of NO_2FA was minor in PLs versus AGs, and nitroalkanes were particularly abundant in TAGs [47]. The supplementation of nitro-NO_2FAs to cell cultures was also used to asses how NO_2FAs can cross membranes[91]. Some works in cellular *in vitro* models studied the endogenous generation of nitroxidized lipids. Supplementation of CLA to a culture of activated macrophages, yielding the nitro- product, was used to confirm the association of nitroxidation with inflammation[53,92]. Nitrated LA and its esterified form with cholesterol were also induced by activated macrophages[74]. Nitro-, nitroso- and other nitroxidized forms of PCs and PEs were detected in cardiomyocytes in a model of starvation[8]. A total of six nitroxidized PCs and two nitroxidized PEs were identified. The nitroxidative modifications found were one and two nitro- groups, combinations of nitro and

nitroso groups and combinations of nitro and hydroxy groups in different proportions. Quantitative values were calculated and expressed as a percentage of conversion versus the non-modified species, with a maximum for NO_2-PC(34:1) of 1%, and as a percentage of the species versus the total amount of the PL class in the estimated value of 0.3% for NO_2-PC(34:1)[8]. In conclusion, methods *in vitro* have been successfully developed and provide a wide array of nitroxidized lipids for its use as standards and as a simplified approach for their characterization and the study of their physiological properties.

1.2.3 Detection of nitroxidized lipids *in vivo*

Nitroxidized lipids have been detected *in vivo* (Table 2), although the information available refers mainly to NO_2FAs. Nitrohydroxy-AA was the first endogenous nitroxidized FA detected, in bovine cardiac tissue[76]. The first study situated the concentrations of nitro-OA and nitro-LA in plasma of healthy individuals in the order of a few hundred nanomolar units [62,67], values that were considered overestimated in subsequent works. The concentration in the plasma of healthy individuals is currently considered to be in the order of a few hundred picomolar units in plasma[52,63,68] for the most abundant species as nitro-OA. The basal value determined in the plasma of healthy individuals was 0.88±0.29 nM for 9-nitro-OA and 0.96 nM for 10-nitro-OA[23,63], and 0.72nM for nitro-CLA [53,90]. Other nitroxidized species as palmitoleic acid (PA), linolenic acid (LNA), AA, eicosapentaenoic acid (EPA), and DHA including nitro- and nitrohydroxy- derivatives have also been detected in urine, plasma, and in red blood cells [52,53,62]. Nitro-CLA in the concentration of 9.97 ± 3.98 pmol/mg creatinine, and its beta-oxidation products have also been reported in human urine of healthy individuals[64].

NO_2FAs have also been detected associated with physiological and pathological conditions. It has been reported that nitro-LA in mitochondrial lipid extracts reaches 3.6pg per milligram of protein in control and up to 186pg per milligram of protein in disease, in a model of ischemia-reperfusion induced in rat hearts[69]. In the mitochondria from the myocardium of rats hearts undergoing ischemia preconditioning associated to acute myocardial infarction, it was reported that nitro-OA increased from 215fmols to 245fmols per mg of protein, while nitro-LA increased from <50fmols to 619fmols in the lipid extracts during disease versus the basal state[66]. Another study in mouse myocardial tissue detected concentrations in the total lipid extract of 9.5nM of nitro-OA and 17.3nM of nitro-LA during the ischemia-reperfusion process[65]. The formation of NO_2FAs was also reported in the plasma and vaginal lavage of

mice infected with herpes virus[93]. It has also been reported an increase of 56% nitro-OA in skin due to psoriasis lesion[94].

Nitroxidized PLs have been recently reported *in vivo*. Melo and co-authors were the first to detect nitro- derivatives of PC and PE[7]. NO_2-PC and NO_2-PE were identified in mitochondria from the myocardium of animal models of type 1 diabetes mellitus[7]. Seven nitro-PCs and one nitro-PEs were observed in samples from diseased subjects but were not detected in control samples. The concentration of these nitrated species was reported as a percentage of conversion, with a maximum up to 9%, for NO_2-PC(34:1), and as percentage versus the total amount of the PL class, with a maximum of 0.75%, for NO_2-PC(34:1). uTAGs containing nitro-CLA were detected in extra-virgin olive oil[73], and CE esterified to nitro-LA was also found in human plasma and lipoproteins[48].

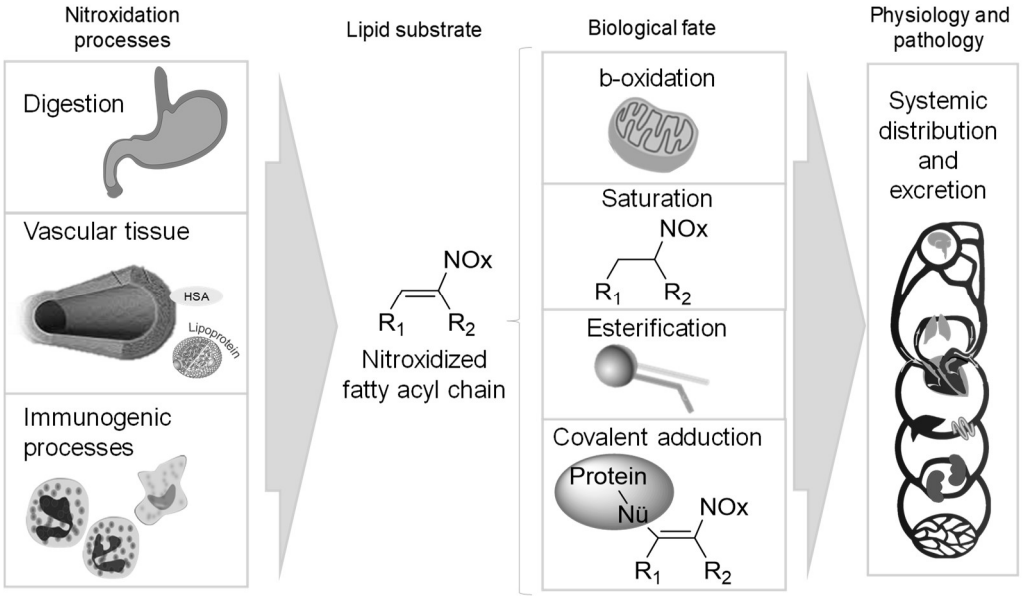

Figure 6: Scheme for the production and physiological fate of nitroxidized lipids.

NO_2FAs were also detected in strategies in which RNS were supplemented, forcing their endogenous occurrence for the study. Plasma and urine of rats fed with CLA and sodium nitrate were shown to produce the nitrated form of CLA[53]. Nitro-CLA acid was also identified in plasma and urine of human volunteers correlated with ingestion of the fatty acid and sodium nitrite or sodium nitrate doses[90]. Similar studies have been done to determine the physiological fate of nitroxidized lipids by supplementing NO_2FAs to animals. Nitro-OA was administered by intravenous injection in murine models and in *ex vivo* blood samples, and was shown to undergo beta-oxidation to FAs C16:1, C14:1 and C12:1, via formation of CoA

thioesters, but products with shorter fatty acid chain length were not observed[95]. This article also reports NO_2FAs saturation (including full saturation to nitroalkanes) and desaturation, as well as Michael addition reactions[95]. The formation of non-electrophilic nitroalkanes from the reduction of NO_2FAs was also identified in the plasma of rats gavaged with nitro-OA[56]. Gavage in rats with nitro-OA, showed the presence of different nitro-TAGs in plasma, with a preferential abundance of nitroalkanes[46]. Similar metabolic products were also detected after administration of pure synthetic nitro-OA to obese mice, but not in non-supplemented animals[47], in a study in which it was also shown the different esterification in AGs, and CEs. It has also been recently described the renal and fecal elimination of 10-nitro-OA after its oral administration in rat and human individuals, reporting metabolized nitroxidized products, including conjugates with N-acetylcysteine, taurine and sulfo-conjugates[96]. Studies of bioavailability also exist based on supplementation. Nitro-OA reaches the skin and serum after subcutaneous injection or topical application[94,97], while nitro-LA was reported in serum and lung tissue after intraperitoneal injection[98]. Based on monitoring of radiolabeled forms of nitro-OA, it was found that an after intravenous injection most of nitro-OA accumulate in the muscle, liver, and urine, in that order, with some lower proportion being present in kidney, plasma, and adipocytes[95]. The estimated recovery of the signal was 64%, a fact which reveals that other collateral pathways exist, that must include the reaction of NO_2FAs with nucleophilic targets, basically proteins[95]. A recent study with gavage of mice with radiolabelled nitro-OA indicates that systemic distribution reaches its maximum around 6h after oral administration and concentrates highly in abdominal and brown adipose tissue[47]. Therefore, abundant information exists that confirms the endogenous occurrence of nitroxidized FAs, PLs, AGs, and CEs, including quantitative values and some aspects about their physiological fate and distribution

Table 2: State of the art of the detection of nitroxidized lipids, including species with free and esterified fatty acids.

Substrate and modification	**Detection Method**	**Experimental model**
Free fatty acids		
PA		
- Nitro[62] - Nitrohydroxy [62]	- C18-HPLC-ESI-MS/MS[62]	*In vivo*: - Human red cells [62] - Human plasma [62] - Human urine [62]

OA		
- Nitro [23,38,94,50,52,53,62,65,66,68,72] - Nitro-allylic [38] -Nitrohydroxy [38,50,62] - Nitroketo [38,65] - Oxonitro [38] - Oligomers of nitro [38] -Multiple nitro, nitroso and nitroxidized [50]	- C18-HPLC-ESI-MS/MS [38,50,53,62,65,66,72,73,94,97] - HILIC-HPLC-ESI-MS/MS [23] - GC-ECNICI-MS [23,38,52,68] - NMR [62] - UV/visible[62], also coupled to HPLC [23,38]	*In vitro*: - Nitroaldol condensation [72] - Nitroselenation [38] - Nitrite in acidic conditions H_2O_2 [62] - NO_2 solution [38] - Peroxynitrite [23,62] - MPO with NO_2^- and H_2O_2 [62] - NO_2BF_4 [50] - Cardiomyocytes culture under SIN-1 nitroxidative stress [50] - Gastric mimetic digestion of extra virgin olive oil [73] - Liver mitochondrial lipid extract with NO_2^- at acidic condition [53] *In vivo*: - Human red cells [62] - Human plasma [23,52,62,68] - Human urine [62] - Mice myocardial tissue in ischemia-reperfusion model [65] - Ischemia preconditioning in rat heart mitochondria [66] - Skin and serum of mice after topical application of nitro-OA [94] - Serum of mice after subcutaneous injection of nitro-OA [97]
LA		
- Nitro [41,48,72,73,75,87,98,50,51,62,65–69] - Nitrohydroxy [50,62,75] -Multiple nitro, nitroso and nitroxidized[50]	- C18-HPLC-ESI-MS/MS [41,50,73,75,87,98,51,53,62,65–67,69,72] - GC-EI-MS [67] - GC-ECNICI-MS [52,67,68] - NMR [41,67,74,75,87]	*In vitro*: - Nitroaldol condensation [72] - Nitrite in acid conditions [41,74,75] - NO_2BF_4 [41,50,51,75] - Nitroselenation [67,87] - NO_2 solution [41,51] - N_2O_3[51]

	- IR [75] - UV [67,74,87] - Preparative TLC [74]	- Peroxynitrite [41,53] - MPO and H_2O_2 [53] - Gastric mimetic digestion for extra virgin olive oil [73] - Liver mitochondrial lipid extract with NO_2^- at acidic condition [53] <u>*In vivo*</u>: - Human red cells [62,67] - Human plasma [52,62,67,68] - Human urine [62] - Mice myocardial tissue in ischemia-reperfusion model [65] - Ischemia-preconditioning in rat heart mitochondria [66] - Ischemia preconditioning in rat myocardium mitochondria [69] - Serum and lung tissue of rats injected with nitro-LA [98]
CLA		
- Nitro [53,64,73,90,92,94] - Nitrohydroxy [50,53] - Nitroketo [53] - Multiple nitro, nitroso and nitroxidized combinations [50]	- C18-HPLC-ESI MS/MS [50,53,64,73,90,92–94] - NMR [53]	<u>*In vitro*</u> - Peroxynitrite [53] - NO_2 gas [53] - MPO with H_2O_2 and NO_2^- [53] - NO_2BF_4 [50] - P-NAP [50] - Liver mitochondrial lipid extract with NO_2^- at acidic condition [53] - Activated macrophages in the presence of CLA [53,92] - Isolated mitochondria supplemented with CLA and NO_2^- [53] <u>*In vivo*</u> - Human urine [64] - Mice peritoneal tissue after induced inflammation and CLA supplementation [92]

		- Gastric generation in rats gavaged with CLA and nitrite, detected in urine, blood, stomach, intestine, colon, and liver [53] - Human plasma [53] - Extra virgin olive oil [73] - Gastric mimetic digestion for extra virgin olive oil [73] - Cardiac tissue in mice subjected to focal myocardial ischemia-reperfusion [53] - Urine of healthy humans after ingestion of nitrite, nitrate, and CLA [90] - Plasma of healthy humans after ingestion of nitrite, nitrate and CLA [90] - Biopsy of skin with psoriasis [94] - Mice plasma and vaginal lavages after infection by herpes simplex virus and CLA inoculation[93]
LNA		
- Nitro [62] - Nitrohydroxy [62]	- C18-HPLC-ESI-MS/MS[62]	- Human red cells [62] - Human plasma [62] - Human urine [62]
AA		
- Nitro [35,50,51,62,76] - Nitro-hydroxy [35,50,62] - Multiple nitro, nitroso and nitroxidized combinations [50]	- C18-HPLC-ESI-MS/MS [35,50,51,62,76] - IR [35] - NMR [35]	<u>*- In vitro*</u>: - NO_2^- in acidic conditions [22,35] - NO_2BF_4 [50,51] - NO_2 solution [51,76] - N_2O_3 [51] - Cardiomyocytes culture unde SIN-1 nitrosative stress [50] <u>*In vivo*</u>: - Human red cells [62] - Human plasma [62] - Human urine [62]
6-methyl-AA		
- Nitro [89]	- HPLC-MS [89] - NMR [89]	<u>*In vitro*</u>: - NO_2^- in acidic pH [89]

	- IR [89]	
EPA		
- Nitro [62] - Nitrohydroxy [62]	- C18-HPLC-ESI MS/MS[62]	*In vivo*: - Human red cells [62] - Human plasma [62] - Human urine [62]
DHA		
- Nitro [50] - Nitrohydroxy [50] - Multiple nitro, nitroso and nitroxidized combinations [50]	- C18-HPLC-ESI -MS/MS[50]	*In vitro*: - NO_2BF_4 [50] - Cardiomyocytes culture with SIN-1 nitrosative stress [50]
Metabolic products of NO_2FAs		
- Nitrated beta-oxidation products [46,56,64,69,92,94,96,97] - Nitrated omega-oxidation products [96] - Acetyl coA derivatives [95] - Nitrated product undergoing saturation and desaturation [46,56,69,92,94–96] - Nitrated dicarboxylic products [96] - Nitrated conjugates with sulphate, N-acetylcysteine and taurin [96]	- C18-HPLC-APCI-MS [46] - C18-HPLC-ESI MS/MS [56,64,69,92,94,95,97]	*In vitro:* - Metabolic products in adipocyte culture supplemented with nitro-OA [46] - Incubation of bovine aortic endothelial cell with nitro-OA [95] - HEK cells transfected with overexpressed prostaglandin reductase [56] - Activated macrophages in the presence of CLA [92] *In vivo*: - Human plasma [56] - Mice blood, after intravenous injection of nitro-OA [69,95] - Mice blood, after intravenous injection of nitro-LA [69] - Peripheral human blood incubated with nitro-OA [95] - Human urine [64] - Langendorff-perfused rat hearts with CLA [64] - Human urine after supplementation of nitro-OA [96] - Rat urine after ingestion fo nitro-OA [96] - Rat blood after injection of nitro-OA [56]

		- Skin and serum of mice after topical application of nitro-OA [94] - Serum of mice after subcutaneous injection of nitro-OA [97]
Esterified FAs		
PC		
- Nitro [7,38,47] - Nitrohydroxy [38] - Nitroketo [38] - Nitroxdized: NO, NO_2 and OH in different proportion [8]	- C18-HPLC-ESI-MS/MS [38] - HILIC-HPLC-ESI-MS/MS [7] - C5-HPLC-ESI-MS/MS [8] - C18-HPLC-ESI-MS/MS(MRM) after SPE fractionation and hydrolysis of FAs [47]	*In vitro*: - NO_2BF_4 [7,8] - Adipocytes supplemented with nitro-OA [47] - Cardiomyocytes cell culture in an induced model of ischemia-reperfusion[8] *In vivo*: - Mitochondria from the myocardium in a model of Type 1 diabetes mellitus [7]
PE		
- Nitro [7,38,47] - Nitroxidized: NO, NO_2 and OH in different proportion [8]	- C18-HPLC-ESI-MS/MS [38] - HILIC-HPLC-ESI-MS/MS [7] - C5-HPLC-ESI-MS/MS [8] - C18-HPLC-ESI-MS/MS(MRM) after SPE fractionation and hydrolysis of FAs [47]	*In vitro*: - NO_2BF_4 [7,8] - Adipocytes supplemented with nitro-OA[47] - Cardiomyocytes cell culture in an induced model of ischemia-reperfusion [8] *In vivo*: - Mitochondria from the myocardium in a model of Type 1 diabetes mellitus [7]
PS		
- Nitro [7,38,47] - Nitrohiydroxy [38] - Nitro-keto [38] - Nitroxidized: NO, NO_2 and	- C18-HPLC-ESI-MS/MS [38] - HILIC-HPLC-ESI-MS/MS [7] - C18-HPLC-ESI-MS/MS(MRM) after SPE	*In vitro*: - NO_2BF_4 [7,8,70] - Adipocytes supplemented with nitro-OA[47] - Cardiomyocytes cell culture in an induced model of ischemia-reperfusion [8] *In vivo*:

OH in different proportion [70]	fractionation and hydrolysis of FAs [47]	- Mitochondria from the myocardium in a model of Type 1 diabetes mellitus [7]
PI		
- Nitro [47]	- C18-HPLC-ESI-MS/MS(MRM) after SPE fractionation and hydrolysis of FAs [47]	<u>*In vitro*</u>: - Adipocytes supplemented with nitro-OA [47]
TAG		
- Nitro [46,47] - Nitrohydroxy [46] - Nitroperoxy [46]	- C18-HPLC-APCI-MS/MS [46] - C18-HPLC-ESI-MS/MS(MRM) after hydrolysis of FAs [46,73] - C18-HPLC-ESI-MS/MS(MRM) after SPE fractionation and hydrolysis of FAs [47]	<u>*In vitro*</u>: - Gastric biomimetic compartment with nitrite [46] - Adipocytes supplemented with nitro-OA [46,47] <u>*In vivo*</u>: - Plasma of rats gavaged with nitro-OA [46] - Extra virgin olive oil [73] - Adipose tissue of rats gavaged with nitro-OA [47]
CE		
-Nitro [43,47,48,74]	- C18-HPLC-ESI-MS/MS with preparative TLC [74] - C18-HPLC-ESI-MS/MS with [43,48] - IR [48] - NMR [74] - UV [74] - C18-HPLC-ESI-MS/MS(MRM) after SPE	<u>*In vitro*</u>: - NO_2BF_4 [43,48] -Nitrite in acidic conditions [43,48,74] - Activated macrophages [74] - Adipocyte supplemented with nitro-OA [46,47] <u>*In vivo*</u>: - Adipose tissue of rats gavaged with nitro-OA [47] - Human plasma [48] - Lipoproteins [43,48]

	fractionation and hydrolysis of FAs [47]	

1.2.4 MS characterization of covalent adducts between nitroxidized lipids and peptides/proteins.

Mass spectrometry has been crucial for the characterization and detection of covalent adduction of nitroxidized lipids to peptides and proteins *in vitro* and *in vivo* (Table 3). Typically, well-established proteomic protocols are used, using the same approaches as done for other post-translational modifications. To date, only peptide and protein adducts with NO_2FAs have been reported, as reviewed in [54]. For protein analysis, bottom-up approaches were used, and protocols usually include digestion, reduction, and carbamidomethylation followed by LC-MS analysis.

The identification of adducts of NO_2FA with peptides and proteins has been done by using ESI and matrix-assisted laser desorption/ionization (MALDI) as the ionization source. Positive mode has been used in all these works, although the possibility of negative mode ionization has also been reported[71]. Modified peptides were identified based on the mass shift of the peptides bearing the modification, and MS^2 characterization allows to confirm its structure. For example, in the case of nitro-OA, a mass shift of 326 Da is observed. MS^2 cleavages in proteins adducted to NO_2FAs occur similarly as the non-modified, with predominant cleavage along the peptidic bonds[99], revealing the modification when the fragment ion includes the NO_2FA and determining the specific amino acid where the adduction occurred. Thus, the identification in the MS^2 spectrum of the sites of adduction is revealed mainly by a mass shift mainly in the *b, y,* and immonium fragments, whose abundances can vary depending on the peptide sequence. The loss of HNO_2 from the fragment ions was occasionally observed, as reported for the adducts of nitro-OA with glutathione[71]. Reversed phase (C18) resins have been the chromatographic stationary phase used to analyze NO_2FA-protein adducts. In these conditions, the modified peptide shows a higher retention time when compared to the non-modified peptide, due to its higher hydrophobicity..

An alternative MS analysis of adducts in proteins has been proposed, by capturing nitroxidized FAs attached to peptides with a transalkylating agent[69]. This approach can evaluate the content of adducted NO_2FAs in a protein pool, as in blood [95], or in particular proteins, either by use of isolated proteins or by identifying the protein following gel

electrophoresis, affinity chromatography or immunoprecipitation protocols. The treatment with the transalkylating agent β-mercaptoethanol captures the NO_2FAs that are released from the protein. A complex is formed between the transalkylating agent and the NO_2FA, that can be readily analyzed and quantitated by MS strategies, revealing the adduction in the protein, although it does not give information about the site of the modification[69,95,100–103]. Hydrolysis of a pool of proteins allowed the detection of adducts by observation of the amino acids bound to NO_2FAs[73].

The detection of adducts of NO_2FAs with proteins by MS has been sometimes bypassed by using different strategies like observing changes in electrophoresis[93,104,105], immunoassays targeting and revealing the modified protein[66,93,106–110], and mutation of the residues that are potentially adducted[111,112]. Still, MS spectrometry characterization must be regarded as the most precise and informative tool to detect this modification in proteins.

1.2.5 *In vitro* models of adduction between nitroxidized lipids and peptides/proteins

Detection of covalent adducts between proteins/peptides and nitroxidized lipids was initially based on *in vitro* experiments (Table 3). To the best of our knowledge, the literature only reports adducts formed with NO_2FAs, namely nitro-OA, nitro-LA, nitro-CLA, and nitro-AA. Biomimetic models based on the incubation of the purified peptide/protein with NO_2FAs in buffers mimicking physiological conditions have been used. Isolated mitochondria and their lipid extract have been incubated too[66,103]. Also, studies in cell cultures overexpressing the proteins and co-cultured with nitrated FAs allowed to detect these adducts[65,66,93,100,101,103,107,110,112,113]. The incubation of the amino acid cysteine with nitro-OA originates adduction through a covalent bond that has been characterized by MS and MS/MS[73]. Adducts of nitro-OA and nitro-LA with glutathione (GSH) have also been characterized using similar approaches[69,71,114]. The MS characterization of adducts of nitro-OA with glyceraldehyde phosphate dehydrogenase (GAPDH) allowed pinpointing six modified His and Cys residues[69,71]. MS characterization reported that the peroxisome-proliferator activated receptor-γ (PPAR-γ) is adducted with nitro-OA in one only residue, Cys(285), when incubated with a lower concentration, and subsequentially, in other histidines after incubation with a higher concentration of nitro-OA[100]. Other proteins were also reported to form adducts with NO_2FAs *in vitro,* such as recombinant Kelch-like ECH-associated protein 1 (KEAP1), with seven nitroalkylated Cys[113], recombinant prometalloproteinase-7 (proMMP-7) on one Cys and His[109], nuclear factor κB (NF-κB) with

predicted modification on Cys of p65 and Cys of p50[65], 5-lipoxygenase on one Cys and six His[115,116], α-synuclein on a His[117], protein disulphide isomerase (PDI) in four Cys[105], adenine nucleotide translocase-1 (ANT-1) in a Cys[66,108], uncoupling protein (UCP) in a residue not determined[66], angiotensin II receptor type 1 (AT1R) in a residue not determined[101], catephsin S in a Cys[110], transient receptor potential A1 (TRPA1) suspected on four Cys and one Lys[112], FP subunit of the mitochondrial complex II in two Cys and three His, and signaling protein stimulator of IFN genes (STING) in two Cys and one His. Noteworthy, STING was proposed to be also modified by nitroso-OA[93]. Details about the experimental models used for identifying these adducts, and indicating the modified amino acids, can be found in Table 3.

Different chemical parameters for the formation of adducts between nitroxidized lipids and proteins have also been tested *in vitro.* By incubating GAPDH adduct with DTT or GSH, that rescue the non-modified protein by capturing the NO_2FA, 85% of the enzymatic activity was recovered, while the reversibility of the reaction was not observed when the protein was oxidized with peroxynitrite or hydroperoxide [71]. Recently, confirmation of the reversibility of the reaction*,* dependence on pH, the existence of non-equivalent electrophilic carbons in the NO_2FA and computational modeling of the mechanism of reaction have been studied, for the adduction of nitro-CLA to thiols by *in vitro* experiments with GSH and low molecular thiols[58]. This work also evaluated the non-covalent interaction of nitro-CLA with HSA reporting binding of four molecules of nitro-CLA per protein, and the abundant covalent binding of nitro-CLA that readily occupies half of the free thiols per mol present in HSA[58]. Therefore, *in vitro* assays have been essential for the characterization of adducts of NO_2FAs and proteins, confirming their formation, and for the study the parameters of the reaction.

1.2.6 Detection *in vivo* of adducts between nitroxidized lipids and proteins

The formation of adducts of proteins and NO_2FAs *in vivo* has been corroborated from different works, mostly with the help of NO_2FAs externally supplemented. First works identifying NO_2FAs adducted to proteins established that only less than 10% of intravenously supplemented nitro-OA in mice remains free, while the rest is more likely adducted to proteins in plasma after a few minutes[95]. In particular, the most significant proportion of nitro-OA, up to 50% of the total pool, is adducted to albumin in the blood, as deduced by comparing total nitro-OA versus the amount adducted to albumin after isolating the protein[95]. Adducts of NO_2FAs with GSH and with GADPH have been detected endogenously without supplementation, formed in human red blood cells[71]. And quantitative

information was obtained for GSH adduct with nitro-OA (3.3nM) and nitro-LA (1.3nM)[71]. Adducts of cysteine with nitro-CLA have been detected in the urine of healthy human volunteers[58] and after hydrolysis of proteins in fresh olive olives[73]. Some other low molecular weight thiols were also detected in human urine adducted to nitro-OA[64]. GSH and cysteine adducts with nitro-OA were also observed in the blood of mice, after intravenous injection of the modified FA[95]. Nitroalkylation of albumin by nitro-OA and nitro-LA have been found in the plasma of mice gavaged with these NO_2FAs[69] or after intravenous injection[95]. Nitroalkylation of nuclear factor κB (NFκB) in the subunit p65 was demonstrated *in vivo* in myocardial tissue of a murine model of ischemia-reperfusion with intravenous supplementation of nitro-OA and nitro-LA[65]. Adducts of soluble epoxide hydrolase (sEH) were also demonstrated in mice fed with nitrite and LA[104]. Experiments showed adduction of nitro-OA and nitro-LA to ANT1 in ischemic hearts perfused with these NO_2FAs[108]. Therefore, although often non-biological levels of NO_2FAs supplemented externally are used for the studies, these results evidence that adducts are formed *in vivo* and are detectable by MS

Table 3: State of the art of the detection of adducts between nitroxidized lipids and proteins.

Protein/ peptide (modified residue)	**Fatty acid adducted**	**Detection method**	**Experimental model**
Cysteine	- nitro-OA [58,64,73] - nitro-CLA [58,64] - Metabolic derivatives of nitro-OA [95] - Metabolic derivatives of nitro-CLA[64]	- C18-HPLC-ESI-MS/MS [58,64,73] - C18-HPLC-ESI-MS/MS with BME transalkylation [95] - UV characterization [64] - UV assessment of the reaction and kinetics [58]	*In vitro*: - Incubation with NO_2FA [58,64,73] *In vivo*: - Human urine [58,64] - Hydrolyzed protein extract from fresh olives [73] - Mice blood, after intravenous injection of nitro-OA [95]
Low molecular weight thiols (homocysteine / cysteine methyl ester / DHLA / cysteinylglycine /BME / TNB /taurine/N-acetyl cysteine)	- nitro-OA [64,114] - nitro-LA [114] - nitro-CLA [58] - Metabolic derivatives of nitro-CLA [64]	- C18-HPLC-ESI-MS/MS [64,95] - UV assessment of the reaction and kinetics [58,114]	*In vitro*: - Incubation with NO_2FA [58,95,114] *In vivo*: - Human urine [64]

GSH (Cys)	- nitro-OA [69,71,95,114] - nitro-LA [69,71,91,114] - nitro-CLA [58] - Metabolic derivatives of nitro-LA [69]	- C18-HPLC-ESI-MS/MS [69,71,91,95] - Direct infusion-ESI-MS [69,71] - UV assessment of the reaction, kinetics or parameters of the reaction [58,91,114]	*In vitro*: - Incubation with NO_2FA [58,69,71,91,114] *In vivo*: - Mice blood, after intravenous injection of nitro-OA [95] - Red Blood cells [71]
Albumin	- nitro-OA [69,95] - nitro-LA [69] - nitro-CLA [58]	- C18-HPLC-ESI-MS/MS after electrophoresis and BME transalkylation [69,95] - Spectrophotometry of non-covalently bound nitro-CLA[58] - Measurement of free thiols [58] - Non-covalent binding by UV-VIS spectrophotometry[58].	*In vitro*: - Incubation with NO_2FA [58] *In vivo*: - Mice blood, after intravenous injection of nitro-OA [95] - Mice blood, after intravenous injection of nitro-OA and nitro-LA [69]
GAPDH (Cys149,153,244 and His 108,327,134)	- nitro-OA [69,71] - nitro-LA [71]	- C18-HPLC-ESI-MS/MS [71] - MALDI-TOF-MS of tryptic digest [71] - C18-HPLC-ESI-MS/MS after electrophoresis and BME transalkylation [69] -MALDI-TOF-MS [71]	*In vitro*: - Incubation with NO_2FA [69,71] *In vivo*: - Red Blood cells [71]
ANT1 (Cys57)	- nitro-LA [66,108]	- Immunoprecipitation for biotinylated FA adduct, electrophoresis, tryptic digestion and MALDI-TOF-TOF-MS/MS [108] - Immunoprecipitation of biotin-FA labeled proteins, and Western Blot anti-ANT1 [66]	*In vitro:* - Mitochondria from rat heart incubated with nitro-LA [66] - Cardiomyocytes incubated with NO_2-LA [66] *In vivo* - Model of ischemia by heart perfusion with biotinylated nitro-LA [108]
UCP	- nitro-LA [66]	- Western Blot suggest the adduct by the disappearance of the band when nitroalkylated [66]	*In vitro*: - Mitochondria from rat heart incubated with nitro-LA [66]
5-LO (Cys416, 418 and His125,	- nitro-OA [115]	- C18-HPLC-ESI-MS/MS after	*In vitro*: - Incubation with nitro-OA [115]

360, 362, 367, 372, 432)		electrophoresis and tryptic digestion [115]	
Keap1 (preferentially Cys273,288, also other 17 Cys)	- nitro-OA [113]	- C18-HPLC-ESI-MS/MS after electrophoresis and tryptic digest [113] - Immunoprecipitation of the protein and C18-HPLC-ESI-MS/MS after BME transnitroalkylation [113]	*In vitro* - Incubation with nitro-OA [113] - HEK cells transfected with recombinant protein and treated with nitro-OA [113]
PPAR gamma (Cys285 and His266, 323, 425, 449)	- nitro-OA[100]	- Immunoprecipitation of the protein and C18-HPLC-ESI-MS/MS after BME transalkylation [100] - C18-HPLC-ESI-MS/MS after electrophoresis and tryptic digest [100]	*In vitro* - Incubation with nitro-OA [100] - HEK cells transfected with recombinant protein and treated with nitro-OA [100]
NFkB (residue non determined, predicted at Cys38 of p65 subunit and Cys62 of p50)	- nitro-OA [65,107]	- Correlated Immunoprecipitation of the adduct with avidin forbiotinylated NO_2FA and and anti-NFκB antibodies[107] - Immunoprecipitation of the protein and BME transalkylation followed by C18-HPLC-ESI-MS/MS[65]	*In vitro*: - Incubation with biotinylated nitro-OA [107] *In vivo*: - Induced *in vivo* myocardial infarction in mice, gavaged with nitro-OA[65]
MMP7 (Cys70 and His105, 126, 196) / MMP9 (residue not determined)	- nitro-OA [109]	- Western-blot for adducted protein containing biotin [109] - Tryptic digestion and C18-HPLC- ESI-MS/MS (ProMMP7)[109]	*In vitro*: - Incubation with biotiniylated nitro-OA [109]
AT1R	- nitro-OA [106]	- Immunoprecipitation AT1R, BME transalkylation followed by C18-LC-ESI-MS/MS[106]	*In vitro*: - HEK293 overexpressing AT1R incubated with nitro OA [106]
TRPA1-Transient Receptor Potential A1	- nitro-OA [112]	- Study of the effect of mutation of the suspected modified aminoacids [112]	*In vitro*: - HEK cell transfected and supplemented with nitro-OA [112]
FP subunit of mitochondrial complex II (Cys	- nitro-OA [103]	- Nano-C18-HPLC-ESI-MS/MS after	*In vitro*: - Incubation with nitro-OA [103]

9 and 14, His 2,5, 6)		electrophoresis and BME transalkylation [103] - Nano-C18-HPLC-ESI-MS/MS of tryptic digest [103]	- Rat heart mitochondrial extracts incubated with nitroalkene[103]
PDI (Cys397, 400, 312 and 343)	- nitro-AA[105]	- C4-HPLC-MS of tryptic digest and electrophoretic mobility assay[105]	*In vitro*: - Recombinant protein incubated with nitroalkene [105]
Catephsin S (Cys 25)	- nitro-OA [110]	- Correlated immunoblot for protein and biotinylated FA [110]	*In vitro*: Incubation with biotinylated nitro-OA[110]
sEH(suspected Cys521)	- nitro-OA [111]	- Electrophoretic mobility assay and study of the effect of mutation of the suspected modified amino acids[111]	*In vivo*: - Mice model of hypertension [111]
STING- (Cys88, 91 and His116)	- nitro-OA[93] - nitroso-OA[93] -nitro-CLA[93]	- Electrophoretic shift and immunoprecipitation of the adduct with biotinylated nitro-FA [93] - Immunoprecipitation of the adduct with biotinylated nitro-FA and MALDI-TOF of tryptic digest [93]	*In vitro:* - THP-1 cells treated with NO_2FAs [93] - HEK cells expressing STING,supplemented with nitro-OA [93]

1.3. Biological roles and clinical implications of lipid nitroxidation

Nitroxidized lipids are nowadays considered as a class of bioactive molecules, after the last two decades of intense research in the field[77,118–122]. It is well-known that their pleiotropic activity is not only related to nitric oxide signaling, but the formation of nitroxidized lipids seems to have other important downstream signaling pathways, remarkably interaction of NO_2FAs with proteins by covalent adduction. It leads to the modulation of enzymatic activity, transcription factors, membrane activity and chemical homeostasis (Figure 7). Following, mechanisms of action are detailed without focusing on the specific NO_2FA given that the key feature for the interaction seems to depend on the presence of the modification rather than the lipid substrate.

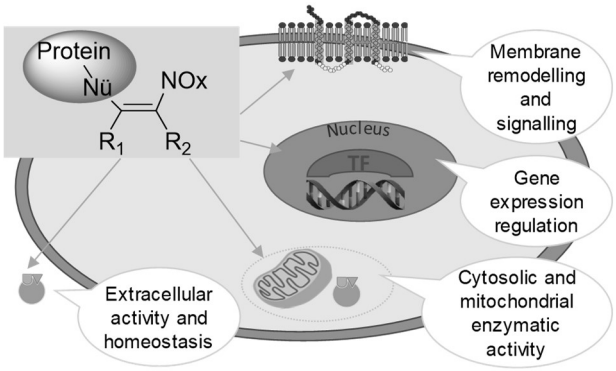

Figure 7: Scheme for the cellular effects of adduction of nitroxidized lipids to proteins.

Most of the information gathered to date refers to NO_2FAs, since these are the best-studied nitroxidized lipids. NO_2FAs have been reported to have important anti-inflammatory effects, modulating different processes in inflammation and immune response. They induce a decrease of the release of cytokines by macrophages activated *in vitro* with lipopolysaccharides, tumor necrosis factor α, or interferon gamma IFNγ[74,92,93,107,123–127]. NO_2FAs have also been reported to reduce the leukocyte number and activity, including processes of recruitment, adhesion, and infiltration[92,94,128–131,97,107,110,123–127]. NO_2FAs also contribute to the resolution of the inflammation process by reducing the synthesis of key mediators, by inhibiting prostaglandin endoperoxide H synthase 1 and 2 (PGHS) or cyclooxygenase 2 (COX2) that diminishes the synthesis of prostaglandins[125,132], by inhibition of 5-lipoxygenase (5-LOX) that hampers production of pro-inflammatory leukotrienes[115,116], and by specific decrease of the levels of prostaglandin E, PGE_2[125]. ROS and RNS production associated with the immune response is also quenched by NO_2FAs and nitro-PLs. Likewise, NO_2FAs and nitro-PLs inhibit the activity of nitric oxide synthases (NOS) [9,92,110,123–126,133], NADPH oxidase (NOX) [126,131,134] and myeloperoxidase (MPO)[126]. NO_2FAs are important repressors of the nuclear factor κB (NFκB), which induces the expression of various pro-inflammatory genes in macrophages and endothelial cells[74,92,107,110,123,124,127,135,136]. The electrophilic addition of NO_2FAs also disrupts upstream processes for the activation of NFκB as the interaction of lipolysaccharides and Toll-like receptor 4 (TLR4) in activated macrophages[137]. Also, the signal transducer and activator of transcription-1, STAT-1, which is a transcription factor for pro-inflammatory enzymes, is potently suppressed by NO_2FAs[123,131,138]. Presence of NO_2FAs upregulates mitogen-activated protein kinase (MPK1) in macrophages, inhibiting inflammatory signals[138]. NO_2FAs are also able to activate the peroxisome proliferator-activated receptor-γ in the

nucleus(PPARγ) with anti-inflammatory effect[62,110,124,127,139,140]. NO_2FAs also reduce the production of pro-inflammatory interferons mediated by the adaptor molecule stimulator of IFN genes (STING)[93].

Antioxidative effects have also been attributed to NO_2FAs. Lipid nitration is considered a terminating product of lipid peroxidation[20,41], and oxidized lipids pool are diminished in the presence of NO_2FAs[126] and nitro-PLs[9]. Protein oxidation is also diminished in the presence of NO_2FAs[131]. It has been described that the Kelch-like ECH-associated protein 1 (Keap1) is adducted to NO_2OA, leading to the release of nuclear factor erythroid 2-related factor 2 (Nrf2) from the cytosolic complex, which enters the nucleus, acting as a transcription factor for the antioxidant phase II responsive gene expression [92,113,135]. One of these enzymes, responsible for the detoxification related to the heme moiety, heme oxygenase-1 (HO-1), is also enhanced by t mechanisms involving its nitroalkylation of HO-1 and the expression of related redox regulatory proteins [74,92,98,141–143]. Heat shock response is activated by nitro-OA, promoting the antioxidative response based on a transcription of heat shock proteins (HSP)[142]. Finally, the levels of ROS, particularly $O_2^{\cdot-}$, have been shown to decrease associated with the presence of NO_2FAs and nitroxidized phospholipids [9,92,133–135,144,145,103,107,110,123–126,130].

It is well-reported that NO_2FAs have a vasculoprotective effect[146,147]. The most direct mechanism is by releasing nitric oxide since, in this sense, they can be considered a reservoir of a vasorelaxant agent [43,62,89,148]. Also, NO_2FAs increase the concentration of nitric oxide by upregulating the eNOS activity [149]. Methylated nitro-AA has been shown to induce vasodilation by increasing cGMP in smooth muscle cells of vessels[89]. The covalent modification of angiotensin II receptor 1 (AT_1R) by nitro-OA, inhibits downstream processes in smooth muscle cells related to G-proteins, diminishing blood pressure[106]. The covalent adduction of nitro-OA to soluble epoxide hydrolase (sEH) leads to inhibition with an anti-hypertensive effect[104]. NO_2FAs also alleviates hypertension by reducing levels of prostaglandin F2 (PGF_2) and proliferation of smooth muscle cells[130], or by downregulating the differentiation of myofibroblasts through Smad2 pathway[144]. NO_2FAs regulate thrombotic mechanisms in blood, by inhibiting platelets activation and clotting[89,150], production of thromboxanes[132] and thrombin-induced aggregation[150]. The prejudicial infiltration of leukocytes in atherosclerotic vascular injury, it is inhibited by NO_2FAs[128].

NO_2FAs also showed to play a role in glucose homeostasis. They have been considered important to improve glucose tolerance[129,151]. NO_2FAs can modulate the PPAR-γ activity[100,114], in its role in adipocyte differentiation and regulating glucose homeostasis.

Also, in endothelial or smooth muscle cells, NO_2FAs can promote glucose uptake by improving insulin sensitivity[100].

Cytoprotective effects of NO_2FAs have also been highlighted. In ischemia-reperfusion events, NO_2FAs reduce the tissue damage by interacting with uncoupling proteins (UCP) and adenine nucleotide translocase-1 (ANT1) in mitochondria, promoting energetic uncoupling that avoids cellular death[65,66,69,108,152]. NO_2FAs have also shown to be able to reverse the mitochondrial dysfunction after myocardium infarction in rats[153], and to enhance the respiratory processes and metabolic adaptation[103]. Finally, some reports showed the antitumoral activity of NO_2FAs by reducing the proliferation of neoplastic cells, and their ability to invade other tissues in metastasis[136,154].

Table 4: Biological roles of nitroxidized lipids.

Anti-inflammatory
- Cytokines ↓[74,92,93,107,123–127] - Leukocytes number and activity ↓ [92,94,128–131,97,107,110,123–127] - PGHS/COX-2 ↓ [123,125,132] - 5-LOX ↓[115,116] - PGE_2 ↓ [125] - iNOS ↓[9,92,110,123–126,133] - NOX ↓[126,134,144] - MPO ↓ [126] - NFκB ↓[74,92,107,110,123,124,127,135,136] - TL4R signalling ↓[137] - STAT1 ↓[123,131,138] - MKP-1 ↑[138] - PPARγ ↑ [62,110,124,127,139,140] - STING ↓ [93]
Antioxidant
- Lipid peroxidation ↓ [9,20,41,126] - Protein oxidation and nitration ↓ [131] - XOR ↓ [145] - Nrf2 ↑ [92,113,135] - Heme oxygenase 1 (HO1) ↑ [74,92,98,141–143] - HSP ↑ [142] - ROS ↓ [9,35,145,92,123,125,126,133–135,144]
Vasorelaxation
- $NO^{\cdot}$ ↑ [43,62,89,148] - eNOS ↑ [149] - cGMP levels in smooth muscle cells ↑ [89]

Antihypertensive
- AT_1R ↓ [106] - sEH ↓[111] - Smooth muscle cell proliferation↓ [130] - Prostaglandin F2 ↓ [130] - Myofibroblast differentiation ↓ [144]
Antithrombotic
- Platelets ↓[89,128] - Thromboxanes ↓[132] - Thrombin activation ↓ [150]
Anti-hyperglycemic
- PPARγ↑ [100,114] - Adipocytes ↑[100,114] - Glucose uptake ↑ [100] - Glucose tolerance ↑ [129]
Antitumoral
- Tumor cells↓[136,154]
Cytoprotective
- ANT1 ↑ [66,108] - UCP ↑ [66] - Mitochondrial function ↑[133,153] - Mitochondrial respiratory complex ↑ [103] - Metabolic adaptation ↑ [103]

The different biological roles played by NO_2FAs have moved the interest of scientists to its analytical determination and diagnostic or therapeutic exploitation. Different studies on NO_2FAs have already correlated their occurrence in clinical cases, that could be exploited in diagnosis. The concentrations can be monitored and compared with healthy subjects as, for example, the ischemia-reperfusion in which the concentration of nitro-linoleic acid was significantly increased [65,66] or the increase of nitro-PLs levels in diabetes mellitus type 1 in a murine model[7]. Recently, a study has proposed the detection of NO_2FAs in urine related to the prognosis of rheumatoid arthritis[155]. Years ago, 10-nitro-OA, whose intellectual property has been licensed by Complexa Inc., was selected for clinical assays and drug development in chronic inflammation and fibrotic diseases[96,119,156]. Nitro-FAs therapeutic

potential against immune-based pathologies is also being exploited by developing drugs with a broad spectrum that can be beneficial against diseases as nephropathy, focal segmental glomerulosclerosis, and pulmonary arterial hypertension (reviewed in [119]). A positive effect against allergic dermatitis has been recently proved by subcutaneous administration of nitro-OA[97]. It is also well-established the potential of NO_2FAs regarding cardiovascular diseases (reviewed in [146,147]). They may help to alleviate general hypertension[104,106], and pulmonary hypertension[130], and to reduce the formation of plaques in atherosclerosis[128,131]. Also, NO_2FAs may promote recovery in myocardial infarction, particularly by influencing the damage and prognosis after ischemia and ischemia-reperfusion injury[65,66,126,153,157]. After endoluminal vessel surgery, nitro-OA helps to minimize the probability of restenosis[143]. Another pathology in which NO_2FAs may have therapeutic potential is diabetes, through reduction of glucose levels, as an alternative to drugs as rosiglitazone [100], and in different aspects of the evolution of the disease, as renal damage[158]. Finally, obesity-related complications also seem to be therapeutically targeted by NO_2FAs[129,151]. Recent studies have also performed structure-function relationship studies of different nitroalkenes with chain lengths ranging from 11 to 24 carbon, and its modulation ability of the activity of Nrf2 and NFκB, revealing that nitro-OA is the most potent effector[135]. The biological relevance between different isomeric forms is not yet clarified, but there are indications of different efficiencies[145].

The discovery of the important bioactivity of NO_2FAs would not have been possible without mass spectrometry for their monitoring and characterization. This work is still ongoing and must still provide important information about their involvement in pathologies, and for diagnosis and drug development.

1.4. Aim of this work

Nitroxidized lipids are important endogenous signaling molecules, and mass spectrometry is a powerful tool for their study. While nitroxidized fatty acids are well-studied, nitroxidized phospholipids have been scarcely addressed. The main objective of this thesis was to expand the knowledge about the impact of nitroxidative stress in the lipidome and the formation of nitroxidized phospholipids, including to study their adduction to peptides/proteins, by using and developing new MS-based approaches. The main goals of this thesis were to:

- To develop LC-MS and MS/MS approaches and to characterize the *in vitro* nitroxidation of cardiolipins, an important phospholipid class associated with cellular bioenergetics and signaling as apoptosis, that remains uncharacterized to date. (CHAPTER 1)

- To characterize by MS and MS/MS the *in vitro* adduction between nitroxidized phospholipids and nucleophilic peptides. (CHAPTER 2)

- To evaluate the adaptation of the lipidome in pathological conditions associated with nitroxidative stress, namely in acute myocardial infarction (CHAPTER 3) and in cancer cachexia. (CHAPTER 4)

1.5. References

1. GC. Brown, V. B. Interaction between nitric oxide, oxygen, reactive oxygen species and reactive nitrogen species. 953–956 (2006).
2. Freeman, B. A. *et al.* Nitro-fatty acid formation and signaling. *J. Biol. Chem.* **283**, 15515–15519 (2008).
3. Trostchansky, A. & Rubbo, H. Nitrated fatty acids: mechanisms of formation, chemical characterization, and biological properties. *Free Radic. Biol. Med.* **44**, 1887–96 (2008).
4. Rubbo, H. & Radi, R. Protein and lipid nitration: Role in redox signaling and injury. *Biochim. Biophys. Acta - Gen. Subj.* **1780**, 1318–1324 (2008).
5. Baker, P. R. S. S. *et al.* Convergence of nitric oxide and lipid signaling: Anti-inflammatory nitro-fatty acids. *Free Radic. Biol. Med.* **46**, 989–1003 (2009).
6. Kalyanaraman, B. Nitrated lipids: a class of cell-signaling molecules. *Proc. Natl. Acad. Sci. U. S. A.* **101**, 11527–8 (2004).
7. Melo, T. *et al.* Recent Advances on Mass Spectrometry Analysis of Nitrated Phospholipids. *Anal. Chem.* **88**, 2622–2629 (2016).
8. Melo, T. *et al.* Characterization of phospholipid nitroxidation by LC-MS in biomimetic models and in H9c2 Myoblast using a lipidomic approach. *Free Radic. Biol. Med.* **106**, 219–227 (2017).
9. Melo, T. *et al.* New Insights into the Anti-Inflammatory and Antioxidant Properties of Nitrated Phospholipids. *Lipids* **53**, 117–131 (2018).
10. Villanueva, C. & Giulivi, C. Subcellular and cellular locations of nitric oxide synthase isoforms as determinants of health and disease. *Free Radic. Biol. Med.* **49**, 307–16 (2010).
11. Förstermann, U. & Sessa, W. C. Nitric oxide synthases: Regulation and function. *Eur. Heart J.* **33**, 829–837 (2012).
12. Franchini, A., Conte, A. & Ottaviani, E. Nitric oxide: an ancestral immunocyte effector molecule. *Adv. Neuroimmunol.* **5**, 463–78 (1995).

13. Aktan, F. iNOS-mediated nitric oxide production and its regulation. *Life Sci.* **75**, 639–653 (2004).

14. Patel, R. P. *et al.* Biological aspects of reactive nitrogen species. *Biochim. Biophys. Acta - Bioenerg.* **1411**, 385–400 (1999).

15. Nalwaya, N. & Deen, W. M. Nitric oxide, oxygen, and superoxide formation and consumption in macrophage cultures. *Chem. Res. Toxicol.* **18**, 486–493 (2005).

16. Pacher, P., Beckman, J. S. & Liaudet, L. Nitric Oxide and Peroxynitrite in Health and Disease. *Physiol. Rev.* **87**, 315–424 (2007).

17. Porterfield, D. M. *et al.* Proteins and lipids define the diffusional field of nitric oxide. *Am. J. Physiol. Cell. Mol. Physiol.* **281**, L904-12 (2001).

18. Davies, M. J. Protein oxidation and peroxidation. *Biochem. J.* **473**, 805–25 (2016).

19. Eiserich, J. P., Butler, J., van der Vliet, a, Cross, C. E. & Halliwell, B. Nitric oxide rapidly scavenges tyrosine and tryptophan radicals. *Biochem. J.* **310 (Pt 3**, 745–9 (1995).

20. O'Donnell, V. B. *et al.* Nitric oxide inhibition of lipid peroxidation: kinetics of reaction with lipid peroxyl radicals and comparison with alpha-tocopherol. *Biochemistry* **36**, 15216–15223 (1997).

21. Ferrer-sueta, G. & Radi, R. Chemical Biology of Peroxynitrite: Kinetics, Diffusion, and Radicals. **4**, 161–177 (2009).

22. Rubbo, H., Trostchansky, A. & O'Donnell, V. B. Peroxynitrite-mediated lipid oxidation and nitration: Mechanisms and consequences. *Arch. Biochem. Biophys.* **484**, 167–172 (2009).

23. Trettin, A. *et al.* GC – MS / MS and LC – MS / MS studies on unlabelled and deuterium-labelled oleic acid (C18 : 1) reactions with peroxynitrite (O N O O −) in buffer and hemolysate support the pM / nM-range of nitro-oleic acids in human plasma ☪. *J. Chromatogr. B* **964**, 172–179 (2014).

24. Möller, M. N. *et al.* Membrane 'lens' effect: Focusing The Formation of Reactive Nitrogen Oxides from the .NO/O2 reaction. *Chem. Res. Toxicol.* **20**, 709–714 (2007).

25. Espey, M. G. *et al.* A chemical perspective on the interplay between NO, reactive oxygen species, and reactive nitrogen oxide species. *Ann. N. Y. Acad. Sci.* **962**, 195–206 (2002).

26. Sampson, J. B., Ye, Y., Rosen, H. & Beckman, J. S. Myeloperoxidase and horseradish peroxidase catalyze tyrosine nitration in proteins from nitrite and hydrogen peroxide. *Arch. Biochem. Biophys.* **356**, 207–13 (1998).

27. Singh, R. J., Goss, S. P., Joseph, J. & Kalyanaraman, B. Nitration of gamma-tocopherol and oxidation of alpha-tocopherol by copper-zinc superoxide dismutase/H2O2/NO2-: role of nitrogen dioxide free radical. *Proc. Natl. Acad. Sci. U. S. A.* **95**, 12912–7 (1998).

28. Malle, E., Marsche, G., Arnhold, J. & Davies, M. J. Modification of low-density lipoprotein by myeloperoxidase-derived oxidants and reagent hypochlorous acid. *Biochim. Biophys. Acta - Mol. Cell Biol. Lipids* **1761**, 392–415 (2006).

29. Eiserich, J. P. *et al.* Formation of Nitric Oxide-derived oxidants by myeloperoxidase

in neutrophils. *Nature* **391**, 393–397 (1998).

30. D'Ischia, M., Napolitano, A., Manini, P. & Panzella, L. Secondary targets of nitrite-derived reactive nitrogen species: Nitrosation/nitration pathways, antioxidant defense mechanisms and toxicological implications. *Chem. Res. Toxicol.* **24**, 2071–2092 (2011).

31. Eiserich, J. P., Patel, R. P. & O'Donnell, V. B. Pathophysiology of nitric oxide and related species: Free radical reactions and modification of biomolecules. *Mol. Aspects Med.* **19**, 221–357 (1998).

32. Durackova, Z. Some Current Insights into Oxidative Stress. **8408**, 459–469 (2010).

33. Foster, M. W., Hess, D. T. & Stamler, J. S. Protein S-nitrosylation in health and disease: a current perspective. *Trends Mol. Med.* **15**, 391–404 (2009).

34. Melo, T., Montero-Bullón, J.-F., Domingues, P. & Domingues, M. R. Discovery of bioactive nitrated lipids and nitro-lipid-protein adducts using mass spectrometry-based approaches. *Redox Biol.* 101106 (2019). doi:10.1016/j.redox.2019.101106

35. Trostchansky, A. *et al.* Synthesis, isomer characterization, and anti-inflammatory properties of nitroarachidonate. *Biochemistry* **46**, 4645–4653 (2007).

36. Balazy, M. & López-Fernández, J. Isomerization and nitro-oxidation of arachidonic acid by NO2. *Adv. Exp. Med. Biol.* **525**, 173–6 (2003).

37. Balazy, M. & Poff, C. D. Biological nitration of arachidonic acid. *Curr. Vasc. Pharmacol.* **2**, 81–93 (2004).

38. Jain, K. *et al.* The mechanism of oleic acid nitration by ???NO2. *Free Radic. Biol. Med.* **45**, 269–283 (2008).

39. Schopfer, F. J. *et al.* Fatty acid transduction of nitric oxide signaling: Nitrolinoleic acid is a hydrophobically stabilized nitric oxide donor. *J. Biol. Chem.* **280**, 19289–19297 (2005).

40. Rubbo, H. *et al.* Nitric Oxide Inhibition of Lipoxygenase-Dependent Liposome and Low-Density Lipoprotein Oxidation : Termination of Radical Chain Propagation Reactions and Formation of Nitrogen-Containing Oxidized Lipid Derivatives. **324**, 15–25 (1995).

41. Donnell, V. B. O. *et al.* Nitration of Unsaturated Fatty Acids by Nitric Oxide-Derived Reactive Nitrogen Species Peroxynitrite , Nitrous Acid , Nitrogen Dioxide , and Nitronium Ion. 83–92 (1999).

42. Pryor, W. A., Castle, L. & Church, D. F. Nitrosation of organic hydroperoxides by nitrogen dioxide/dinitrogen tetraoxide. *J. Am. Chem. Soc.* **107**, 211–217 (1985).

43. Lima, É. S. *et al.* Nitrated lipids decompose to nitric oxide and lipid radicals and cause vasorelaxation. *Free Radic. Biol. Med.* **39**, 532–539 (2005).

44. Su, Y.-H., Wu, S.-S. & Hu, C.-H. Release of nitric oxide from nitrated fatty acids: Insights from computational chemistry. *J. Chinese Chem. Soc.* **66**, 41–48 (2019).

45. Gorczynski, M. J., Huang, J., Lee, H. & King, S. B. Evaluation of nitroalkenes as nitric oxide donors. *Bioorg. Med. Chem. Lett.* **17**, 2013–2017 (2007).

46. Fazzari, M. *et al.* Generation and esterification of electrophilic fatty acid nitroalkenes in triacylglycerides. *Free Radic. Biol. Med.* **87**, 113–124 (2015).

47. Fazzari, M. *et al.* Nitro-fatty acid pharmacokinetics in the adipose tissue compartment. *J. Lipid Res.* **58**, 375–385 (2017).

48. Lima, E. S., Di Mascio, P. & Abdalla, D. S. P. Cholesteryl nitrolinoleate, a nitrated lipid present in human blood plasma and lipoproteins. *J. Lipid Res.* **44**, 1660–1666 (2003).

49. Lancaster, J. R. Nitroxidative, nitrosative, and nitrative stress: Kinetic predictions of reactive nitrogen species chemistry under biological conditions. *Chem. Res. Toxicol.* **19**, 1160–1174 (2006).

50. Milic, I. *et al.* Profiling and relative quantification of multiply nitrated and oxidized fatty acids. *Anal. Bioanal. Chem.* 5587–5602 (2015). doi:10.1007/s00216-015-8766-3

51. Chakravartula, S. V. S. S. V. S. & Balazy, M. Characterization of nitro arachidonic acid and nitro linoleic acid by mass spectrometry. *Anal. Lett.* **45**, 2412–2424 (2012).

52. Tsikas, D. *et al.* Specific GC-MS/MS stable-isotope dilution methodology for free 9- and 10-nitro-oleic acid in human plasma challenges previous LC-MS/MS reports. *J. Chromatogr. B Anal. Technol. Biomed. Life Sci.* **877**, 2895–2908 (2009).

53. Bonacci, G. *et al.* Conjugated linoleic acid is a preferential substrate for fatty acid nitration. *J. Biol. Chem.* **287**, 44071–44082 (2012).

54. Geisler, A. C. & Rudolph, T. K. Nitroalkylation - A redox sensitive signaling pathway. *Biochim. Biophys. Acta - Gen. Subj.* **1820**, 777–784 (2012).

55. Domingues, R. M. *et al.* Lipoxidation adducts with peptides and proteins: Deleterious modifications or signaling mechanisms? *J. Proteomics* **92**, 110–131 (2013).

56. Vitturi, D. A. *et al.* Modulation of Nitro-fatty Acid Signaling: prostaglandin reductase-1 is a nitroalkene reductase. *J. Biol. Chem.* **288**, 25626–25637 (2013).

57. Franz, J. *et al.* Nitrated Fatty Acids Modulate the Physical Properties of Model Membranes and the Structure of Transmembrane Proteins. *Chem. - A Eur. J.* **23**, 9690–9697 (2017).

58. Turell, L. *et al.* The Chemical Basis of Thiol Addition to Nitro-conjugated Linoleic Acid, a Protective Cell-signaling Lipid. *J. Biol. Chem.* **292**, 1145–1159 (2017).

59. Wang, M., Wang, C., Han, R. H. & Han, X. Novel advances in shotgun lipidomics for biology and medicine. *Prog. Lipid Res.* **61**, 83–108 (2016).

60. Herzog, R. *et al.* A novel informatics concept for high-throughput shotgun lipidomics based on the molecular fragmentation query language. *Genome Biol.* **12**, R8 (2011).

61. Schoeman, J. C. *et al.* Development and application of a UHPLC–MS/MS metabolomics based comprehensive systemic and tissue-specific screening method for inflammatory, oxidative and nitrosative stress. *Anal. Bioanal. Chem.* **410**, 2551–2568 (2018).

62. Baker, P. R. S. *et al.* Multiple nitrated unsaturated fatty acid derivatives exist in human blood and urine and serve as endogenous peroxisome proliferator-activated receptor ligands. *J. Biol. Chem.* **280**, 42464–42475 (2005).

63. Tsikas, D., Zoerner, A. A. & Jordan, J. Oxidized and nitrated oleic acid in biological systems: Analysis by GC-MS/MS and LC-MS/MS, and biological significance. *Biochimica et Biophysica Acta - Molecular and Cell Biology of Lipids* **1811**, 694–705

(2011).

64. Salvatore, S. R. *et al.* Characterization and quantification of endogenous fatty acid nitroalkene metabolites in human urine. *J. Lipid Res.* **54**, 1998–2009 (2013).

65. Rudolph, V. *et al.* Endogenous generation and protective effects of nitro-fatty acids in a murine model of focal cardiac ischaemia and reperfusion. *Cardiovasc. Res.* **85**, 155–166 (2010).

66. Nadtochiy, S. M., Baker, P. R. S., Freeman, B. A. & Brookes, P. S. Mitochondrial nitroalkene formation and mild uncoupling in ischaemic preconditioning: Implications for cardioprotection. *Cardiovasc. Res.* **82**, 333–340 (2009).

67. Baker, P. R. S., Schopfer, F. J., Sweeney, S. & Freeman, B. A. Red cell membrane and plasma linoleic acid nitration products: synthesis, clinical identification, and quantitation. *Proc. Natl. Acad. Sci. U. S. A.* **101**, 11577–82 (2004).

68. Tsikas, D., Zoerner, A. A., Mitschke, A. & Gutzki, F. M. Nitro-fatty acids occur in human plasma in the picomolar range: A targeted nitro-lipidomics GC-MS/MS study. *Lipids* **44**, 855–865 (2009).

69. Schopfer, F. J. *et al.* Detection and quantification of protein adduction by electrophilic fatty acids: mitochondrial generation of fatty acid nitroalkene derivatives. *Free Radic. Biol. Med.* **46**, 1250–1259 (2009).

70. Neves, B. *et al.* Profile of Phosphatidylserine Modifications under Nitroxidative Stress Conditions Using a Liquid Chromatography-Mass Spectrometry Based Approach. *Molecules* **24**, 107 (2018).

71. Batthyany, C. *et al.* Reversible post-translational modification of proteins by nitrated fatty acids *in vivo*. *J. Biol. Chem.* **281**, 20450–20463 (2006).

72. Bonacci, G. *et al.* Gas-phase fragmentation analysis of nitro-fatty acids. *J. Am. Soc. Mass Spectrom.* **22**, 1534–1551 (2011).

73. Fazzari, M. *et al.* Olives and olive oil are sources of electrophilic fatty acid nitroalkenes. *PLoS One* **9**, (2014).

74. Ferreira, A. M. *et al.* Macrophage activation induces formation of the anti-inflammatory lipid cholesteryl-nitrolinoleate. *Biochem. J.* **417**, 223–234 (2009).

75. Lima, É. S., Di Mascio, P., Rubbo, H. & Abdalla, D. S. P. Characterization of linoleic acid nitration in human blood plasma by mass spectrometry. *Biochemistry* **41**, 10717–10722 (2002).

76. Balazy, M. *et al.* Vicinal nitrohydroxyeicosatrienoic acids: vasodilator lipids formed by reaction of nitrogen dioxide with arachidonic acid. *J. Pharmacol. Exp. Ther.* **299**, 611–619 (2001).

77. Schopfer, F. J., Cipollina, C. & Freeman, B. A. Formation and Signaling Actions of Electrophilic Fatty Acids. 5997–6021 (2011).

78. Pulfer, M. & Murphy, R. C. Electrospray mass spectrometry of phospholipids. *Mass Spectrom. Rev.* **22**, 332–364 (2003).

79. Shearer, G. C., Chen, J., Chen, Y. & Harris, W. S. Myocardial infarction does not affect fatty-acid profiles in rats. *Prostaglandins Leukot. Essent. Fat. Acids* **81**, 411–416 (2009).

80. Campos, A. M. *et al.* Lipidomics of Mesenchymal Stromal Cells: Understanding the Adaptation of Phospholipid Profile in Response to Pro-Inflammatory Cytokines. *J. Cell. Physiol.* **231**, 1024–1032 (2016).

81. Sousa, B. *et al.* Alteration in Phospholipidome Profile of Myoblast H9c2 Cell Line in a Model of Myocardium Starvation and Ischemia. *J. Cell. Physiol.* **231**, 2266–2274 (2016).

82. Woodcock, S. R., Bonacci, G., Gelhaus, S. L. & Schopfer, F. J. Nitrated fatty acids: Synthesis and measurement. *Free Radic. Biol. Med.* **59**, 14–26 (2013).

83. Zanoni, G. *et al.* Improved Synthesis of (*E*)-12-Nitrooctadec-12-enoic acid, a Potent PPARγ Activator. Development of a “Buffer-Free” Enzymatic Method for Hydrolysis of Methyl Esters. *J. Org. Chem.* **75**, 8311–8314 (2010).

84. Dunny, E. & Evans, P. Stereocontrolled Synthesis of the PPAR-γ Agonist 10-Nitrolinoleic Acid. *J. Org. Chem.* **75**, 5334–5336 (2010).

85. Gorczynski, M. J., Huang, J. & King, S. B. Regio- and stereospecific syntheses and nitric oxide donor properties of (E)-9- and (E)-10-nitrooctadec-9-enoic acids. *Org. Lett.* **8**, 2305–8 (2006).

86. Woodcock, S. R., Marwitz, A. J. V, Bruno, P. & Branchaud, B. P. Synthesis of nitrolipids. All four possible diastereomers of nitrooleic acids: (E)- and (Z)-, 9- and 10-nitro-octadec-9-enoic acids. *Org. Lett.* **8**, 3931–3934 (2006).

87. Manini, P. *et al.* Chemistry of nitrated lipids: Remarkable instability of 9-nitrolinoleic acid in neutral aqueous medium and a novel nitronitrate ester product by concurrent autoxidation/nitric oxide-release pathways. *J. Org. Chem.* **73**, 7517–7525 (2008).

88. Hayama, T., Tomoda, S., Takeuchi, Y. & Nomura, Y. Synthesis of conjugated nitroalkenes via nitroselenenylation of alkenes. *Tetrahedron Lett.* **23**, 4733–4734 (1982).

89. Blanco, F. *et al.* 6-Methylnitroarachidonate: A novel esterified nitroalkene that potently inhibits platelet aggregation and exerts cGMP-mediated vascular relaxation. *Free Radic. Biol. Med.* **50**, 411–418 (2011).

90. Delmastro-greenwood, M. *et al.* Nitrite and nitrate-dependent generation of anti-in fl ammatory fatty acid nitroalkenes. *Free Radic. Biol. Med.* **89**, 333–341 (2015).

91. Richard L. Alexander, ‡, Darcy J. P. Bates, ‡, Marcus W. Wright, §, S. Bruce King, § and & Charles S. Morrow*, ‡. Modulation of Nitrated Lipid Signaling by Multidrug Resistance Protein 1 (MRP1): Glutathione Conjugation and MRP1-Mediated Efflux Inhibit Nitrolinoleic Acid-Induced, PPARγ-Dependent Transcription Activation†. (2006). doi:10.1021/BI0605639

92. Villacorta, L. *et al.* In situ generation, metabolism and immunomodulatory signaling actions of nitro-conjugated linoleic acid in a murine model of inflammation. *Redox Biol.* **15**, 522–531 (2018).

93. Hansen, A. L. *et al.* Nitro-fatty acids are formed in response to virus infection and are potent inhibitors of STING palmitoylation and signaling. *Proc. Natl. Acad. Sci. U. S. A.* **115**, E7768–E7775 (2018).

94. Mathers, A. R. *et al.* Topical electrophilic nitro-fatty acids potentiate cutaneous inflammation. *Free Radic. Biol. Med.* **115**, 31–42 (2018).

95. Rudolph, V. *et al.* Nitro-fatty acid metabolome: saturation, desaturation, b-oxidation, and protein adduction. *J. Biol. Chem.* **284**, 1461–1473 (2009).

96. Salvatore, S. R. *et al.* Evaluation of 10-Nitro Oleic Acid Bio-Elimination in Rats and Humans. *Sci. Rep.* **7**, 39900 (2017).

97. Mathers, A. R. *et al.* Electrophilic nitro-fatty acids suppress allergic contact dermatitis in mice. **1**, (2016).

98. Iles, K. E. *et al.* Fatty acid transduction of nitric oxide signaling: nitrolinoleic acid mediates protective effects through regulation of the ERK pathway. *Free Radic. Biol. Med.* **46**, 866–875 (2009).

99. Wysocki, V. H., Resing, K. A., Zhang, Q. & Cheng, G. Mass spectrometry of peptides and proteins. *Methods* **35**, 211–222 (2005).

100. Schopfer, F. J. *et al.* Covalent peroxisome proliferator-activated receptor gamma adduction by nitro-fatty acids: Selective ligand activity and anti-diabetic signaling actions. *J. Biol. Chem.* **285**, 12321–12333 (2010).

101. Zhang, J. *et al.* Nitro-oleic acid inhibits angiotensin II-induced hypertension. *Circ. Res.* **107**, 540–548 (2010).

102. Kansanen, E., Jyrkkänen, H. K. & Levonen, A. L. Activation of stress signaling pathways by electrophilic oxidized and nitrated lipids. *Free Radic. Biol. Med.* **52**, 973–982 (2012).

103. Koenitzer, J. R. *et al.* Fatty acid nitroalkenes induce resistance to ischemic cardiac injury by modulating mitochondrial respiration at complex II. *Redox Biol.* **8**, 1–10 (2016).

104. Charles, R. L. *et al.* Protection from hypertension in mice by the Mediterranean diet is mediated by nitro fatty acid inhibition of soluble epoxide hydrolase. *Proc. Natl. Acad. Sci.* **111**, 8167–8172 (2014).

105. González-Perilli, L. *et al.* Nitroarachidonic acid (NO 2 AA) inhibits protein disulfide isomerase (PDI) through reversible covalent adduct formation with critical cysteines. *Biochim. Biophys. Acta - Gen. Subj.* **1861**, 1131–1139 (2017).

106. Zhang, J. *et al.* Nitro-Oleic Acid Inhibits Angiotensin II – Induced Hypertension. 540–548 (2010). doi:10.1161/CIRCRESAHA.110.218404

107. Cui, T. *et al.* Nitrated fatty acids: Endogenous anti-inflammatory signaling mediators. *J. Biol. Chem.* **281**, 35686–35698 (2006).

108. Nadtochiy, S. M. *et al.* Nitroalkenes Confer Acute Cardioprotection via Adenine Nucleotide Translocase 1. *J. Biol. Chem.* **287**, 3573–3580 (2012).

109. Bonacci, G. *et al.* Electrophilic fatty acids regulate matrix metalloproteinase activity and expression. *J. Biol. Chem.* **286**, 16074–16081 (2011).

110. Reddy, A. T. *et al.* Nitrated Fatty Acids Reverse Cigarette Smoke-Induced Alveolar Macrophage Activation and Inhibit Protease Activity via Electrophilic S-Alkylation. *PLoS One* **11**, e0153336 (2016).

111. Charles, R., Freeman, B. & Eaton, P. Nitro-Oleic Acid Inhibits Soluble Epoxide Hydrolase Via Adduction at Cys521 to Provide Cardioprotection Against Ischemia and Reperfusion Injury. *Free Radic. Biol. Med.* **87**, S48 (2015).

112. Taylor-Clark, T. E., Ghatta, S., Bettner, W. & Undem, B. J. Nitrooleic acid, an endogenous product of nitrative stress, activates nociceptive sensory nerves via the direct activation of TRPA1. *Mol. Pharmacol.* **75**, 820–9 (2009).

113. Kansanen, E. *et al.* Electrophilic nitro-fatty acids activate Nrf2 by a Keap1 cysteine 151-independent mechanism. *J. Biol. Chem.* **286**, 14019–14027 (2011).

114. Baker, L. M. S. *et al.* Nitro-fatty acid reaction with glutathione and cysteine: Kinetic analysis of thiol alkylation by a Michael addition reaction. *J. Biol. Chem.* **282**, 31085–31093 (2007).

115. Awwad, K. *et al.* Electrophilic fatty acid species inhibit 5-lipoxygenase and attenuate sepsis-induced pulmonary inflammation. *Antioxid. Redox Signal.* **20**, 2667–80 (2014).

116. Maucher, I. V *et al.* Michael acceptor containing drugs are a novel class of 5-lipoxygenase inhibitor targeting the surface cysteines C416 and C418. *Biochem. Pharmacol.* **125**, 55–74 (2017).

117. Souza, J. M. *et al.* Posttranslational Modification of Human Alpha-Synuclein by Nitro-Oleic Acid. *Free Radic. Biol. Med.* **49**, S158 (2010).

118. Rom, O., Khoo, N. K. H., Chen, Y. E. & Villacorta, L. Inflammatory signaling and metabolic regulation by nitro-fatty acids. *Nitric Oxide* (2018). doi:10.1016/J.NIOX.2018.03.017

119. Schopfer, F. J., Vitturi, D. A., Jorkasky, D. K. & Freeman, B. A. Nitro-fatty acids: New drug candidates for chronic inflammatory and fibrotic diseases. *Nitric Oxide* **79**, 31–37 (2018).

120. Deen, A. J. *et al.* Regulation of stress signaling pathways by nitro-fatty acids. *Nitric Oxide* (2018). doi:10.1016/J.NIOX.2018.03.012

121. Trostchansky, A. & Rubbo, H. Anti-inflammatory signaling actions of electrophilic nitro-arachidonic acid in vascular cells and astrocytes. *Arch. Biochem. Biophys.* 1–7 (2016). doi:10.1016/j.abb.2016.10.003

122. Trostchansky, A., Bonilla, L., González-Perilli, L. & Rubbo, H. Nitro-Fatty Acids: Formation, Redox Signaling, and Therapeutic Potential. *Antioxid. Redox Signal.* **19**, 1257–1265 (2013).

123. Ambrozova, G. *et al.* Nitro-oleic acid modulates classical and regulatory activation of macrophages and their involvement in pro-fibrotic responses. *Free Radic. Biol. Med.* **90**, 252–260 (2016).

124. Reddy, A. T. *et al.* The nitrated fatty acid 10-nitro-oleate attenuates allergic airway disease. *J. Immunol.* **191**, 2053–63 (2013).

125. Wang, H. *et al.* Nitro-oleic acid protects against endotoxin-induced endotoxemia and multiorgan injury in mice. *Am. J. Physiol. Physiol.* **298**, F754–F762 (2010).

126. Liu, H. *et al.* Nitro-oleic acid protects the mouse kidney from ischemia and reperfusion injury. *Am. J. Physiol. Physiol.* **295**, F942–F949 (2008).

127. Hwang, J., Lee, K. E., Lim, J.-Y. & Park, S. I. Nitrated fatty acids prevent TNFα-stimulated inflammatory and atherogenic responses in endothelial cells. *Biochem. Biophys. Res. Commun.* **387**, 633–640 (2009).

128. Coles, B. *et al.* Nitrolinoleate Inhibits Superoxide Generation, Degranulation, and Integrin Expression by Human Neutrophils: Novel antiinflammatory properties of nitric oxide-derived reactive species in vascular cells. *Circ. Res.* **91**, 375–381 (2002).

129. Kelley, E. E. *et al.* Fatty acid nitroalkenes ameliorate glucose intolerance and pulmonary hypertension in high-fat diet-induced obesity. *Cardiovasc. Res.* **101**, 352–63 (2014).

130. Klinke, A. *et al.* Protective Effects of 10-nitro-oleic Acid in a Hypoxia-Induced Murine Model of Pulmonary Hypertension. *Am. J. Respir. Cell Mol. Biol.* **51**, 155–162 (2014).

131. Rudolph, T. K. *et al.* Nitro-fatty acids reduce atherosclerosis in apolipoprotein E-deficient mice. *Arterioscler. Thromb. Vasc. Biol.* **30**, 938–945 (2010).

132. Trostchansky, A. *et al.* Nitroarachidonic acid, a novel peroxidase inhibitor of prostaglandin endoperoxide H synthases 1 and 2. *J. Biol. Chem.* **286**, 12891–900 (2011).

133. Sánchez-calvo, B., Cassina, A., Rios, N. & Peluffo, G. Nitro-Arachidonic Acid Prevents Angiotensin II-Induced Mitochondrial Dysfunction in a Cell Line of Kidney Proximal Tubular Cells. 1–17 (2016). doi:10.1371/journal.pone.0150459

134. González-Perilli, L. *et al.* Nitroarachidonic acid prevents NADPH oxidase assembly and superoxide radical production in activated macrophages. *Free Radic. Biol. Med.* **58**, 126–33 (2013).

135. Khoo, N. K. H., Li, L., Salvatore, S. R., Schopfer, F. J. & Freeman, B. A. Electrophilic fatty acid nitroalkenes regulate Nrf2 and NF-κB signaling:A medicinal chemistry investigation of structure-function relationships. *Sci. Rep.* **8**, 2295 (2018).

136. Woodcock, C.-S. C. *et al.* Nitro-fatty acid inhibition of triple-negative breast cancer cell viability, migration, invasion, and tumor growth. *J. Biol. Chem.* **293**, 1120–1137 (2018).

137. Villacorta, L. *et al.* Electrophilic nitro-fatty acids inhibit vascular inflammation by disrupting LPS-dependent TLR4 signalling in lipid rafts. *Cardiovasc. Res.* **98**, 116–124 (2013).

138. Ichikawa, T. *et al.* Nitroalkenes Suppress Lipopolysaccharide-Induced Signal Transducer and Activator of Transcription Signaling in Macrophages: A Critical Role of Mitogen-Activated Protein Kinase Phosphatase 1. *Endocrinology* **149**, 4086–4094 (2008).

139. Borniquel, S., Jansson, E. Å., Cole, M. P., Freeman, B. A. & Lundberg, J. O. Nitrated oleic acid up-regulates PPARγ and attenuates experimental inflammatory bowel disease. *Free Radic. Biol. Med.* **48**, 499–505 (2010).

140. Schopfer, F. J. *et al.* Nitrolinoleic acid: an endogenous peroxisome proliferator-activated receptor gamma ligand. *Proc. Natl. Acad. Sci. U. S. A.* **102**, 2340–5 (2005).

141. Wright, M. M. *et al.* Human haem oxygenase-1 induction by nitro-linoleic acid is mediated by cAMP, AP-1 and E-box response element interactions. *Biochem. J.* **422**, 353–61 (2009).

142. Kansanen, E. *et al.* Nrf2-dependent and -independent responses to nitro-fatty acids in human endothelial cells: identification of heat shock response as the major pathway activated by nitro-oleic acid. *J. Biol. Chem.* **284**, 33233–41 (2009).

143. Cole, M. P. *et al.* Nitro-fatty acid inhibition of neointima formation after endoluminal vessel injury. *Circ. Res.* **105**, 965–972 (2009).

144. Rudolph, T. K. *et al.* Nitrated fatty acids suppress angiotensin II-mediated fibrotic remodelling and atrial fibrillation. *Cardiovasc. Res.* **109**, 174–184 (2016).

145. Kelley, E. E. *et al.* Nitro-oleic acid, a novel and irreversible inhibitor of xanthine oxidoreductase. *J. Biol. Chem.* **283**, 36176–36184 (2008).

146. Villacorta, L., Gao, Z., Schopfer, F. J., Freeman, B. a & Chen, Y. E. Nitro-fatty acids in cardiovascular regulation and diseases: characteristics and molecular mechanisms. *Front. Biosci. (Landmark Ed.* **21**, 873–89 (2016).

147. Mollenhauer, M., Mehrkens, D. & Rudolph, V. Nitrated fatty acids in cardiovascular diseases. *Nitric Oxide* (2018). doi:10.1016/J.NIOX.2018.03.016

148. Lim, D. G. *et al.* Nitrolinoleate, a nitric oxide-derived mediator of cell function: Synthesis, characterization, and vasomotor activity. *Proc. Natl. Acad. Sci.* **99**, 15941–15946 (2002).

149. Shin, E. *et al.* Nitrooleate Mediates Nitric Oxide Synthase Activation in Endothelial Cells. 457–466 (2014). doi:10.1007/s11745-014-3893-8

150. Coles, B. *et al.* Nitrolinoleate inhibits platelet activation by attenuating calcium mobilization and inducing phosphorylation of vasodilator-stimulated phosphoprotein through elevation of cAMP. *J. Biol. Chem.* **277**, 5832–40 (2002).

151. Khoo, N. K. H. *et al.* Electrophilic nitro-oleic acid reverses obesity-induced hepatic steatosis. *Redox Biol.* **22**, 101132 (2019).

152. Nadtochiy, S. M., Madukwe, J., Hagen, F. K. & Brookes, P. S. Mitochondrially targeted nitro-linoleate : a new tool for the study of cardioprotection. 2091–2098 (2014). doi:10.1111/bph.12405

153. Hoose, P. M. Van, Kelm, N. Q., Piell, K. M. & Cole, M. P. Conjugated linoleic acid and nitrite attenuate mitochondrial dysfunction during myocardial ischemia. *J. Nutr. Biochem.* **34**, 8–16 (2016).

154. Kühn, B. *et al.* Anti-inflammatory nitro-fatty acids suppress tumor growth by triggering mitochondrial dysfunction and activation of the intrinsic apoptotic pathway in colorectal cancer cells. *Biochem. Pharmacol.* **155**, 48–60 (2018).

155. Fu, J. *et al.* Metabolomics profiling of the free and total oxidised lipids in urine by LC-MS / MS : application in patients with rheumatoid arthritis. *Anal. Bioanal. Chem.* 6307–6319 (2016). doi:10.1007/s00216-016-9742-2

156. Rodriguez-Duarte, J. *et al.* Electrophilic nitroalkene-tocopherol derivatives: synthesis, physicochemical characterization and evaluation of anti-inflammatory signaling responses. *Sci. Rep.* **8**, 12784 (2018).

157. Qipshidze-Kelm, N., Piell, K. M., Solinger, J. C. & Cole, M. P. Co-treatment with conjugated linoleic acid and nitrite protects against myocardial infarction. *Redox Biol.* **2**, 1–7 (2013).

158. Menon, M. C., Chuang, P. Y. & He, J. C. Nitro-oleic acid is a novel anti-oxidative therapy for diabetic kidney disease. 1542–1543 (2013). doi:10.1152/ajprenal.00489.2013

CHAPTER 2. Liquid chromatography/tandem mass spectrometry characterization of nitroso, nitrated and nitroxidized cardiolipin products.

The content presented in this section was integrally published as follows:

Montero-Bullon, J.-F., Melo, T., Rosário M Domingues, M. & Domingues, P. Liquid chromatography/tandem mass spectrometry characterization of nitroso, nitrated and nitroxidized cardiolipin products. *Free Radic. Biol. Med.* (2019). doi:10.1016/j.freeradbiomed.2019.05.009

Free Radical Biology and Medicine xxx (xxxx) xxx–xxx

Contents lists available at ScienceDirect

Free Radical Biology and Medicine

journal homepage: www.elsevier.com/locate/freeradbiomed

Liquid chromatography/tandem mass spectrometry characterization of nitroso, nitrated and nitroxidized cardiolipin products

Javier-Fernando Montero-Bullon[a], Tânia Melo[a,b], M. Rosário M Domingues[a,b], Pedro Domingues[a,*]

[a] Centro de Espectrometria de Massa, Departamento de Química & QOPNA, Universidade de Aveiro, Campus Universitário de Santiago, 3810-193 Aveiro, Portugal
[b] Departamento de Química & CESAM, Universidade de Aveiro, Campus Universitário de Santiago, 3810-193 Aveiro, Portugal

ARTICLE INFO

Keywords:
Phospholipids
Cardiolipin
Nitroxidative stress
Nitroso
Nitration
Nitroxidized
LC/MS

ABSTRACT

Cardiolipins (CL) are anionic dimeric phospholipids bearing four fatty acids, found in inner mitochondrial membrane as structural components and are involved in several processes as oxidative phosphorylation or apoptotic signalling. As other phospholipids, CL can be modified by reactive oxygen species (ROS) and reactive nitrogen species (RNS), which can modulate various cellular functions. Modifications of CL by RNS remain largely unstudied although other nitrated lipids are emerging as bioactive molecules. In this work, we developed a C30-LC-HRMS/MS methodology to identify the nitrated and nitroxidized tetralinoleoyl-cardiolipin (TLCL), using a biomimetic model of nitration, and to disclose specific fragmentation pathways under HCD MS/MS. Using this lipidomics approach, we were able to separate and identify nitro, nitroso, nitronitroso, and nitroxidized TLCL derivatives, comprising 11 different nitrated compounds. These products were identified using accurate mass measurements and the fragmentation pattern acquired in higher-energy collision dissociation (HCD)-tandem MS/MS experiments. These spectra showed classifying fragmentation pathways, yielding phosphatidic acid (PA^-), lysophosphatidic acid (LPA^-), and carboxylate fragment ions with the modifying moiety. Remarkably, the typical neutral losses associated with the added moieties were not observed. In conclusion, this work has developed a new method for the identification of nitroso, nitrated and nitroxidized cardiolipin products by using a C30LC-MS platform method, potentially allowing their detection in biological samples.

1. Introduction

Cardiolipins (CL) are phospholipids that in mammals are found exclusively in mitochondria, more predominantly in the internal membrane, where they are involved in critical biological processes as energy production through electron transport chain and oxidative phosphorylation [1], or in apoptosis [2]. The average abundance of CLs in the total cellular lipid content is minor, but depending on cell type and tissues, it can achieve a percentage up to 24% of total phospholipids of the mitochondrial membrane [3,4]. In high energy-demand tissues with large numbers of mitochondria, like the brain, liver or muscle, and the cardiac muscle, an increased amount of CL is observed, in the range of nanomolar per mg of protein [5]. Structurally, CLs are dimeric anionic glycerophospholipids with two phosphate groups and three glycerol moieties, allowing the presence of four fatty acids. *In vivo*, the combinations of fatty acids are limited, with a high predominance of chains of 18 carbons with one or two unsaturations (C18:1 and C18:2), and, in less proportion, chains of 16 carbons [5] and, especially in the brain, poly-unsaturated chains of C20:4 and C22:6 [6]. Due to the presence of unsaturated fatty acids, CLs are prone to chemical modification by radicals like reactive oxygen species (ROS) and reactive nitrogen species (RNS), similarly to other phospholipids [7].

Oxidized phospholipids formed by ROS are well-known, showing altered functionality and were linked to pathophysiological conditions [8–10]. Chemical oxidation of CLs is also well-studied [6,11–15]. Long-chain oxidation products of CL have been characterized by LC-MS [12,14,15], as well as short-chain products [16]. Oxidized CLs have been detected *in vivo* and *in vitro* and correlated with important biological processes. They have been detected in endothelial cells and *in vitro* in cultures of neuronal cells under stress and apoptotic stimuli [12], in lymphoblast's treated with rotenone [17], in lung tissue of mice under hyperoxia [12], acute injury [18] or gamma radiation-induced injury [19], in intestinal tissue of mice under gamma radiation [20], in kidney tissue of rats under nephrotoxic conditions [16], and in brain of rats under chronic stress-induced depression [21]. Nowadays, CL oxidation

* Corresponding author. Department of Chemistry, Campus Universitário Santiago, 3810-193 Aveiro, Portugal.
E-mail address: p.domingues@ua.pt (P. Domingues).

https://doi.org/10.1016/j.freeradbiomed.2019.05.009
Received 1 March 2019; Received in revised form 26 April 2019; Accepted 7 May 2019

is considered an important mechanism participating in processes such as apoptosis [6] and with implications in diseases as neurodegeneration, myocardial ischaemia, diabetes, or ageing [13]. Notwithstanding, the modification on CLs by RNS remains unexplored.

It is well-known that RNS can be highly expressed in associated with inflammation, cardiovascular homeostasis, and digestion [22], exerting nitroxidative stress that chemically modifies biomolecules. Nitration of proteins is widely recognized as a marker of cellular dysfunction, usually evaluated by the increase of tyrosine nitration and S-nitrosylation [23,24]. Regarding lipids, the susceptibility of fatty acids and their esterified forms to be modified by RNS has been recently explored. The natural occurrence of nitrated fatty acids is well established, and their biological implications have been addressed [25], evidencing a resolving role in different pathologies as cardiovascular disease [26] and diabetes [27,28]. Indeed, most of the studies in lipid nitroxidation have focused on nitro-fatty acids establishing their role as anti-inflammatory and antioxidant agents [29], antagonizing the effects of oxidation products. The possibility of other nitroxidative changes as the addition of nitroso group or combination with several oxidative moieties has also been observed *in vitro* and *in vivo* [30]. More recently, some of these modifications have also been characterized in phospholipids, namely PEs, PCs and PSs *in vitro* [28,31,32] and *in vivo* [28]. The possible physiological role of nitroxidized phospholipids has just started to be unravelled, indicating that they had antioxidant and anti-inflammatory properties [33]. However, cardiolipins, an important phospholipid class, and their nitroxidation products have not been studied. CLs are a likely target of RNS given that RNS interact with mitochondria and regulate its function [34], and therefore may diffuse in the proximity of mitochondrial membrane promoting CL nitroxidation.

Knowledge of modified fatty acids and phospholipids have been facilitated by previous detailed structural characterization by mass spectrometry (MS). Mass spectrometry is a powerful technique, especially when coupled to liquid chromatography, for molecular characterization of complex samples containing molecules as oxidized phospholipids [7], nitroxidized fatty acids [35] and phospholipids [28,31]. *In vitro* assays allow the biomimetic generation of these species and their characterization, making possible further detection in complex matrixes, particularly *in vivo*. The aim of this work was to apply LC-MS strategies to identify and characterize *in vitro* products of CLs nitroxidation. We produced nitrated and nitroxidized CL molecular species using a biomimetic protocol of lipid nitration. LC-MS analysis of the products was performed using a C30 reversed-phase column, providing a new method and list of modified CLs that may help to detect and study their functions *in vivo*.

2. Experimental

2.1. Materials

3′-Bis[1,2-Di-(9Z-12Z-octadecadienoyl)-*sn*-glycero-3-phospho]-*sn*-glycerol or tetralinoleoyl cardiolipin (TLCL) was bought from Avanti® Polar Lipids, Inc. (Alabaster, USA) and used without further purification. Nitronium tetrafluoroborate (NO_2BF_4) was purchased from Sigma-Aldrich (Madrid, Spain). Ammonium molybdate ($NaMoO_4{\cdot}4H_2O$) and sodium phosphate monobasic dihydrate ($NaH_2PO_4{\cdot}2H_2O$) were purchased from Riedel-de Haën (Seelze, Germany) and ascorbic acid from VWR International (Leicestershire, UK) HPLC grade chloroform, methanol, isopropanol, formic acid and ammonium acetate were purchased from Fisher Scientific Ltd. (Leicestershire, U.K.). Milli-Q water was used for all experiments, filtered through a 0.22 µm filter and obtained using a Milli-Q Millipore system (Synergy®, Millipore Corporation, Billerica, MA, USA).

2.2. In vitro nitroxidation

Cardiolipin (TLCL) nitration (1 mg) was carried out with an excess of nitronium tetrafluoroborate (approximately 5 mg) in chloroform (1 mL) at room temperature for 1 h, under orbital shaking at 750 rpm. Nitration was quenched with water (2 mL), vortexing for 30 s and centrifuged for 5 min at 1000 rpm in a Mixtasel Centrifuge (Selecta, Barcelona, Spain). The water phase containing products from the hydrolysis of the excess of NO_2BF_4 and salts, in general, was discarded, while the lower organic phase containing the cardiolipin was dried under a nitrogen stream and stored at −20 °C to be further quantified using phosphorus assay and analysed by C30-HPLC-ESI-MS and MS/MS.

2.3. Phospholipid quantification

The total amount of non-modified and modified CL recovered after reaction and extraction were quantified using colourimetric phosphorus assay as previously described by Bartlett and Lewis [36]. Briefly, 125 µL of concentrated perchloric acid (70% w/v), $HClO_4$, were added to 10 µL of 25 µg of dried lipid extract. Samples were then incubated for 1 h at 180 °C in the heating block (Stuart, UK). Afterwards, 0.825 mL of H_2O, 0.125 mL of 2.5% ammonium molybdate (m/v: 2.5 g of $NaMoO_4{\cdot}4H_2O$ in 100 mL of H_2O) and 10% ascorbic acid (m/v; 0.1 g in 1 mL H_2O) were added to all samples. The reaction mixture was homogenized in a vortex mixer and incubated for 10 min at 100 °C in a water bath. Then, the reaction mixture was quickly cooled down to stop the reaction. Standards with 0.1–2 µg of phosphorus (in the form of $NaH_2PO_4{\cdot}2H_2O$ salt) were simultaneously treated. Finally, the absorbance of standards and samples was measured at 797 nm in a Multiskan GO Microplate Spectrophotometer (Thermo Fisher Scientific, Waltham, MA, USA). The amount of phosphorus present in each sample was calculated by linear interpolation, based on the calibration curve of the response of absorbance versus phosphorus present in the standards. The mass of phospholipid was calculated by considering the ratio between the molecular mass of the phosphorus detected and molecular mass of tetralinoleoyl cardiolipin.

2.4. C30-ESI-LC-HRMS and MS/MS analysis

Sample separation was performed using an Accucore C30 column (150 mm*2.1 mm,2.6 µm, 150 Å, Thermo Fisher Scientific) with an UltiMate U3000RS system, coupled to a high resolution (HR) Orbitrap Q-Exactive mass spectrometer (Thermo Fisher Scientific). The column was run with a flow rate of 300 µL/min and a column temperature set to 40 °C. For each run, 10 µL of a sample containing 5 µg of nitroxidized cardiolipin in methanol was injected. The gradient used was 25% B for 2 min, 25–86% B in 18 min, 86–95% B in 1 min, 95% B for 14 min. The solvents used were acetonitrile/water/formic acid (95/5/0.1; v/v/v), 5 mM ammonium acetate (A) and isopropanol/acetonitrile/water/formic acid (85/10/5/0.1; v/v/v/v), 5 mM ammonium acetate (B).

The mass spectrometer was operated in negative ion mode (electrospray voltage 2.7 kV; capillary temperature, 350 °C; sheath gas flow 45 units, auxiliary gas flow 15 units) acquiring a survey mass spectrum with resolving power 70,000 (full width half maximum), m/z = 1395–1750 using an automatic gain control (AGC) target of $10E^6$ and a maximum injection time of 100 ms. The 5 most intense ions were selected for higher-energy collisional dissociation (HCD) fragmentation (20, 23, and 25% normalized collision energy) and MS/MS spectra were generated with an AGC target of $10E^5$ and a maximum injection time of 200 ms at a resolution of 17,500. The mass spectrometer worked in data-dependent mode, with an inclusion list containing an m/z list of possible nitroxidative modifications and dynamic exclusion of 30 s.

After analysing this data, a second MS/MS method was run using data-independent acquisition (DIA), for acquiring better quality MS/MS spectra and attempting to identify isomers. For these experiments, a list of the identified nitroxidative products and the respective RT was

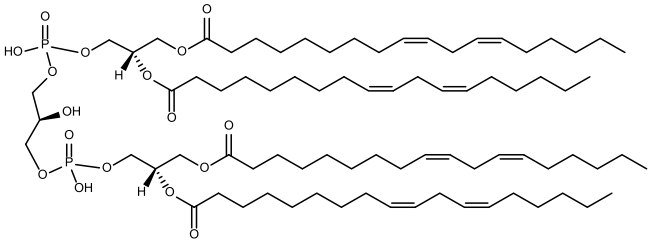

Fig. 1. Structure of tetralinoleoyl-cardiolipin (TLCL).

created. The method surveyed these ranges of *m/z* using a 1 *m/z* quadrupole isolation windows and multiplexing at the maximum 4 of these windows. Maximum injection times were of 300 ms, AGC values were set to 2x10e5 for MS/MS scans. Data acquisition was carried out using the Xcalibur data system (V3.3, Thermo Fisher Scientific, Waltham, MA, USA).

3. Results

In this study, we analysed the *in vitro* nitration tetralinoleoyl-cardiolipin (TLCL) products (Fig. 1) using an C30-LC-HRMS platform. These products, generated by using a biomimetic protocol of lipid nitration using NO_2BF_4, were observed in the negative ion mode, as mono-charged deprotonated molecular ions $[M\text{-}H]^-$. Initial structural identification and annotation of the nitration reaction products were based on accurate mass (< 5 ppm) to provide possible products containing nitro and nitroso moieties and enabled the assignment of several products (Table 1). These ions were assigned as nitroso-TLCL derivatives (NO-TLCL, $(NO)_2$-TLCL, $(NO)_3$-TLCL and $(NO)_4$-TLCL) and nitro-TLCL derivatives (NO_2-TLCL and $(NO_2)_2$-TLCL). We have also assigned a nitronitroso product, with both NO with NO_2 groups $(NO_2)(NO)$-TLCL, and few nitroxidized CL derivatives namely hydroxy or hydroperoxy TLCL with a nitroso group (NO + O-TLCL, $(NO)_2 + 2O$-TLCL) and a nitronitroso derivative ($(NO_2)(NO) + O$-TLCL. Weak signals attributed to the well-known oxidized derivatives, namely keto, hydroxy and hydroperoxy derivatives, were also observed, but not studied because they were out of the scope of this work (data not shown).

For each of the assigned ions, we plotted a reconstructed ion chromatogram (RIC) and, to confirm its identification (Fig. 2), we analysed the HCD MS/MS spectra acquired for each RT of the peaks (also annotated in Table 1), using the conditions previously described. Overall, species with more modifications eluted at shorter retention times, as expected for the LC conditions used. In the following text, we will describe the results obtained for each of the ions presented in Table 1. By using LC-MS/MS data, we will explore the possibility of the presence of positional isomers and of structural isomers. For example,

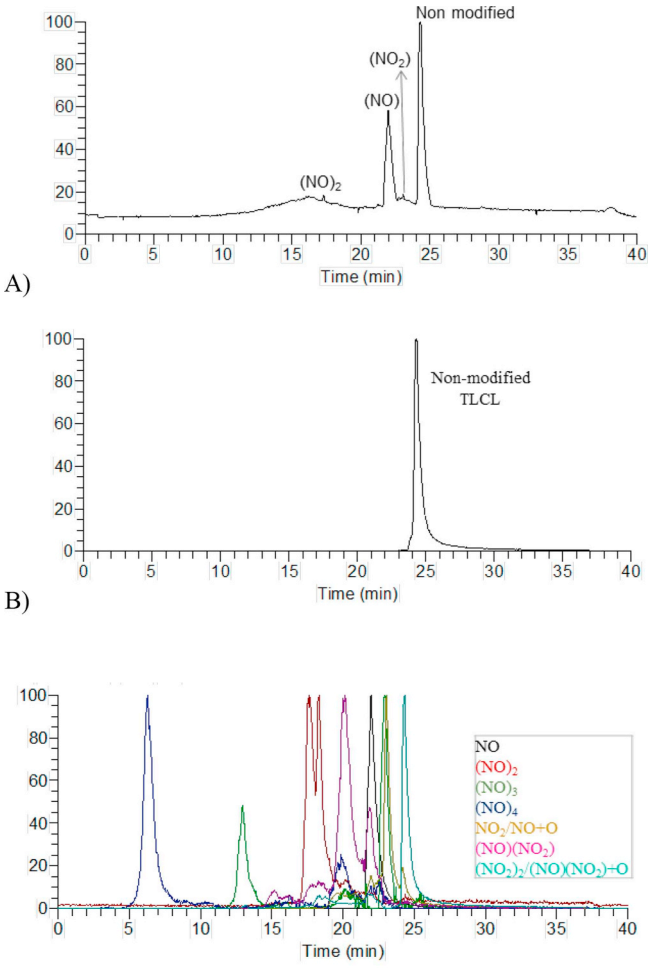

Fig. 2. Total ion chromatogram (TIC) obtained after nitroxidation of TLCL (A), reconstructed ion chromatogram (RIC) of non modified TLCL (B) and RIC of the nitroso and nitrated derivatives (C) observed by C30 RP LC-HR-MS as $[M\text{-}H]^-$ ions and identified by accurate mass measurement and MS/MS fragmentation pattern, shown in Table 1.

the compounds NO + O-TLCL and NO_2-TLCL are structural isomers and thus indistinguishable by exact mass measurements but can be separated using chromatography.

In Fig. 3A, we show the RIC of the species annotated as NO-TLCL, $[M\text{-}H]^-$, at *m/z* 1476.95, corresponding to a mass shift of 29Da (NO)

Table 1
Nitrated and nitroso products of tetralinoleoyl-cardiolipin (TLCL) formed by treatment with NO_2BF_4, identified by C30 RP LC-HR-MS as $[M\text{-}H]^-$ ions and confirmed by accurate mass measurements and MS/MS data analysis. The relative abundance RA (%) of the various nitrated species was determined by integrating the peak area for each species.

m/z theoretical	*m/z* observed	Error (ppm)	Shift (Da)	Modification	RT (min)	RA(%)
1447.9644	1447.9686	2.9	0	–	24.2	–
1476.9546	1476.9595	3.3	29	NO	21.9	60.9
1505.9447	1505.9497	3.3	58	$(NO)_2$	17.5	4.1
1505.9447	1505.9501	3.6	58	$(NO)_2$	18.3	3.8
1534.9349	1534.9396	3.1	87	$(NO)_3$	12.9	1.3
1563.9251	1563.9279	1.8	116	$(NO)_4$	6.2	2.9
1492.9495	1492.9542	3.2	45	NO_2	23.0	11.9
1492.9495	1492.9539	3.0	45	NO_2	21.8	2.6
1492.9495	1492.9518	1.6	45	NO + O	19.6	2.4
1521.9396	1521.9447	3.4	74	$(NO)(NO_2)$	21.9	1.7
1521.9396	1521.9446	3.3	74	$(NO)(NO_2)$	20.2	5.4
1537.9346	1537.9376	2.0	90	$(NO_2)_2$	21.3	1.3
1537.9346	1537.9373	1.8	90	$(NO)(NO_2) + O$	18.3	1.5

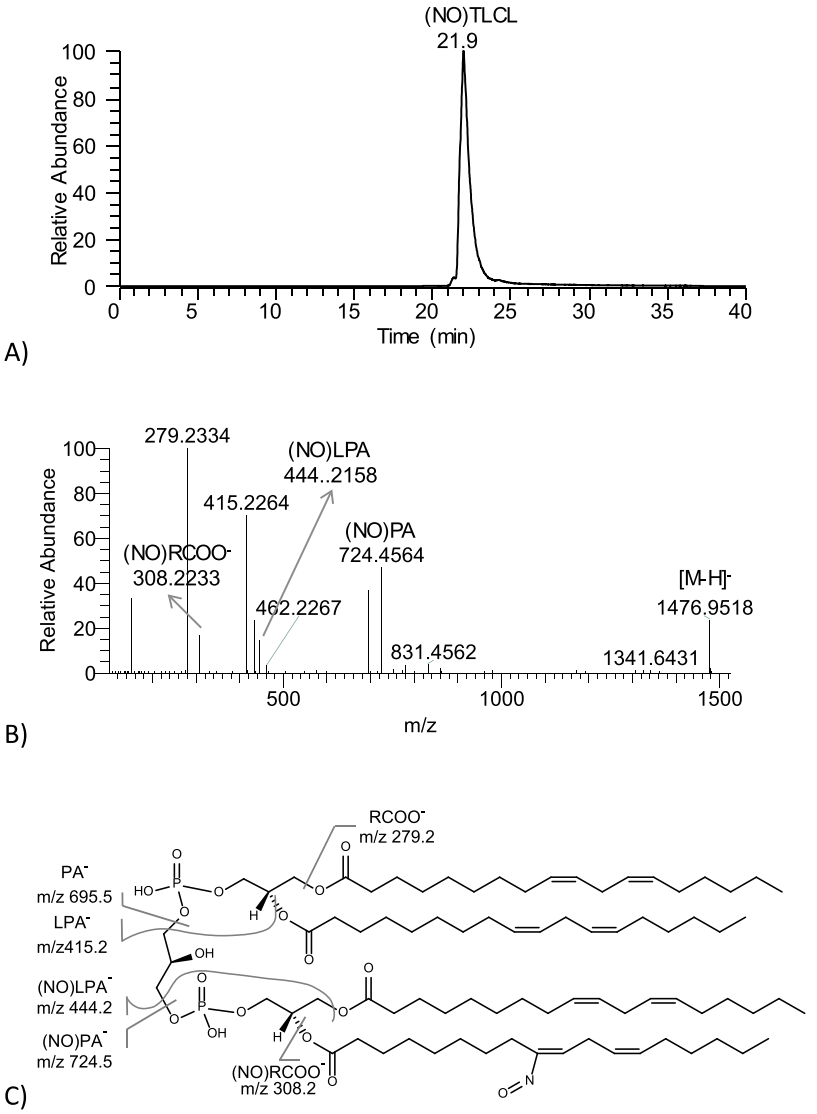

Fig. 3. A) Reconstructed ion chromatogram for species with a mass shift of +29Da. B) Correspondent HCD MS/MS spectrum of the species, acquired at RT 21.9 min. C) and its main fragmentation pathways.

from the native TLCL. The observation of the RIC suggests the presence of only one isomer, although the NO modification could be present in each of the double bonds of the four linoleyl fatty acyl chains. The MS/MS spectra acquired at RT 21.9 min (Fig. 3B), validated this identification. In fact, the presence of the diagnostic fragment ions of nitroso phosphatidic acid $(NO)PA^-$ at *m/z* 724.46, the carboxylate anion of the nitroso fatty acid $(NO)RCOO^-$ at *m/z* 308.22, and nitroso lysophosphatidic acid $(NO)LPA^-$ at *m/z* 444.22, allows identifying this species (Fig. 3C). However, the neutral loss of HNO was not observed in this analysis, as reported in previous work using an ion trap instrument for nitroso PC and PE [31]. The MS/MS spectra do not give information allowing to assign the position in the fatty acid were NO group in linked. Thus, the structure present in Fig. 2C is one possibility since nitration of linoleic FA can occur in C (9,10,12 or 13).

Fig. 4A shows the RIC at *m/z* 1505.94, corresponding to a mass shift of 58Da from the native TLCL. These species were annotated in Table 1 as $(NO)_2$-TLCL. The RIC suggest that we are in the presence of two main isomers with RT of 17.5 min and 18.4 min. The MS/MS spectra acquired at RT 17.5 min show the fragment ions identified as nitroso phosphatidic acid fragments $(NO)PA^-$ at *m/z* 724.46, nitroso fatty acid $(NO)RCOO^-$ at *m/z* 308.22, and the nitroso lysophosphatidic acid $(NO)LPA^-$ at *m/z* 444.22 (Fig. 4B). These fragment ions suggest the presence of a dinitroso TLCL derivative, with each nitroso group present in different fatty acids and in a different glycerodiacyl monomer of the cardiolipin. The MS/MS of the species eluting latter, at RT 18.3 (Fig. 4C), show the fragment ion $(NO)_2PA^-$ at *m/z* 753.45 and the fragment ions $(NO)LPA^-$ at *m/z* 444.22 and $(NO)RCOO^-$ at *m/z* 308.22, indicating that, in this isomer, the two nitroso groups were in the same monomer of the cardiolipin, but not in the same linoleyl group. This identification also suggests that the modifications in the same monomer make the nitroso cardiolipin more apolar than when the same modifications occur in different monomers.

In Fig. 5A, we show the RIC of the species at *m/z* 1534.92, with a mass shift of 87Da from the native TLCL, corresponding to the addition of three nitroso groups, and annotated in Table 1 as $[M-H]^-$ of the $(NO)_3$-TLCL species. The observation of the RIC suggests the presence of, at least, one abundant isomer that eluted at RT 12.9 min. The MS/MS spectra acquired at RT 12.9 min, shows the presence of the fragment ions $(NO)PA^-$ at *m/z* 724.46 and $(NO)_2PA^-$ at *m/z* 753.45 that validates the interpretation that the isomers bear two NO groups in one monomer and a third one in the other monomer. Each NO group seems to be in different fatty acyl chain as indicated by the presence of $(NO)LPA^-$ at *m/z* 444.22 and $(NO)RCOO^-$ at *m/z* 308.22, and due to the absence of the fragments of $(NO)_2LPA^-$ nor $(NO)_2RCOO^-$. The peak

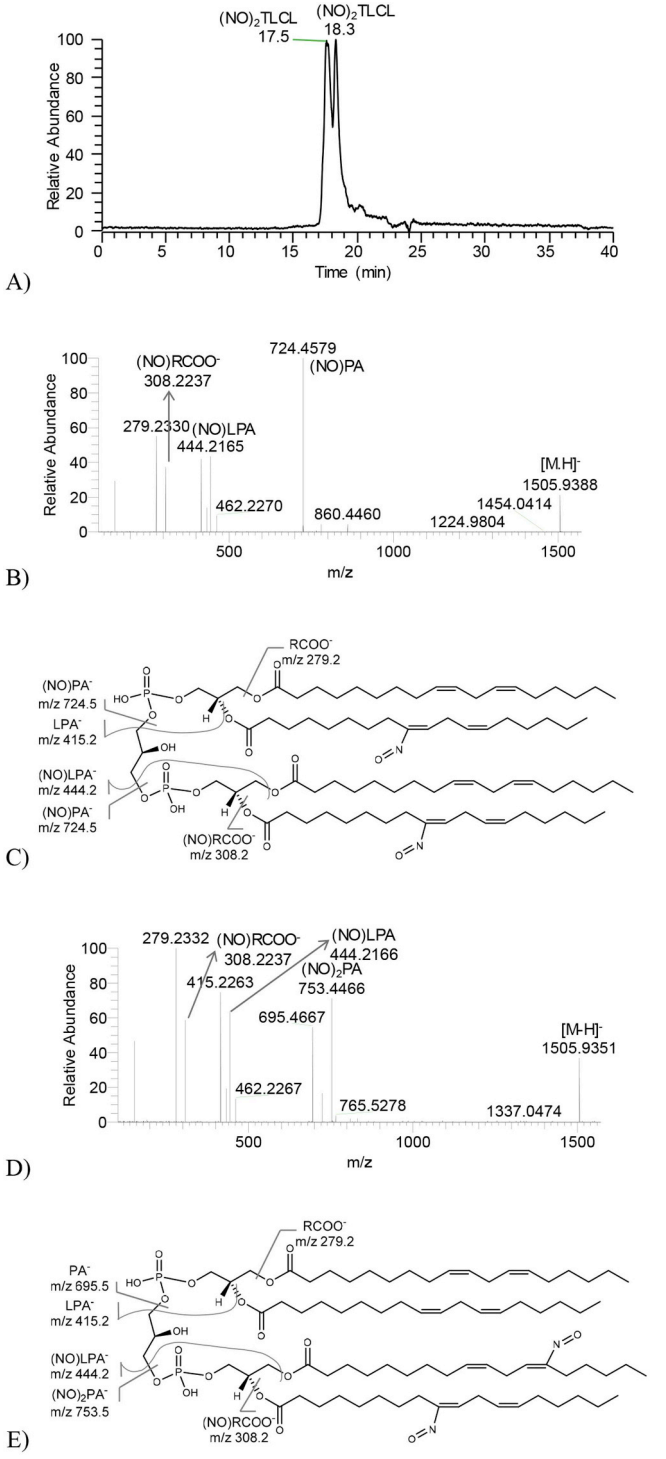

Fig. 4. A) Reconstructed ion chromatogram for nitroso species $(NO)_2$-TLCL. MS/MS spectra of the ion at *m/z* 1505.94 acquired at B) RT 17.5 min with C) its fragmentation pathways and D) RT 18.3 min with E) its fragmentation pathways.

observed at RT 23.2 corresponded to an unrelated contaminant at *m/z* 1534.94.

In Fig. 6A, we show the RIC of the species at *m/z* 1563.93, with a mass shift of 116Da, corresponding to the addition of four nitroso groups to TLCL, and annotated as the molecular ion $[M\text{-}H]^-$ of $(NO)_4$-TLCL, in Table 1. The observation of the RIC suggests the presence of one isomer. The MS/MS spectra acquired at RT 6.2 min shows the presence of fragment ions identified as $(NO)PA^-$ at *m/z* 308.22 and

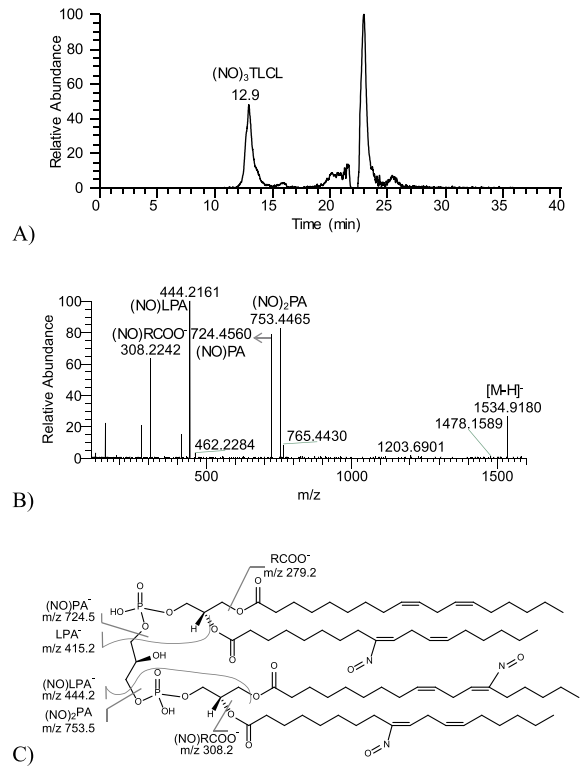

Fig. 5. A) Reconstructed ion chromatogram for nitroso species $(NO)_3$-TLCL. B) MS/MS spectrum of the ion at *m/z* 1534.92 acquired at RT 12.9 min with C) its fragmentation pathways.

$(NO)LPA^-$ at *m/z* 444.22 and $(NO)_2PA^-$ at *m/z* 753.45 (Fig. 6B). This fragmentation pattern is consistent with the presence of one compound with four NO-modified linoleyl fatty acyl chains, thus with each NO group linked to each linoleic acid.

Fig. 7A shows the RIC of the *m/z* 1492.93, corresponding to a mass shift of 45Da from the native TLCL. These species were annotated in Table 1 as NO_2-TLCL$^-$ and (NO) + (OH)-TLCL$^-$. The RIC shows an abundant species eluting at RT 23.0 min and several other minor species eluting before (RT 19.6 min; RT 21.8 min) and after (RT 24.4 min). The MS/MS spectrum acquired at RT 23.0 min (Fig. 7B) shows the fragment ions $(NO_2)PA^-$ at *m/z* 740.45, lysophosphatidic acid $(NO_2)LPA^-$ at *m/z* 460.21, and fatty acid carboxylate anions $(NO_2)RCOO^-$ at *m/z* 324.22. This suggests that this species corresponds to nitrated derivative, NO_2-TLCL. The presence of NO(OH)CL derivative isobaric of NO2CL, could not be excluded, although if it occurs, it is expected to be in lower abundance. The informative neutral loss of HNO_2 or HNO was not observed in this HCD MS/MS spectrum, as it has been previously reported in the CID-MS/MS of other nitrated phospholipids [28,31], thus inducing some uncertainty in the assignments.

Fig. 7C shows the MS/MS spectrum of the ion at *m/z* 1492.93, acquired at RT 19.6 min. This spectrum shows the fragment ions identified as $(NO)PA^-$ at *m/z* 724.46 and $(PA + O)^-$ at *m/z* 711.46, $(NO)LPA^-$ at *m/z* 444.22 and $(LPA + O)^-$ at *m/z* 431.22, and $(NO)RCOO^-$ at *m/z* 308.22 and $(RCOO + O)^-$ at *m/z* 295.23. Altogether, this information strongly suggests that this compound is the $(NO + O\text{-TLCL})^-$ isomer, thus a nitroso hydroxy derivative. Also, these fragment ions suggest that the two groups (nitroso, NO and hydroxy, OH) are present in different fatty acyl chains.

The MS/MS spectra acquired at RT 21.8 min (Fig. 7D) is similar to the one described in Fig. 7B, corresponding to NO_2-TLCL. This most probably can be an indication that we are in the presence of an isomeric species, with the nitro group, NO_2, located in a different position of the fatty acyl chain or in other fatty acid in the TLCL, although the MS/MS

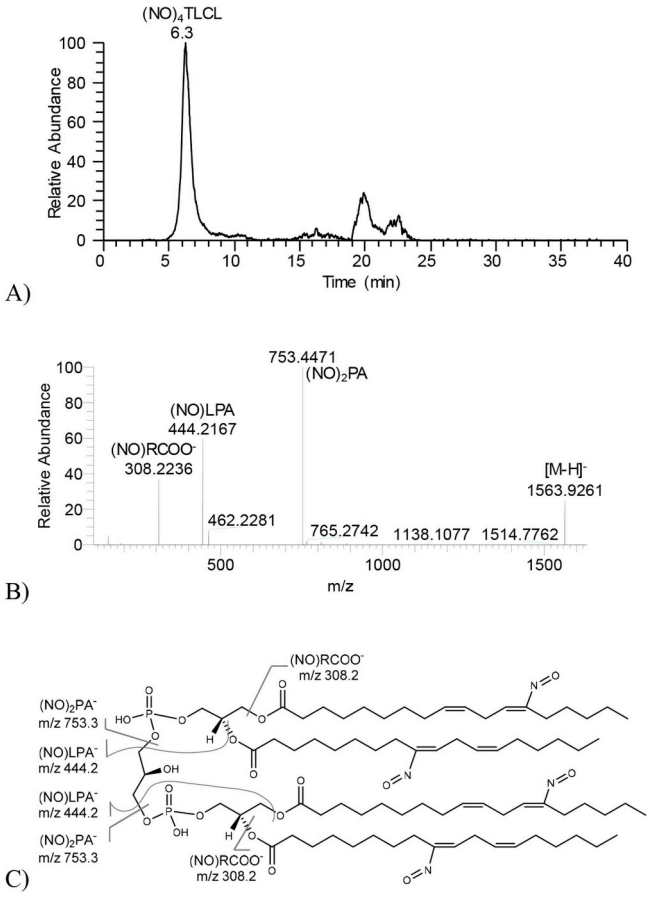

Fig. 6. A) Reconstructed ion chromatogram for nitroso species $(NO)_4$-TLCL. B) MS/MS spectrum of the ion at *m/z* 1563.93 acquired at RT 6.2 min with C) its fragmentation pathways.

spectra provide no evidence of the exact location of the modification. The MS/MS acquired at RT 24.4 min (Fig. 7E) does not allow a positive confirmation of the species eluting at this RT.

Fig. 8A shows the RIC of the ion at *m/z* 1521.93, corresponding to a mass shift of 74Da from the native TLCL. These species were annotated in Table 1 as (NO + NO_2-TLCL)$^-$. The RIC shows two major peaks at RT 20.2 min and 21.9 min. The MS/MS spectrum acquired at RT 20.2min (Fig. 8B) shows the fragment ions $(NO)PA^-$ at *m/z* 724.45 and $(NO_2)PA^-$ at *m/z* 740.45 indicating that both modifications co-exist and are present in different fatty acyl chains. The MS/MS spectrum acquired at RT 21.9min (Fig. 7C) does not allow a positive confirmation of the species eluting at this RT. Nevertheless, the presence of the fragment ion at *m/z* 308.22 identified as (NO)RCOO$^-$also suggest the presence of a (NO + NO_2-TLCL)$^-$, although this fragment ion can also be present due to carryover.

Fig. 9A shows the RIC of the *m/z* 1537.93, corresponding to a mass shift of 90Da from the native TLCL. These species were annotated in Table 1 as $((NO_2)_2$-TLCL)$^-$ and ((NO)(NO_2) + O-TLCL)$^-$, eluting at RT 21.3 and 18.3, respectively. The MS/MS spectrum acquired at RT 21.3min (Fig. 9B) shows the fragment ion $(NO_2)PA^-$ at *m/z* 740.45. The absence of a fragment ion corresponding to $(NO_2)_2PA^-$ suggest that each of the NO_2 group is located in different monomers. The MS/MS spectrum acquired at RT 18.3min (Fig. 9C) shows the fragment ions $(NO)PA^-$ at *m/z* 724.46 and $(NO)LPA^-$ at *m/z* 444.21, suggesting that this is a nitroso nitro cardiolipin. Although no fragment ion evidencing the presence of a NO_2 group was observed, the exact mass measurements and the retention time suggest that this is ((NO)(NO_2) + O-TLCL)$^-$. The MS/MS spectrum acquired at RT 24.3min (Fig. 9D) does not allow performing a positive identification of this species, corresponding to an unrelated contaminant, probably arising from the nitration reaction.

4. Discussion

Cardiolipins are structurally a unique phospholipid group, consisting of a dimeric structure, that forms clusters in cell membranes, stabilizing the geometry of curved regions of the membrane [37]. Due to its characteristic structure, cardiolipins form a very large group of diverse molecules, since they include a different combination of fatty acyl chains, in its tetrameric structure, and also with large pools of structural isomers. Recently, using a C8 RP column, G. Oemer et al. separated 135 cardiolipins with different masses and referred to the presence of several isobaric CL with limited different retention times [4]. For several years we have been working to characterize biologically-relevant modified phospholipids, mainly by oxidative stress, including the identification of oxidized cardiolipin (OxCL) that allowed to identify and characterize by MS-based approaches different structural and isomeric OxCL [10,14,16]. Lately, we have published a series of papers identifying phospholipid nitroxidation using LC-MS approaches, through Hydrophilic Interaction Liquid Chromatography-Mass Spectrometry (HILIC-ESI-MS) [28], and reversed phase C5 LC-MS [31]. In these papers, we focused on the identification of nitroalkenes derivatives of phosphatidylcholines, phosphatidylethanolamines, and phosphatidylserines. These LC/MS approaches suffer from a lack of resolution and the ability to separate isomers. The present study extends our previous structural identification platform, by utilizing a C30-ESI-LC-MS and HCD MS/MS analysis to identify nitrated cardiolipins.

The use, for the first time of this platform for the identification of nitrated cardiolipin, has allowed us to separate and identify several isomers of nitroso-TLCL, nitro-TLCL, nitronitroso-TLCL and nitroxidized CL derivatives. In this C30 column TLCL elutes with an RT of 22.3 min, and as expected, nitrated compounds, because they are more polar, elute with a shorter RT. Also, the nitroso compound has shorter retention times than the corresponding nitro derivative. For example, the NO-TLCL has an RT of 21.9 min while the NO_2-TLCL has a retention time of 23.1 min. Remarkably, this platform also allowed to separate positional isomers with good resolution. For example, two different isomers of dinitroso TLCL, $(NO)_2$-TLCL isomers were separated, with an RT difference of 48 s and identified (Fig. 3A). As previously described, the MS/MS data allowed to suggest that one of the isomers had the modification on different monomers of the molecule, while the other had the two nitroso groups in the same monomer of the cardiolipin, but in the different linoleyl group. This data that was further corroborated by other isomers described in this study, suggesting that in linoleyl fatty acids, nitration does not co-occur in the same fatty acid.

By using the platform described in this study, we were also able to resolve and identify several isomeric structures. For example, for the ion at *m/z* 1537.93, corresponding to a mass shift of 90Da from the native TLCL, we were able to identify 3 structures, $((NO_2)_2$-TLCL)$^-$, ((NO)(NO_2) + O-TLCL)$^-$ and $((NO)_2$ + 2O-TLCL)$^-$, with considerable differences in the retention times (RT 21.3, 18.3 and 13.7, respectively) (Fig. 8A).

The results of this study clearly show that under biomimetic lipid nitration using NO_2BF_4, a wide variety of nitrated structures are formed. Altogether, we have separated and identified in this study 11 different nitrated compounds comprising 7 different mass shifts. Thus, considering the different possible combination of FA in CL in biological samples, the possibility of different nitrated cardiolipins in biological samples increase exponentially, making difficult its detection and identification. To this end, our results show that it is vital to use a high-sensibility, high-resolution instrument, together with good chromatographic selectivity, able to separate isomeric and close related isomeric nitrated cardiolipins.

In this work, we have used higher-energy collision dissociation, HCD-MS/MS spectra to identify the nitrated cardiolipin compounds. These spectra showed the main patterns previously observed in CL [14–16,38]. The main, most informative fragmentation pathways included the cleavage to phosphatidic acid monomers (PA^-) fragment

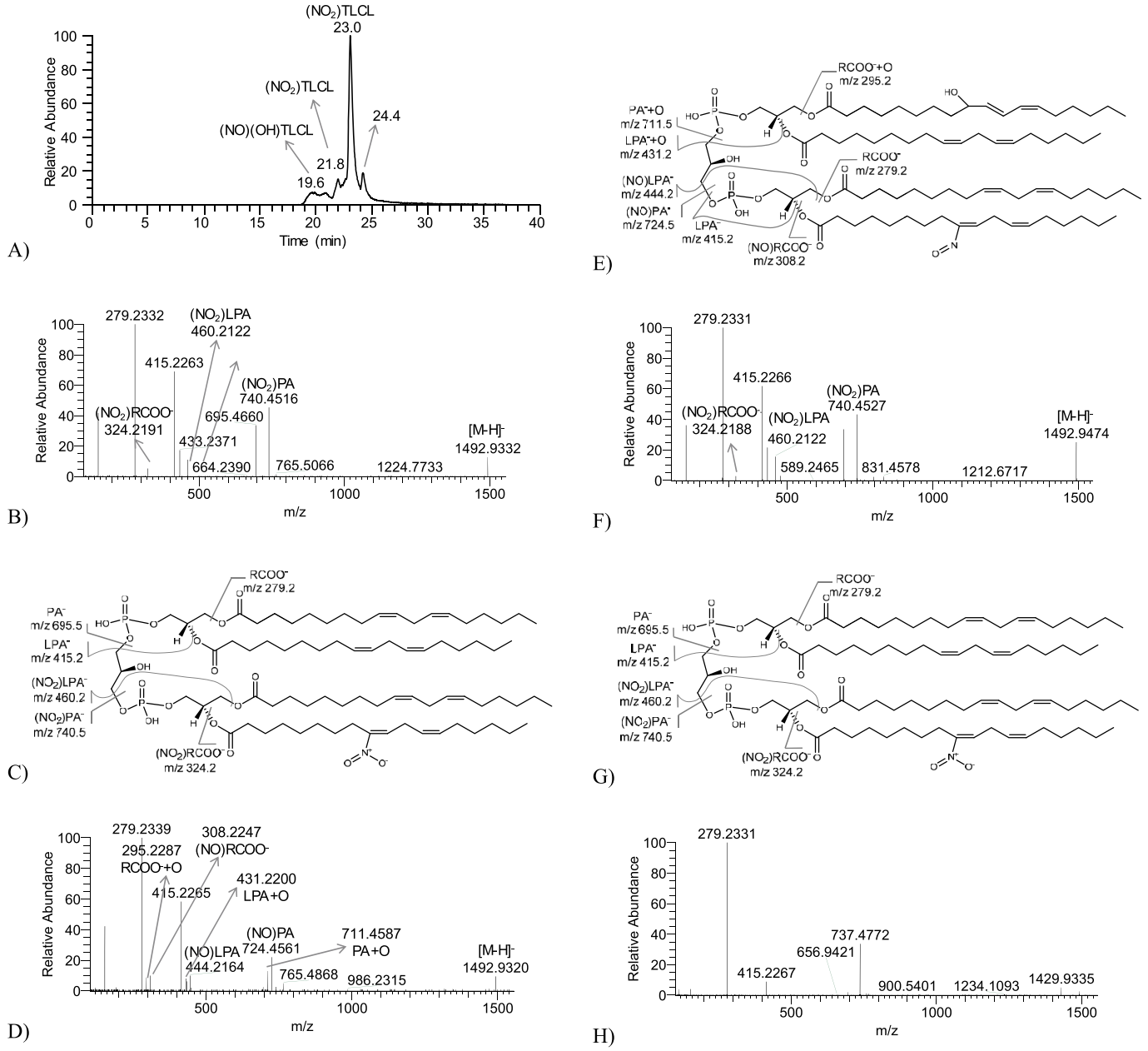

Fig. 7. A) Reconstructed ion chromatogram for species *m/z* 1492.93, corresponding to a mass shift of 45Da from the native TLCL. MS/MS spectrum of the ion at *m/z* 1492.93 acquired at B) RT 23.0 min with C) its fragmentation pathways; D) RT 19.6 min with E) its fragmentation pathways; F) RT 21.8 min with G) its fragmentation pathways; and H) RT 24.4 min.

ions, that may lose fatty acids yielding the lysophosphatidic acid monomers (LPA^-), and the carboxylate product ions (RCOO-). PA^- and LPA^- fragment ions were also observed with remaining glycerol (+56) or glycerol-phosphate (+136) moieties from the other monomer of the molecule. Remarkably, the typical neutral losses associated with the modifying moieties, such as neutral loss (NL) of HNO (NL of 31 Da), NO (NL 30) or HNO_2 (NL of 47 Da) from the NO or NO_2 nitrated TLCL precursor ions were not observed, in contrast with the previous works [28,31], which were performed using low-energy collision-induced dissociation (CID). HCD uses higher energy dissociations (< 100eV) than those used in resonant-excitation CID (< 2 eV), enabling different and more abundant fragmentation pathways [39]. As such, it is important to select the diagnostic ions according to the fragmentation method that it is used.

5. Conclusions

We have applied C30LC-HRMS and HCD MS/MS to study the nitration products of tetralinoleoyl cardiolipin, after biomimetic lipid nitration using NO_2BF_4. The system performed with high-sensibility, high-resolution and high chromatographic selectivity, allowing to separate and identify a wide variety of nitrated structures. We have separated and identified 11 different nitrated compounds comprising 7 different classes of nitro, nitroso, nitronitroso, and nitroxidized TLCL derivatives. The system also allowed to separate isomers with good chromatographic selectivity. These nitrated cardiolipins were further identified by analysing the LC-HCD-MS/MS spectra. The observed fragmentation pathways included the cleavage to phosphatidic acid monomers (PA^-), lysophosphatidic acid monomers (LPA^-) and carboxylate product ions with the modifying nitro, nitroso, nitronitroso, or nitroxidized moieties, which allowed to identify the nitrated compounds.

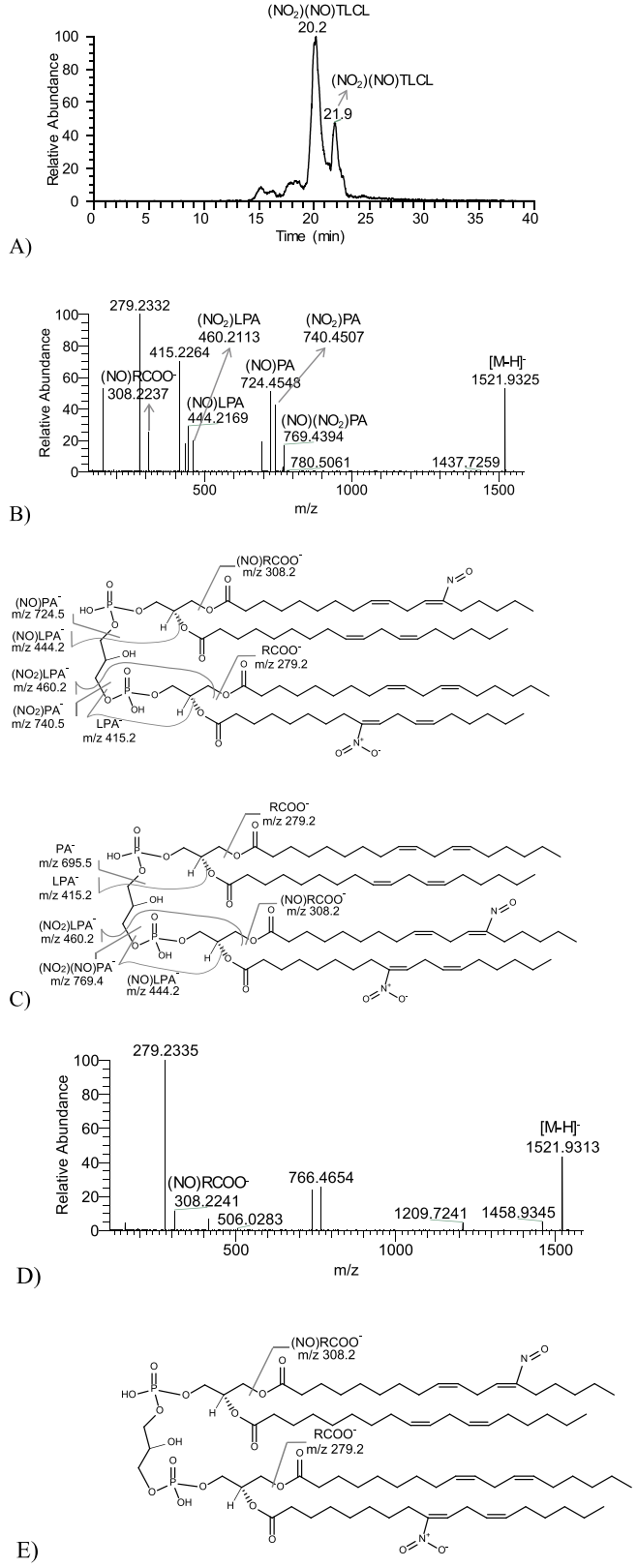

Fig. 8. A) Reconstructed ion chromatogram for species *m/z* 1521.93, corresponding to a mass shift of 74Da from the native TLCL. MS/MS spectrum of the ion at *m/z* 1521.93 acquired at B) RT 20.2 min with C) fragmentation pathways for the two possible positional isomers, and D) at 21.9 min with E) its fragmentation pathways.

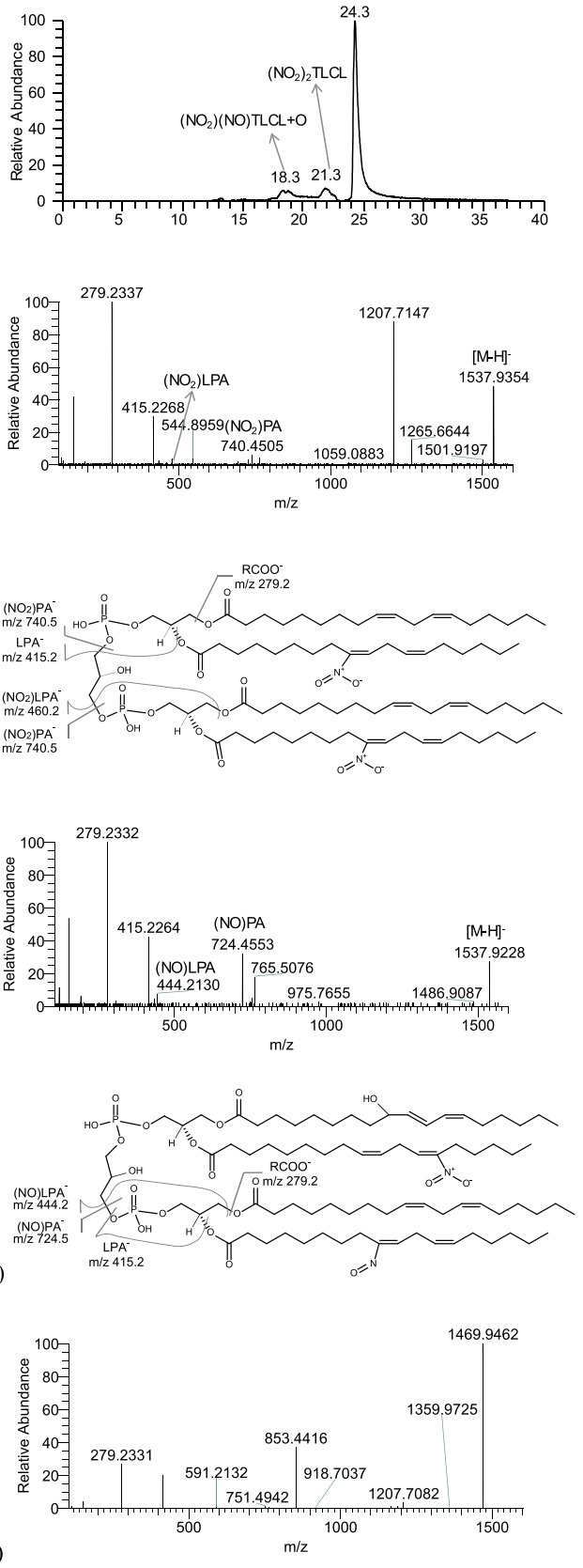

Fig. 9. A) Reconstructed ion chromatogram for species at *m/z* 1537.93, corresponding to a mass shift of 90Da from the native TLCL. MS/MS spectra of the ion *m/z* 1537.93 acquired at B) 21.3 min with C) its fragmentation pathways; D) 18.3 min with E) its fragmentation pathways, and F) at 24.3 min.

Acknowledgements

This work was supported by funding from European Commission's Horizon 2020 research and innovation programme under the Marie Sklodowska-Curie grant agreement number 675132 (MSCA-ITN-ETN MASSTRPLAN) to University of Aveiro. Thanks are due to University of Aveiro, FCT/MEC, European Union, QREN, COMPETE for the financial support to the QOPNA-LAQV (FCT UID/QUI/00062/2019) and CESAM (UID/AMB/50017/2019), through national funds and where applicable co-financed by the FEDER, within the PT2020 Partnership Agreement, to the RNEM, Portuguese Mass Spectrometry Network (LISBOA-01-0145-FEDER-402-022125). Tânia Melo is grateful for her Post-Doc grant (BPD/UI 51/5388/2017).

References

[1] G. Paradies, V. Paradies, V. De Benedictis, F.M. Ruggiero, G. Petrosillo, Functional role of cardiolipin in mitochondrial bioenergetics, Biochim. Biophys. Acta Bioenerg. 1837 (2014) 408–417, https://doi.org/10.1016/j.bbabio.2013.10.006.

[2] Y.A. Vladimirov, E.V. Proskurnina, A.V. Alekseev, Molecular mechanisms of apoptosis. Structure of cytochrome c-cardiolipin complex, Biochem 78 (2013) 1086–1097, https://doi.org/10.1134/S0006297913100027.

[3] J.J.R. Krebs, H. Hauser, E. Carafoli, Asymmetric distribution of phospholipids in the inner membrane of beef heart mitochondria*, J. Biol. Chem. 254 (1979) 5308–5316.

[4] G. Oemer, K. Lackner, K. Muigg, G. Krumschnabel, K. Watschinger, S. Sailer, H. Lindner, E. Gnaiger, S.B. Wortmann, E.R. Werner, J. Zschocke, M.A. Keller, Molecular structural diversity of mitochondrial cardiolipins, Proc. Natl. Acad. Sci. Unit. States Am. 115 (2018) 4158 LP–4163, https://doi.org/10.1073/pnas.1719407115.

[5] X. Han, K. Yang, J. Yang, H. Cheng, R.W. Gross, Shotgun lipidomics of cardiolipin molecular species in lipid extracts of biological samples, J. Lipid Res. 47 (2006) 864–879, https://doi.org/10.1194/jlr.D500044-JLR200.

[6] V.E. Kagan, Y.Y. Tyurina, V.A. Tyurin, D. Mohammadyani, J.P.F. Angeli, S. V Baranov, J. Klein-Seetharaman, R.M. Friedlander, R.K. Mallampalli, M. Conrad, H. Bayir, Cardiolipin signaling mechanisms: collapse of asymmetry and oxidation, Antioxidants Redox Signal. 22 (2015) 1667–1680, https://doi.org/10.1089/ars.2014.6219.

[7] A. Reis, C.M. Spickett, Chemistry of phospholipid oxidation, Biochim. Biophys. Acta Biomembr. 1818 (2012) 2374–2387, https://doi.org/10.1016/J.BBAMEM.2012.02.002.

[8] C.M. Spickett, A.R. Pitt, Oxidative lipidomics coming of age: advances in analysis of oxidized phospholipids in physiology and pathology, Antioxidants Redox Signal. 22 (2015) 1646–1666, https://doi.org/10.1089/ars.2014.6098.

[9] G. Aldini, M.R. Domingues, C.M. Spickett, P. Domingues, A. Altomare, F.J. Sánchez-Gómez, C.L. Oeste, D. Pérez-Sala, Protein lipoxidation: detection strategies and challenges, Redox Biol 5 (2015) 253–266, https://doi.org/10.1016/j.redox.2015.05.003.

[10] Y.Y. Tyurina, R.M. Domingues, V.A. Tyurin, E. Maciel, P. Domingues, A.A. Amoscato, H. Bayir, V.E. Kagan, Characterization of cardiolipins and their oxidation products by LC–MS analysis, Chem. Phys. Lipids 179 (2014) 3–10, https://doi.org/10.1016/j.chemphyslip.2013.12.003.

[11] S.L. Iverson, S. Orrenius, The cardiolipin-cytochrome c interaction and the mitochondrial regulation of apoptosis, Arch. Biochem. Biophys. 423 (2004) 37–46.

[12] V.A. Vladimir Tyurin, Y.Y. Tyurina, M.-Y. Jung, M.A. Tungekar, K.J. Wasserloos, H. Bayır, J.S. Greenberger, P.M. Kochanek, A.A. Shvedova, B. Pitt, V.E. Kagan, Mass-spectrometric analysis of hydroperoxy-and hydroxy-derivatives of cardiolipin and phosphatidylserine in cells and tissues induc1, J. Chromatogr., B 877 (2009) 2863–2872, https://doi.org/10.1016/j.jchromb.2009.03.007.

[13] H. Yin, M. Zhu, Free radical oxidation of cardiolipin: chemical mechanisms, detection and implication in apoptosis, mitochondrial dysfunction and human diseases, Free Radic. Res. 46 (2012) 959–974, https://doi.org/10.3109/10715762.2012.676642.

[14] E. Maciel, P. Domingues, M.R.M. Domingues, Liquid chromatography/tandem mass spectrometry analysis of long-chain oxidation products of cardiolipin induced by the hydroxyl radical, Rapid Commun. Mass Spectrom. 25 (2011) 316–326, https://doi.org/10.1002/rcm.4866.

[15] J. Kim, P.E. Minkler, R.G. Salomon, V.E. Anderson, C.L. Hoppel, Cardiolipin: characterization of distinct oxidized molecular species, J. Lipid Res. 52 (2011) 125–135, https://doi.org/10.1194/jlr.M010520.

[16] E. Maciel, P. Domingues, D. Marques, C. Simões, A. Reis, M.M. Oliveira, R.A. Videira, F. Peixoto, M.R.M. Domingues, Cardiolipin and oxidative stress: identification of new short chain oxidation products of cardiolipin in in vitro analysis and in nephrotoxic drug-induced disturbances in rat kidney tissue, Int. J. Mass Spectrom. 301 (2011) 62–73, https://doi.org/10.1016/J.IJMS.2010.06.036.

[17] Y.Y. Tyurina, D.E. Winnica, V.I. Kapralova, A.A. Kapralov, V.A. Tyurin, V.E. Kagan, LC/MS characterization of rotenone induced cardiolipin oxidation in human lymphocytes: implications for mitochondrial dysfunction associated with Parkinson's disease, Mol. Nutr. Food Res. 57 (2013) 1410–1422, https://doi.org/10.1002/mnfr.201200801.

[18] Y.Y. Tyurina, V.A. Tyurin, A.M. Kaynar, V.I. Kapralova, K. Wasserloos, J. Li, M. Mosher, L. Wright, P. Wipf, S. Watkins, B.R. Pitt, V.E. Kagan, Oxidative lipidomics of hyperoxic acute lung injury: mass spectrometric characterization of cardiolipin and phosphatidylserine peroxidation, Am. J. Physiol. Cell. Mol. Physiol. 299 (2010) L73–L85, https://doi.org/10.1152/ajplung.00035.2010.

[19] Y.Y. Tyurina, V.A. Tyurin, V.I. Kapralova, K. Wasserloos, M. Mosher, M.W. Epperly, J.S. Greenberger, B.R. Pitt, V.E. Kagan, Oxidative lipidomics of γ-radiation-induced lung injury: mass spectrometric characterization of cardiolipin and phosphatidylserine peroxidation, Radiat. Res. 175 (2011) 610–621, https://doi.org/10.1667/RR2297.1.

[20] Y.Y. Tyurina, V.A. Tyurin, M.W. Epperly, J.S. Greenberger, V.E. Kagan, Oxidative lipidomics of γ-irradiation-induced intestinal injury, Free Radic. Biol. Med. 44 (2008) 299–314, https://doi.org/10.1016/J.FREERADBIOMED.2007.08.021.

[21] R. Faria, M.M. Santana, C.A. Aveleira, C. Simões, E. Maciel, T. Melo, D. Santinha, M.M. Oliveira, F. Peixoto, P. Domingues, C. Cavadas, M.R.M. Domingues, Alterations in phospholipidomic profile in the brain of mouse model of depression induced by chronic unpredictable stress, Neuroscience 273 (2014) 1–11, https://doi.org/10.1016/J.NEUROSCIENCE.2014.04.042.

[22] M.C. Martínez, R. Andriantsitohaina, Reactive nitrogen species: molecular mechanisms and potential significance in health and disease, Antioxidants Redox Signal. 11 (2009) 669–702, https://doi.org/10.1089/ars.2007.1993.

[23] D.A. Butterfield, T. Reed, R. Sultana, Roles of 3-nitrotyrosine- and 4-hydroxynonenal-modified brain proteins in the progression and pathogenesis of Alzheimer's disease, Free Radic. Res. 45 (2011) 59–72, https://doi.org/10.3109/10715762.2010.520014.

[24] M.W. Foster, D.T. Hess, J.S. Stamler, Protein S-nitrosylation in health and disease: a current perspective, Trends Mol. Med. 15 (2009) 391–404, https://doi.org/10.1016/j.molmed.2009.06.007.

[25] A.J. Deen, V. Sihvola, J. Härkönen, T. Patinen, S. Adinolfi, A.-L. Levonen, Regulation of Stress Signaling Pathways by Nitro-Fatty Acids, Nitric Oxide, (2018), pp. S1089–S8603, https://doi.org/10.1016/J.NIOX.2018.03.012 17 30323–3.

[26] L. Villacorta, Z. Gao, F.J. Schopfer, B. a Freeman, Y.E. Chen, Nitro-fatty acids in cardiovascular regulation and diseases: characteristics and molecular mechanisms, Front. Biosci. 21 (2016) 873–889.

[27] F.J. Schopfer, Y. Lin, P.R.S. Baker, T. Cui, M. Garcia-Barrio, J. Zhang, K. Chen, Y.E. Chen, B.A. Freeman, Nitrolinoleic acid: an endogenous peroxisome proliferator-activated receptor gamma ligand, Proc. Natl. Acad. Sci. U.S.A. 102 (2005) 2340–2345, https://doi.org/10.1073/pnas.0408384102.

[28] T. Melo, P. Domingues, R. Ferreira, I. Milic, M. Fedorova, S.M. Santos, M.A. Segundo, M.R.M. Domingues, Recent advances on mass spectrometry analysis of nitrated phospholipids, Anal. Chem. 88 (2016) 2622–2629, https://doi.org/10.1021/acs.analchem.5b03407.

[29] A. Trostchansky, L. Bonilla, L. González-Perilli, H. Rubbo, Nitro-fatty acids: formation, redox signaling, and therapeutic potential, Antioxidants Redox Signal. 19 (2013) 1257–1265, https://doi.org/10.1089/ars.2012.5023.

[30] I. Milic, E. Griesser, V. Vemula, N. Ieda, H. Nakagawa, N. Miyata, J.M. Galano, C. Oger, T. Durand, M. Fedorova, Profiling and relative quantification of multiply nitrated and oxidized fatty acids, Anal. Bioanal. Chem. 407 (2015) 5587–5602, https://doi.org/10.1007/s00216-015-8766-3.

[31] T. Melo, P. Domingues, T.M. Ribeiro-Rodrigues, H. Girão, M.A. Segundo, M.R.M. Domingues, Characterization of phospholipid nitroxidation by LC-MS in biomimetic models and in H9c2 Myoblast using a lipidomic approach, Free Radic. Biol. Med. 106 (2017) 219–227, https://doi.org/10.1016/j.freeradbiomed.2017.02.033.

[32] B. Neves, P. Domingues, M. Oliveira, M. Domingues, T. Melo, B. Neves, P. Domingues, M.M. Oliveira, M. do R. Domingues, T. Melo, Profile of phosphatidylserine modifications under nitroxidative stress conditions using a liquid chromatography-mass spectrometry based approach, Molecules 24 (2018) 107, https://doi.org/10.3390/molecules24010107.

[33] T. Melo, S.S. Marques, I. Ferreira, M.T. Cruz, P. Domingues, M.A. Segundo, M.R.M. Domingues, New insights into the anti-inflammatory and antioxidant properties of nitrated phospholipids, Lipids 53 (2018) 117–131, https://doi.org/10.1002/lipd.12007.

[34] F.J. Larsen, T.A. Schiffer, E. Weitzberg, J.O. Lundberg, Regulation of mitochondrial function and energetics by reactive nitrogen oxides, Free Radic. Biol. Med. 53 (2012) 1919–1928, https://doi.org/10.1016/j.freeradbiomed.2012.08.580.

[35] S.R. Woodcock, G. Bonacci, S.L. Gelhaus, F.J. Schopfer, Nitrated fatty acids: synthesis and measurement, Free Radic. Biol. Med. 59 (2013) 14–26, https://doi.org/10.1016/j.freeradbiomed.2012.11.015.

[36] E.M. Bartlett, D.H. Lewis, Spectrophotometric determination of phosphate esters in the presence and absence of orthophosphate, Anal. Biochem. 36 (1970) 159–167, https://doi.org/10.1016/0003-2697(70)90343-X.

[37] K.C. Huang, R. Mukhopadhyay, N.S. Wingreen, A curvature-mediated mechanism for localization of lipids to bacterial poles, PLoS Comput. Biol. 2 (2006) e151, https://doi.org/10.1371/journal.pcbi.0020151.

[38] F.F. Hsu, J. Turk, E.R. Rhoades, D.G. Russell, Y. Shi, E.A. Groisman, Structural characterization of cardiolipin by tandem quadrupole and multiple-stage quadrupole ion-trap mass spectrometry with electrospray ionization, J. Am. Soc. Mass Spectrom. 16 (2005) 491–504, https://doi.org/10.1016/j.jasms.2004.12.015.

[39] J.V. Olsen, B. Macek, O. Lange, A. Makarov, S. Horning, M. Mann, Higher-energy C-trap dissociation for peptide modification analysis, Nat. Methods 4 (2007), https://doi.org/10.1038/nmeth1060 709–1.

CHAPTER 3. Characterization of Nitrophospholipid-Peptide Covalent Adducts by Electrospray Tandem Mass Spectrometry: A First Screening Analysis Using Different Instrumental Platforms

The content presented in this section was integrally published as follows:

Montero-Bullon, J.-F., Melo, T., Domingues, M. R. & Domingues, P. Characterization of Nitrophospholipid-Peptide Covalent Adducts by Electrospray Tandem Mass Spectrometry: A First Screening Analysis Using Different Instrumental Platforms. *Eur. J. Lipid Sci. Technol.* 120, 1800101 (2018).

SHORT COMMUNICATION

Tandem Mass Spectrometry

European Journal of Lipid Science and Technology

www.ejlst.com

Characterization of Nitrophospholipid-Peptide Covalent Adducts by Electrospray Tandem Mass Spectrometry: A First Screening Analysis Using Different Instrumental Platforms

Javier-Fernando Montero-Bullon, Tânia Melo, Maria Rosário Domingues, and Pedro Domingues*

Lipids are well-known targets of reactive nitrogen species and this reaction leads to the formation of nitrated lipids that have been associated with anti-inflammatory and cytoprotective effects. Nitro-fatty acids (NO_2-FA) are highly electrophilic compounds that can form covalent adducts with proteins, leading to the formation of lipoxidation adducts, which modulate the protein structure and function. Nitrated phospholipids (NO_2-PL) have been detected recently in biological samples, but their biological effects are unknown, although similarly to what has been described for nitrated lipids, it has been hypothesized that they may react with peptides and proteins. In this study, in vitro biomimetic assays are used to synthetize adducts of nitrated POPC (NO_2POPC), already detected in biological samples, and GSH peptide. The formation of NO_2POPC-GSH adducts is studied by ESI-MS and MS^2, using both low and high energy CID in different MS platforms: a LXQ linear ion trap, a Q-TOF 2, and a Q-Exactive Hybrid Quadrupole-Orbitrap. Typical product ions observed under MS^2 conditions are modified b, y, and C ions bearing NO_2POPC covalently linked that unequivocally confirms the presence of the lipid-peptide adduct. Typical loss of HNO_2 is only observed in the MS^2 of the mono-charged precursor ions, $[M+H]^+$. Product ions at *m/z* 184 or neutral loss of 183 Da are assigned as typical fragmentations that confirm the presence of the phosphatidylcholine. In summary, the characterization of nitro PL-peptide adducts by MS and MS^2 allows the identification of the structure and specific MS^2 reporter ions to be used to pinpoint these adductions in biological systems.

***Practical Applications*: The covalent interaction between nitro phospholipids and peptides suggests a new pathway in cellular transduction of nitroxidative stress signal. This adduction can be considered a post-translational modification (PTM) of lipoxidation type, similarly as it has been described for nitro-fatty acids and with important physiological implications. The identification and characterization of the nitro phospholipids and peptides adducts are possible by MS and tandem MS. This analytical technique also represents a robust and sensitive approach for detection of nitro-lipids adduction to peptides or proteins in biological samples, allowing to disclose their physiological and clinical implications. Tandem MS fingerprinting is an essential feature for this purpose, so in this work, the identification of the reporter ions typical for this type of lipoxidation adducts is provided. These reporter ions can be used to design target (NL, PIS, or MRM) approaches to detect these type of PTM in biological environments.**

J.-F. Montero-Bullon, Dr. T. Melo, Dr. M. R. Domingues, Dr. P. Domingues
Centro de Espectrometria de Massa
Departamento de Química & QOPNA
Universidade de Aveiro
Campus Universitário de Santiago
3810-193 Aveiro, Portugal
E-mail: mrd@ua.pt

DOI: 10.1002/ejlt.201800101

1. Introduction

Phospholipids, main components of lipoproteins and cell membranes, are prone to be modified by reactive oxygen species (ROS) and reactive nitrogen species (RNS), leading to a plethora of oxidized or nitrated and nitroxidized lipids. Among these, oxidized lipids bearing terminal carbonyl group and nitrated lipids are highly reactive electrophilic compounds, and can form covalent adducts with proteins, leading to the formation of lipoxidation adducts.[1,2] These reactions are main routes of protein post-translational modifications[3,4] being responsible for modulation of protein's structure and function. Most of the studies have been focused on lipoxidation adducts formed between peptides and proteins with electrophilic-oxidized lipids[5,6] and, usually, these adducts are reported to have deleterious effects associated with inflammation and several diseases.[1]

More recently, peptide and protein modifications by covalent adduction to nitrated fatty acids have been described[7] and have been associated with beneficial and health protective effects.[7] Nitro-fatty acids (NO_2-FA) have been found both in vitro and in vivo, namely in red blood cells,[8,9] plasma,[8–11] and in different tissues, either in normal or in inflammatory conditions.[12] Several published works described the NO_2-FA adducts with GSH,[13,14] GAPDH,[13,14] NF-κB,[15] and PPARγ.[16] This type of post-translational modification seems to be an important regulatory pathway for the modulation of enzymatic activity, redox homeostasis, and in signaling events[7,13,17] associated with inhibition of inflammatory process and pro-survival responses. Also, NO_2-FA and their protein adducts have been identified in olive and olive oil and were correlated with the beneficial effects of this food and of the Mediterranean diet.[18]

The identification in vitro or in vivo of lipoxidation adducts and of nitrolipid-peptide/protein adducts is usually done by using

mass spectrometry (MS)-based approaches.[13] This approach allows to specify the electrophilic molecule that is covalently linked to peptide or protein, and to localize the addition site.[5] This structural information is obtained by analysis of the fragmentation pattern of peptide-electrophilic adducts obtained using tandem mass spectrometry experiments.[5,6]

Very recently, nitro-phospholipids (NO_2-PL) were detected in in vitro and in vivo systems, by our group,[19,20] using MS-based approaches. Nitro derivatives of phosphatidylcholines (NO_2-PC) and phosphatidylethanolamines (NO_2-PE), mainly bearing oleic acid (OA) were detected in cardiomyocytes[20] and in cardiac mitochondria from diabetic rats.[19] These results showed that not only free NO_2-FA, but also esterified NO_2-FA in PL, can be a target of RNS and can be formed in vivo. NO_2-PL was correlated with beneficial effects in the recovery phase in a cellular model of myocardium infarction in autophagy.[20] Also, NO_2POPC showed antioxidant properties as scavenging agent and anti-inflammatory properties by inhibiting the expression of iNOS in Raw 264.7 macrophages stimulated with LPS.[21]

However, there are no studies on the possible adduction of NO_2-PLs to peptides. Thus, the aim of our work was to identify for the first time the typical tandem MS fragmentation pattern of the covalent adducts formed between GSH and NO_2POPC, one of the NO_2-PL species reported in biological samples,[19,20] and that may have important biological properties. Analysis by tandem MS was performed in three different instruments commonly used in lipidomics and proteomics approaches: an LXQ linear ion trap (LXQ-LIT), a Q-TOF hybrid quadrupole time-of-flight, and a high-resolution Q Exactive Hybrid Quadrupole-Orbitrap. Herein, we have characterized the covalent Michael adduct formed between GSH and NO_2-POPC by MS-based approaches, opening a new field of study for nitroxidative stress downstream processes and to unveil the possible role of NO_2-PL in protein's post-translational modifications.

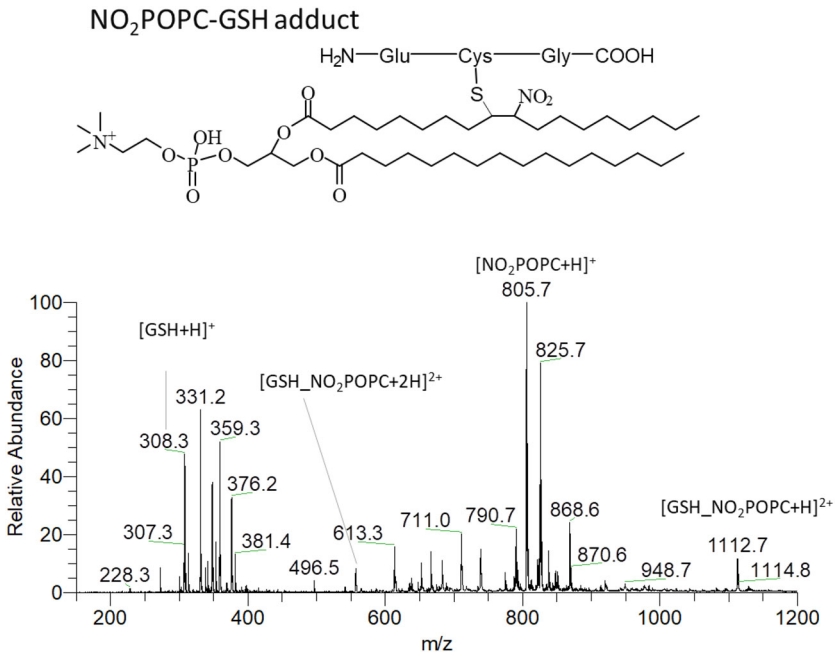

Figure 1. ESI-MS spectrum obtained after reaction between GSH and NO_2POPC, showing the NO_2POPC-GSH indentified by the presence of the $[M+2H]^{2+}$ ions at *m/z* 556.8 and $[M+H]^+$ ions at *m/z* 1112.7.

2. Experimental Section

Phospholipid nitration was carried out with nitronium tetrafluoroborate (NO_2BF_4; Sigma–Aldrich, St. Louis, MO, USA), as previously described.[19,20,22] A solution of 1-palmitoyl-2-oleoyl-SN-glycero-3-phosphocholine (POPC; 1 mg; Avanti Polar Lipids, Inc., Alabaster, USA) in chloroform (1 mL; Fisher Scientific Ltd., Leicestershire, UK) was prepared in an amber vial tube. Then, an excess of the solid NO_2BF_4 (≈1 mg) was added. The vial containing the reaction mixture was purged with nitrogen stream, prior to the incubation at room temperature (20 °C) for 1 h, under orbital shaking at 750 rpm. This allows that the reaction occur under nitrogen atmosphere in order to avoid decomposition of the nitro phospholipid formed. After incubation, the reaction was stopped by solvent extraction with Milli-Q water. The organic layer containing the phospholipid products was collected, and was dried under a nitrogen stream. The recovered nitrated PL was quantified using phosphorous assay and analyzed by ESI-MS and MS/MS in an LXQ linear ion trap (LIT) mass spectrometer (ThermoFinnigan, San Jose, CA, USA) in positive-ion mode. After analysis of ESI-MS spectrum, it was possible to identify the $[NO_2POPC+H]^+$ ion at *m/z* 805.7, confirming the formation of the NO_2POPC. A smaller ion attributed to the fluorinated derivative $[NO_2POCP+HF+Na]^+$ is also observed at *m/z* 847.7, as observed previously for the nitration of fatty acids (data not shown),[22] and may correspond to the addition of fluoride to the double bond of the monounsaturated fatty acid. Since nitroso or nitroxidized derivatives were not identified in our reaction, in contrast with what was reported before by Melo et al.[20] and Milic et al.[22] (because in the previously published work nitration was performed in the presence of air, favoring oxidation and decomposition of nitro POPC) and considering that the hydrofluoride nitro-POPC derivative lose the double bond, thus is not reactive toward protein/peptides, the NO_2POPC was used without further purification steps. The adducts between the NO_2POPC and GSH (reduced form; Sigma–Aldrich) were obtained by mixing 0.25 µmol of NO_2POPC with 1.25 µmol of GSH in 50 µL of NH_4HCO_3 buffer (5 mM, pH 7.4; Sigma–Aldrich), under a N_2 atmosphere. The mixture was vortexed for 15 min, sonicated for 5 min, and incubated at 37 °C for 6 h in a shaker at 750 rpm. Aliquots of 4 µL of product mixture were diluted to 200 µL of MeOH:H_2O (3:1, v/v) with 1% formic acid (Sigma–Aldrich), and analyzed by ESI-MS using different instruments operating in positive-ion mode: a LXQ linear ion trap (LIT) (ThermoFinnigan), a Q-TOF 2 hybrid

European Journal of Lipid Science and Technology
www.ejlst.com

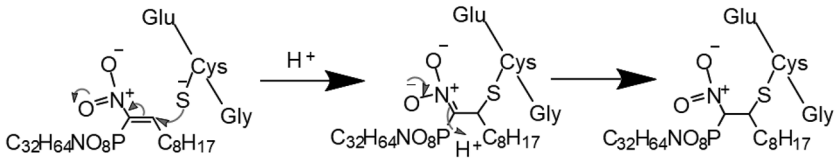

Scheme 1. The general mechanism of reaction for adduction of NO_2-PL to GSH with the formation of Michael adducts. The reaction of NO_2POPC with GSH should occur in aqueous media, as proposed for nitro oleic acid (NO_2-OA).[23]

quadrupole time-of-flight (Micromass, Manchester, UK) and a high resolution Q Exactive Hybrid Quadrupole-Orbitrap (Thermo Fisher Scientific, Bremen, Germany) mass spectrometers.

The operating conditions used in ESI-LXQ-LIT mass spectrometer were as follows: samples were introduced at a flow rate of 8 μL min^{-1}; electrospray voltage was +5 kV; capillary temperature was 275 °C; and the sheath gas flow of 8 (arbitrary units). Nitrogen was used as nebulizing and drying gas. Full scan MS spectra were acquired over the *m/z* range 150–1200. For MS/MS experiments, spectra were acquired by CID using helium as the collision gas. The normalized collision energy used was 28 (arbitrary units). Data acquisition and analysis were performed using Xcalibur Data System (version 2.0, ThermoFinnigan).

In the ESI-Q-TOF2 mass spectrometer, the flow rate was 10 μL min^{-1}; cone voltage was set at 30 V; capillary voltage was maintained at +3 kV; source temperature was 80 °C, and desolvation temperature was 150 °C. Full scan MS was acquired scanning the mass range from *m/z* 150 to 1200. MS/MS spectra were acquired using argon as the collision gas. The normalized collision energy used was 25 (arbitrary units). Data acquisition and analysis were performed using MassLynx 4.0 data system.

In the ESI Q Exactive Hybrid Quadrupole-Orbitrap mass spectrometer (Thermo Fisher Scientific), samples were introduced through direct infusion at flow rate of 10 μL min^{-1} and the operating conditions were as follows: the electrospray voltage was +3 kV; capillary temperature was 250 °C; sheath gas (nitrogen) flow of 5 (arbitrary units); isolation width of 1 Da; AGC target of 5E06; maximum injection time (IT) was 250 ms; and resolution was set at 140 000 in *m/z* range 150–1200. In MS/MS experiments, the resolution was set at 70 000 full width at half maximum (FWHM); AGC target of 1E05; maximum IT 250 ms; isolation window of 1.0 *m/z*; and normalized collision energy was 23 for mono charged and 20 for double-charged ions, arbitrary units. Collision gas was N_2. Data acquisition was carried out using the Xcalibur data system (V3.3, Thermo Fisher Scientific, USA).

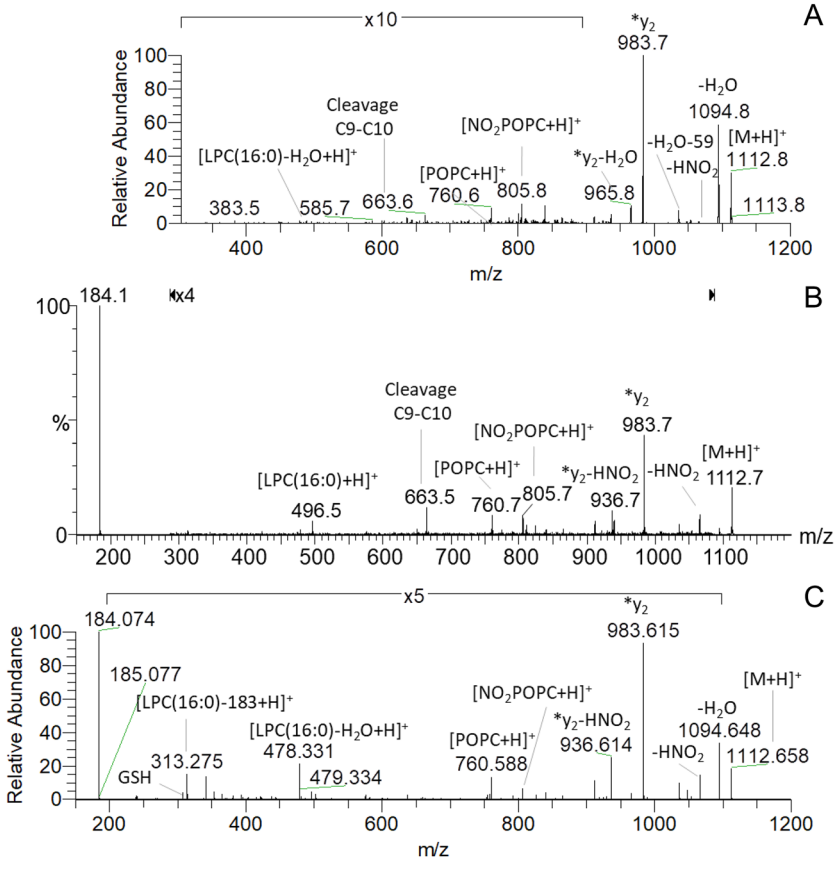

Figure 2. ESI-MS/MS spectra of $[NO_2POPC\text{-}GSH+H]^+$ in A) LXQ Linear Ion trap, B) Q-TOF 2, and C) Q-Exactive Orbitrap.

3. Results and Discussion

The covalent adduct of NO_2POPC and GSH was identified in the ESI-MS spectra by the presence of the $[M+2H]^{2+}$ ions at *m/z* 556.832 and $[M+H]^+$ ions at *m/z* 1112.656 (**Figure 1**), as confirmed by exact mass measurement in the high resolution Q Exactive Orbitrap (not shown), and also by tandem MS. These adducts are formed via Michael addition reaction between reduced cysteine of GSH with the double bond of the NO_2-PL, in a similar way as previously proposed for NO_2-FA-GSH adducts[13,14] (**Scheme 1**). The reaction of NO_2POPC with GSH should occur in aqueous media, as proposed for nitro oleic acid (NO_2-OA). A recent study evaluated the position of the nitro group of NO_2-OA in PC liposomes used as a model of membranes. By fluorescence measurements, vibrational spectroscopy, and coarse-grained computer simulations demonstrated that NO_2-OA changes the lipid organization and are mainly accumulated at the membrane–water interface.[23] NO_2-OA is able to shape the molecular organization of model membranes along the bilayer, and the nitro group is preferentially located near the head group of the phospholipid.[23] This arrangement facilitates the location of the nitro group more closely to

the membrane–water interface that favors the electrophilic adduction of the nitro-lipids with the anionic sulfhydryl moiety of the cysteine in peptides and proteins, in an aqueous medium.

Analysis of the MS/MS spectra of both mono- and double-charged ions, $[M+H]^+$ and $[M+2H]^{2+}$, allowed to identify the fragmentation pathways and to suggest reporter ions that can be further used to confirm the identity of these adducts. The MS/MS spectra obtained in three different mass spectrometers, an LXQ linear ion trap (CID), a Q-TOF (CID) and a Q Exactive Orbitrap (HCD) are shown in **Figure 2** and 3. These MS platforms were selected because they are, nowadays, the most used for the detection of lipid–protein adducts either in biomimetic systems or in searching these compounds in biological samples analysis.[13,24]

The MS/MS spectra of the mono-charged $[M+H]^+$ ions of NO_2POPC-GSH adduct, obtained in the three instruments (Figure 2) showed some common fragmentation pathways such as the ion arising from the neutral loss of HNO_2 ($[M+H-HNO_2]^+$, at m/z 1065.658, confirming the presence of NO_2-PL species. It was also observed the mono-charged y_2 fragment ion linked to the nitrated POPC, designed as $^*y_2^+$ (at m/z 983.615) product ion (where * indicates that the product ion has a nitrated POPC moiety) formed by the cleavage of the peptide backbone in the vicinity of Cys where the NO_2-POPC is linked (**Scheme 2**). These MS/MS spectra showed also the loss of HNO_2 from $^*y_2^+$, inferred by the observation of the product ion at m/z 936.614. A product ion at m/z 663.5, arising from the cleavage of the C9-C10 bond of the modified fatty acyl chain, was only observed in the tandem spectra acquired in the ESI-Linear ion trap and Q-TOF instruments. The presence of product ions attributed to $[NO_2POPC+H]^+$ (at m/z 805.6), $[POPC+H]^+$ (at m/z 760.6) and at phosphatidylcholine head (at m/z 184.1), allowed to confirm the identity of NO_2-PL. No loss of HNO was observed in the MS/MS spectra of the $[M+H]^+$, and of the $[M+2H]^{2+}$, thus excluding the contribution of possible nitroso derivatives.

The tandem mass spectra of the double charged $[M+2H]^{2+}$ ions showed, in all instruments (**Figure 3**), the common product ions $^*y_2^{2+}$ (at m/z 492.311), $^*b_2^{2+}$ (at m/z 519.316), and $^*C_1^{2+}$ (at m/z 440.797), all corresponding to peptide fragments adducted to NO_2POPC. All these product ions confirmed the presence of the NO_2POPC covalently linked to the Cys residue of glutathione. Loss of HNO_2 was absent or observed with very low abundance. In all MS/MS spectra was also possible to detect the loss of phosphocholine (−183 Da), observed either from the precursor ion with formation of the product ion at m/z 929.591, or also combined with cleavages of the peptide product ions: $^*y_2^+$-183 (at m/z 800.5471) and $^*b_2^{2+}$-183 (at m/z 854.558). Similarly, as observed in the case of the mono-charged ion, the $[POPC+H]^+$ product ion (at m/z 760.588) and the PC polar head (at m/z 184.074), were observed in all spectra. All these product ions confirmed the presence of a phosphatidylcholine covalently linked to the peptide.

Overall, comparing the MS/MS spectra from the three mass spectrometers, we can highlight as common features that clearly identify the presence of NO_2POPC-GSH adducts, the product ions $^*y_2$, and the product ions and combined neutral losses associated with the phosphocholine polar head (m/z 184 or loss of 183 Da). Other important reporter ions were $^*y_2$-HNO_2 (observed in the case of fragmentation of mono-charged ions), the $^*b_2$ and $^*C_1$ (observed in the case of fragmentation of double-charged ions). Typical neutral loss (NLs) of HNO_2 was observed in the case of mono-charged ions. The presence of the fragment ions $^*y_2$, $^*y_2$-HNO_2 together with the cysteine immonium ions $^*C_1$ support the hypothesis that the lipid backbone of the NO_2POPC was bonded to the cysteine-moiety of GSH. The main product ions, identified as y_2, b_2^{2+}, and C_1, now observed for the NO_2POPC-GSH adduct, were also reported in tandem MS of the $[M+H]^+$ ions of the NO_2-FA-GSH adduct.[13] In consequence, these product ions ($^*y_2$, $^*b_2$, $^*C_1$) can be considered as reporter ions for the target analysis of these nitro lipoxidation adducts in biological samples. However, in this case of the NO_2FA adducts, loss of HNO_2 was not observed in the MS/MS spectrum but was only observed by MS^3 of $^*y_2$, when using the ion trap instrument.[13]

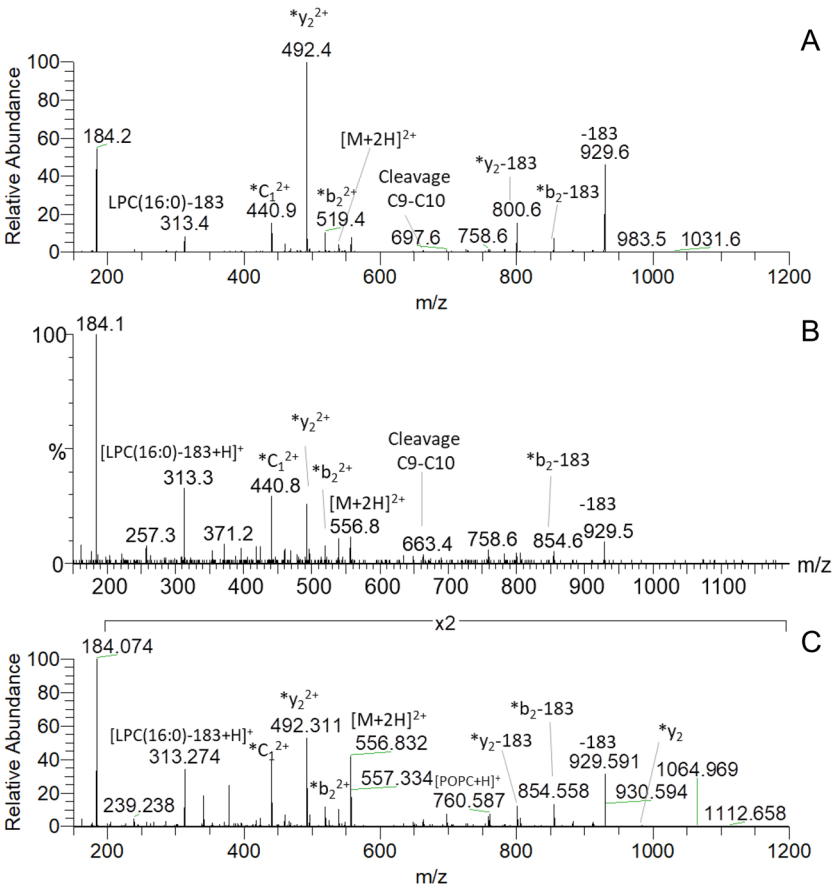

Figure 3. ESI-MS/MS spectra of $[NO_2POPC\text{-}GSH+2H]^{2+}$ in A) LXQ Linear Ion trap, B) Q-TOF 2, and C) Q-Exactive Orbitrap.

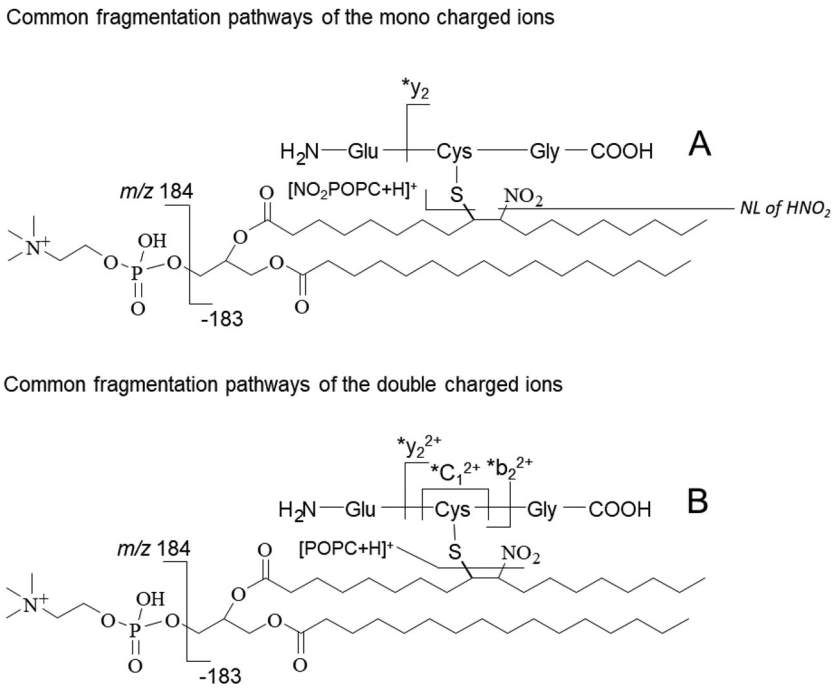

Scheme 2. Main fragmentation pathways observed in the ESI-MS/MS spectra of the NO_2POPC-GSH adducts detected in all the mass spectrometers, A) mono charged $[M+H]^+$ ion and B) double charged $[M+2H]^{2+}$.

The mass spectrometry approach used in this work was able to identify the formation of adducts between nitrated phospholipids and peptides, as exemplified for GSH. POPC is one of the most abundant phospholipids and its nitration in vivo has been previously shown.[19,20] GSH is intracellularly biosynthesized but it is also found in the extracellular medium, as in plasma. In spite of being a hydrophilic peptide, it was chosen for this experiment due to its facility to oxidize and the availability of its cysteine residue. In fact, the susceptibility of being oxidized by the nitro-fatty acyl chain embedded in the bilayer of liposomes shows the accessibility for interaction between NO_2-PL and peptides. This suggests the idea that a great number of peptides, but also proteins can be considered targets of nitrated phospholipids, especially those with a closer relationship with the membrane, which should be further investigated.

4. Conclusions

In summary, in this work we have characterized a nitro phospholipid-peptide adduct by MS and MS^2. This approach allows to identify the nature of modified phospholipid that is covalently bound to the peptide/protein and the reported ions identified can be used to pinpoint these adductions in biological systems. The biological effects of these new kind of adducts remains to be studied but it can be considered as promising, based on the importance of nitroxidation events in physiological and pathophysiological circumstances.

Abbreviations

NO_2-FA, nitrated fatty acids; NO_2-PL, nitrated phospholipids.

Acknowledgments

Thanks are due to University of Aveiro, Fundação para a Ciência e Tecnologia and Ministério da Educação e Ciência (FCT/MEC), European Union, QREN, COMPETE for the financial support to the QOPNA research Unit (FCT UID/QUI/00062/2013) and, through national funds and where applicable co-financed by the FEDER, within the PT2020 Partnership Agreement, and also to the Portuguese Mass Spectrometry Network (LISBOA-01-0145-FEDER-402-022125) and to the funding from European Commission's Horizon 2020 research and innovation programme under the Marie Sklodowska-Curie grant agreement number 675132 (MSCA-ITN-ETN MASSTRPLAN). T.M. (BPD/UI51/5388/2017) is grateful to FCT for her post-doctoral grant.

Conflict of Interest

The authors declare no conflict of interest.

Keywords

lipoxidation, nitration, nitrophospholipids, post-translational modifications, protein adducts

Received: March 7, 2018
Revised: July 20, 2018
Published online: October 24, 2018

[1] M. R. Domingues, P. Domingues, T. Melo, D. Pérez-Sala, A. Reis, C. Spickett, *J. Proteomics* **2013**, *92*, 110.
[2] I. Milic, T. Melo, M. R. Domingues, P. Domingues, M. Fedorova, *J. Mass Spectrom.* **2015**, *50*, 603.
[3] A. M. Silva, A. C. Borralho, S. A. Pinho, M. R. Domingues, P. Domingues, *Rapid Commun. Mass Spectrom.* **2011**, *25*, 1413.
[4] G. Aldini, M. R. Domingues, C. M. Spickett, P. Domingues, A. Altomare, F. J. Sánchez-Gómez, C. L. Oeste, D. Pérez-Sala, *Redox Biol.* **2015**, *5*, 253.
[5] M. Fedorova, R. C. Bollineni, R. Hoffmann, *Mass Spectrom. Rev.* **2014**, *33*, 79.
[6] Y. V. Vasil'ev, S. C. Tzeng, L. Huang, C. S. Maier, *Mass Spectrom. Rev.* **2014**, *33*, 157.
[7] A. C. Geisler, T. K. Rudolph, *Biochim. Biophys. Acta* **2012**, *1820*, 777.
[8] P. R. Baker, F. J. Schopfer, S. Sweeney, B. A. Freeman, *Proc. Natl. Acad. Sci. USA* **2004**, *101*, 11577.
[9] E. S. Lima, P. Di Mascio, D. S. Abdalla, *J. Lipid Res.* **2003**, *44*, 1660.
[10] E. S. Lima, P. Di Mascio, H. Rubbo, D. S. Abdalla, *Biochemistry* **2002**, *41*, 10717.
[11] D. Tsikas, A. A. Zoerner, A. Mitschke, F. M. Gutzki, *Lipids* **2009**, *44*, 855.
[12] L. Villacorta, Z. Gao, F. J. Schopfer, B. A. Freeman, Y. E. Chen, *Front. Biosci. (Landmark Ed)* **2016**, *21*, 873.
[13] C. Batthyany, F. J. Schopfer, P. R. Baker, R. Duran, L. M. Baker, Y. Huang, C. Cervenansky, B. P. Branchaud, B. A. Freeman, *J. Biol. Chem.* **2006**, *281*, 20450.
[14] L. M. Baker, P. R. Baker, F. Golin-Bisello, F. J. Schopfer, M. Fink, S. R. Woodcock, B. P. Branchaud, R. Radi, B. A. Freeman, *J. Biol. Chem.* **2007**, *282*, 31085.

[15] T. Cui, F. J. Schopfer, J. Zhang, K. Chen, T. Ichikawa, P. R. Baker, C. Batthyany, B. K. Chacko, X. Feng, R. P. Patel, A. Agarwal, B. A. Freeman, Y. E. Chen, *J. Biol. Chem*. **2006**, *281*, 35686.
[16] P. R. Baker, Y. Lin, F. J. Schopfer, S. R. Woodcock, A. L. Groeger, C. Batthyany, S. Sweeney, M. H. Long, K. E. Iles, L. M. Baker, B. P. Branchaud, Y. E. Chen, B. A. Freeman, *J. Biol. Chem*. **2005**, *280*, 42464.
[17] G. Bonacci, F. J. Schopfer, C. I. Batthyany, T. K. Rudolph, V. Rudolph, N. K. Khoo, E. E. Kelley, B. A. Freeman, *J. Biol. Chem*. **2011**, *286*, 16074.
[18] M. Fazzari, A. Trostchansky, F. J. Schopfer, S. R. Salvatore, B. Sánchez-Calvo, D. Vitturi, R. Valderrama, J. B. Barroso, R. Radi, B. A. Freeman, H. Rubbo, *PLoS ONE* **2014**, *9*, e84884.
[19] T. Melo, P. Domingues, R. Ferreira, I. Milic, M. Fedorova, S. M. Santos, M. A. Segundo, M. R. M. Domingues, *Anal. Chem*. **2016**, *88*, 2622.
[20] T. Melo, P. Domingues, T. M. Ribeiro-Rodrigues, H. Girao, M. A. Segundo, M. R. M. Domingues, *Free Radic. Biol. Med*. **2017**, *106*, 219.
[21] T. Melo, S. S. Marques, I. Ferreira, M. T. Cruz, P. Domingues, M. A. Segundo, M. R. M. Domingues, *Lipids* **2018**, *53*, 117.
[22] I. Milic, E. Griesser, V. Vemula, N. Ieda, H. Nakagawa, N. Miyata, J. M. Galano, C. Oger, T. Durand, M. Fedorova, *Anal. Bioanal. Chem*. **2015**, *407*, 5587.
[23] J. Franz, T. Bereau, S. Pannwitt, V. Anbazhagan, A. Lehr, U. Nubbemeyer, U. Dietz, M. Bonn, T. Weidner, D. Schneider, *Chemistry* **2017**, *23*, 9690.
[24] S. R. Salvatore, D. A. Vitturi, P. R. Baker, G. Bonacci, J. R. Koenitzer, S. R. Woodcock, B. A. Freeman, F. J. Schopfer, *J. Lipid Res*. **2013**, *54*, 1998.

CHAPTER 4. Exercise training counteracts cachexia-induced alterations in skeletal muscle mitochondria phospholipidome in animal model of urothelial carcinoma

The content presented in this section has been integrally submitted as follows:

Javier-Fernando Montero-Bullon, Tânia Melo, Rita Ferreira, Ana Isabel Padrão, Paula A. Oliveira, M Rosário M Domingues, Pedro Domingues. Exercise training counteracts urothelial carcinoma-induced alterations in skeletal muscle mitochondria phospholipidome in an animal model. Under revision in Scientific Reports journal.

Exercise training counteracts urothelial carcinoma-induced alterations in skeletal muscle mitochondria phospholipidome in an animal model

Javier-Fernando Montero-Bullon[1], Tânia Melo[1,4], Rita Ferreira[1], Ana Isabel Padrão[1,2], Paula A. Oliveira[3], M Rosário M Domingues[1,4], Pedro Domingues[1*]

[1]Centro de Espectrometria de Massa, Departamento de Química & QOPNA, Universidade de Aveiro, Campus Universitário de Santiago, 3810-193 Aveiro, Portugal

[2]CIAFEL, Faculty of Sports, University of Porto, Porto, Portugal

[3]CITAB, Department of Veterinary Sciences, School of Agrarian and Veterinary Sciences, University of Trás-os-Montes and Alto Douro (UTAD), Vila Real, Portugal

[4]Departamento de Química & CESAM&ECOMARE, Universidade de Aveiro, Campus Universitário de Santiago, 3810-193 Aveiro, Portugal

*Corresponding author: Rosário Domingues, Department of Chemistry, Campus Universitário Santiago, 3810-193 Aveiro, Portugal. Email: mrd@ua.pt

Abstract

Cancer associated body wasting is the cause of physical disability, reduced tolerance to anticancer therapy and reduced survival of cancer patients and, similarly to cancer, its incidence is increasing. There is no cure for this clinical condition, and the pathophysiological process involved is largely unknown. Exercise training appears as the gold standard non-pharmacological therapy for the management of this wasting syndrome. Herein we used a lipidomics approach based on liquid chromatography coupled with high-resolution mass spectrometry (LC-HR-MS) to study the effect of exercise in the modulation of phospholipids profile of mitochondria isolated from *gastrocnemius* muscle of a pre-clinical model of urothelial carcinoma-related body wasting (BBN induced), submitted to 13 weeks of treadmill exercise after diagnosis. Multivariate analysis showed a close relationship between the BBN exercise group and both control groups (control sedentary and control exercise), while the BBN sedentary group was significantly separated from the control groups and the BBN exercise group. Univariate statistical analysis revealed differences mainly in phosphatidylserine (PS) and cardiolipin (CL), although some differences were also observed in phosphatidylinositol (PI, LPI) and phosphatidylcholine (PC) phospholipids. PS with shorter fatty acyl chains were up-regulated in the BBN sedentary group, while the other species of PS with longer FA and a higher degree of unsaturation were down-regulated, but the BBN exercise group was mostly similar to control groups. Remarkably, exercise training prevented these alterations and had a positive impact on the ability of mitochondria to produce ATP, restoring the healthy phospholipid profile. The remodelling of mitochondria phospholipid profile in rats with urothelial carcinoma allowed confirming the importance of the lipid metabolism in mitochondria dysfunction in cancer-induced skeletal muscle remodelling. The regulation of phospholipid biosynthetic pathways observed in the BBN exercise group supported the current perspective that exercise is an adequate therapeutic approach for the management of cancer-related muscle remodeling.

Keywords

lipidomics, cancer, body wasting, cardiolipin, phosphatidylserine

4.1. Introduction

The incidence of cancer has increased in the last years and, consequently, paraneoplastic syndromes such as cachexia have also increased. Cachexia is an insidious syndrome associated with cancer, estimated to occur in 60-80% of the cases, and is mainly characterized by body weight decrease due to skeletal muscle loss[1,2]. This muscle wasting contributes to physical disability, weakness, reduced tolerance to anticancer therapy and reduced survival of cancer patients [1,2]. Mitochondrial dysfunction is an early molecular event reported in cancer-related skeletal muscle wasting [3–6]. ATP production has been shown to be impaired[7], mainly due to the downregulation of oxidative phosphorylation (OXPHOS) complexes I, II, IV and V expression and activity[8,9], and by energy dissipation through uncoupling proteins (UCP)[8–10]. Changes in mitochondrial phospholipids profile has been described and seem to be mainly characterized by the decrease of cardiolipin (CL), its precursor phosphatidylglycerol (PG) and phosphatidic acid (PA), and by the increase of phosphatidylcholine (PC) and phosphatidylserine (PS) contents [8]. CL is the only lipid that is synthesized in mitochondria [11], where it performs a critical role in the organization of mammalian OXPHOS complexes and in the maintenance of inner mitochondrial membrane potential [11]. So, decreased levels of CL in mitochondria seem to explain, at least in part, the impaired ability of skeletal muscle from tumour-bearing animals to synthesize ATP [8]. Oxidative stress is also involved in cachexia and increased ROS cause oxidation of biomolecules, and could be one of the causes of decreased CL content and mitochondrial dysfunction[8,12].

Exercise training appears as the gold standard non-pharmacological therapy for increasing muscle function and counteracting the dramatic reduction of muscle strength and endurance that characterizes cancer cachexia [6,13–15]. The practice of exercise was shown to decrease the serum levels of pro-inflammatory cytokines[13,16,17], to increase muscle protein synthesis and attenuate proteolysis [10], and to improve mitochondrial dynamics[17,18]. Indeed, the benefits of exercise training on skeletal muscle involves mitochondrial adaptations mainly characterized by increased mitochondrial biogenesis, which are linked to improved metabolic health[19]. A single bout of endurance exercise was shown to induce a rapid and sustained increase of PGC-1α, a central player in mitochondria biogenesis in skeletal muscle[20]. Moreover, PGC-1α seems to mediate exercise training-related increase of the enzymes involved in CL and PI synthesis[21]. However, the molecular events underpinning the benefits of exercise training in counteracting cancer-induced muscle wasting, particularly the ones harboured in mitochondria, remain elusive.

In the present study, we use a lipidomics MS-based approach to study the effect of exercise in the modulation of phospholipids profile of mitochondria isolated from *gastrocnemius* muscle of a pre-clinical model of urothelial carcinoma-related body wasting submitted to 13 weeks of treadmill exercise after diagnosis. The identification of changes in the phospholipid profile permits to hypothesize about the physiological processes involved, and possible biomarkers and therapeutic targets of cancer-related muscle remodelling and physical exercise beneficial role.

4.2. Results

The phospholipidome of the total lipid extracts obtained from mitochondria of control rats (CTsed), healthy rats undertaking exercise (CTex), rats with urothelial carcinoma (BBNsed), and rats with urothelial carcinoma and submitted to exercise training (BBNex), were analysed by HILIC-MS and MS/MS and statistic analysis.

Data obtained from bladder histological analysis confirmed that animals from BBN groups developed urothelial lesions whereas animals from control groups did not develop any lesion. BBN-exposed animals with activity confined to the cage's space presented more aggressive lesions in the bladder and inflammation compared to exercised ones (data not shown). Morover, tumor-bearing animals evidenced significantly lower body weight ($p < 0.05$ vs CTsed; Table 1), suggestive of cachexia. Trained BBN rats also evidenced a 15% reduction of body mass ($p < 0.001$ vs. CTex; Table 1). No significant effect of BBN exposure was noticed on *gastrocnemius* mass; however, an approximately 10% increase of the ratio between gastrocnemius mass to body weight was noticed in BBNex group ($p < 0.05$ vs CTex; Table 1). The effect of BBN exposure was noticed in the ability of gastrocnemius muscle to produce ATP. Indeed, tumor-bearing animals showed a significant decrease in ATP synthase activity ($p<0.01$ vs CTsed) but exercise training counteracted this effect ($p<0.001$ vs BBNsed).

Table 1: Characterization of the animals` response to the BBN-induced muscle wasting and/or exercise training in terms of body weight, *gastrocnemius* mass and of the ratio *gastrocnemius*-to-body weight and mitochondrial ATP synthase activity.

	Experimental groups			
	CTsed	**BBNsed**	**CTex**	**BBNex**
body weight (g)	484.80 ± 31.90	440.66 ± 22.44*	502.70 ± 11.87	426.12 ± 33.51¥¥¥
***gastrocnemius* mass (g)**	4.92 ± 0.46	4.66 ± 0.31	5.18 ± 0.53	4.86 ± 0.41
***gastrocnemius*-to-body weight (mg/g)**	10.15 ± 0.68	10.57 ± 0.55	10.32 ± 1.20	11.42 ± 0.61¥
mitochondrial ATP synthase activity (µmol mg^{-1} min^{-1})	5.84 ± 0.56	4.58 ± 1.19**	6.80 ± 1.15	6.44 ± 1.45###

Values are expressed as mean ± standard deviation.

*p<0.05 vs CTsed; **p<0.01 vs CTsed; ###p<0.001 vs BBNsed; ¥p<0.05 vs CTex; ¥¥¥p<0.001 vs CTex.

Using high resolution LC-MS, mass accuracy and by interpretation of LC-MS/MS data we identified and semi-quantified 211 molecular species of 12 lipid classes: PC, LPC, SM, PE, LPE, Cer, PG, PI, LPI, PA, PS, and CL (Supplementary Table S1). The identification was made using as criteria the *m/z* value, the retention time and manual analysis of the MS/MS spectra (Supplementary Table S1, Figures S1-S12). The molecular species of the classes PC, LPC, SM, PE, LPE, Cer were identified as $[M+H]^+$ ions while PG, PI, LPI, PA, and PS, were identified as $[M-2H]^{2-}$ ions for CL.

The phospholipid profiles were then compared between the four conditions using univariate and multivariate analysis. To reduce the dimensionality of the data and visualize sample grouping, we performed principal component analysis (PCA) on the phospholipidomics data set. The visual observation of the PCA bi-plot for principal components 1 and 2 identified two outliers from the control exercise group (data not shown), which were removed from further analysis. The principal component analysis showed that the eigenvalues of the two first principal components represented 73.3% of the total variance (PC1 58.5%; PC2 14.8%) of the observations (Figure 1). Figure 1 also shows significant segregation of the four cohorts along the second dimension, which is related to the variability of the distributions, whereas the first dimension is influenced by the values of the means within cohorts. The PCA of lipid profiles showed a close relationship between the BBNex, CTsed and CTex groups, while the BBNsed group was significantly separated from the CTsed and CTex

groups. Remarkably, these results show that BBNex group is much more related to the CTsed group that of the BBNsed group.

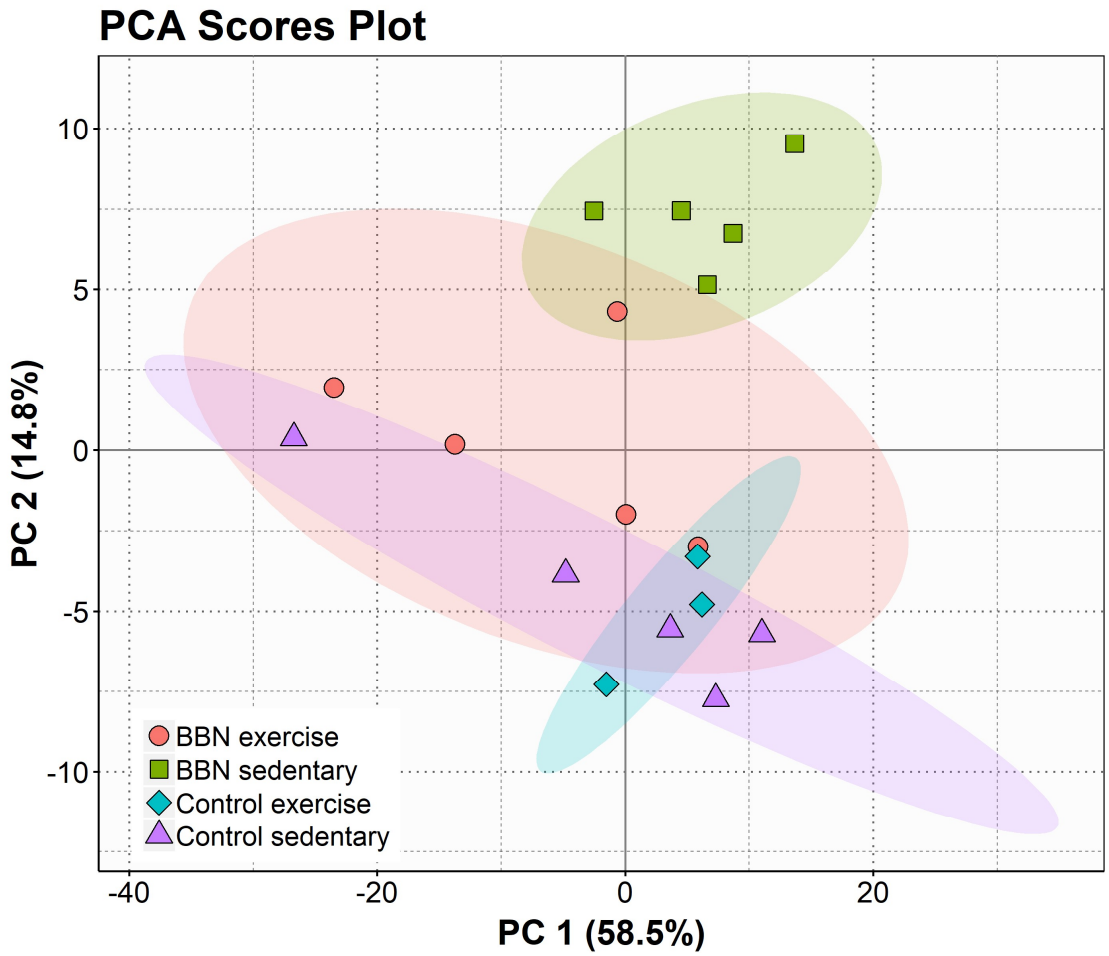

Figure 1: PCA score plot of the of the first two PCs of phospholipid data set acquired by LC-MS, of the four biological groups: Control sedentary, Control with exercise, urothelial cancer (BBN sedentary) and urothelial cancer submitted to exercise (BBN exercise).

We ranked the estimated coefficients (loadings) of component 2 of the PCA and selected the major 16 contributors. These species are shown in the box plots in figure 2. As it can be observed, the main contributors belong to PS (6 species) and CL (8 species). Figure 2 shows that a lower relative abundance of several CL species, independently of the number of carbons and unsaturations, occurs in the sedentary disease group (BBNsed). However, mitochondria from trained tumor-bearing rats (BBNex) presented relative abundances of CL at the levels of the control groups (CTex and CTsed). The PS content was found to be increased in the BBNsed group when compared with the CTsed, CTex and BBNex groups.

Species as PC(40:9) and the plasmenyl PEp(38:3) were also important species, both of them showing a tendency to have lower relative abundance in the control groups.

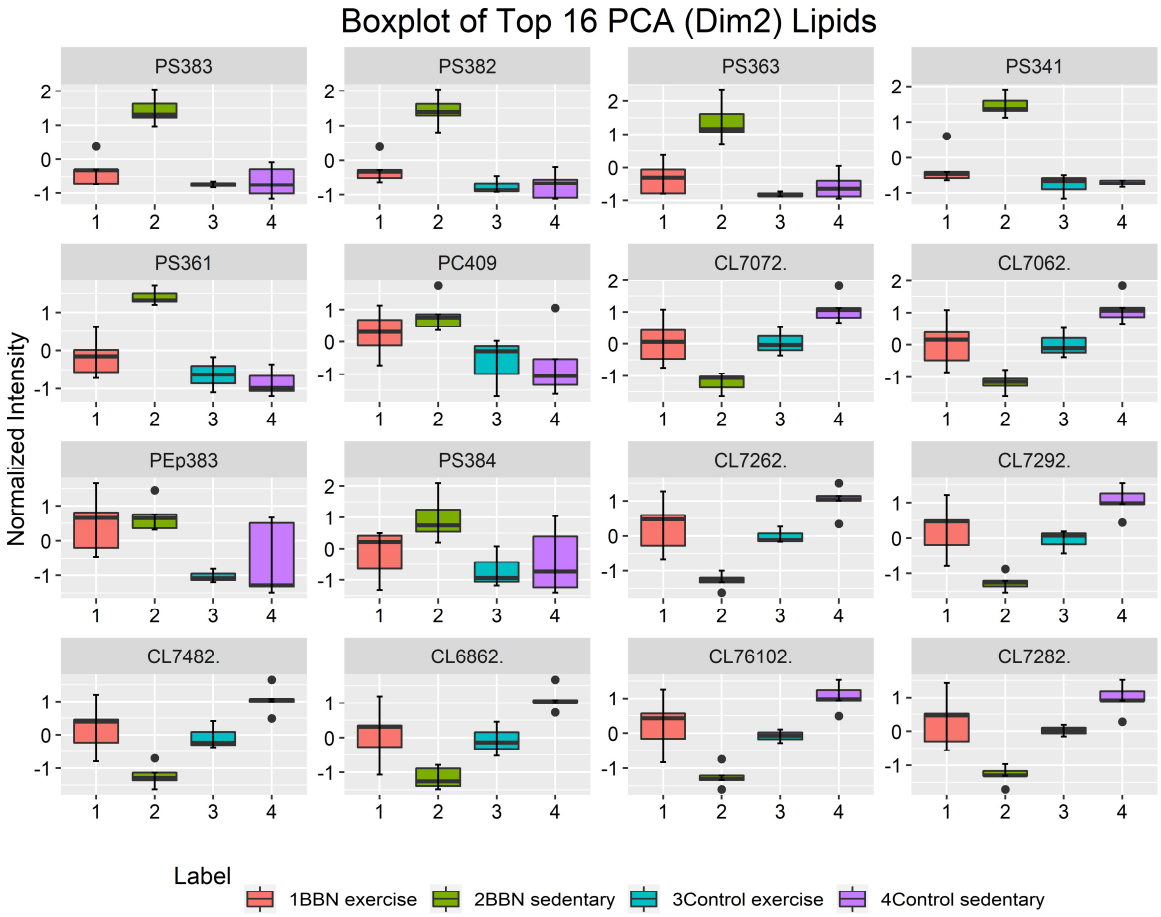

Figure 2: Boxplots of the 16 major phospholipid contributors of component 2 of the PCA. Labels of the species are according to the following notation: AAxxic (AA=lipid class; xx=total of carbon atoms in fatty acid; i=number of unsaturations; c=charge(cardiolipins)

We performed a *univariate analysis* (Kruskal-Wallis and the post hoc *Dunn's* multiple comparisons tests) of the various phospholipid species on the transformed dataset to test the association of these variables with the four clusters. This analysis allowed the identification of 45 species with $p<0.05$, although after FDR correction, all had a $p>0.05$ (Supplementary Table S2). Nevertheless, we have used the information from the univariate analysis to create a *dendrogram* with a two-dimensional hierarchical clustering, using the top 25 p-values phospholipid species ($p<0.02$) (Figure 3). The primary split in the upper hierarchical dendrogram shows that the samples clustered independently in two groups: one cluster for BBNSed group, and another one for the remaining groups. The clustering of

individual phospholipids with respect to their similarity in changes in phospholipid expression shows that they cluster in three groups. The first cluster of five PS species is clearly upregulated in disease BBNsed (cluster 3, figure 3B). A second group contains eighteen CL species that are decreased in the BBNSed group (cluster 3, figure 3B). And a third cluster includes LPI (16:0) and PC(42:10) also downregulated in the BBNSed group (cluster 1, figure 3B).

A

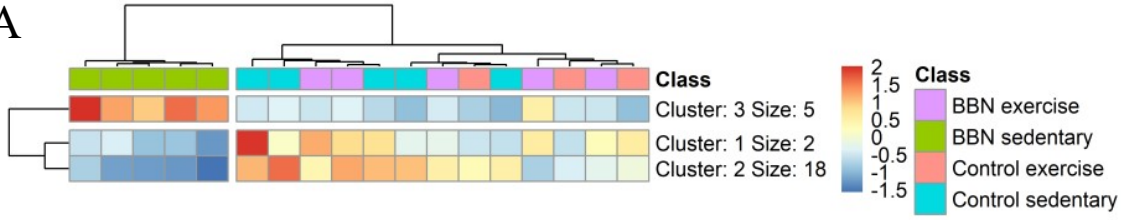

B

Cluster 1	Cluster 2	Cluster 3
LPI160	CL7411	PS341
PC4210	CL707	PS361
	CL7613	PS382
	CL729	PS363
	CL749	PS383
	CL7410	
	CL706	
	CL7611	
	CL7612	
	CL748	
	CL725	
	CL726	
	CL727	
	CL728	
	CL705	
	CL7610	
	CL686	
	CL685	

Figure 3: Two-dimensional hierarchical clustering heat map of the phospholipid data of the four studied groups. Levels of relative abundance are shown on the colour scale, with numbers indicating the fold difference from the mean (Figure 3A). The clustering of the sample groups is represented by the dendrogram in the top, showing a cluster for BBNSed group, and another one for the remaining groups. The clustering of individual phospholipid species with respect to their similarity in changes of relative abundance is represented by the dendrogram to the left, showing 3 clusters. The members of each of these clusters are

listed in figure 3B. Labels of the species are according to the following notation: AAxxic (AA=lipid class; xx=total of carbon atoms in fatty acid; i=number of unsaturations.

To conclude exploring the underlying phospholipid variations in the studied conditions, we undertook a pairwise phospholipid expression profiling analysis. The volcano plot displays significantly expressed phospholipid abundances against fold-change (log2 (ratio)) and p-value (-log10 (p-value), based on *Mann-Whitney* statistics for two treatments) (Figure 4). The volcano plot in Figure 4A showed the significant upregulated and downregulated differentially expressed phospholipids of the BBNsed versus the sedentary control group (CTsed). The volcano plot-based method revealed 35 differentially expressed phospholipids, of which 5 were upregulated in the BBNsed group, and 30 were downregulated. Downregulation was observed as the prominent regulation in tumor-bearing sedentary rats (BBNsed). The downregulated phospholipids comprised two different groups: Cardiolipins, with higher fold changes and lower p-values, and a different group with lower fold changes and higher p-values containing PS (4 species), PI (7 species) and LPI (1 species). Comparing with the sedentary control rats (CTsed), five PS were up-regulated in the sedentary rats that suffered from cachexia (BBNsed)((Supplementary Table S3). These PS contained shorter fatty acids (one C34, two C36 and two C38) than those that were upregulated (PS with C40 and C42).

The volcano plot in Figure 4B showed the significant upregulated and downregulated differentially expressed phospholipids of the BBNex versus the BBNsed groups. The volcano plot revealed 51 differentially expressed phospholipids, of which 44 were upregulated in the BBNsed group, and 7 were downregulated. The downregulated phospholipids comprised 6 PS with shorter chain fatty acid (four C36 and two C38) and one PA. Of the upregulated group, cardiolipins (17species), with lower fold changes and lower p-values were the most significant feature. Other up-regulated species included PI (10 species), LPE (10 species) PS (2 species), LPI (1 species), PG (1 species), PCp (1 species), PE (1 species), LPC (1 species). The volcano plot in Figure 4C showed the significant upregulated and downregulated differentially expressed phospholipids of the BBNex vs CTsed group. Remarkably, only one differential expressed phospholipid was observed, CL70:5, which was downregulated (Supplementary Table S3).

A

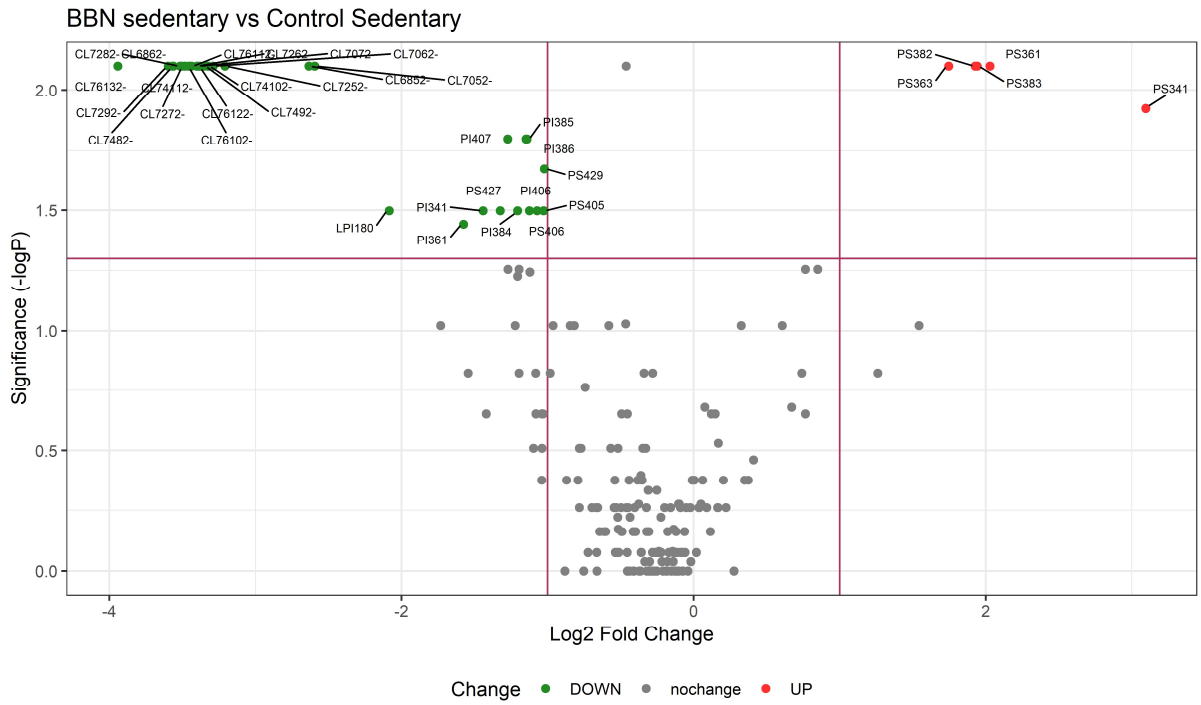
BBN sedentary vs Control Sedentary
Significance (-logP)
Log2 Fold Change
Change DOWN nochange UP

B

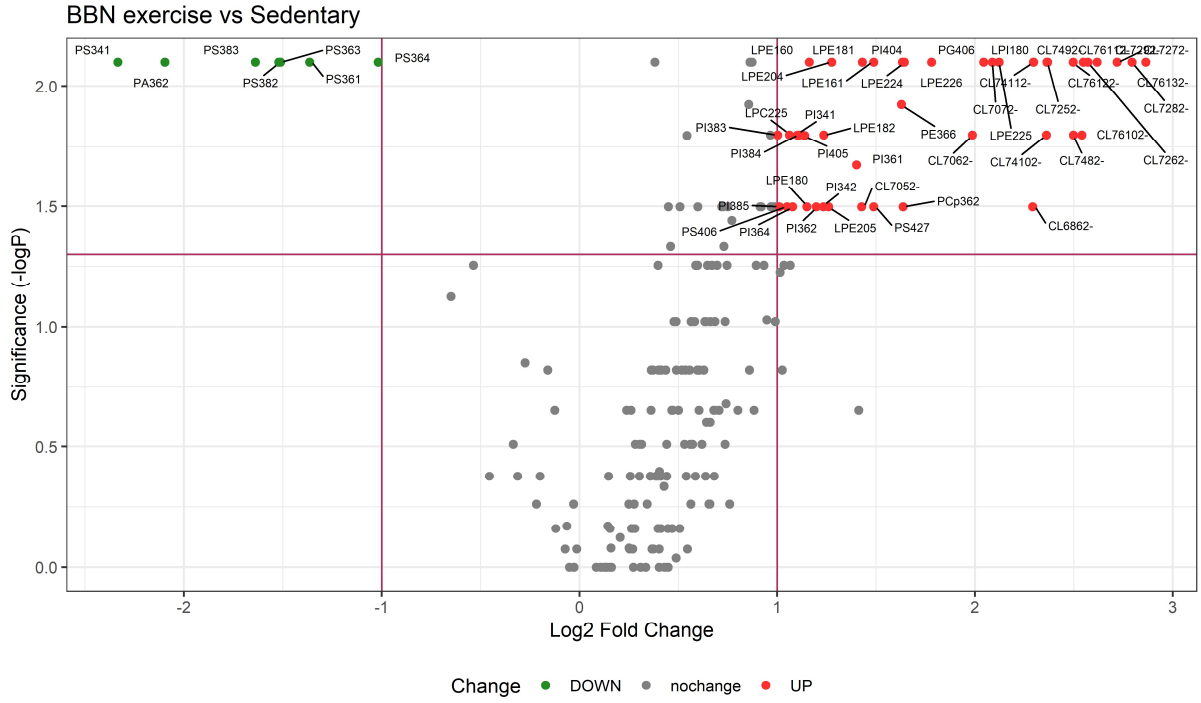
BBN exercise vs Sedentary
Significance (-logP)
Log2 Fold Change
Change DOWN nochange UP

C

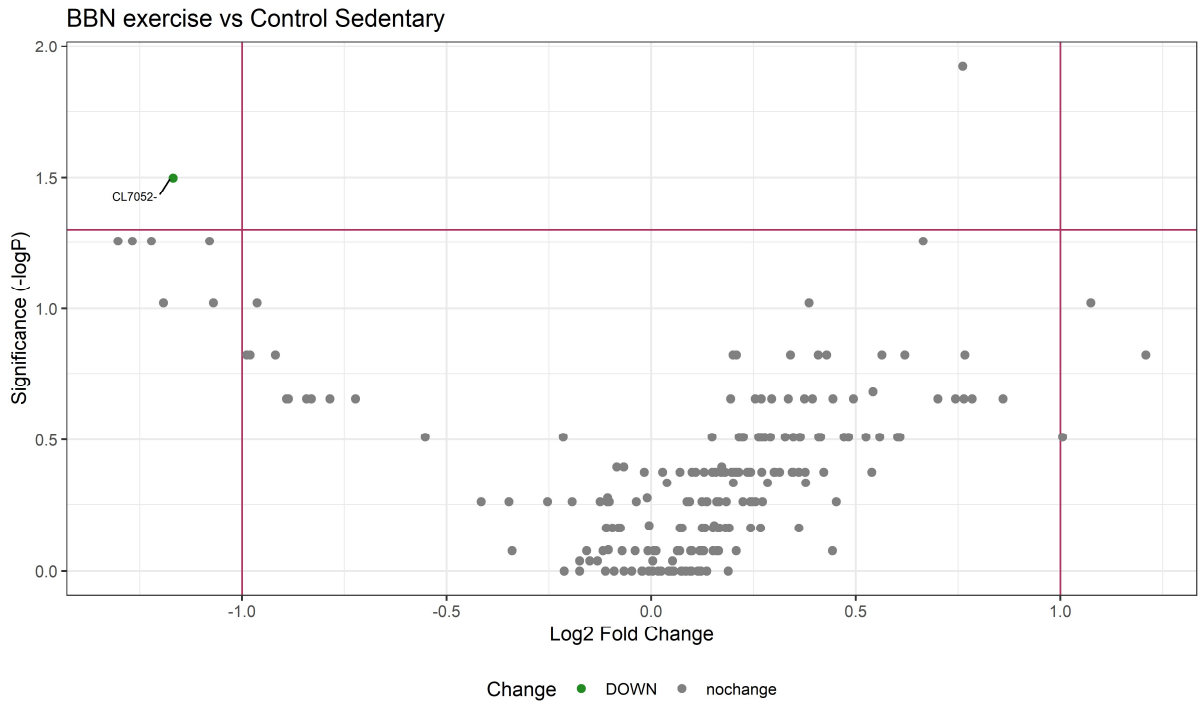

Figure 4: Volcano plot of all pairwise comparisons. Comparisons of all phospholipids from A) BBN sedentary (n = 5) vs control sedentary (n = 5); B) BBN sedentary (n = 5) vs BBN exercise (n = 5) and C) BBN exercise (n = 5) vs control sedentary (n = 5). The volcano plot displays the relationship between fold-change and significance between the two groups. Significant phospholipids were selected by fold change (>2- or < –2-fold) and adjusted *Mann-Whitney* p-value (<0.05). Each dot denotes a phospholipid. The dashed red line *shows* where p = 0.05 and fold change = 2. Phospholipids identified as significant are coloured in red and labelled on the plot. Labels of the species are according to the following notation: AAxxic (AA=lipid class; xx=total of carbon atoms in fatty acid; i=number of unsaturations; c=charge(cardiolipins)

4.3. Discussion

Body wasting is a major contributor to the high morbidity and mortality in cancer, but the molecular mechanism responsible for this condition remains unclear. Nevertheless, it is hypothesized that changes in mitochondrial functionality drive skeletal remodelling in cancer. Oxidative stress and alterations of the mitochondrial phospholipid composition has been strongly correlated to mitochondria malfunction[35]. To date, very few works addressed the relation between phospholipid composition and cancer-related muscle remodelling[36–38]

and only one was performed in mitochondria, reporting the variation of the relative content of few phospholipid classes related to skeletal muscle mitochondrial dysfunction in a rat model of urothelial carcinoma[8]. To the best of our knowledge, there are no studies that characterized the impact of exercise training on urothelial carcinoma-induced alterations in skeletal muscle mitochondrial lipidome.

In the present study, we report a comprehensive analysis of the variation of the mitochondrial phospholipidome of the skeletal muscle from rats with urothelial carcinoma, using high-resolution LC-MS, aiming to evaluate the beneficial effect of the exercise in cachexia. Multivariate principal component analysis (PCA) together with hierarchical cluster analysis (HCA) were used for data visualization and analysis. PCA revealed that CTsed, CTex and BBNex clustered in one group, but the BBNsed group clustered distinctly (Figure 1). In the PCA, the BBNex group clustered closely to both control groups, revealing a lipidic chemo-phenotype more closely related to the non-pathological conditions. This tendency supported that exercise has modulatory effects in the phospholipid metabolism and interferes with some of the molecular mechanisms involved in the development of cachexia. The 16 molecular species that mostly contributed to the PCA discrimination between conditions (Figure 2) included 6 PS with shorter fatty acyl chains and low degree of unsaturation, that were up-regulated in BBNsed, and 8 CL that were down-regulated in BBNsed. One PC and one pPE species were down-regulated in both BBN conditions.
We have selected the 25 more discriminant species, showing smaller p values in the univariate analysis, to create a dendrogram (Figure 3). The hierarchical clustering showed that in the primary dendrogram, there was noteworthy discrimination between BBNsed and the other groups, as previously shown in the PCA analysis. The secondary dendrogram produced 3 nodes with different composition in phospholipids; the first one included one LPI and one PC with long FA and unsaturated chains; the second was composed by CL species and the third with PS species with shorter FA. This also corroborates the tendency presented in the PCA, showing a closer phenotype of BBNex with CT groups, and the benefits of exercise in modulating the PL profile, particularly in PS and CL species.

To date, there is no effective pharmacological therapeutic approach to treat cancer-related body wasting; however, exercise training is known to promote benefit systemic and muscle adaptations, overcoming muscle maladaptive adaptations [6,14,39–43]. The results from our work showed that exercise training promoted a positive remodelling of the mitochondrial phospholipidome of the skeletal muscle from rats with urothelial carcinoma, evidenced by the increased ability to produce ATP, which seems to be associated with the regulation of

phospholipid metabolism. Indeed, exercise training of rats with urothelial carcinoma counteracted the down-regulation of major CL species and the up-regulation of PS (figures 4A and 4C). Also, comparing BBNsed and BBNex (figure 4B), we can see that there is an up-regulation of CL and PI species and a down-regulation of PS species in the exercised BBNex animals, corroborating the positive effect of exercise training in the regulation of PL profile in mitochondria in order to restore the healthier one. Altogether, these results also suggest that the modification of the phospholipid metabolism can be used to classify cancer cachexia since there is distinct mitochondrial phospholipidome phenotype for this group.

Cardiolipin is a dimeric phospholipid found almost exclusively in mitochondria and play essential roles in modulating the properties and the homeostasis of the membrane structure[44]. Also, this is a very important lipid class in the regulation of the activity of several mitochondria proteins, particularly oxidative phosphorylation (OXPHOS) complexes, and bioenergetics related proteins[45]. The decrease of CL content and disturbance of the CL profile was reported as an early event in apoptosis and to be present in several pathologies such as Barth syndrome[46] and others. Cardiolipin peroxidation in enhanced under oxidative stress condition and could be one of the main responsible for the decrease of CL and mitochondrial dysfunction and cell death[47]. In cancer, a decrease of mitochondria CL was found to be accompanied by a decrease in the expression of cytochrome c, and an increase of the ratio Bax/Bcl-2, and was correlated to OXPHOS dysfunction and consequently to muscle catabolism associated with cancer[8]. In the present study, we observed that the reduced ability of skeletal muscle mitochondria to produce ATP, was reverted by exercise (Table 1). Based on these results, we hypothesized that the decrease of mitochondrial ATP production is related to a decrease in the cardiolipin content, which negatively affects the mitochondrial function.

Alterations of PS profile in mitochondria have been scarcely addressed, and its effect in the mitochondrial function is still unknown. There is some evidence that PS is important for the mitochondria regulation, due to its role as a precursor of PE biosynthesis. PS is usually transported from the endoplasmatic reticulum to the mitochondria via mitochondria-associated membranes (MAM)[21]and is converted to PE in a reaction catalysed by the inner mitochondrial enzyme phosphatidylserine decarboxylase (PSD)[48]. The observed increase of PS in BBNsed could be due to impaired conversion of PS to PE. In fact, the lack of PS decarboxylase in PSD knockout mice was correlated with mitochondrial defects and dysfunction[49]. However, in this study, only very few PE species were down-regulated in BBNsed, most probably because the other PE biosynthetic routes in mitochondria also

regulate the PE levels. Interestingly, we saw an increase of LPE species when BBNex is compared with BBNsed (Figure 4B). LPE is a lysophospholipid recognized as an intercellular signalling molecule, but its function is far from being completely known[50]. LPE mobilizes intracellular Ca^{2+} through G-protein-coupled receptor (GPCR) in some cells types and was recently reported to exhibit anti-apoptotic activity in PC-12 cells[51] Very recently, it was reported that treatment of PISD patients, a mitochondrial disease gene encoding phosphatidylserine decarboxylase proenzyme, causing skeletal dysplasia, with lyso-PE allowed to restore mitochondrial morphology. In PISD, there is an impairment of the conversion of PS to PE and the administration of LPE seemed to increase the PE mitochondrial pool, restoring the normal mitochondrial function. Likewise, the increase of LPE with exercise, observed in this study, could be a factor contributing to balance the PE biosynthesis and reverting the mitochondrial dysfunction associated with cachexia.

In this work, a decrease of PI species in the BBNsed group was also observed, but its metabolic role in mitochondria is still unknown. However, PI seems to be correlated with the production of phosphatidylinositol (3,4,5)-trisphosphate (PIP3) and with signalling events[45]. This, it is expected that a change on the PI homeostasis impacts negatively on the mitochondrial function.

Skeletal muscle mitochondria have a unique phospholipid composition that is highly dynamic and can adapt to face different energetic demands. It was reported that the PL profile is adapted to diet and exercise training[21]. Upon moderate intensity exercise there was an upregulation of CL production, probably to face the high demand for energy[21]. Treadmill exercise training in rats appears to increase mitochondrial PC without affecting PE, CL or PI relative abundances[52]. In our work, no major alterations were observed between CTsed and CTex rats, but additional studies on exercise-induced adaptation of mitochondrial phospholipids are needed, taking in consideration the type, intensity and duration of training programs. However, our results provide strong molecular evidence of the mitochondrial phospholipidome remodelling promoted by exercise training on the set of cancer-related muscle remodelling . In conclusion, modification of the mitochondria phospholipidome was observed in the skeletal muscle in response to urothelial carcinoma, which could be correlated to mitochondria dysfunction. The observed phospholipid signature on this group was mainly characterized by a decrease of the content of cardiolipin and phosphatidylinositol, and an increased content of phosphatidylserine. Exercise training prevented these alterations and had a positive impact on the ability of mitochondria to produce ATP. While exercise had a limited impact in the phospholipidome in control rats,

exercise promoted a significant modification in tumor-bearing rats, restoring the healthy phospholipid profile.

4.4. Methods

4.4.1 Reagents/Chemicals

N-butyl-N-(4-hydroxybutyl)-nitrosamine (BBN) was purchased from Tokyo Kasey Kogyo (Japan). Phospholipids internal standards used were (1,3-bis[1,2-dimyristoyl-sn-glycero-3-phospho]-sn-glycerol) ($CL(14:0)_4$), 1,2-dimyristoyl-sn-glycero-3-phosphocholine (dMPC), 1-nonadecanoyl-2-hydroxy-sn-glycero-3-phosphocholine (LPC(19:0)), 1,2-dimyristoyl-sn-glycero-3-phosphoethanolamine (dMPE), 1,2-dimyristoyl-sn-glycero-3-phosphate (dMPA), 1,2-dimyristoyl-sn-glycero-3-phospho-(10-rac-glycerol) (dMPG), 1,2-dimyristoyl-sn-glycero-3-phospho-L-serine (dMPS), 1,2-dipalmitoyl-sn-glycero-3-phospho-(10-myo-inositol) (dPPI), N-heptadecanoyl-D-erythro-sphingosylphosphorylcholine (SM(17:0/d18:1)) and N-heptadecanoyl-D-erythro-sphingosine (Cer(17:0/d18:1)), purchased to Avanti polar lipids Inc (Alabaster, AL). Organic solvents (chloroform, methanol, acetonitrile), purchased from Fisher Scientific (Leicestershire, UK), were HPLC grade and used without further purification Ammonium acetate was purchased from Sigma-Aldrich (St. Louis, MO, USA), perchloric acid ($HClO_7$, 70%) and ammonium molybdate tetrahydrate ($(NH_4)_6Mo_7O_{24}\cdot 4H_2O$) from Panreac (Barcelona, Spain), ascorbic acid ($C_6H_8O_6$) from VWR International (Leicestershire, UK), sodium dihydrogen phosphate dihydrate ($NaH_2PO4\cdot 2H_2O$) from Riedel-de Haën (Seelze, Germany). MilliQ water was used, filtered through a 0.22 um filter in a Milli-Q Millipore system (MilliQ plus 185).

4.4.2 Animals and experimental design

Forty-four male Wistar rats (aged 5 weeks) were obtained from Harlan (Barcelona, Spain) and randomly housed in groups of 4 rats/cage, in a controlled environment at 22 ± 2ºC of temperature and 60 ± 5% of relative humidity with 12/12 hour dark-light inverted cycle, with free access to food (standard laboratory diet 4RF21®, Mucedola, Italy) and water. After one week of acclimatization, the animals were randomly divided into two experimental groups: exposed to 0.05 % BBN in the drinking water over the course of 20 weeks (BBN group, n=24) and with access to tap water (CT, n=20). After this 20 week-period, half of the animals from each group started an exercise program in a treadmill running for 13 weeks (subgroups

BBNex (n=12) and CTex (n=10)). The animal protocol was approved by the Portuguese Ethics Committee for Animal Experimentation, Direção Geral de Alimentação e Veterinária (license number 008962) and was performed in accordance with the European Directive 2010/63/EU.

Animals from the EX group were submitted to a treadmill exercise training program on an electric treadmill (Treadmill Control® LE 8710, Panlab, Harvard Apparatus, ISA) for 13 weeks during 5 days/week. In the first two weeks, exercise duration and treadmill speed were gradually increased until it reached 60 min per day at 20 m per min, which was maintained for 11 weeks. At the end of the experimental protocol, all animals were weighed and sacrificed with ketamine/xylazine (Imalgen® and Rompun®, respectively). All noticeable tumours were counted and removed for histological analysis. Gastrocnemius muscle was removed, weighed, and immediately prepared for mitochondria isolation.

4.4.3 Mitochondria isolation from gastrocnemius muscle

Mitochondria isolation was performed using the conventional methods of differential centrifugation, as previously described[22] All the procedures were performed on ice or below 4 °C. Briefly, muscles were immediately excised and minced in ice-cold isolation medium containing 100mM sucrose, 0.1mM ethylene glycol tetraacetic acid, 50mM Tris–HCl, 100mM KCl, 1mM KH_2PO_4, and 0.2% free fatty acid bovine serum albumin (BSA), pH 7.4. Minced blood-free tissue was rinsed and suspended in 10 mL of fresh medium containing 0.2 mg/mL bacterial proteinase (Nagarse E.C.3.4.21.62, type XXVII; Sigma) and stirred for 2 min. The sample was then carefully homogenized with a tightly fitted Potter-Elvehjem homogenizer and a Teflon pestle. An aliquot of homogenized was separated for biochemical analysis. After homogenization, three volumes of Nagarse-free isolation medium were added to the homogenate, which was then centrifuged at 700 g for 10 min. The resulting supernatant suspension was centrifuged at 10,000g for 10 min. The pellet was gently re-suspended in the isolation medium (1.3 mL/100 mg initial tissue) and centrifuged at 7000g for 3 min. The final pellet, containing the mitochondrial fraction, was gently re-suspended (0.4 mL/mg initial tissue) in a medium containing 225mM mannitol, 75mM sucrose, 10mM Tris, and 0.1mM EDTA, pH 7.4. Mitochondrial protein content was determined using the Bio-Rad RC-DC assay.

4.4.4 Determination of ATP synthase

The activity of ATP synthase was measured as previously described[8] In brief, the phosphate produced by the hydrolysis of ATP reacts with ammonium molybdate, in the presence of reducing agents, forming a blue-colour complex. The colour intensity was proportional to the concentration of phosphate in solution. Optical densities were measured at 610 nm in a Multiskan GO Microplate Spectrophotometer (Thermo Scientific). Oligomycin was used as an inhibitor of mitochondrial ATPase activity.

4.4.5 Extraction of mitochondrial phospholipids

Lipid extraction of each mitochondrial fraction was performed according to the Bligh and Dyer method[23]. Briefly, 3.75 mL of chloroform/methanol 1:2 (v/v) was added to 1 mL of mitochondrial fraction (corresponding approximately to 8 mg of protein). Then, the tubes were well-vortexed and incubated on ice for 30 min (vortex every 5 min). An additional volume of 1.25 mL chloroform and 1.25 mL milli-Q H_2O were added. Finally, following vigorous vortex, samples were centrifuged at 1000 rpm ((Mixtasel centrifuge, Selecta), for 5 min at room temperature to obtain a two-phase system: aqueous top phase and organic bottom phase from which lipids were obtained. The organic phase was collected to a new tube, and the aqueous phase was washed with 1.88 mL of chloroform. At last, the extracts were dried in a nitrogen flow, dissolved in 1 mL of chloroform for subsequent quantification by the phosphorus assay.

4.4.6 Quantification of phospholipids content by phosphorus assay

The total amount of phospholipids in each lipid extract was determined in two replicate experiments by Barlett and Lewis colourimetric assay, based on the measurement of inorganic phosphorus. Briefly, an aliquot of 10 µL of the extract was dried and incubated 1h at 180 °C with 125 µL of perchloric acid (70%) in a heating block (Stuart, U.K.) to hydrolyse the inorganic phosphorus of the phospholipids. Afterwards, and once cooled down to room temperature, the solutions were mixed by vortexing with 825 µL of MilliQ water, 125 µL of ammonium molybdate tetrahydrate 2.5% and 125 µL of ascorbic acid 10% freshly prepared. Samples and standards (8 standards solutions, with different concentrations of phosphorus) were simultaneously incubated at 100ºC in a water bath for 10 min and cooled down. The content of inorganic acid was measured in a microplate spectrophotometer (Multiscan 90, ThermoScientific) at 797 nm.

4.4.7 HILIC-ESI-MS and MS/MS

An amount of lipid extract equivalent to 5 µg of total phospholipid in 5 µL of chloroform was mixed with 4 µL of the standards solution (0.02 µg dMPC, 0.02 µg dMPE, 0.04 µg dMPS, 0.012 µg dMPG, 0.08 µg dMPA, 0.08 µg dPPI, 0.02 µg SM(17:0/d18:1), 0.02 µg Cer(17:0/d18:1), 0.08 µg $CL(14:0)_4$ and 0.02 µg LPC(19:0)) and 91µL of initial HPLC conditions solvent mixture. For the HPLC-MS analysis, 5 µL were injected in an Ultimate 3000 Dionex ultra high-performance LC (UHPLC) system (Thermo Fisher Scientific, Bremen, Germany) coupled to a Q-Exactive hybrid quadrupole mass spectrometer (Thermo Fisher, Scientific, Bremen, Germany). A microbore chromatographic column Ascentis Si HPLC column, 15 cm length×1.0mm internal diameter×3 µm particle size(Sigma–Aldrich) was used for the separation. A biphasic gradient was used with solvents A (25% water / 50% acetonitrile / 25% methanol (v/v/v), 1 mM of ammonium acetate) and B (60% acetonitrile /40% methanol (v/v), 1 mM of ammonium acetate). Initial condition with 40% of mobile phase A was held isocratically for 8 min, followed by a linear increase to 60% of A within 7 min and an isocratic period of 5 min, and return to the initial condition in linear decrease during 5 min with final 10 min of equilibration. The flow rate through the column was established 40 µL/min and the temperature at 30 ºC. The Q-Exactive Orbitrap was operated with a HESI source simultaneously in positive mode (3kV) and negative mode (-2.7kV), with capillary temperature 250ºC, and sheath gas flow 15U and auxiliary gas 5U. The MS spectra were acquired at high resolution (70,000), with the AGC target set to $10E^6$ and maximum injection time of 200 ms. MS^2 spectra were acquired in a different run and separately for positive and negative mode, with a pool of all the replicates of each condition adjusted to the same concentration as each replicate. For MS^2, a ten data-dependent MS/MS scans were repeated continuously throughout the experiments with a resolution of 17500, AGC target of $1E^5$, maximum injection time of 50 ms, minimum intensity threshold of $1E^4$, dynamic exclusion of 60 s, APEX trigger of 10 to 30 s, and isolation window of 1Da. The normalized collision energy was stepped (25,30,35). Data acquisition was carried out using the Xcalibur data system (V3.3, Thermo Fisher Scientific, Waltham, MA, USA).

4.4.8 Data analysis and statistics

Data from LC-MS and MS/MS was analysed with XCalibur Qual Browser (Thermo Fisher Scientific, Waltham, MA, USA) for chromatographic, high-accuracy MS and MS^2

identification of species. LC-MS data was checked against a the theoretic list of species, with exact *m/z* values of species that were probable and with retention times adapted based on the internal standard for each PL class. The program MZmine 2.26[24] was used for high-resolution identification (5ppm) including retention time alignment, and plotting the chromatograms of the identified species together with the quantification of the area under the curve. Data pre-processing including baseline correction, peak deconvolution, deisotoping, alignment, and gap-filling was applied. Data of the area of each species was exported to an Excel data spreadsheet (Excel, Microsoft, Redmond, WA) and normalized by the ratio against a selected internal standard. The internal standards were endogenously non-occurring PL species, and each standard is employed for normalization of all the species of its class.

Multivariate and univariate analyses were performed using R version 3.5[25] in Rstudio version 1.1.4[26]. Data were glog transformed and autoscaled using the R package Metaboanalyst[27]. Principal Component Analysis (PCA) was conducted for exploratory data analysis, with the R built-in function and ellipses were drawn using the R package ellipse[28], assuming a multivariate normal distribution and a level of 0.95. *Kruskal-Wallis* test *followed by Dunn's post-hoc* comparisons were performed with the R built-in function. Heatmaps were created using the R package pheatmap[29] using "Euclidean" as clustering distance, and "ward.D" as the clustering method. Finally, volcano plots of fold change vs significance for a pairwise comparison using Wilcoxon test were performed in R. All graphics and boxplots were created using the R package ggplot2[30]. Other R packages used for data management and graphics included plyr[31], dplyr[32], tidyr[33] and ggrepel[34].

Acknowledgements

This work was supported by funding from European Commission's Horizon 2020 research and innovation programme under the Marie Sklodowska-Curie grant agreement number 675132 (MSCA-ITN-ETN MASSTRPLAN). Thanks are due for the financial support to to QOPNA research Unit (FCT UID/QUI/00062/2019), to CESAM (UID/AMB/50017 - POCI-01-0145-FEDER-007638), to the Portuguese Mass Spectrometry Network (LISBOA-01-0145-FEDER-402-022125), to FCT/MCTES through national funds (PIDDAC), and the co-funding by the FEDER, within the PT2020 Partnership Agreement and Compete 2020.

References

1. Mattox, T. W. Cancer Cachexia: Cause, Diagnosis, and Treatment. *Nutr. Clin. Pract.* **32,** 599–606 (2017).

2. Argilés, J. M., Busquets, S., Stemmler, B. & López-Soriano, F. J. Cancer cachexia: Understanding the molecular basis. *Nat. Rev. Cancer* **14,** 754–762 (2014).

3. van der Ende, M. *et al.* Mitochondrial dynamics in cancer-induced cachexia. *Biochim. Biophys. Acta - Rev. Cancer* **1870,** 137–150 (2018).

4. Argilés, J. M., López-Soriano, F. J. & Busquets, S. Muscle wasting in cancer: The role of mitochondria. *Curr. Opin. Clin. Nutr. Metab. Care* **18,** 221–225 (2015).

5. Vanderveen, B. N., Fix, D. K. & Carson, J. A. Disrupted Skeletal Muscle Mitochondrial Dynamics, Mitophagy, and Biogenesis during Cancer Cachexia: A Role for Inflammation. *Oxid. Med. Cell. Longev.* **2017,** 24–27 (2017).

6. Vitorino, R., Moreira-Gonçalves, D. & Ferreira, R. Mitochondrial plasticity in cancer-related muscle wasting: Potential approaches for its management. *Curr. Opin. Clin. Nutr. Metab. Care* **18,** 226–233 (2015).

7. Argilï¿½s, J. *et al.* Nuclear magnetic resonance in conjunction with functional genomics suggests mitochondrial dysfunction in a murine model of cancer cachexia. *Int. J. Mol. Med.* **27,** 15–24 (2010).

8. Antunes, D. *et al.* Molecular insights into mitochondrial dysfunction in cancer-related muscle wasting. *Biochim. Biophys. Acta - Mol. Cell Biol. Lipids* **1841,** 896–905 (2014).

9. TZIKA, A. A. *et al.* Skeletal muscle mitochondrial uncoupling in a murine cancer cachexia model. *Int. J. Oncol.* **43,** 886–894 (2013).

10. Padrão, A. I. *et al.* Bladder cancer-induced skeletal muscle wasting: Disclosing the role of mitochondria plasticity. *Int. J. Biochem. Cell Biol.* **45,** 1399–1409 (2013).

11. Haines, T. H. & Dencher, N. A. Cardiolipin: a proton trap for oxidative phosphorylation. *FEBS Lett.* **528,** 35–9 (2002).

12. Ábrigo, J. *et al.* Role of Oxidative Stress as Key Regulator of Muscle Wasting during Cachexia. *Oxid. Med. Cell. Longev.* **2018,** 1–17 (2018).

13. Padrão, A. I. *et al.* Long-term exercise training prevents mammary tumorigenesis-induced muscle wasting in rats through the regulation of TWEAK signalling. *Acta Physiol.* **219,** 803–813 (2017).

14. Argilés, J. M., Busquets, S., López-Soriano, F. J., Costelli, P. & Penna, F. Are there any benefits of exercise training in cancer cachexia? *J. Cachexia. Sarcopenia Muscle* **3,** 73–76 (2012).

15. Morley, J. E., Anker, S. D. & von Haehling, S. Prevalence, incidence, and clinical impact of sarcopenia: facts, numbers, and epidemiology-update 2014. *J. Cachexia. Sarcopenia Muscle* **5,** 253–259 (2014).

16. Hardee, J. P. *et al.* Eccentric contraction-induced myofiber growth in tumor-bearing mice. *J. Appl. Physiol.* **120,** 29–37 (2016).

17. Puppa, M. J. *et al.* The effect of exercise on IL-6-induced cachexia in the Apc Min /+ mouse. *J. Cachexia. Sarcopenia Muscle* **3,** 117–137 (2012).

18. Pigna, E. *et al.* Aerobic Exercise and Pharmacological Treatments Counteract

Cachexia by Modulating Autophagy in Colon Cancer. *Sci. Rep.* **6,** 26991 (2016).

19. Trewin, A., Berry, B. & Wojtovich, A. Exercise and Mitochondrial Dynamics: Keeping in Shape with ROS and AMPK. *Antioxidants* **7,** 7 (2018).

20. Hawley, J. A., Hargreaves, M., Joyner, M. J. & Zierath, J. R. Integrative Biology of Exercise. *Cell* **159,** 738–749 (2014).

21. Heden, T. D., Neufer, P. D. & Funai, K. Looking Beyond Structure: Membrane Phospholipids of Skeletal Muscle Mitochondria. *Trends Endocrinol. Metab.* **27,** 553–562 (2016).

22. Tonkonogi, M. & Sahlin, K. Rate of oxidative phosphorylation in isolated mitochondria from human skeletal muscle: effect of training status. *Acta Physiol. Scand.* **161,** 345–353 (1997).

23. Bligh, E. G. & Dyer, W. J. A rapid method of total lipid extraction and purification. *Can. J. Biochem. Physiol.* **37,** 911–917 (1959).

24. Pluskal, T., Castillo, S., Villar-Briones, A. & Oresic, M. MZmine 2: modular framework for processing, visualizing, and analyzing mass spectrometry-based molecular profile data. *BMC Bioinformatics* **11,** 395 (2010).

25. R Core Team. R: A language and environment for statistical computing.R Foundation for Statistical Computing, Vienna, Austria. (2018).

26. Rstudio Team. RStudio: Integrated Development Environment for R. (2016).

27. Xia, J. & Wishart, D. S. Using MetaboAnalyst 3.0 for Comprehensive Metabolomics Data Analysis. in *Current Protocols in Bioinformatics* **55,** 14.10.1-14.10.91 (John Wiley & Sons, Inc., 2016).

28. Murdoch, D. & Chow, E. ellipse: Functions for drawing ellipses and ellipse-like confidence regions. R package version 0.4.1. (2018).

29. Kolde, R. pheatmap: Pretty Heatmaps. R package version 1.0.12. (2019).

30. Wickham, H. ggplot2 – Elegant Graphics for Data Analysis. Springer Verlag New York. (2016).

31. Wickham, H. The Split-Apply-Combine Strategy for Data Analysis. *J. Stat. Softw.* **40,** (2011).

32. Wickham, H., François, R., Henry, L. & Müller, K. dplyr: A Grammar of Data Manipulation. R package version 0.7.7. (2018).

33. Wickham, H. & Henry, L. tidyr: Easily Tidy Data with ‘spread()’ and ‘gather()’ Functions. (2018).

34. Slowikowski, K. ggrepel: Automatically Position Non-Overlapping Text Labels with ‘ggplot2’. R package version 0.8.0. (2018).

35. Dalal, S. Lipid metabolism in cancer cachexia. *Ann. Palliat. Med.* **8,** 13–23 (2019).

36. Penet, M.-F. *et al.* Metabolic Signatures Imaged in Cancer-Induced Cachexia. *Cancer Res.* **71,** 6948–6956 (2011).

37. Winnard, P. T. *et al.* Detection of Pancreatic Cancer-induced Cachexia using a Fluorescent Myoblast Reporter System and Analysis of Metabolite Abundance Running Title: Imaging pancreatic cancer-induced cachexia. (2015).

doi:10.1158/0008-5472.CAN-15-1740

38. Kliewer, K. L. *et al.* Adipose tissue lipolysis and energy metabolism in early cancer cachexia in mice. *Cancer Biol. Ther.* **16,** 886–897 (2015).

39. Lira, F. S., Neto, J. C. R. & Seelaender, M. Exercise training as treatment in cancer cachexia. *Appl. Physiol. Nutr. Metab.* **39,** 679–686 (2014).

40. Ardies, C. M. Exercise, Cachexia, and Cancer Therapy: A Molecular Rationale. *Nutr. Cancer* **42,** 143–157 (2002).

41. Gould, D. W., Lahart, I., Carmichael, A. R., Koutedakis, Y. & Metsios, G. S. Cancer cachexia prevention via physical exercise: molecular mechanisms. *J. Cachexia. Sarcopenia Muscle* **4,** 111–124 (2013).

42. Hardee, J. P., Counts, B. R. & Carson, J. A. Understanding the Role of Exercise in Cancer Cachexia Therapy. *Am. J. Lifestyle Med.* 155982761772528 (2017). doi:10.1177/1559827617725283

43. Battaglini, C. *et al.* Cancer Cachexia: Muscle Physiology and Exercise Training. *Cancers (Basel).* **4,** 1247–1251 (2012).

44. Lopes, S. C., Ivanova, G., de Castro, B. & Gameiro, P. Revealing cardiolipins influence in the construction of a significant mitochondrial membrane model. *Biochim. Biophys. Acta - Biomembr.* **1860,** 2465–2477 (2018).

45. Mejia, E. M. & Hatch, G. M. Mitochondrial phospholipids: role in mitochondrial function. *J. Bioenerg. Biomembr.* **48,** 99–112 (2016).

46. Schlame, M. & Ren, M. Barth syndrome, a human disorder of cardiolipin metabolism. *FEBS Lett.* **580,** 5450–5455 (2006).

47. Bayir, H. & Kagan, V. E. Bench-to-bedside review: Mitochondrial injury, oxidative stress and apoptosis – there is nothing more practical than a good theory. *Crit. Care* **12,** 206 (2008).

48. Szymański, J. *et al.* Interaction of Mitochondria with the Endoplasmic Reticulum and Plasma Membrane in Calcium Homeostasis, Lipid Trafficking and Mitochondrial Structure. *Int. J. Mol. Sci.* **18,** 1576 (2017).

49. Steenbergen, R. *et al.* Disruption of the Phosphatidylserine Decarboxylase Gene in Mice Causes Embryonic Lethality and Mitochondrial Defects. *J. Biol. Chem.* **280,** 40032–40040 (2005).

50. Lee, J.-M., Park, S.-J. & Im, D.-S. Calcium Signaling of Lysophosphatidylethanolamine through LPA $_1$ in Human SH-SY5Y Neuroblastoma Cells. *Biomol. Ther. (Seoul).* **25,** 194–201 (2017).

51. Nishina, A. *et al.* Lysophosphatidylethanolamine in *Grifola frondosa* as a neurotrophic activator via activation of MAPK. *J. Lipid Res.* **47,** 1434–1443 (2006).

52. Dohm, G. L., Barakat, H., Stephenson, T. P., Pennington, S. N. & Tapscott, E. B. Changes in muscle mitochondrial lipid composition resulting from training and exhaustive exercise. *Life Sci.* **17,** 1075–80 (1975).

4.5. Supplementary information

Supplementary Table S 1: Summary for LC-MS and MS/MS identification of the phospholipid molecular species that were quantified in the present study. Fatty acyl chain composition was deduced from the carboxylate ions observed in negative mode. In the cases in which a positive charge ion was chosen for the detection, the negative ion counterpart was checked to assign the fatty acyl chain composition. Exceptionally, sphingomyelins and ceramides fatty acyl composition was observed in positive mode based on the sphingoid base ions. Species are annotated as: PL(C:N), where PL is the phospholipid class, C the number of carbons and N the number of double bonds

Species assigned	Ion	Exact m/z	Observed m/z	Error (ppm)	RT	Most probable fatty acyl chain content according to MS^2 data
Cer(d34:1)	$[M+H]^+$	538.5194	538.5206	2.2	3.4	(d18:1/16:0)
Cer(d36:1)	$[M+H]^+$	566.5507	566.5521	2.5	3.4	(d18:1/18:0)
Cer(d36:2)	$[M+H]^+$	564.5350	564.5363	2.3	3.4	-
Cer(d38:1)	$[M+H]^+$	594.5820	594.5828	1.3	3.4	(d18:1/20:0)
Cer(d38:2)	$[M+H]^+$	592.5663	592.5678	2.5	3.4	-
Cer(d40:1)	$[M+H]^+$	622.6133	622.6140	1.1	3.4	(d18:1/22:0)
Cer(d42:1)	$[M+H]^+$	650.6446	650.6456	1.6	3.4	(d18:1/24:0)
Cer(d42:2)	$[M+H]^+$	648.6289	648.6300	1.7	3.4	(d18:1/24:1)
CL(68:5)	$[M-2H]^{2-}$	698.4710	698.4703	-1.0	2.7	(16:1/16:1/18:0/18:3)
CL(68:6)	$[M-2H]^{2-}$	697.4632	697.4639	1.0	2.6	(16:1/16:1/18:2/18:2)
CL(70:5)	$[M-2H]^{2-}$	712.4867	712.4840	-3.8	2.7	-
CL(70:6)	$[M-2H]^{2-}$	711.4788	711.4771	-2.3	2.6	(16:1/18:1/18:2/18:2)
CL(70:7)	$[M-2H]^{2-}$	710.4710	710.4711	0.2	2.6	(16:1/18:2/18:2/18:2) (16:2/18:1/18:2/18:2)
CL(72:5)	$[M-2H]^{2-}$	726.5023	726.4988	-4.9	2.7	(18:0/18:1/18:2/18:2)
CL(72:6)	$[M-2H]^{2-}$	725.4945	725.4915	-4.2	2.6	(18:0/18:1/18:2/18:3)
CL(72:7)	$[M-2H]^{2-}$	724.4840	724.4828	-1.6	2.6	(18:0/18:2/18:2/18:3) (18:1/18:2/18:2/18:2)
CL(72:8)	$[M-2H]^{2-}$	723.4788	723.4796	1.1	2.6	(18:2/18:2/18:2/18:2)
CL(72:9)	$[M-2H]^{2-}$	722.4710	722.4731	2.9	2.6	(18:2/18:2/18:2/18:3)
CL(74:10)	$[M-2H]^{2-}$	735.4788	735.4805	2.4	2.6	(18:2/18:2/18:2/20:4)
CL(74:11)	$[M-2H]^{2-}$	734.4710	734.4729	2.5	2.6	(16:1/18:2/18:2/22:6)
CL(74:8)	$[M-2H]^{2-}$	737.4945	737.4931	-1.8	2.6	(18:1/18:2/18:3/20:2) (18:1/18:1/18:3/20:3)
CL(74:9)	$[M-2H]^{2-}$	736.4867	736.4852	-2.1	2.6	(18:2/18:2/18:3/20:2)
CL(76:10)	$[M-2H]^{2-}$	749.4945	749.4915	-3.9	2.6	(16:0/16:0/22:5/22:5) (18:1/18:1/18:2/22:6) (18:0/18:2/18:2/22:6)

CL(76:11)	$[M-2H]^{2-}$	748.4867	748.4856	-1.5	2.6	(16:0/16:0/22:5/22:6) (16:0/18:0/20:5/22:6) (18:1/18:2/18:2/22:6)
CL(76:12)	$[M-2H]^{2-}$	747.4788	747.4807	2.6	2.6	(16:0/16:0/22:6/22:6) (18:1/18:2/18:3/22:6) (18:0/18:3/18:3/22:6)
CL(76:13)	$[M-2H]^{2-}$	746.4710	746.4702	-1.1	2.6	(16:0/16:1/22:6/22:6) (18:0/18:3/20:5/20:5) (18:1/18:2/20:5/20:5)
LPC(16:0)	$[M+H]^{+}$	496.3398	496.3411	2.6	12.6	-
LPC(16:1)	$[M+H]^{+}$	494.3241	494.3253	2.4	12.7	(16:1)
LPC(18:0)	$[M+H]^{+}$	524.3711	524.3724	2.4	12.1	(18:0)
LPC(18:1)	$[M+H]^{+}$	522.3554	522.3574	3.8	12.3	(18:1)
LPC(18:2)	$[M+H]^{+}$	520.3398	520.3375	-4.3	12.4	(18:2)
LPC(18:3)	$[M+H]^{+}$	518.3241	518.3232	-1.8	12.6	(18:3)
LPC(20:3)	$[M+H]^{+}$	546.3554	546.3548	-1.0	12.1	-
LPC(20:4)	$[M+H]^{+}$	544.3398	544.3400	0.4	11.3	(20:4)
LPC(20:5)	$[M+H]^{+}$	542.3241	542.3235	-1.2	12.4	(20:5)
LPC(22:4)	$[M+H]^{+}$	572.3711	572.3705	-1.1	11.8	-
LPC(22:5)	$[M+H]^{+}$	570.3554	570.3554	0.1	11.3	-
LPC(22:6)	$[M+H]^{+}$	568.3398	568.3415	3.0	11.2	(22:6)
LPCp(16:1)	$[M+H]^{+}$	480.3448	480.3460	2.5	12.0	-
PA(36:2)	[M-H]-	699.4952	699.497	0.0	3.8	(16:0/20:2) (18:0/18:2) (18:1/18:1)
PC(32:0)	$[M+H]^{+}$	734.5694	734.5704	1.4	8.8	(16:0/16:0)
PC(32:1)	$[M+H]^{+}$	732.5538	732.5517	-2.8	8.8	(16:0/16:1)
PC(32:2)	$[M+H]^{+}$	730.5381	730.5401	2.7	8.7	(16:1/16:1)
PC(34:1)	$[M+H]^{+}$	760.5851	760.5838	-1.8	8.6	(16:0/18:1) (16:1/18:0)
PC(34:2)	$[M+H]^{+}$	758.5694	758.5715	2.7	8.6	(16:0/18:2)
PC(34:3)	$[M+H]^{+}$	756.5538	756.5558	2.7	8.6	(16:1/18:2) (16:0/18:3)
PC(34:4)	$[M+H]^{+}$	754.5381	754.5393	1.5	8.5	-
PC(34:5)	$[M+H]^{+}$	752.5225	752.5229	0.6	8.6	-
PC(36:1)	$[M+H]^{+}$	788.6164	788.6143	-2.7	8.4	(18:1/18:0)
PC(36:2)	$[M+H]^{+}$	786.6007	786.6019	1.5	8.4	(18:0/18:2) (18:1/18:1)
PC(36:3)	$[M+H]^{+}$	784.5851	784.5852	0.2	8.4	(16:1/20:2) (18:1/18:2)
PC(36:4)	$[M+H]^{+}$	782.5694	782.5713	2.4	8.2	(16:0/20:4) (18:2/18:2)
PC(36:5)	$[M+H]^{+}$	780.5538	780.5543	0.6	8.3	(16:0/20:5)
PC(36:6)	$[M+H]^{+}$	778.5381	778.5406	3.2	8.3	-
PC(38:2)	$[M+H]^{+}$	814.6320	814.6316	-0.6	8.3	(16:1/22:1)

						(18:0/20:2) (18:1/20:1) (18:2/20:0)
PC(38:4)	$[M+H]^+$	810.6007	810.6038	3.9	8.0	(16:0/22:4) (18:0/20:4)
PC(38:5)	$[M+H]^+$	808.5851	808.5842	-1.1	8.1	(16:0/22:5) (18:0/20:5) (18:1/20:4)
PC(38:6)	$[M+H]^+$	806.5694	806.5717	2.9	8.1	(16:0/22:6) (16:1/22:5) (18:1/20:5)
PC(38:7)	$[M+H]^+$	804.5538	804.5541	0.4	8.1	(16:1/22:6)
PC(38:8)	$[M+H]^+$	802.5381	802.5384	0.3	8.2	(16:2/22:6) (20:4/18:4)
PC(40:4)	$[M+H]^+$	838.6320	838.6327	0.9	8.1	(16:0/24:4) (18:0/22:4) (20:0/20:4)
PC(40:5)	$[M+H]^+$	836.6164	836.6158	-0.7	8.0	(16:0/24:5) (18:0/22:5) (20:2/20:3) (20:1/20:4)
PC(40:6)	$[M+H]^+$	834.6007	834.6028	2.5	7.9	(18:0/22:6) (16:0/24:6) (18:1/22:5)
PC(40:7)	$[M+H]^+$	832.5851	832.5862	1.3	7.9	(18:1/22:6) (18:2/22:5)
PC(40:8)	$[M+H]^+$	830.5694	830.5705	1.3	8.0	(18:2/22:6)
PC(40:9)	$[M+H]^+$	828.5538	828.5524	-1.6	8.0	(18:3/22:6) (20:4/20:5)
PC(42:10)	$[M+H]^+$	854.5694	854.5670	-2.8	7.8	-
PC(42:11)	$[M+H]^+$	852.5538	852.5523	-1.7	7.9	-
PC(42:6)	$[M+H]^+$	862.6320	862.6308	-1.3	7.9	-
PC(42:7)	$[M+H]^+$	860.6164	860.6170	0.7	7.9	(16:1/26:6)
PC(42:8)	$[M+H]^+$	858.6007	858.5991	-1.9	7.9	-
PC(42:9)	$[M+H]^+$	856.5851	856.5833	-2.2	7.8	-
PC(44:10)	$[M+H]^+$	882.6007	882.5990	-2.0	7.7	-
PC(44:11)	$[M+H]^+$	880.5851	880.5857	0.7	7.7	-
PC(44:12)	$[M+H]^+$	878.5694	878.5733	4.4	7.6	-
PCp(32:0)	$[M+H]^+$	720.5902	720.5904	0.3	9.0	(p16:0/16:0)
PCp(32:1)	$[M+H]^+$	718.5745	718.5760	2.1	8.7	(p16:1/16:0)
PCp(34:0)	$[M+H]^+$	748.6215	748.6198	-2.2	8.8	(p18:1/16:0)
PCp(34:1)	$[M+H]^+$	746.6058	746.6067	1.2	8.8	(p18:1/16:0/) (p16:0/18:1)
PCp(34:2)	$[M+H]^+$	744.5902	744.5918	2.2	8.6	(p16:0/18:2)
PCp(34:3)	$[M+H]^+$	742.5745	742.5755	1.4	8.5	(p16:1/18:2)

PCp(36:2)	$[M+H]^+$	772.6215	772.6213	-0.3	8.5	(p18:0/18:2)
PCp(36:3)	$[M+H]^+$	770.6058	770.6062	0.5	8.4	(p18:1/18:2)
PCp(36:4)	$[M+H]^+$	768.5902	768.5894	-1.0	8.4	(p16:0/20:4)
PCp(36:5)	$[M+H]^+$	766.5745	766.5761	2.1	8.1	-
PCp(36:6)	$[M+H]^+$	764.5589	764.5577	-1.6	8.2	-
PCp(38:5)	$[M+H]^+$	794.6058	794.6040	-2.3	8.2	(p18:1/20:4) (p16:0/22:5)
PCp(38:6)	$[M+H]^+$	792.5902	792.5911	1.2	8.1	(p16:0/22:6)
PCp(38:7)	$[M+H]^+$	790.5745	790.5767	2.8	8.0	-
PCp(40:6)	$[M+H]^+$	820.6215	820.6220	0.7	8.0	(p18:0/22:6)
PCp(40:7)	$[M+H]^+$	818.6058	818.6034	-2.9	7.9	(p18:1/22:6)
PE(32:0)	$[M+H]^+$	692.5225	692.5229	0.6	4.5	-
PE(32:1)	$[M+H]^+$	690.5068	690.5070	0.3	4.4	(16:1/16:0)
PE(34:1)	$[M+H]^+$	718.5381	718.5359	-3.1	4.4	(16:0/18:1) (16:1/18:0)
PE(34:2)	$[M+H]^+$	716.5225	716.5241	2.2	4.4	(16:0/18:2)
PE(34:3)	$[M+H]^+$	714.5068	714.5090	3.1	4.4	(16:1/18:2)
PE(36:2)	$[M+H]^+$	744.5538	744.5565	3.6	4.4	(18:0/18:2) (18:1/18:1)
PE(36:3)	$[M+H]^+$	742.5400	742.5396	-0.6	4.4	(18:1/18:2)
PE(36:4)	$[M+H]^+$	740.5225	740.5243	2.4	4.3	-
PE(36:5)	$[M+H]^+$	738.5068	738.5079	1.5	4.4	(16:0/20:5)
PE(36:6)	$[M+H]^+$	736.4912	736.4920	1.1	4.4	-
PE(38:4)	$[M+H]^+$	768.5538	768.5545	0.9	4.2	(18:0/20:4)
PE(38:5)	$[M+H]^+$	766.5381	766.5364	-2.3	4.3	(16:0/22:5) (18:1/20:4) (18:0/20:5)
PE(38:6)	$[M+H]^+$	764.5225	764.5242	2.2	4.2	(16:0/22:6) (18:2/20:4)
PE(38:7)	$[M+H]^+$	762.5068	762.5086	2.3	4.3	(16:1/22:6)
PE(38:8)	$[M+H]^+$	760.4912	760.4935	3.0	4.4	(18:4/20:4)
PE(40:10)	$[M+H]^+$	784.4912	784.4916	0.5	4.6	-
PE(40:4)	$[M+H]^+$	796.5851	796.5860	1.1	4.2	(18:0/22:4)
PE(40:5)	$[M+H]^+$	794.5694	794.5660	-4.3	4.2	-
PE(40:6)	$[M+H]^+$	792.5538	792.5567	3.7	4.2	(18:0/22:6)
PE(40:7)	$[M+H]^+$	790.5381	790.5390	1.1	4.3	(18:1/22:6) (18:2/22:5)
PE(40:8)	$[M+H]^+$	788.5225	788.5212	-1.6	4.2	(18:2/22:6)
PE(40:9)	$[M+H]^+$	786.5068	786.5047	-2.7	4.3	-
PE(42:10)	$[M+H]^+$	812.5225	812.5213	-1.4	4.2	-
PE(42:11)	$[M+H]^+$	810.5068	810.5038	-3.7	4.3	-
PE(42:7)	$[M+H]^+$	818.5694	818.5704	1.2	4.2	-
PE(42:8)	$[M+H]^+$	816.5538	816.5522	-2.0	4.2	-
PE(42:9)	$[M+H]^+$	814.5381	814.5364	-2.1	4.2	-

PEp(34:1)	$[M+H]^+$	704.5589	704.5589	-0.1	4.4	(p18:1/16:0) (p16:1/18:0)
PEp(34:2)	$[M+H]^+$	702.5432	702.5403	-4.2	4.4	(p18:1/16:1) (p16:1/18:1)
PEp(34:3)	$[M+H]^+$	700.5276	700.5289	1.9	4.4	(p16:1/18:2)
PEp(36:2)	$[M+H]^+$	730.5745	730.5748	0.4	4.4	-
PEp(36:3)	$[M+H]^+$	728.5589	728.5604	2.1	4.4	(p18:1/18:2)
PEp(36:4)	$[M+H]^+$	726.5432	726.5437	0.7	4.4	-
PEp(36:5)	$[M+H]^+$	724.5276	724.5298	3.0	4.3	(p16:1/20:4)
PEp(38:3)	$[M+H]^+$	756.5902	756.5905	0.4	4.4	-
PEp(38:4)	$[M+H]^+$	754.5745	754.5718	-3.6	4.3	(p18:0/20:4)
PEp(38:5)	$[M+H]^+$	752.5589	752.5592	0.4	4.3	(p18:1/20:4)
PEp(38:6)	$[M+H]^+$	750.5432	750.5403	-3.8	4.3	(p16:1/22:5) (p16:0/22:6)
PEp(38:7)	$[M+H]^+$	748.5276	748.5297	2.8	4.2	(p16:1/22:6)
PEp(38:8)	$[M+H]^+$	746.5125	746.5112	-1.7	4.3	-
PEp(40:10)	$[M+H]^+$	770.5125	770.5110	-1.9	4.2	-
PEp(40:5)	$[M+H]^+$	780.5902	780.5872	-3.8	4.2	-
PEp(40:6)	$[M+H]^+$	778.5745	778.5778	4.3	4.2	-
PEp(40:7)	$[M+H]^+$	776.5589	776.5607	2.4	4.2	(p18:1/22:6)
PEp(40:8)	$[M+H]^+$	774.5438	774.5447	1.2	4.2	-
PEp(40:9)	$[M+H]^+$	772.5281	772.5266	-2.0	4.2	-
PEp(42:10)	$[M+H]^+$	798.5438	798.5412	-3.2	4.2	-
LPE(16:0)	$[M+H]^+$	454.2940	454.2942	0.3	5.3	(16:0)
LPE(16:1)	$[M+H]^+$	452.2783	452.2783	0.0	5.3	(16:1)
LPE(18:0)	$[M+H]^+$	482.3253	482.3257	0.8	5.2	(18:0)
LPE(18:1)	$[M+H]^+$	480.3098	480.3098	0.0	5.2	(18:1)
LPE(18:2)	$[M+H]^+$	478.2940	478.2940	0.0	5.2	(18:2)
LPE(20:3)	$[M+H]^+$	504.3072	504.3072	0.0	5.2	-
LPE(20:4)	$[M+H]^+$	502.2938	502.2938	0.0	5.1	(20:4)
LPE(20:5)	$[M+H]^+$	500.2768	500.2769	0.2	5.2	-
LPE(22:4)	$[M+H]^+$	530.3222	530.3222	0.1	5.0	-
LPE(22:5)	$[M+H]^+$	528.3083	528.3083	0.0	5.0	-
LPE(22:6)	$[M+H]^+$	526.2943	526.2943	0.0	5.0	(22:6)
LPEp(16:0)	$[M+H]^+$	438.2988	438.2988	0.0	5.2	-
LPEp(18:0)	$[M+H]^+$	466.3305	466.3305	0.0	5.1	-
PG(32:0)	[M-H]-	721.5025	721.5038	1.8	2.8	(16:0/16:0)
PG(34:0)	[M-H]-	749.5338	749.5303	-4.7	2.8	(16:0/18:0)
PG(34:1)	[M-H]-	747.5182	747.5202	2.7	2.8	(16:0/18:1)
PG(34:2)	[M-H]-	745.5025	745.5041	2.2	2.8	(16:0/18:2) (16:1/18:1)
PG(36:0)	[M-H]-	777.5651	777.5637	-1.8	2.8	-
PG(36:1)	[M-H]-	775.5495	775.5495	0.0	2.8	(18:0/18:1)
PG(36:2)	[M-H]-	773.5338	773.5335	-0.4	2.8	(18:0/18:2)

PG(36:3)	[M-H]-	771.5182	771.5188	0.8	2.8	(18:1/18:2)
PG(36:4)	[M-H]-	769.5025	769.5033	1.0	2.8	(18:2/18:2)
PG(38:4)	[M-H]-	797.5338	797.5345	0.9	2.8	(18:1/20:3)
PG(38:5)	[M-H]-	795.5182	795.5184	0.2	2.8	(18:2/20:3) (18:3/20:2)
PG(38:6)	[M-H]-	793.5025	793.5053	3.6	2.8	(18:2/20:4)
PG(40:6)	[M-H]-	821.5338	821.5355	2.1	2.8	(18:0/22:6)
PG(40:7)	[M-H]-	819.5182	819.5188	0.7	2.7	(18:1/22:6) (18:2:22:5)
PG(40:8)	[M-H]-	817.5025	817.5040	1.9	2.7	(18:2/22:6)
PI(34:1)	[M-H]-	835.5342	835.5361	2.3	2.8	(16:0/18:1) (16:1/18:0)
PI(34:2)	[M-H]-	833.5186	833.5204	2.1	2.8	(16:0/18:2) (16:1/18:1)
PI(36:1)	[M-H]-	863.5655	863.5668	1.5	2.8	(18:0/18:1)
PI(36:2)	[M-H]-	861.5499	861.5510	1.3	2.8	(18:0/18:2) (18:1/18:1)
PI(36:3)	[M-H]-	859.5342	859.5309	-3.8	2.8	(16:0/20:3) (16:1/20:2) (18:0/18:3) (18:1/18:2)
PI(36:4)	[M-H]-	857.5186	857.5207	2.4	2.8	(16:0/20:4)
PI(38:3)	[M-H]-	887.5655	887.5659	0.4	2.8	(16:0/22:3)
PI(38:4)	[M-H]-	885.5499	885.5523	2.8	2.8	(18:0/20:4) (18:2/20:2)
PI(38:5)	[M-H]-	883.5342	883.5359	1.9	2.8	(16:0/20:5) (18:1/20:4) (18:2/20:3)
PI(38:6)	[M-H]-	881.5186	881.5209	2.7	2.8	(18:2/20:6)
PI(40:4)	[M-H]-	913.5812	913.5788	-2.6	2.8	-
PI(40:5)	[M-H]-	911.5655	911.5651	-0.4	2.8	(16:0/22:5)
PI(40:6)	[M-H]-	909.5499	909.5521	2.4	2.8	(18:0/22:6)
PI(40:7)	[M-H]-	907.5342	907.5363	2.3	2.8	(18:1/22:6)
LPI(16:0)	[M-H]-	571.2889	571.2905	2.8	2.9	(16:0)
LPI(18:0)	[M-H]-	599.3202	599.3222	3.3	2.9	(18:0)
PS(34:1)	[M-H]-	760.5134	760.5159	3.3	5.1	(16:0/18:1) (16:1/18:0)
PS(34:2)	[M-H]-	758.4978	758.4982	0.5	5.1	(16:0/18:2) (16:1/18:1) (16:2/18:0)
PS(36:1)	[M-H]-	788.5447	788.5470	2.9	5.3	(18:0/18:1)
PS(36:2)	[M-H]-	786.5291	786.5327	4.6	5.3	(18:0/18:2) (18:1/18:1)
PS(36:3)	[M-H]-	784.5134	784.5169	4.4	5.1	-
PS(36:4)	[M-H]-	782.4978	782.5003	3.3	5.0	-

PS(38:2)	[M-H]-	814.5604	814.5592	-1.5	5.1	(16:0/22:2) (16:1/22:1) (18:2/20:0)
PS(38:3)	[M-H]-	812.5447	812.5453	0.7	5.0	(16:1/22:2) (18:2/20:1)
PS(38:4)	[M-H]-	810.5291	810.5303	1.5	4.9	(16:0/22:4) (18:0/20:4) (18:2/20:2)
PS(38:5)	[M-H]-	808.5134	808.5134	0.0	5.0	-
PS(38:6)	[M-H]-	806.4978	806.5003	3.1	4.9	(16:0/22:6) (18:2/20:4) (18:4/20:2)
PS(40:4)	[M-H]-	838.5604	838.5608	0.5	5.0	(20:0/20:4) (16:1/24:3) (18:0/22:4) (18:2/22:2) (20:1/20:3)/
PS(40:5)	[M-H]-	836.5447	836.5439	-0.9	4.9	(18:0/22:5) (16:0/24:5) (18:2/22:3)
PS(40:6)	[M-H]-	834.5291	834.5308	2.1	4.9	(16:0/24:6) (18:0/22:6) (18:2/22:4) (20:1/20:5) (20:2/20:4)
PS(40:7)	[M-H]-	832.5134	832.5151	2.1	4.9	(18:1/22:6) (18:2/22:5) (18:3/22:4)
PS(42:7)	[M-H]-	860.5447	860.5440	-0.9	4.9	(18:1/24:6) (18:2/24:5) (18:3/24:4) (20:1/22:6)
PS(42:8)	[M-H]-	858.5291	858.5281	-1.2	4.4	(18:2/24:6) (20:2/22:6) (20:3/22:5)
PS(42:9)	[M-H]-	856.5134	856.5127	-0.8	5.0	(20:3/22:6) (20:4/22:5) (20:5/22:4)
SM(d34:1)	$[M+H]^+$	703.5748	703.5762	1.9	10.4	(d18:1/16:0)
SM(d36:1)	$[M+H]^+$	731.6061	731.6079	2.5	10.2	(d18:1/18:0)
SM(d36:2)	$[M+H]^+$	729.5905	729.5923	2.5	10.2	(d18:1/18:1)
SM(d38:1)	$[M+H]^+$	759.6374	759.6386	1.5	10.1	(d18:1/20:0)
SM(d38:2)	$[M+H]^+$	757.6218	757.6234	2.1	10.0	(d18:1/20:1)
SM(d40:0)	$[M+H]^+$	789.6844	789.6812	-4.0	9.7	-
SM(d40:1)	$[M+H]^+$	787.6687	787.6688	0.1	9.8	(d18:1/22:0)

SM(d40:2)	$[M+H]^+$	785.6531	785.6537	0.7	9.9	-
SM(d42:1)	$[M+H]^+$	815.7000	815.7015	1.8	9.6	-
SM(d42:2)	$[M+H]^+$	813.6844	813.6863	2.4	9.7	-
SM(d42:3)	$[M+H]^+$	811.6687	811.6688	0.1	9.7	-

Supplementary Table S 2: Results of the Kluskal-Wallis univariate analysis. All the PL species are detailed and ranked by its p value. Species with p value under 0.05 are marked with shading.

PL specie	p value				
PS(34:1)	0.003	SM(d38:1)	0.081	PC(38:6)	0.387
CL(74:11)	0.003	PS(38:5)	0.082	PS(42:8)	0.390
CL(70:7)	0.004	PS(38:6)	0.083	SM(d34:1)	0.390
CL(76:13)	0.004	SM(d42:2)	0.083	PC(38:5)	0.392
CL(72:9)	0.004	PE(p36:3)	0.085	Cer(d36:2))	0.400
CL(74:9)	0.004	LPE(18:2)	0.085	PE(p36:5)	0.402
CL(74:10)	0.004	PC(42:8)	0.088	PE(34:2)	0.408
CL(70:6)	0.004	LPE(20:5)	0.089	Cer(d40:1)	0.412
CL(76:11)	0.005	LPE(p18:0)	0.089	PE(36:3)	0.414
CL(76:12)	0.005	PC(44:11)	0.091	LPC(16:0)	0.416
CL(74:8)	0.005	PC(p32:1)	0.093	Cer(d34:1)	0.419
CL(72:5)	0.005	PC(p36:2)	0.095	LPC(18:0)	0.428
CL(72:6)	0.005	PC(p36:6)	0.095	PC(p34:3)	0.428
CL(72:7)	0.005	PC(42:6)	0.107	LPC(18:3)	0.436
CL(72:8)	0.005	LPE(18:0)	0.107	PE(42:7)	0.440
PS(36:1)	0.005	PI(34:2)	0.112	PE(p34:1)	0.455
CL(70:5)	0.005	PC(p36:3)	0.114	PC(40:8)	0.472
CL(76:10)	0.005	PG(36:2)	0.114	LPC(16:1)	0.480
CL(68:6)	0.006	PC(38:2)	0.117	PC(34:3)	0.480
PS(38:2)	0.007	PC(36:4)	0.119	PE(p40:10)	0.494
PS(36:3)	0.008	LPE(18:1)	0.128	PE(40:7)	0.498
PS(38:3)	0.010	PS(36:2)	0.132	LPC(20:3)	0.508
CL(68:5)	0.015	PG(38:4)	0.132	PC(34:1)	0.516
LPI(16:0)	0.016	SM(d40:1)	0.136	PC(p38:6)	0.519
PC(42:10)	0.021	PE(p42:10)	0.138	LPC(p16:1)	0.533
PS(36:4)	0.023	PE(p40:6)	0.138	PE(40:5)	0.538
PC(p32:0)	0.024	PG(36:4)	0.140	PE(40:10)	0.569
LPI(18:0)	0.027	PI(36:3)	0.142	PE(40:4)	0.578
PI(40:5)	0.029	LPC(22:5)	0.144	PE(p38:4)	0.588
PI(36:1)	0.029	PG(34:0)	0.147	PE(38:5)	0.594
PC(42:11)	0.029	PC(38:4)	0.148	PC(40:6)	0.596
PI(38:4)	0.032	LPE(p16:0)	0.159	PE(40:8)	0.596
PC(p36:5)	0.033	SM(d40:0)	0.163	PC(32:2)	0.605
PI(38:5)	0.035	LPE(20:4)	0.165	PE(p34:3)	0.617
PC(p34:0)	0.036	LPC(22:6)	0.165	LPC(20:5)	0.628
PC(42:9)	0.037	PG(36:1)	0.168	PC(38:8)	0.629
PI(34:1)	0.037	PE(38:7)	0.168	Cer(d38:2)	0.644
PC(44:10)	0.037	LPE(20:3)	0.169	PC(32:1)	0.651
PG(40:6)	0.037	PC(40:7)	0.195	PE(38:6)	0.656

PI(38:3)	0.038	PC(p40:6)	0.202	PE(38:4)	0.657
PC(32:0)	0.039	LPC(20:4)	0.205	PE(32:0)	0.664
PI(40:4)	0.040	PE(34:3)	0.215	PC(34:4)	0.670
PI(40:6)	0.046	PG(40:8)	0.227	PE(p40:5)	0.683
PS(42:9)	0.047	LPC(18:1)	0.227	PS(40:4)	0.703
PS(40:6)	0.047	PG(38:5)	0.231	PE(p40:9)	0.706
SM(d38:2)	0.051	PG(36:3)	0.234	PE(36:5)	0.717
PS(42:7)	0.055	PC(38:7)	0.243	PE(40:9)	0.739
PI(36:4)	0.056	PE(p38:5)	0.243	PC(34:2)	0.744
SM(d36:2)	0.057	LPC(22:4)	0.247	Cer(d38:1)	0.758
PE(p36:2)	0.058	PS(34:2)	0.250	PC(34:5)	0.767
PS(40:5)	0.059	PC(40:4)	0.250	PS(40:7)	0.774
PA(36:2)	0.062	PG(36:0)	0.262	PE(42:8)	0.780
LPE(16:1)	0.063	Cer(d36:1)	0.263	PE(p34:2)	0.783
PE(36:6)	0.063	PC(44:12)	0.265	PE(36:2)	0.783
LPE(16:0)	0.064	PG(34:1)	0.265	PE(40:6)	0.797
LPE(22:6)	0.064	PG(32:0)	0.271	PE(32:1)	0.798
SM(d40:2)	0.065	PC(p40:7)	0.271	PE(p40:7)	0.841
PC(40:9)	0.065	Cer(d42:2)	0.277	PC(p38:7)	0.866
PI(38:6)	0.065	PC(36:1)	0.278	PE(p40:8)	0.877
PE(p38:3)	0.066	PE(p36:4)	0.280	PE(36:4)	0.881
PI(40:7)	0.066	PC(36:3)	0.284	PE(42:9)	0.919
PI(36:2)	0.070	PC(40:5)	0.294	PE(42:11)	0.940
PC(p34:1)	0.071	PG(38:6)	0.304	PC(36:6)	0.944
PC(p34:2)	0.072	PC(36:2)	0.305	PE(p38:7)	0.951
PS(38:4)	0.073	PE(p38:8)	0.321	PE(p38:6)	0.955
SM(d42:1)	0.073	PC(p36:4)	0.326	PE(34:1)	0.957
PC(42:7)	0.076	SM(d36:1)	0.350	PC(36:5)	0.962
PC(p38:5)	0.076	LPC(18:2)	0.353	PE(42:10)	0.968
LPE(22:5)	0.078	Cer(d42:1)	0.369	PG(40:7)	0.998
SM(d42:3)	0.078	PE(38:8)	0.377		
LPE(22:4)	0.079	PG(34:2)	0.381		

Supplementary Table S 3: Species showing significant differences (p value<0.05) and up- or downregulation in the Wilcoxon Pairwise test. Comparison between CTex and Ctsed, BBNsed and CTsed, and BBN and BBNex are included in the table, together with the sense of the variation (up/down).

BBNex vs CTsed		BBNsed vs Ctsed		BBNex vs BBNsed	
PL specie	Regulation	PL specie	Regulation	PL specie	Regulation
CL(70:5)	DOWN	PS(34:1)	UP	PA(36:2)	DOWN
		PS(36:1)	UP	PS(34:1)	DOWN
		PS(38:3)	UP	PS(36:1)	DOWN
		PS(38:2)	UP	PS(36:3)	DOWN
		PS(36:3)	UP	PS(36:4)	DOWN
		PS(42:9)	DOWN	PS(38:2)	DOWN
		PS(40:5)	DOWN	PS(38:3)	DOWN
		PS(40:6)	DOWN	CL(68:6)	UP
		PI(40:6)	DOWN	CL(70:5)	UP
		PI(38:5)	DOWN	CL(70:6)	UP
		PI(38:6)	DOWN	CL(70:7)	UP
		PI(38:4)	DOWN	CL(72:5)	UP
		PI(40:7)	DOWN	CL(72:6)	UP
		PS(42:7)	DOWN	CL(72:7)	UP
		PI(34:1)	DOWN	CL(72:8)	UP
		PI(36:1)	DOWN	CL(72:9)	UP
		LPI(18:0)	DOWN	CL(74:10)	UP
		CL(70:5)	DOWN	CL(74:11)	UP
		CL(68:5)	DOWN	CL(74:8)	UP
		CL(72:5)	DOWN	CL(74:9)	UP
		CL(70:6)	DOWN	CL(76:10)	UP
		CL(74:10)	DOWN	CL(76:11)	UP
		CL(74:9)	DOWN	CL(76:12)	UP
		CL(76:12)	DOWN	CL(76:13)	UP
		CL(70:7)	DOWN	LPC(22:5)	UP
		CL(72:6)	DOWN	LPE(16:0)	UP
		CL(76:11)	DOWN	LPE(16:1)	UP
		CL(76:10)	DOWN	LPE(18:0)	UP
		CL(68:6)	DOWN	LPE(18:1)	UP
		CL(72:7)	DOWN	LPE(18:2)	UP
		CL(72:8)	DOWN	LPE(20:4)	UP
		CL(74:11)	DOWN	LPE(20:5)	UP

		CL(74:8)	DOWN	LPE(22:4)	UP
		CL(72:9)	DOWN	LPE(22:5)	UP
		CL(76:13)	DOWN	LPE(22:6)	UP
				LPI(18:0)	UP
				PC(p36:2)	UP
				PE(36:6)	UP
				PG(40:6)	UP
				PI(34:1)	UP
				PI(34:2)	UP
				PI(36:1)	UP
				PI(36:2)	UP
				PI(36:4)	UP
				PI(38:3)	UP
				PI(38:4)	UP
				PI(38:5)	UP
				PI(40:4)	UP
				PI(40:5)	UP
				PS(40:6)	UP
				PS(42:7)	UP

A)

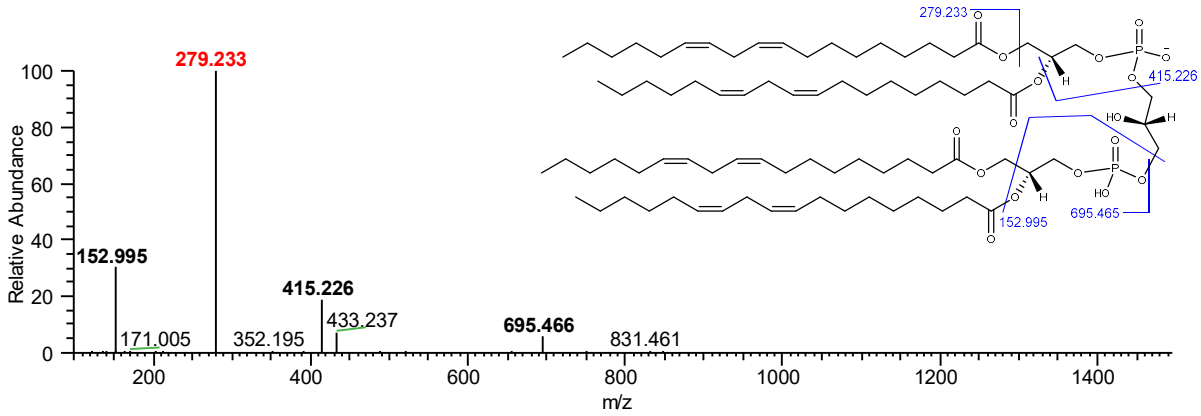

B)

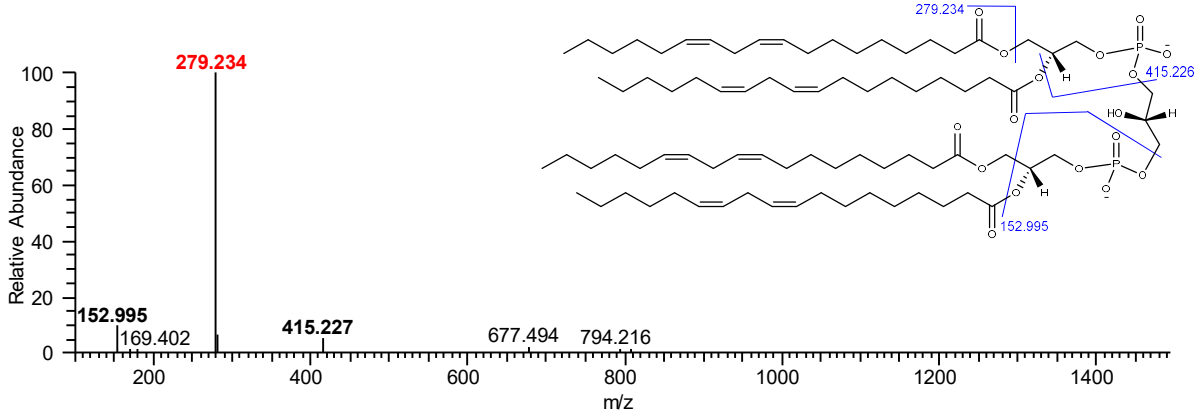

CL(72:8)

Supplementary Figure S 1: Representative LC-ESI-MS/MS spectra of cardiolipin species, CL(72:8) as A) $[M-H]^-$ ion and B) $[M-2H]^{2-}$ ion. Informative fragments for the class are highlighted in bold and ions corresponding to the fatty acyl chains in red, all indicated in the structure scheme also shown.

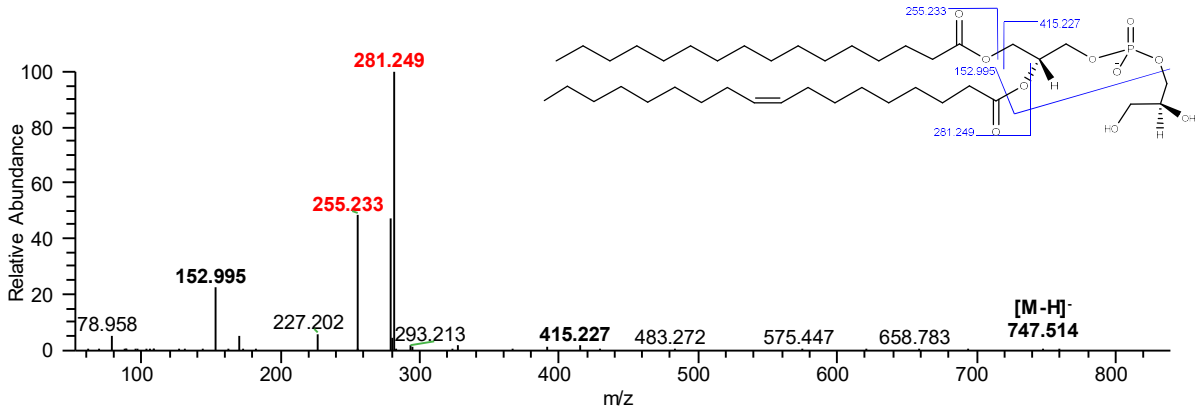

Supplementary Figure S 2: Representative LC-ESI-MS/MS spectrum of phosphatidylglycerol species: PG(34:1) as $[M-H]^-$ ion. Informative fragments for the class are highlighted in bold and ions corresponding to the fatty acyl chains in red, all indicated in the structure scheme also shown.

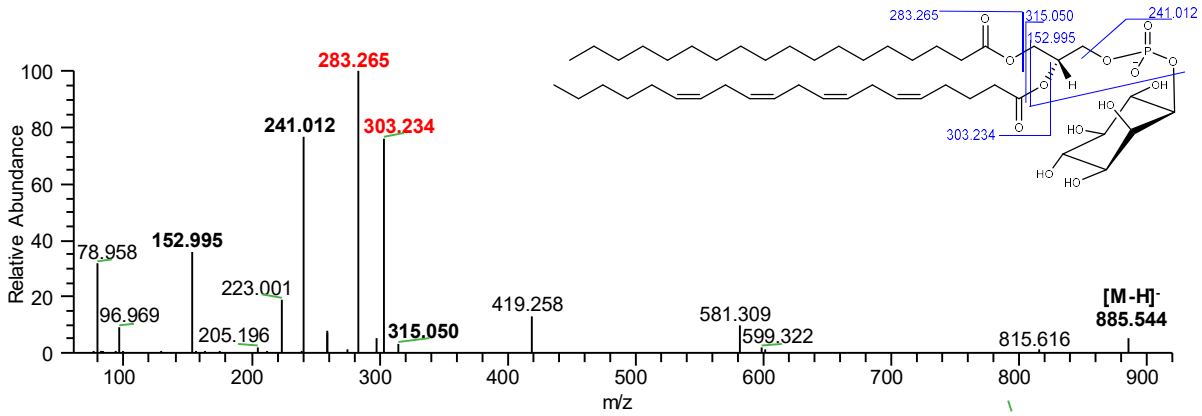

Supplementary Figure S 3: Representative LC-ESI-MS/MS spectrum of phosphatidylinositol species: PI(38:4) as $[M-H]^-$ ion. Informative fragments for the class are highlighted in bold and ions corresponding to the fatty acyl chains in red, all indicated in the structure scheme also shown.

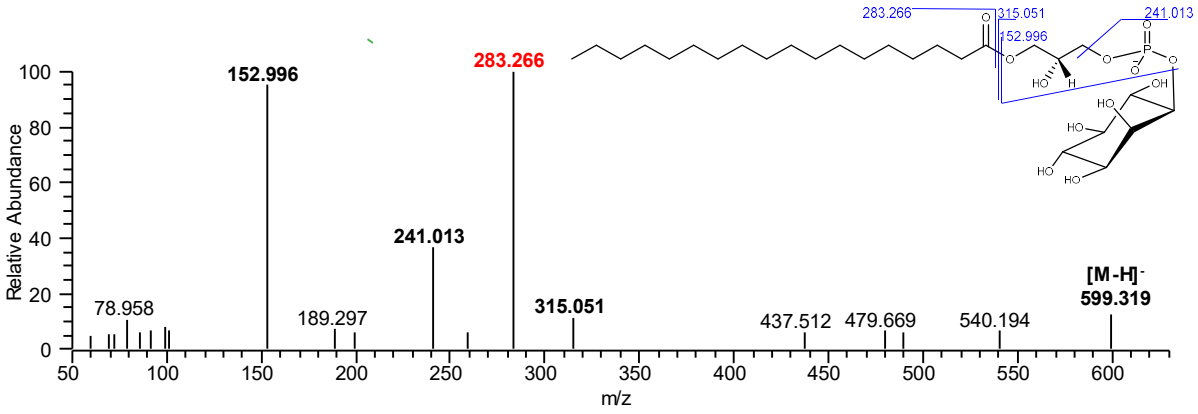

LPI(18:0)

Supplementary Figure S 4: Representative LC-ESI-MS/MS spectrum of lysophosphatidylinositol species: LPI(18:0) as $[M-H]^-$ ion. Informative fragments for the class are highlighted in bold and ions corresponding to the fatty acyl chains in red, all indicated in the structure scheme also shown.

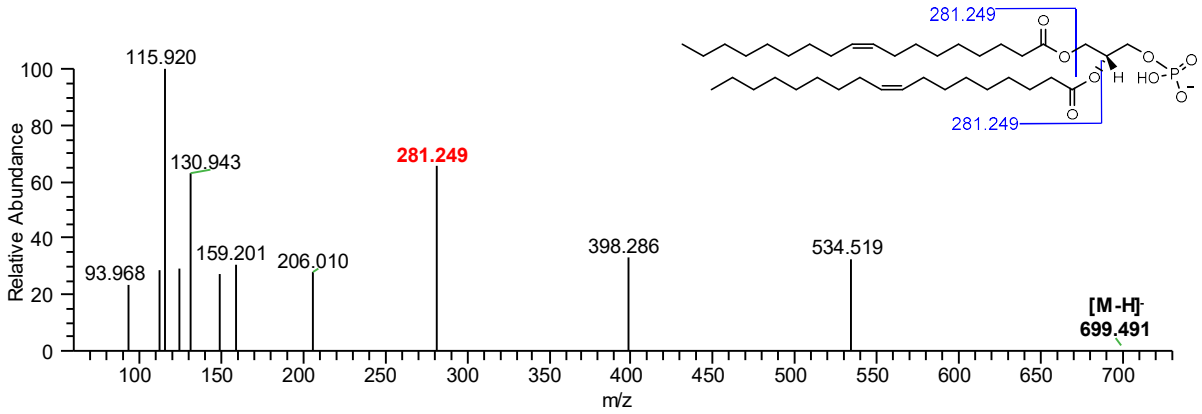

PA(36:2)

Supplementary Figure S 5: Representative LC-ESI-MS/MS spectrum of phosphatidic acid species: PA(36:2) as $[M-H]^-$ ion. Informative fragments for the class are highlighted in bold and ions corresponding to the fatty acyl chains in red, all indicated in the structure scheme also shown.

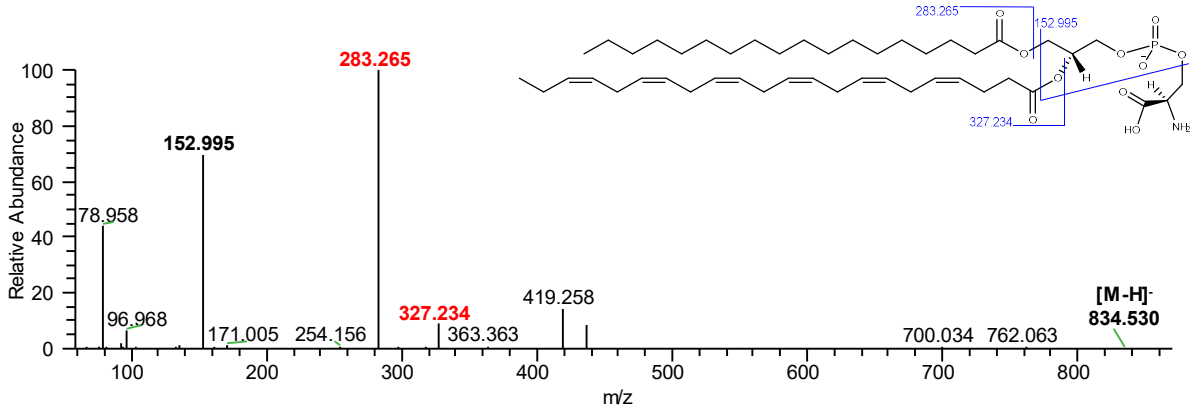

PS(40:6)

Supplementary Figure S 6: Representative LC-ESI-MS/MS spectrum of phosphatidylserine species: PS(40:6) as $[M-H]^-$ ion. Informative fragments for the class are highlighted in bold and ions corresponding to the fatty acyl chains in red, all indicated in the structure scheme also shown.

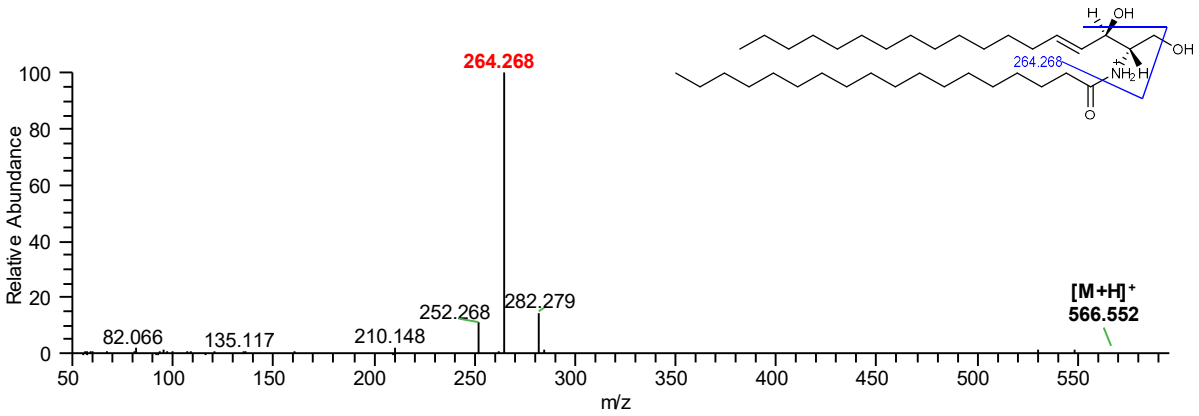

Cer(d36:1)

Supplementary Figure S 7: Representative LC-ESI-MS/MS spectrum of ceramide species: Cer(d36:1) as $[M+H]^+$ ion. Informative fragments for the class are highlighted in bold and ions corresponding to the fatty acyl chains in red, all indicated in the structure scheme also shown.

A)

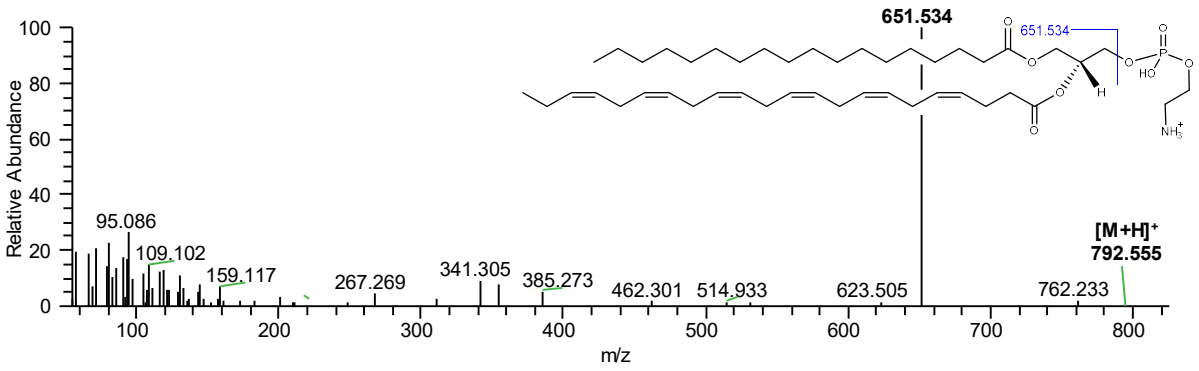

B)

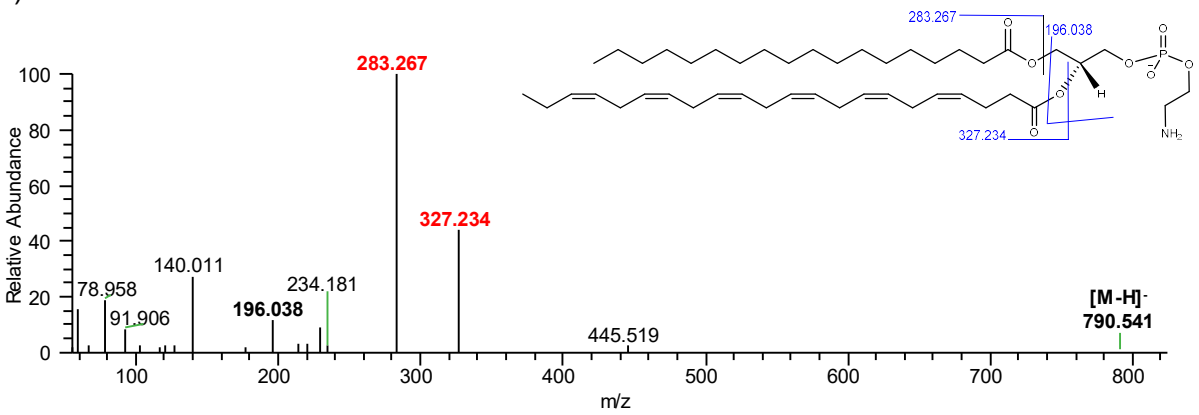

PE(40:6)

Supplementary Figure S 8: Representative LC-ESI-MS/MS spectra of phosphatidylethanolamine species: PE(40:6) as A)$[M+H]^+$ ion and B)$[M-H]^-$. Informative fragments for the class are highlighted in bold and ions corresponding to the fatty acyl chains in red, all indicated in the structure scheme also shown.

A)

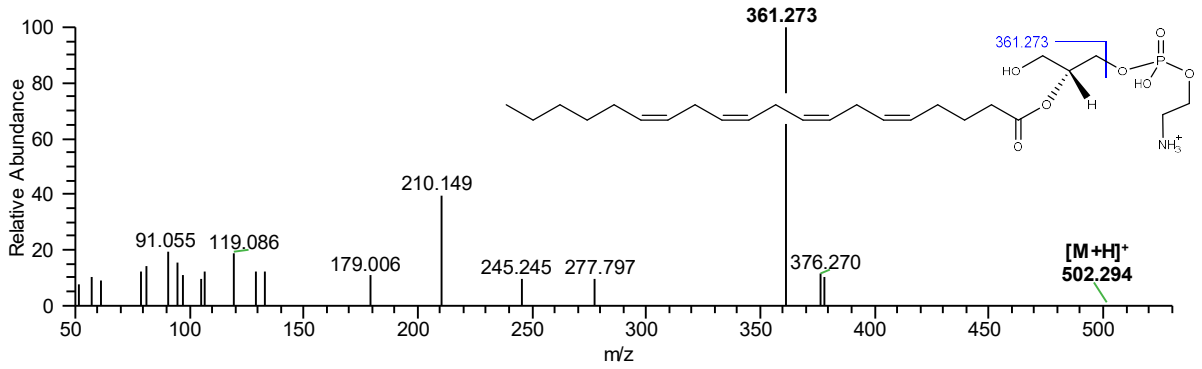

B)

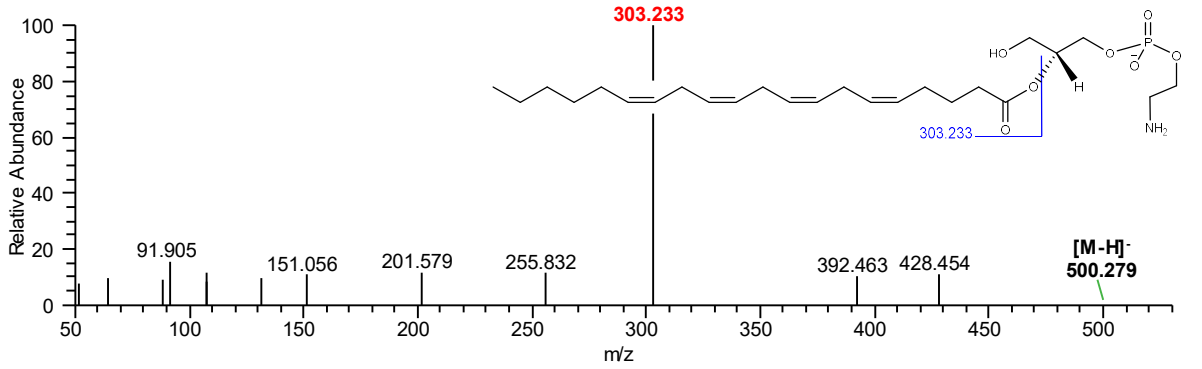

LPE(20:4)

Supplementary Figure S 9: Representative LC-ESI-MS/MS spectra of lysophosphatidylethanolamine species: LPE(20:4) as A)$[M+H]^+$ ion and B)$[M-H]^-$. Informative fragments for the class are highlighted in bold and ions corresponding to the fatty acyl chains in red, all indicated in the structure scheme also shown.

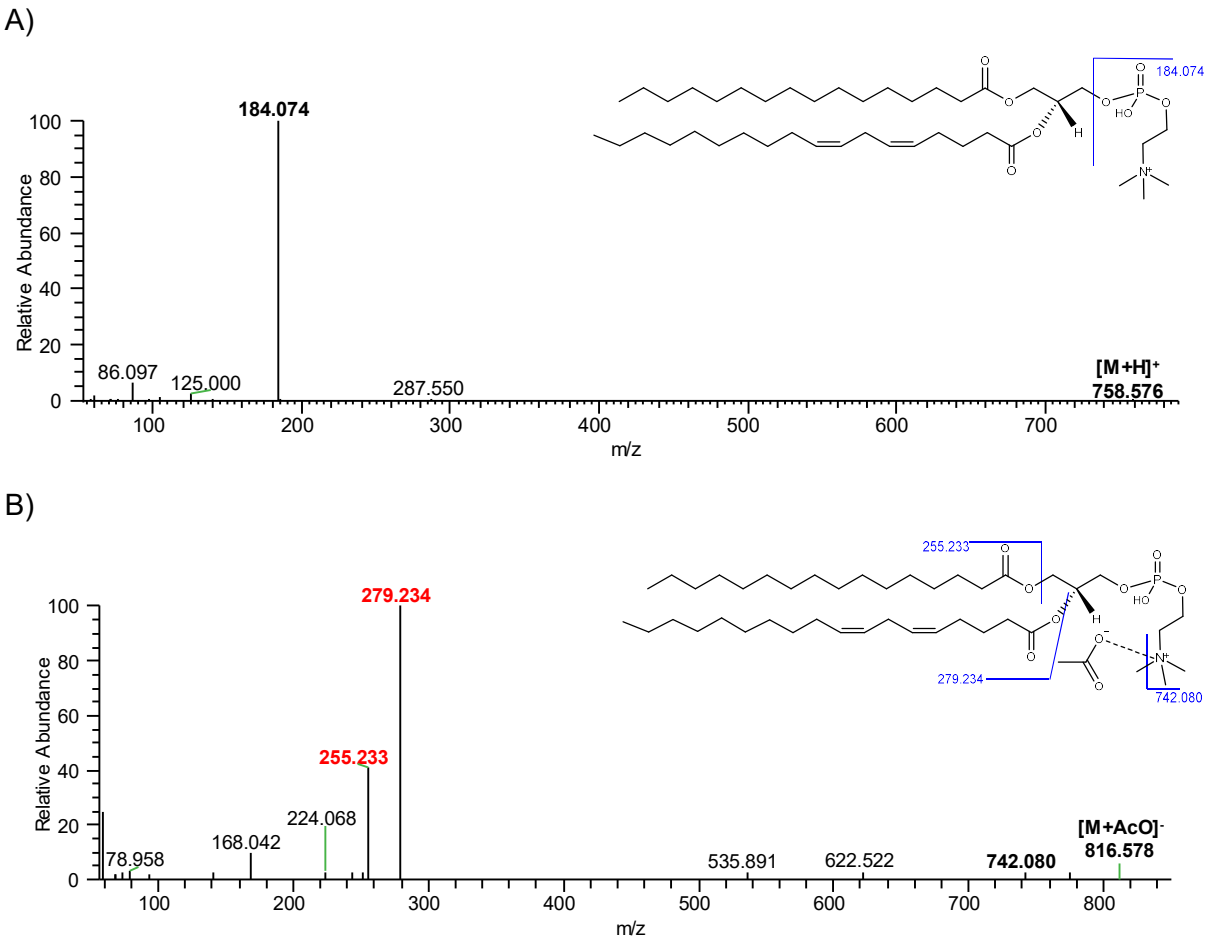

Supplementary Figure S 10: Representative LC-ESI-MS/MS spectra of phosphatidylcholine species: PC(38:4) as A)$[M+H]^+$ ion and B)$[M-AcO]^-$. Informative fragments for the class are highlighted in bold and ions corresponding to the fatty acyl chains in red, all indicated in the structure scheme also shown.

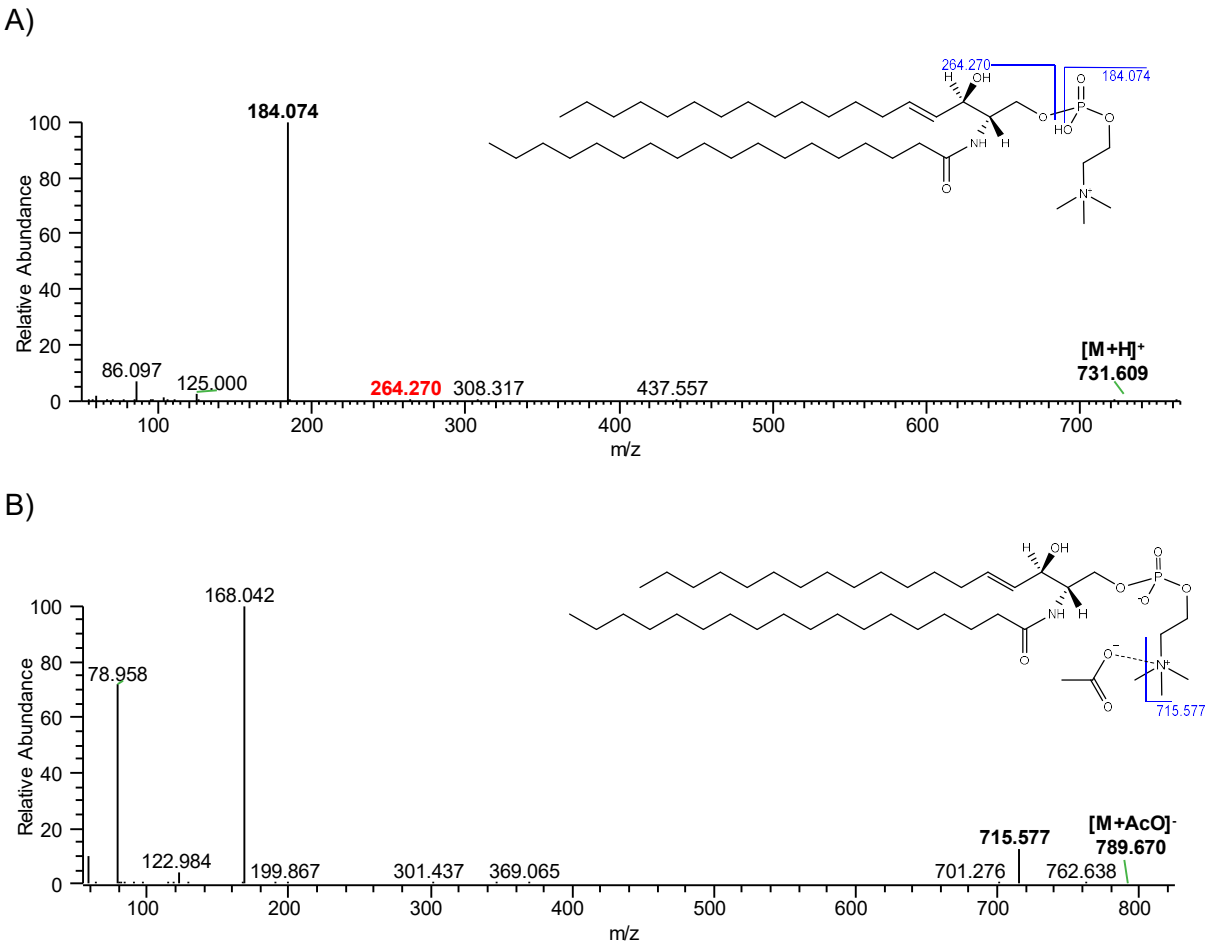

SM(d36:1)

Supplementary Figure S 11: Representative LC-ESI-MS/MS spectra of sphyngomyeline species: SM(d36:1) as A)$[M+H]^+$ ion and B)$[M\text{-}AcO]^-$. Informative fragments for the class are highlighted in bold and ions corresponding to the fatty acyl chains in red, all indicated in the structure scheme also shown.

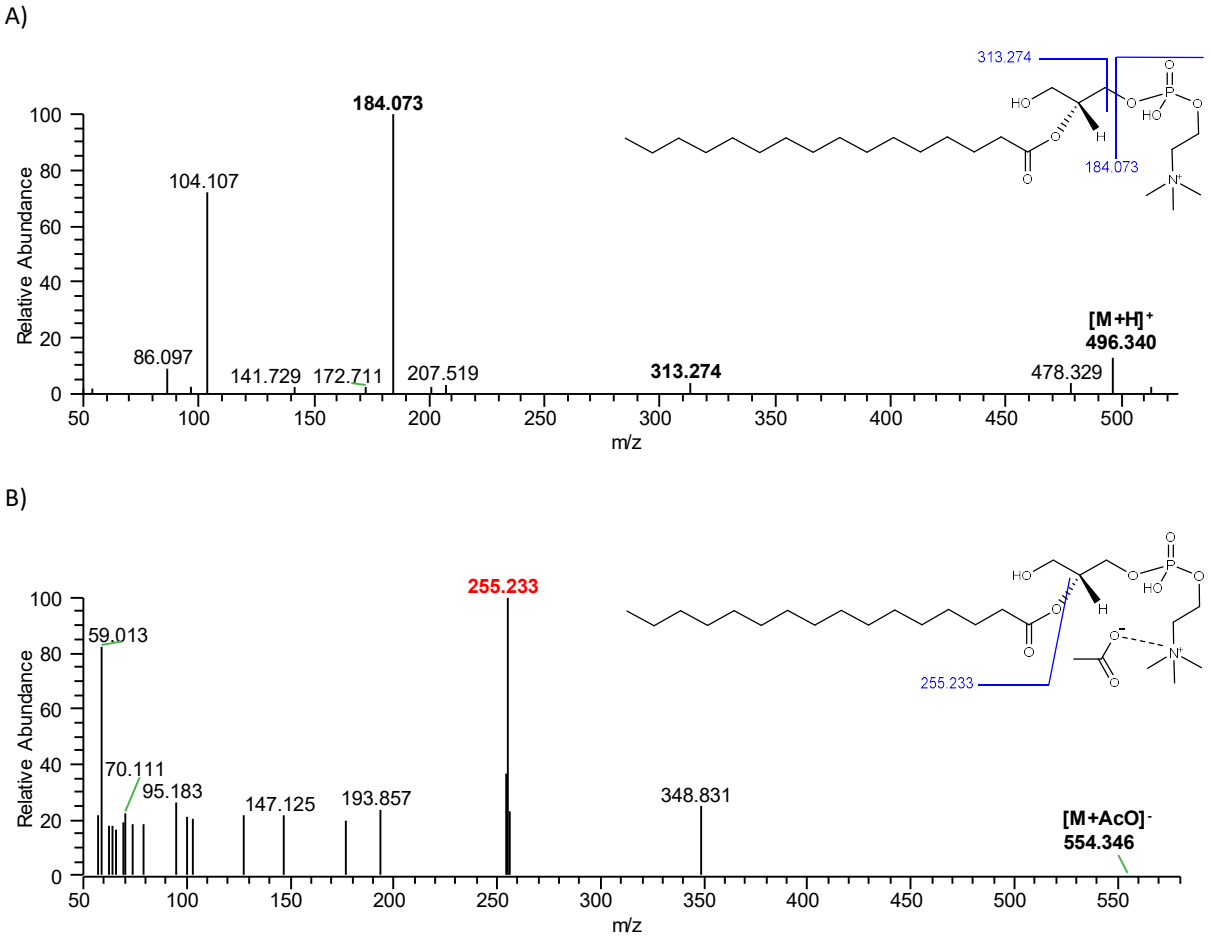

LPC(16:0)

Supplementary Figure S 12: Representative LC-ESI-MS/MS spectra of lyosphosphatidylcholine species: LPC(16:0) as A)$[M+H]^+$ ion and B)$[M-AcO]^-$. Informative fragments for the class are highlighted in bold and ions corresponding to the fatty acyl chains in red, all indicated in the structure scheme also shown.

CHAPTER 5. Adaptation of Phospholipidome profile in heart associated with acute myocardial infarction and ischemia-reperfusion in an *ex vivo* rat model

The content presented in this section has been integrally submitted as follows:

Javier-Fernando Montero-Bullon, Tânia Melo, Tania Martins-Marques, Henrique Girão, M. Rosário M. Domingues, Pedro Domingues. Adaptation of myocardial phospholipidome during acute myocardial infarction and ischemia-reperfusion in an *ex vivo* rat model. Under revision in Molecules MDPI journal.

Adaptation of myocardial phospholipidome during acute myocardial infarction and ischemia-reperfusion in an *ex vivo* rat model

Javier-Fernando Montero-Bullon[1], Tânia Melo[1,2], Tânia Martins-Marques[3,4], Henrique Girão[3,4], M Rosário M Domingues[1,2], Pedro Domingues[1*]

1. Centro de Espectrometria de Massa, Department of Chemistry & QOPNA, University of Aveiro, Campus Universitário Santiago, 3810-193 Aveiro, Portuga
2. I Department of Chemistry & CESAM, University of Aveiro, Campus Universitário Santiago, 3810-193 Aveiro, Portugal
3. Coimbra Institute for Clinical and Biomedical Research (iCBR), Faculty of Medicine, University of Coimbra, Coimbra, Portugal
4. CNC.IBILI, University of Coimbra, Coimbra, Portugal

*Corresponding author:

Pedro Domingues, Department of Chemistry, University of Aveiro, Campus Universitário Santiago, 3810-193 Aveiro, Portugal. Email: p.domingues@ua.pt

Abstract

Acute myocardial infarction (AMI) is the leading cause of mortality, morbidity and cost of health care worldwide. In AMI, an abrupt blockage of the blood flow causes myocardial ischemia and cell death, therefore timely restoration of coronary blood flow is essential to prevent irreversible tissue injury. However, reperfusion after ischemia has paradoxical effects and may exacerbate the myocardial cellular injury, a process known as ischemic reperfusion injury. In this work, we performed a modern lipidomics approach using high-resolution LC-MS and GC-MS to evaluate the lipidome of isolated rat hearts, either maintained in control perfusion (CT), submitted to global ischemia (ISC) or ischemia followed by reperfusion (I/R). We observed a decrease in the relative abundance (RA) of linoleic acid and an increase in palmitic acid during ISC and I/R, which is consistent with the presence of oxidative damage. Multivariate prediction models based on partial least squares-discriminant analysis (PLS-DA) and hierarchical cluster analysis performed on the phospholipidome data, discriminated with high accuracy among the three profiles. From the 219 phospholipid species identified in this study, 49 phospholipid levels were significantly different between the conditions, but most of these occurred between ISC and I/R, suggesting that I/R induces deeper changes than ISC. Generally, the relative abundances of important features were lower in ISC when compared with CT, and lowest in the I/R group. These included mainly phosphatidylcholines, phosphatidylethanolamines, and their plasmalogens, containing polyunsaturated fatty acids, which is also consistent with the presence of oxidative stress under these conditions and the deployment of defence mechanisms. We also observed some CL species whose RA was lower in ISC and I/R, compared with controls conditions, and the observed changes may result in mitochondrial dysfunction, and death of cardiomyocytes. Unveiling adaptation of the heart lipidome during ISC and I/R might reflect the impact of AMI in the lipidome at a cellular level and brings new insights into the role of lipids in the pathophysiology of acute myocardial infarction.

Keywords

Lipidomics; acute myocardial infarction: heart attack; ischemia; reperfusion, phospholipidome, liquid chromatography, mass spectrometry

5.1. Introduction

Acute myocardial infarction (AMI) is one of the cardiovascular diseases (CVD) responsible for higher rates of mortality and morbidity worldwide, both in developed and non-developed countries. According to the World Health Organization, AMI contributes to about 10% of the total worldwide mortality[1]. AMI is characterised by myocardial tissue damage and cell death that occurs as the consequence of an abrupt shortage of blood flow, causing lack of nutrients and oxygen to a region of the heart[2,3]. AMI injury is the consequence of a multifactorial pathological process, including oxidative stress and increased production of reactive oxygen species (ROS), as well as mitochondrial dysfunction, which ultimately leads to death of cardiomyocytes[4,5]. Free radicals can cause alteration of redox homeostasis, resulting not only in the oxidation of lipids and proteins, but also in the activation of several signalling pathways and inflammation[6,7]. This pro-inflammatory response in AMI contributes to cell dysfunction, cardiomyocyte death and myocardial injury[8]. The outcome and the recovery in AMI largely depend on the extent of the ischemic event and the activation of the cell response by cytoprotective mechanisms[9,10], such as autophagy[11–14], and also on a timely restoration of blood flow.

Response following myocardial ischemia/reperfusion (I/R) may have paradoxical effects. Although necessary to restore nutrients and oxygen supply, reperfusion may exacerbate cellular damage in a process known as I/R injury[15], which has been associated with a burst of oxidative stress and inflammation[3,16,17]. Despite the fact that ROS have been consistently associated with I/R injury, the mechanisms and signals implicated in this damaging process remain largely elusive. This lack of knowledge hampers the definition of AMI outcomes, diagnostic and prognostic factors, impairing advances in health care[18–20].

Lipids are involved in CVD and AMI, not only as targets of ROS but also due to the adaptation of lipid metabolism under these processes. Some studies have associated a disturbance of the lipid profile with AMI, in diverse tissues or biofluids. Lipidomics analysis carried out in plasma revealed increased levels of free fatty acids during the onset of AMI[21]. Omega-3 and stearic acid correlated inversely with the risk of AMI, whereas arachidonic acid and oxylipins showed a positive correlation[22]. Changes in phospholipids and sphingolipids have also been reported in AMI[23,24] and correlated with the incidence of CVD[25], mortality[26], or prognosis[27]. The variation in phosphatidylcholines (PC) levels were correlated with CVD risk[28], whereas a decrease of plasmalogens levels was also found in plasma of AMI patients[29] and reported in cardiac remodelling and cardiac function restoration[30].

Changes in the lipid profile associated with AMI and I/R in the cardiac tissue of animal models or cells have also been shown. Variation of the profile of different glycerolipids, sphingolipids and free fatty acid species[31], as well as depletion of cardiolipins (CLs)[32] were reported in rat hearts under simulated infarction. Furthermore, the sphingolipids profile was demonstrated to vary both in blood samples from rats with AMI[33,34,35] and in infarcted heart[36]. Recently, it was shown that the phospholipids profile of myoblast cells, namely, phosphatidylcholines (PCs), lysophosphatidylcholines (LPCs), phosphatidylethanolamines (PEs), phosphatidylserines (PSs), phosphatidylinositolS (PIs), cardiolipins (CLs) and sphingomyelins (SMs) classes, changes in ischemia[37]. However, up to now, no studies have addressed the phospholipid profile associated with ischemia (ISC) and subsequent reperfusion (I/R).

In the present study, we compared the cardiac tissue lipidome, in isolated rat hearts from either control (CT), myocardium ischemia (ISC) or ischemia-reperfusion (I/R), whether ISC and ischemia-I/R would induce distinct changes in the cardiac tissue lipidome. For this purpose, high-resolution hydrophilic interaction liquid chromatography-mass spectrometry (HILIC LC-MS) was used for the phospholipidomics profiling of the cardiac tissue of animal models using the *ex vivo* Langendorff apparatus[38]. Statistical analysis was used to evaluate the degree of lipid content variation in both conditions and to provide a more comprehensive picture of lipid remodelling in AMI, ISC and I/R.

5.2. Results

The phospholipidome profile of the lipid extracts obtained from rat hearts maintained in control perfusion (CT), or subjected to ischemia (ISC), or ischemia and reperfusion (I/R) was analysed using two complementary approaches. These were GC-MS, to study the profile of the esterified fatty acids (FA), and high-resolution HILIC LC-MS and MS/MS to study the lipid profile at the molecular level.

Using GC-MS analysis of the lipid extracts, we semi-quantified seven fatty acids (FA) methyl esters present in the three conditions CT, ISC and I/R. Under all conditions, stearic acid (C18:0) was the FA more abundant, followed by linoleic acid (C18:2), arachidonic acid (C20:4), docosahexaenoic acid (C22:6) and palmitic acid (C16:0), which is in agreement with the FA profile reported in the literature for cardiac tissue[39]. As depicted in Figure 1, the main variation in relative abundance (RA) of the FA in the order of events (CT to ISC to I/R) was an increase in the relative abundance (RA) of C18:0, and a decrease in the RA of

C18:2 FA. These relative abundance variations were statistically significant for the C18:0 ($q<0.01$) and C18:2 ($q<0.05$) species. For the C18:0 fatty acid, significant differences were found between CT and I/R ($q<0.01$), whereas for the C18:2, significant differences were found between CT and I/R ($q<0.01$) and ISC and I/R ($q<0.05$).

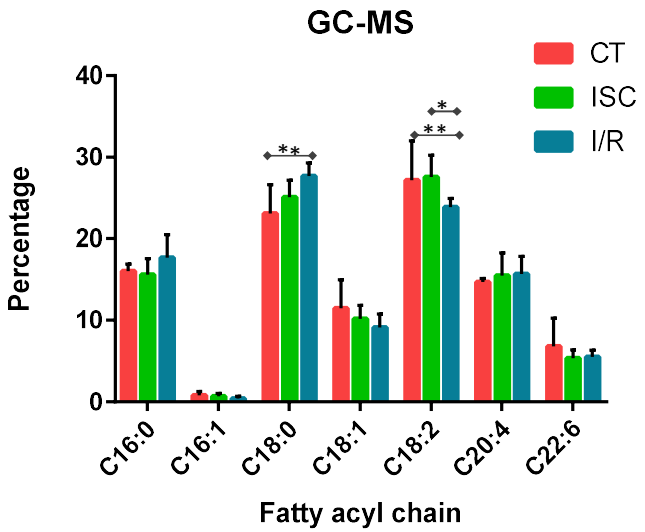

Figure 1: Bar graph of the fatty acids profile obtained by GC-MS, for the three biological conditions: control (CT), ischemia (ISC) and reperfusion (I/R). Bars represent the percentage of each fatty acid species in the tissue (esterified). Kruskal-Wallis test followed by Dunn multicomparison test was used to determine significant variations, marked with * if $q<0.05$ and ** if $q<0.01$.

In this study, we also evaluated the lipid profile of CT, ISC and I/R heart by high-resolution LC-MS and MS/MS analysis. We identified and semi-quantified a total of 219 phospholipid species distributed in 11 phospholipid classes: phosphatidylcholines (PC), lysophosphatidylcholines (LPC), phosphatidylethanolamines (PE), lysophosphatidylethanolamines (LPE), phosphatidylglycerols (PG), phosphatidylinositols (PI), lysophosphatidylinositol (LPI), phosphatidic acids (PA), phosphatidylserines (PS), cardiolipins (CL), sphingomyelins (SM) and also ceramides (Cer) class (Supplementary Table 1). The principal component analysis (PCA) of lipid profiles of the samples did not show unambiguous clusters of specific groups, although the PCA scores plot (PC1 vs PC3) showed an almost complete discriminative separation of the subjects for the ISC and I/R groups (Figure 2). The proportions of the variance explained were of 33.6%, 23.3% and 10.7% for the first, second and third factors, respectively. The variables with contributions

to the first principal component >1% included 10 PCs, 2 PGs, 1 PS, 1 phosphatidylcholine plasmenyl, also called plasmalogens (PC-P) and 1 PI species (Figure 2 and Supplementary Table S 2A) with a total contribution of 17.1%. The variables with contributions to the third principal component >2% included 6 LPEs, 2 SMs, 2 PEs and 2 lysophosphatidylethanolamine plasmanyl (LPE-O) species with a total contribution of 29.1% (Supplementary Table 2B).

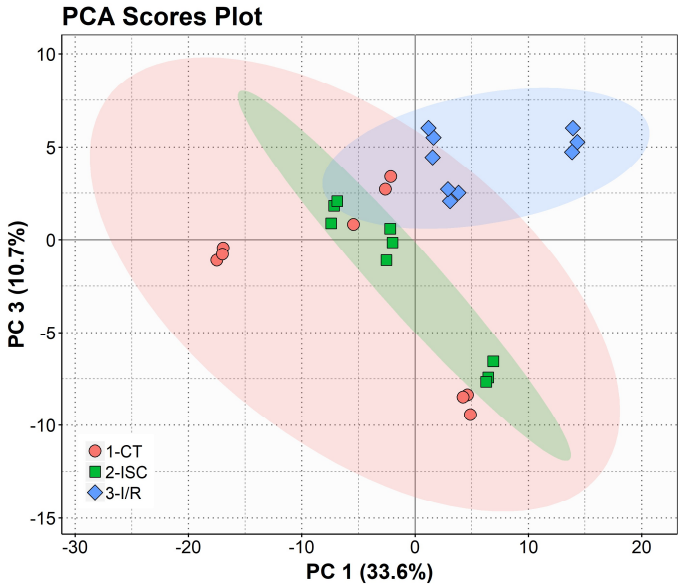

Figure 2: PCA score plot of the first and third principal components of PCA for the phospholipid dataset acquired by LC-MS, of the three biological groups: control (CT), ischemia (ISC) and reperfusion (I/R).

Partial least squares discriminant analysis (PLS-DA) clustered the samples from each condition with high predictive accuracy (Q^2 0.5503, R^2 0.68177)[40], allowing discrimination between the three conditions (Figure 3 A). The score plot shows the grouping of the samples based on component 1, with 30.1% of the variability of the model explained, and component 2 with 14.2%. The clustering shows main discrimination along the x-axis that represents component 1. Figure 3 B shows the list of the variable importance in projection (VIP) score with the top 16 species sorted by their contribution to the classification accuracy (mean decrease accuracy) for the PLS-DA model. These included 7 PCs, 4 PEs, 2 PAs, 1 LPE, 1 PE-P and 1 LPC species. Overall, the relative abundance of these species is higher in control samples and lower in I/R sample. Most of these phospholipid species have highly unsaturated FA.

A)

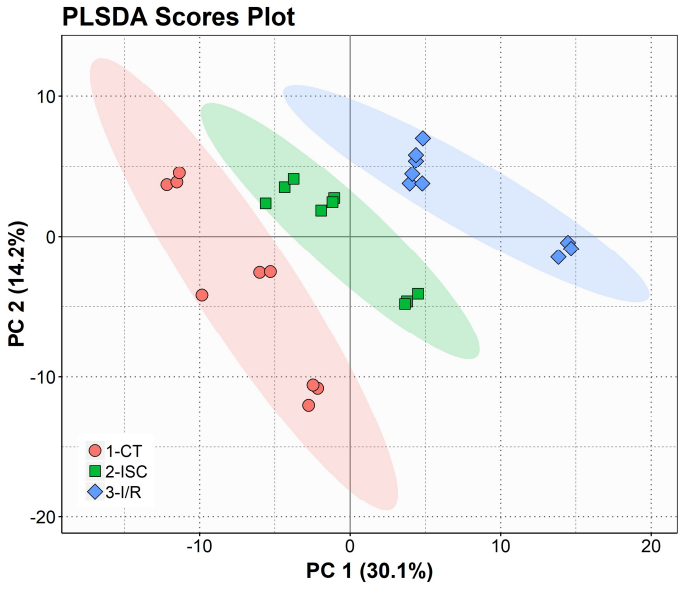

B)

Species	Comp. 1
PC 38:5	1.98
PA 34:1	1.95
PC 36:7	1.93
PC 36:6	1.91
PC 34:4	1.84
PE 40:10	1.82
LPE 16:0	1.79
PC 34:5	1.78
PE 42:8	1.76
PC 38:8	1.76
PC 36:5	1.74
PE 42:10	1.70
LPC 22:6	1.67
PEP-42:7	1.66
PA 36:2	1.63
PE 38:7	1.62

Figure 3: A) PLS-DA score plot of the data set plots indicating the separation between controls (CT) ischemia (ISC) and ischemia-reperfusion (I/R) models. Validation 1 comp: Q^2 0.5503, R^2 0.68177, Accuracy 0.55556) and B) list of top 16 phospholipids species based on variable importance in projection (VIP). Notation: AA-xxi (AA=lipid class; xx=total of carbon atoms in fatty acid; i= number of double bonds).

Univariate analysis (Kruskal–Wallis followed by a Dunn post-hoc analysis) was used to test for significant differences between phospholipid species among the three conditions (CT, ISC and I/R). The Kruskal-Wallis H test showed that the differences in 49 phospholipids scores were statistically significant (24 species with $q<0.01$ and 25 species with $q<0.05$) (Supplementary Table S3). These phospholipid species included 12 PCs, 11 PEs, 10 PE-P, 2 LPCs,2 LPEs, 4 CLs, 2 PGs, 1 LPI, 3 PAs, 1 PE-O, and 1 Cer. Phosphatidylethanolamines (PE) and lysophosphatidylethanolamines (LPE) represented a total of 20 species, including a high number of PE-P, phosphatidylethanolamine plasmalogens.

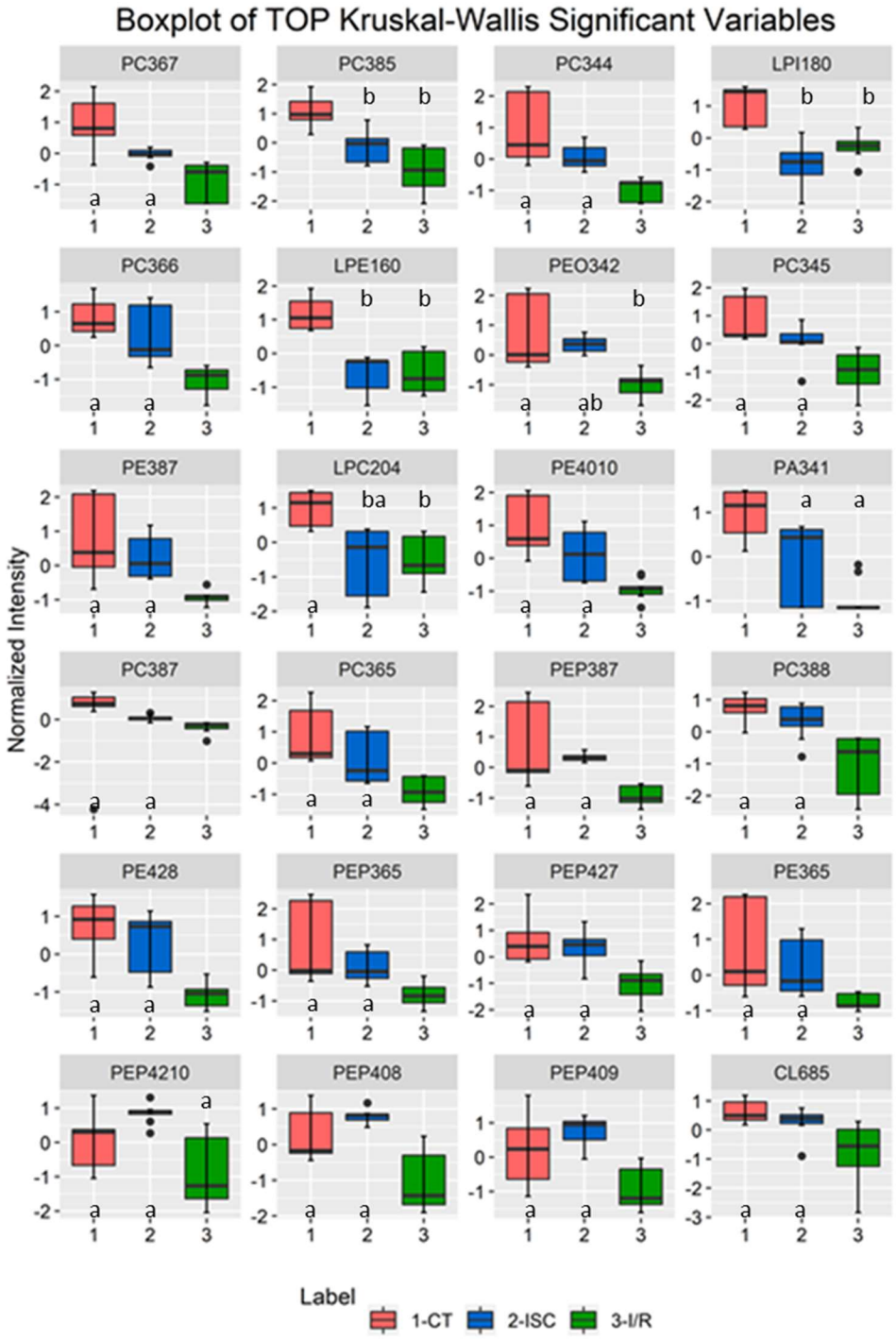

Figure 4: Boxplots of the top 24 Kruskal-Wallis H test q values followed by Dunn multicomparison test of the phospholipid species. Labels of the species are according to the following notation: AA-xxi (AA=lipid class; xx=total of carbon atoms in fatty acid; i= number of double bonds). Median values sharing the same letter did not differ statistically ($p > 0.05$).

Dunn's test of multiple comparisons revealed that 11 species were significantly different between CT and ISC, 34 between CT and I/R and 23 between ISC and I/R, as detailed in Supplementary Table S4. The boxplot of the top 24 Kruskal-Wallis H test q values of the phospholipid species, along with the Dunn's test of multiple comparisons for these species is shown in Figure 4.

Figure 5 shows a heatmap of the mean intensities of the phospholipids signals of the 25 lowest Kruskal-Wallis H test variable q values, together with a two-dimensional hierarchical cluster analysis dendrogram for biological conditions and variables (Figure 5). The trees to the left of the heat map and above the heat map show the relationships between the phospholipids and between samples, respectively. The dendrogram showed a good separation, with a tendency of variation of the relative abundance of the phospholipid species, where I/R levels were lower. These lower levels clustered the I/R group from CT and ISC, that remained more similar and with higher abundance of the phospholipid species. The clustering of individual phospholipid species as to their similarity in relative abundance changes showed two main groups. One group included three lyso species with lower abundance both in ISC and I/R compared with CT, and the second group included several lipids species mainly from PE (diacyl PE and PE-P species), PC, PA and CL. This second cluster is separated into two different branches, the first including three PE-P species, with higher relative abundance in the ISC group and lower relative abundance in the I/R group. The second cluster included, among others, 7 PE and PE-P species with higher relative abundance in CT and lowered relative abundance in the I/R group.

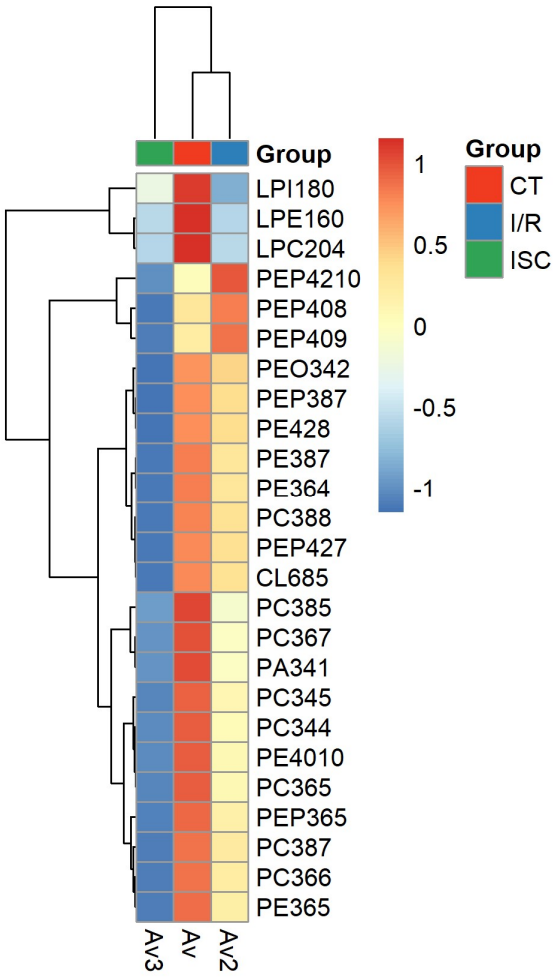

Figure 5: Two-dimensional hierarchical clustering heat map of the phospholipid data for the average of signal intensities of the 25 lowest Kruskal-Wallis H test q values. Levels of relative abundance are shown on the color scale, with numbers indicating the fold difference from the mean. The dendrogram in the top represents the clustering of the sample groups, showed three clusters, one for each condition. The lipid species were clustered in two main groups, one containing three lyso PL, which were less abundant in both disease conditions compared with control. The second cluster included mainly PC, PE and PE-P species with PUFAs. This second cluster was divided into two main branches, one containing 3 PE-P , which were more abundant in ISC and less abundant in IR. The second branch presented mainly polyunsaturated PC and PE species, which were more abundant in CT and less abundant in I/R. Labels of the species are according to the following notation: AA-xxi (AA=lipid class; xx=total of carbon atoms in fatty acid; i= number of double bonds).

5.3. Discussion

AMI is one of the main causes of morbidity and mortality worldwide. It is well known that AMI, usually caused by a sudden blockage in a coronary artery leading to inadequate blood supply to the heart, with the consequent lack of nutrients and hypoxia at the cellular level, elicit various injury-inducing signalling pathways. Hypoxia causes an increase in oxidative stress and ROS production and inflammation, ultimately leading to muscle cell death in myocardial ischemia. The timely reestablishment of blood flow to the infarcted region is very important for myocardial salvage. However, reperfusion after ischemia can have opposing effects mainly by inducing a burst of oxidative stress and ROS production[41], which can lead to severe myocardial injury and increased morbidity and mortality[16,17]. The pathophysiological mechanisms associated with myocardial damage following AMI remain unclear, which difficult the establishment of effective therapeutic strategies to prevent extensive cell death and I/R injury. Lipids are the main targets of ROS, whose levels are increased during ISC and even more during I/R. In fact, some studies have identified lipid peroxidation products have been identified in AMI patients due to I/R[42]. It should be noted that oxidised lipids are present in small amounts *in vivo* and are difficult to quantify[43].

Dysregulation of lipid metabolism is also a hallmark of CVD, although far from being fully understood. Although it has been scarcely used, lipidomics is now emerging as a promising approach in the study of CVD[44,45]. In this work, we evaluated the changes of the lipidome in an *ex vivo* model of ischemia (ISC) and ischemia-reperfusion (I/R) – the isolated Langendorff rat heart. To address this question, we evaluated the fatty acid content by GC-MS and the phospholipid profile by high-resolution LC-MS and MS/MS.

Data on FAs showed an increased level of C18:0 and a decreased level of C18:2 in ISC. These changes were greater in I/R, similarly to what was reported in previous studies in cardiomyocytes cell lines[37] and human serum and heart tissue after AMI[22,39,46]. This decrease of polyunsaturated fatty acids (PUFAs) can occur as a consequence of oxidative damage since the unsaturated fatty acyl chains are very sensitive to oxidation by ROS. Remarkably, we did not observe a significant change in the relative abundance of either C20:4 or C22:6 FAs, although the RA of C22:6 tended to decrease in ISC and I/R.

Besides FAs, we also evaluated the effect of ISC and I/R on the phospholipids profile in the heart. Regarding PCA (Figure 2), the PC1 distance between the ISC and I/R groups indicates that there were variations in phospholipid levels. The main contributors for the first dimension included 10 PC species out of 15 with contributions greater than 1% (Supplementary Table S 2). Given that PCs are the major component of biological

membranes, these results suggest constitutional modifications at the cell membrane level during ISC and I/R. These changes were confirmed in PLS-DA analysis (Figure 3), showing that CT, ISC e I/R were separately clustered into three groups. The PLS-DA plot shows that I/R is more distant of CT than ISC, which indicates that deeper changes in the phospholipidome have occurred. As in PCA, the VIP list (Figure 3B) also shows a high percentage of PC and PE as the main contributors. Also, these major phospholipid contributors in the VIP list had a high number of double bonds, suggesting that the relative abundance of these species was more influenced by the ISC and I/R conditions. Taken together, these results strongly suggest that ISC, but mainly I/R, induce changes in structural phospholipids, which can be mainly ascribed to the oxidation of these species.

Of the 219 phospholipid species identified in this study, 49 phospholipid levels were significantly different between the conditions ($p<0,05$) (Figure 4, Supplementary Table S3). Notably, multiple pairwise comparisons (Figure 4, Supplementary Table S 5) showed that most of these significant variations in the relative abundance of phospholipids occurred between ISC and I/R. This suggests that I/R induces deeper changes than ISC, which is in agreement with previous studies that showed that in ischemia an increase in oxidative stress occurs and this increase is intensified during reperfusion[17,47–50]. The 25 phospholipids with the lowest p-value, included 8 PC, 6 PE-P, 5 PE, 1 CL, 1 PA, 1 LPC, 1 LPE, 1 PE-O and 1 LPI. We used these selected phospholipids to perform a hierarchical cluster analysis (Figure 3).

The result of the hierarchical cluster analysis, represented as a heatmap (Figure 5), shows the phospholipids patterns in ISC, and I/R, compared to the controls. The two conditions varied significantly in relation to the pattern observed in the control samples, with the largest difference occurring between control and I/R, which was in a different branch. This is consistent with the PCA, as observed above (Figure 3). Phospholipids more distantly placed within branches show the greatest differences in relative abundance between conditions. As described above, the three lyso PL grouped in the first branch of HCA, classified the three conditions independently. An earlier study reported a decrease in the concentration of phosphatidylcholine and phosphatidylcholine plasmalogens in plasma and serum of patients with incident myocardial infarction[29,51]. A decrease in circulating PE plasmalogens in the serum of AMI patients was also observed[29]. Consistently, other studies have implicated a decrease of plasmalogens in cardiovascular diseases[27,29,52–54]. In accordance, the results obtained in our study associate variation of these plasmalogens with heart tissue. Cardiac tissue contains high levels of plasmalogens, with a greater amount of plasmenyl

ethanolamines (around 43-59% of PEs and around 30-40% of PCs are plasmalogens)[55]. Although abundant in important functional organs, as the heart, the role of plasmalogens is far from being fully disclosed, but it appears to play a crucial role in health and disease[56–58]. Plasmalogens remodelling can occur in different pathological conditions and among others functions, they have been reported as crucial antioxidants during cellular oxidative stress, being considered vital endogenous antioxidants as scavengers of ROS[59,60]. Under oxidative stress, plasmalogens are preferentially oxidised and avoid damage by lipid peroxidation, which may justify the observed decrease of PE and PC plasmalogens in our study. The vinyl-ether bond at the sn-1 position of these plasmalogens can readily react with ROS, supporting their antioxidant roles[57]. Interestingly, in our study, we observed an increase of 3 PE plasmalogens with longer and polyunsaturated FA in ISC, which could represent an attempt to restore the levels of these endogenous antioxidants, to counteract and prevent oxidative damage. These 3 PE plasmalogens showed opposite variation in the two disease conditions when compared with control, being decreased in I/R hearts

Another hallmark of this study was the variation of the RA of several PC and PE species containing PUFAs. PC and PE with PUFA are prone to radical oxidation[61], and its oxidative degradation may justify the decrease observed during ISC and I/R. Although the effect of AMI in the myocardial lipidome is scarcely addressed, the decrease in PE and PCs was previously reported in I/R[52,53]. The decrease in the PUFAs content in PE and PC has been previously reported in other cardiac disorders, such as diabetes-associated cardiomyopathy[62]. Also, increase of lipid peroxidation[42] and the presence oxidized PC molecular species were reported following myocardial ischemia and associated with cardiomyocytes cell death[63]. This increase in lipid peroxidation was further evidenced by the presence of oxidised PC species, as 1-palmitoyl-2-(5-oxovaleroyl) PC (POVPC) and 1-palmitoyl-2-glutaroyl PC (PGPC) associated with ischemia and reperfusion[64].

Our results showed that an LPI (18:0), an LPE (16:0) and two LPC (22:6 and 20:4) levels were lower in ISC and I/R, compared with the control (Figure 3 and Supplementary Tables S 6 and S4). LPC22:6 and LPC20:4 lysolipids were associated with anti-inflammatory effects. Therefore, it is likely that the decrease observed in this study is associated with a decrease in anti-inflammatory defences during ISC and I/R[65,66].

PC and PE are the major components of cell membranes, and changes in structural phospholipids were associated with changes in membrane properties such as Ca^{2+} defect and permeability changes in myocardium membranes[49,50], which can ultimately lead to cell death by membrane destabilisation. The metabolism of phospholipids is affected during

myocardium ischemia, and most of the studies that report the modulation of PL profile are due to oxidised phospholipids[42,64] and its degradation by phospholipase A2 (PLA2) with the formation of bioactive eicosanoids and lysoPLs,that are important inflammatory mediators[65–67].

Finally , we observed the 4 CL species (68:5, 78:12, 70:7 and 70:6; Supplementary Tables S 3 and S 4) whose RA were lower in ISC and I/R, compared with CT, likely due to oxidative degradation. These results are in agreement with previous studies that reported the loss of myocardial cardiolipin content during myocardial infarction[32,68,69]. Oxidised CL are well-known players in mitochondrial dysfunction and crucial to the cell apoptosis.,[70] and the observed changes may result in mitochondrial dysfunction, and death of cardiomyocytes [68,69,71–74].

In summary, this study demonstrates a clear modification of the PL profile during ischemia and reperfusion, with an overall decrease of levels of some of PLs, including PC and PE containing PUFAs and PE plasmalogens. We also observed a decrease of some CL, as well as some lysoPls. In general, the changes detected were more pronounced in the I/R phase than in ISC, which is consistent with the hypothesis that much of the myocardial damage occurs during reperfusion. Our results provide molecular evidence of the impact of AMI in the lipidome of the myocardial tissue and open new insights into the role of lipids in its pathophysiology, which may be useful in developing new therapeutic strategies and diagnostic markers.

5.4. Material and methods

5.4.1 Chemicals

Phospholipids internal standards for LC-MS were 1,3-bis[1,2-dimyristoyl-sn-glycero-3-phospho]-sn-glycerol) ($CL(14:0)_4$), 1,2-dimyristoyl-sn-glycero-3-phosphocholine (dMPC), 1-nonadecanoyl-2-hydroxy-sn-glycero-3-phosphocholine (LPC(19:0)), 11,2-dimyristoyl-sn-glycero-3-phosphoethanolamine (dMPE), 1,2-dimyristoyl-sn-glycero-3-phosphate (dMPA), 1,2-dimyristoyl-sn-glycero-3-phospho-(10-rac-glycerol) (dMPG), 1,2-dimyristoyl-sn-glycero-3-phospho-L-serine (dMPS), 1,2-dipalmitoyl-sn-glycero-3-phospho-(10-myo-inositol) (dPPI) and N-heptadecanoyl-D-erythro-sphingosylphosphorylcholine (SM(17:0/d18:1)), purchased to Avanti polar lipids Inc. (Alabaster, AL). Organic solvents (chloroform, methanol, acetonitrile and hexane) of HPLC grade were purchased to Fisher Scientific (Leicestershire, UK) and used without further purification. Ammonium acetate was

purchased from Sigma-Aldrich (St. Louis, MO, USA), perchloric acid ($HClO_7$, 70%) and ammonium molybdate tetrahydrate ($(NH_4)_6Mo_7O_{24}\cdot 4H_2O$) from Panreac (Barcelona, Spain), ascorbic acid ($C_6H_8O_6$) from VWR International (Leicestershire, UK), sodium dihydrogen phosphate dihydrate ($NaH_2PO_4\cdot 2H_2O$) from Riedel-de Haën (Seelze, Germany) and potassium hydroxide (KOH) from Merck (Darmstadt, Germany). MilliQ water was obtained from a Milli-Q Millipore system (MilliQ plus 185).

5.4.2 *Ex vivo* Langendorff heart perfusion model

10-week-old female Wistar rats (400±25 g) were anaesthetized with 85 mg/kg ketamine and 10 mg/kg xylazine and heparinized, after which hearts were excised and perfused on a Langendorff apparatus. Modified Krebs–Henseleit (KH) buffer (118 mM NaCl, 25 mM $NaHCO_3$, 4.7mM KCl, 1.2mM $MgSO_4$, 1.2mM KH_2PO_4, 10 mM Hepes, 1.25 mM $CaCl_2$ and 10 mM glucose, pH 7.4) was used to perfuse the isolated hearts, at a constant flow rate of 15 ml/min, equilibrated with 95%O_2/5%CO_2 at 37ºC. After a 10 min stabilization period, hearts were either perfused for further 20 min (CT), subjected to 20 min of no-flow ischemia (ISC), or to 20 min of reperfusion after ischemia (I/R). After the experiments, hearts were snap-frozen in liquid nitrogen before subsequent analysis.

5.4.3 Tissue sampling and lipid extraction

Myocardial tissue (0.1 grams) was excised from the hearts of the rats, and the tissue was transferred to a mortar and homogenized by adding liquid nitrogen and grounding with a pestle. The grounded tissue was collected in an ice-cold glass tube, and 1.5 mL MeOH was added, followed by liquid-liquid lipid extraction with methyl *tert*-butyl ether (MTBE) as previously described[75]. Briefly, 5 ml of MTBE were added to each sample and incubated during one hour on ice with an orbital shaker (750 rpm), and 1.25mL of water were added and incubated in the same conditions for another 10 min. After centrifugation (568 rcf, 10 min) in a Mixtasel centrifuge (Selecta) a two-phase system was obtained, and the upper organic phase containing the extracted lipids was collected and kept on ice. The lower phase was re-extracted with 2 mL of MTBE, 600 µL of MeOH, and 500 µL H_2O (10*/*3*/*2.5, v*/*v*/*v), centrifuged and combined with the previous organic phase. After being dried under a nitrogen stream, the lipid extract was resuspended in $CHCl_3$ and used for the MS analysis and the quantitation of phospholipids. All analyses were performed on three biological replicates.

5.4.4 Quantification of phospholipids content by phosphorous assay

The total phospholipid content of samples was determined according to Bartlett and Lewis[76]. Briefly, an aliquot of 10 µL of the extract was dried and incubated for 1h at 180 ºC with 125 µL of perchloric acid (70%) in a heating block (Stuart, U.K.). This solution and eight standards solutions, with different concentrations of sodium dihydrogen phosphate dihydrate, were mixed with 825 µL of MilliQ water, 125 µL of ammonium molybdate tetrahydrate (2.5% m/v) and 125 µL of freshly prepared ascorbic acid (10% m/v). Samples and standards were then simultaneously incubated at 100 ºC in a water bath for 10 min, and the content of inorganic acid was measured in a microplate spectrophotometer at 797 nm wavelength (Multiscan 90, ThermoScientific). The abundance of phospholipids was calculated with the ratio between the mass of inorganic phosphorus and the phospholipids average.

5.4.5 Fatty acids profiling by GC-MS

FAMEs (fatty acids methyl esters) were obtained by transesterification of total lipid extract. The lipid extract (30 µg in $CHCl_3$) were dried under N_2 stream, redissolved in 1mL of hexane, and mixed with 200 µL of a 2M solution of KOH in methanol[37]. After 2 min vortexing, the reaction products were washed with 2mL of saturated NaCl solution and the upper organic phase collected after centrifugation (568 rcf, 5 min) in a Mixtasel centrifuge (Selecta). The fraction was dried and resuspended in 80 µL of hexane, of which 4 µL were injected in an Agilent Technologies 6890N Network GC spectrometer (Santa Clara, CA) equipped with a polar DB-FFAP column of 30 m of length, 0.32 mm of internal diameter, and 0.25 um film thickness (J&W Scientific, Folsom, CA). The GC equipment was connected to an Agilent 5973 Network Mass Selective Detector (Santa Clara, CA) scanning between *m/z* range 40–500 in a 1s cycle of full scan mode acquisition and electron impact adjusted at 70 eV of energy. The oven temperature was programmed with an initial temperature of 80 °C, following a linear increase to 160 °C at 25 °C/min, a linear increase to 210 °C at 2 °C/min, and finally linear increase until 250 °C at 30 °C/min, where it was held for 10 min before returning to the initial conditions. The injector and detector temperatures were 220 and 280 °C, respectively. Helium was used as carrier gas at a flow rate of 0.5 mL/min. A mixture of fatty acid methyl ester standards (Supelco 37 Component FAME Mix, CRM47885, Sigma

Aldrich, St. Louis, MO, USA) was injected in the same session. Three technical replicates were used to confirm reproducibility.

5.4.6 Lipid profiling by HILIC-ESI-MS and MS/MS

An amount of lipid extract equivalent to 5 µg of total phospholipid were suspended in 200 µL of eluent B (60% ACN/40% MeOH (v/v), 1 mM ammonium acetate). The solution was spiked with 1 µL of a mixture of standards prepared dissolving 25 µg of dMPC, 25 µg of dMPG, 25 µg of dMPE, 100 µg of dMPS, 50 µg of dPPI, 100 µg of dMPA, and 50 µg of LPC(19:0), 25 µg of SM(17:0/d18:1), 100µg of $CL(14:0)_4$ to final volume of 1 mL of $CHCl_3$:MeOH (1:1). The preparation was transferred to a vial, and 5ul were injected in a high-performance HPLC system with an autosampler (Accela™ Thermo Fisher Scientific, Waltham, MA, USA) coupled online to an Orbitrap Q-Exactive mass spectrometer (Thermo Fisher Scientific, Waltham, MA, USA). The chromatographic column was a microbore Ascentis Si HPLC Pore column (15 cm × 1.0 mm, 3 µm; Sigma–Aldrich). The solvent system consisted in a biphasic gradient with solvents A (50% acetonitrile / 25% methanol / 25%water (v/v/v), 1mM ammonium acetate) and B (60% ACN/40% MeOH (v/v), 1 mM of ammonium acetate). The initial condition with 0% of mobile phase A *held isocratically* for 8 min, followed by a linear increase to 60% of A within 7 min and again held isocratically for 15 min, returning to the initial conditions in 5 min and equilibrating during 10 min. The flow rate was at 40 µL/min, and the column compartment was held at 30 ºC. The Orbitrap Q-Exactive was operated simultaneously in positive mode (3kV) and negative mode (-2.7kV), with capillary temperature 250ºC, flow 15U of sheath gas and 5U of auxiliary gas (arbitrary units). The acquisition mode was data dependent, with MS at high resolution (resolution of 70000, AGC target 10E6) and data dependent MS^2 for the ten more intense peaks (resolution of 17500, AGC target $10E^5$, dynamic exclusion 30s and threshold $10E^4$, and normalised collision energy ranged between 20, 30, and 35eV). Data acquisition was carried out during the initial 35 minutes of the run using the Xcalibur data system (V3.3, Thermo Fisher Scientific, Waltham, MA, USA). At least three technical replicates were employed to confirm reproducibility.

5.4.7 Data analysis and statistics

All GC-MS chromatograms were analyzed using the MSD Cessation software version D.00.00.38 (Agilent Technologies, Santa Clara, CA, USA). The peaks were automatically

integrated, the fatty acids were identified, and the percentages of the total peak area were calculated. The FAMEs were identified by comparing their mass spectrum with the fragmentation patterns in the AOCS lipid library and matching peak retention times with fatty acid methyl esters standards.

LC-MS data were analyzed with Xcalibur Qual Browser (Thermo Fisher Scientific, Waltham, MA, USA) for chromatographic profiling, and high-accuracy MS and MS/MS identification of the phospholipid species. The species positively identified were quantified in MZMine 2.26 [77]. Data pre-processing, including baseline correction, peak deconvolution, deisotoping and alignment, and gap-filling, was applied. The identification of all lipid species was based on mass accuracy, retention time and manual analysis of MS/MS data. PE, LPE, PC, LPC, SM and Cer were analyzed in positive ion mode and identified as $[M+H]^+$ molecular ions, while PS, PI, LPI, PA, PG and CL were identified in negative ion mode and identified as $[M-H]^-$ molecular ions. Semi-quantification was performed by integrating the area under the curve using the LC-MS chromatographic peak of the main ion (charge state, adduct and polarity) of each of the phospholipid species. Data (peak areas) were normalized by calculating the ratio against a selected internal standard. The internal standards, described in the Chemical section, were endogenously non-occurring PL species, and each standard was employed for normalization of all the species of its class.

Multivariate and univariate analyses were performed using R version 3.5[78] in Rstudio version 1.1.4[79]. GC data were glog transformed and LC-MS data were glog transformed and autoscaled using the R package Metaboanalyst[80]. Principal Component Analysis (PCA) was conducted for exploratory data analysis, with the R built-in function and ellipses were drawn using the R package ellipse[81], assuming a multivariate normal distribution and a level of 0.95. Partial least square discriminant analysis (PLS-DA) was conducted using the R package Metaboanalyst. *Kruskal-Wallis* test *followed by Dunn's post-hoc* comparisons were performed with the R built-in function. P-values were corrected for multiple testing using the BH Benjamini, Hochberg, and Yekutieli method (q values)[82]. Heatmaps were created using the R package pheatmap[83] using "Euclidean" as clustering distance, and "ward.D" as the clustering method. All graphics and boxplots were created using the R package ggplot2[84]. Other R packages used for data management and graphics included plyr[85], dplyr[86], tidyr[87] and ggrepel[88].

Funding

This work was supported by funding from European Commission's Horizon 2020 research and innovation programme under the Marie Sklodowska-Curie grant agreement number 675132 (MSCA-ITN-ETN MASSTRPLAN) to University of Aveiro. Thanks are due to the University of Aveiro, QOPNA-LAQV (UID/QUI/00062/2019) and CESAM (UID/AMB/50017/2019), and Portuguese Mass Spectrometry Network (LISBOA-01-0145-FEDER-402-022125) to FCT/MCTES through national funds (PIDDAC), and the co-funding by the FEDER, within the PT2020 Partnership Agreement and Compete 2020. Tânia Melo is grateful for her Post-Doc grant (BPD/UI 51/5388/2017).

This work was supported by the European Regional Development Fund (ERDF) through the Operational Program for Competitiveness Factors (COMPETE) [under the projects PAC "NETDIAMOND" POCI-01-0145-FEDER-016385; HealthyAging2020 CENTRO-01-0145-FEDER-000012-N2323; POCI-01-0145-FEDER-007440, CENTRO-01-0145-FEDER-032179, CENTRO-01-0145-FEDER-032414 and FCTUID/NEU/04539/2013 to CNC.IBILI]. TMM was supported by PD/BD/106043/2015 from Fundação para a Ciência e a Tecnologia (FCT).

Conflicts of Interest: The authors declare no conflict of interest.

References

1. Mendis, S. *et al.* World Health Organization definition of myocardial infarction: 2008-09 revision. *Int. J. Epidemiol.* **40**, 139–146 (2011).
2. Tibaut, M., Mekis, D. & Petrovic, D. Pathophysiology of Myocardial Infarction and Acute Management Strategies. *Cardiovasc. Hematol. Agents Med. Chem.* **14**, 150–159 (2017).
3. Jennings, R. B. Historical perspective on the pathology of myocardial ischemia/reperfusion injury. *Circulation Research* **113**, 428–438 (2013).
4. Hausenloy, D. J. & Yellon, D. M. The mitochondrial permeability transition pore: its fundamental role in mediating cell death during ischaemia and reperfusion. *J. Mol. Cell. Cardiol.* **35**, 339–41 (2003).
5. SOUSSI, B., IDSTRÖM, J.-P., SCHERSTÉN, T. & BYLUND-FELLENIUS, A.-C. Cytochrome c oxidase and cardiolipin alterations in response to skeletal muscle ischaemia and reperfusion. *Acta Physiol. Scand.* **138**, 107–114 (1990).
6. Neri, M. *et al.* Cardiac oxidative stress and inflammatory cytokines response after myocardial infarction. *Curr. Vasc. Pharmacol.* **13**, 26–36 (2015).

7. Kurian, G. A., Rajagopal, R., Vedantham, S. & Rajesh, M. The Role of Oxidative Stress in Myocardial Ischemia and Reperfusion Injury and Remodeling: Revisited. *Oxid. Med. Cell. Longev.* **2016**, 1–14 (2016).

8. Ong, S.-B. *et al.* Inflammation following acute myocardial infarction: Multiple players, dynamic roles, and novel therapeutic opportunities. *Pharmacol. Ther.* **186**, 73–87 (2018).

9. Williams, R. S. & Benjamin, I. J. Protective responses in the ischemic myocardium. *J. Clin. Invest.* **106**, 813–8 (2000).

10. Rudolph, T. K. *et al.* Nitro-fatty acids reduce atherosclerosis in apolipoprotein E-deficient mice. *Arterioscler. Thromb. Vasc. Biol.* **30**, 938–945 (2010).

11. Gustafsson, Å. B., Gottlieb, R. A., Gustafsson, A. B. & Gottlieb, R. A. Autophagy in Ischemic Heart Disease. *Circ. Res.* **104**, 150–158 (2009).

12. Ma, S., Wang, Y., Chen, Y. & Cao, F. The role of the autophagy in myocardial ischemia/reperfusion injury ☆. *BBA - Mol. Basis Dis.* **1852**, 271–276 (2015).

13. Huang, C. *et al.* Autophagy induced by ischemic preconditioning is essential for cardioprotection. *J. Cardiovasc. Transl. Res.* **3**, 365–73 (2010).

14. Martins-Marques, T. *et al.* Ischaemia-induced autophagy leads to degradation of gap junction protein connexin43 in cardiomyocytes. *Biochem. J.* **467**, 231–245 (2015).

15. Simonis, G., Strasser, R. H. & Ebner, B. Reperfusion injury in acute myocardial infarction. *Crit. Care* **16**, A22 (2012).

16. Cadenas, S. ROS and redox signaling in myocardial ischemia-reperfusion injury and cardioprotection. *Free Radic. Biol. Med.* **117**, 76–89 (2018).

17. Granger, D. N. & Kvietys, P. R. Reperfusion injury and reactive oxygen species: The evolution of a concept. *Redox Biol.* **6**, 524–551 (2015).

18. Thygesen, K. *et al.* Third Universal Definition of Myocardial Infarction. *Circulation* **126**, (2012).

19. Fathil, M. F. M. *et al.* Diagnostics on acute myocardial infarction: Cardiac troponin biomarkers. *Biosens. Bioelectron.* **70**, 209–220 (2015).

20. Farthing, D. E., Farthing, C. A. & Xi, L. Inosine and hypoxanthine as novel biomarkers for cardiac ischemia: From bench to point-of-care. *Exp. Biol. Med.* **240**, 821 (2015).

21. Opie, L. H. Metabolic Management of Acute Myocardial Infarction Comes to the Fore and Extends Beyond Control of Hyperglycemia. *Circulation* **117**, 2172–2177 (2008).

22. Sun, Y. *et al.* Plasma fatty acids, oxylipins, and risk of myocardial infarction: the Singapore Chinese Health Study. *J. Lipid Res.* **57**, 1300–7 (2016).

23. Park, J. Y., Lee, S.-H., Shin, M.-J. & Hwang, G.-S. Alteration in Metabolic Signature and Lipid Metabolism in Patients with Angina Pectoris and Myocardial Infarction. *PLoS One* **10**, e0135228 (2015).

24. Hinterwirth, H., Stegemann, C. & Mayr, M. Lipidomics: quest for molecular lipid biomarkers in cardiovascular disease. *Circ. Cardiovasc. Genet.* **7**, 941–54 (2014).

25. Ganna, A. *et al.* Large-scale Metabolomic Profiling Identifies Novel Biomarkers for Incident Coronary Heart Disease. *PLoS Genet.* **10**, e1004801 (2014).

26. Sigruener, A. *et al.* Glycerophospholipid and Sphingolipid Species and Mortality: The Ludwigshafen Risk and Cardiovascular Health (LURIC) Study. *PLoS One* **9**, e85724 (2014).

27. Meikle, P. J. *et al.* Plasma Lipidomic Analysis of Stable and Unstable Coronary Artery Disease. *Arterioscler. Thromb. Vasc. Biol.* **31**, 2723–2732 (2011).

28. Syme, C. *et al.* Glycerophosphocholine Metabolites and Cardiovascular Disease Risk Factors in Adolescents: A Cohort Study. *Circulation* **134**, 1629–1636 (2016).

29. Moxon, J. V. *et al.* Baseline serum phosphatidylcholine plasmalogen concentrations are inversely associated with incident myocardial infarction in patients with mixed peripheral artery disease presentations. *Atherosclerosis* **263**, 301–308 (2017).

30. Tham, Y. K. *et al.* Distinct lipidomic profiles in models of physiological and pathological cardiac remodeling, and potential therapeutic strategies. *Biochim. Biophys. Acta - Mol. Cell Biol. Lipids* **1863**, 219–234 (2018).

31. Nam, M., Jung, Y., Ryu, D. H. & Hwang, G.-S. A metabolomics-driven approach reveals metabolic responses and mechanisms in the rat heart following myocardial infarction. *Int. J. Cardiol.* **227**, 239–246 (2017).

32. Paradies, G. *et al.* Decrease in mitochondrial complex I activity in ischemic/reperfused rat heart: involvement of reactive oxygen species and cardiolipin. *Circ. Res.* **94**, 53–9 (2004).

33. Knapp, M. *et al.* Myocardial infarction differentially alters sphingolipid levels in plasma, erythrocytes and platelets of the rat. *Basic Res. Cardiol.* **107**, 294 (2012).

34. Reforgiato, M. R. *et al.* Inhibition of ceramide de novo synthesis as a postischemic strategy to reduce myocardial reperfusion injury. *Basic Res. Cardiol.* **111**, 12 (2016).

35. Berêsewicz, A., Dobrzyñ, A. & Górski, J. ACCUMULATION OF SPECIFIC CERAMIDES IN ISCHEMIC/REPERFUSED RAT HEART; EFFECT OF ISCHEMIC PRECONDITIONING. *J. Physiol. Pharmacol.* **53**, 371–382 (2002).

36. Knapp, M., Żendzian-Piotrowska, M., Kurek, K. & Błachnio-Zabielska, A. Myocardial Infarction Changes Sphingolipid Metabolism in the Uninfarcted Ventricular Wall of the Rat. *Lipids* **47**, 847–853 (2012).

37. Sousa, B. *et al.* Alteration in Phospholipidome Profile of Myoblast H9c2 Cell Line in a Model of Myocardium Starvation and Ischemia. *J. Cell. Physiol.* **231**, 2266–2274 (2016).

38. Herr, D. J., Aune, S. E. & Menick, D. R. Induction and Assessment of Ischemia-reperfusion Injury in Langendorff-perfused Rat Hearts. *J. Vis. Exp.* e52908 (2015). doi:10.3791/52908

39. Shearer, G. C., Chen, J., Chen, Y. & Harris, W. S. Myocardial infarction does not affect fatty-acid profiles in rats. *Prostaglandins Leukot. Essent. Fat. Acids* **81**, 411–416 (2009).

40. Henseler, J. Partial Least Squares Path Modeling. in 361–381 (2017). doi:10.1007/978-3-319-53469-5_12

41. Bagheri, F. *et al.* Reactive oxygen species-mediated cardiac-reperfusion injury: Mechanisms and therapies. *Life Sci.* **165**, 43–55 (2016).

42. Lu, J. *et al.* Comprehensive metabolomics identified lipid peroxidation as a prominent feature in human plasma of patients with coronary heart diseases. *Redox Biol.* **12**, 899–907 (2017).

43. Tyurina, Y. Y. *et al.* “Redox lipidomics technology: Looking for a needle in a haystack”. *Chem. Phys. Lipids* **221**, 93–107 (2019).

44. Alshehry, Z. H. *et al.* Plasma Lipidomic Profiles Improve on Traditional Risk Factors for the Prediction of Cardiovascular Events in Type 2 Diabetes Mellitus. *Circulation* **134**, 1637–1650 (2016).

45. Kohno, S., Keenan, A. L., Ntambi, J. M. & Miyazaki, M. Lipidomic insight into cardiovascular diseases. *Biochem. Biophys. Res. Commun.* (2018). doi:10.1016/J.BBRC.2018.04.106

46. Wurtz, P. *et al.* Metabolite Profiling and Cardiovascular Event Risk: A Prospective Study of 3 Population-Based Cohorts. *Circulation* **131**, 774–785 (2015).

47. Llitjos, J.-F., Mira, J.-P., Duranteau, J. & Cariou, A. Hyperoxia toxicity after cardiac arrest: What is the evidence? *Ann. Intensive Care* **6**, 23 (2016).

48. Sjöberg, F. *et al.* The medical use of oxygen: a time for critical reappraisal. *J. Intern. Med.* **274**, 505–528 (2013).

49. Vishwakarma, V. K., Upadhyay, P. K., Gupta, J. K. & Yadav, H. N. Pathophysiologic role of ischemia reperfusion injury: A review. *J. Indian Coll. Cardiol.* **7**, 97–104 (2017).

50. Budib Dorsa Pontes, H. *et al. Ischemia and Reperfusion Injury: General Aspects and Mechanisms*. *EC Cardiology* **2**, (2016).

51. Reiner, Ž. *et al.* Lipid lowering drug therapy in patients with coronary heart disease from 24 European countries – Findings from the EUROASPIRE IV survey. *Atherosclerosis* **246**, 243–250 (2016).

52. Sutter, I. *et al.* Plasmalogens of high-density lipoproteins (HDL) are associated with coronary artery disease and anti-apoptotic activity of HDL. *Atherosclerosis* **241**, 539–546 (2015).

53. Sutter, I. *et al.* Decreased phosphatidylcholine plasmalogens – A putative novel lipid signature in patients with stable coronary artery disease and acute myocardial infarction. *Atherosclerosis* **246**, 130–140 (2016).

54. Nishimukai, M. *et al.* Serum choline plasmalogens—those with oleic acid in sn− 2—are biomarkers for coronary artery disease. *Clin. Chim. Acta* **437**, 147–154 (2014).

55. Nagan, N. & Zoeller, R. A. Plasmalogens: biosynthesis and functions. *Prog. Lipid Res.* **40**, 199–229 (2001).

56. Dean, J. M. & Lodhi, I. J. Structural and functional roles of ether lipids. *Protein Cell* **9**, 196–206 (2018).

57. Lessig, J. & Fuchs, B. Plasmalogens in biological systems: their role in oxidative processes in biological membranes, their contribution to pathological processes and aging and plasmalogen analysis. *Curr. Med. Chem.* **16**, 2021–41 (2009).

58. Paul, S., Lancaster, G. I. & Meikle, P. J. Plasmalogens: A potential therapeutic target for neurodegenerative and cardiometabolic disease. *Prog. Lipid Res.* **74**, 186–195 (2019).

59. Wallner, S. Plasmalogens the neglected regulatory and scavenging lipid species. *Chem. Phys. Lipids* **164**, 573–589 (2011).

60. Hermansson, M., Hokynar, K. & Somerharju, P. Mechanisms of glycerophospholipid homeostasis in mammalian cells. *Prog. Lipid Res.* **50**, 240–257 (2011).

61. Reis, A. & Spickett, C. M. Chemistry of phospholipid oxidation. *Biochim. Biophys. Acta - Biomembr.* **1818**, 2374–2387 (2012).

62. Li, W. *et al.* Profile of cardiac lipid metabolism in STZ-induced diabetic mice. *Lipids Health Dis.* **17**, 231 (2018).

63. Yeang, C. *et al.* Reduction of myocardial ischaemia–reperfusion injury by inactivating oxidized phospholipids. *Cardiovasc. Res.* **115**, 179–189 (2019).

64. Ganguly, R. *et al.* Alpha linolenic acid decreases apoptosis and oxidized phospholipids in cardiomyocytes during ischemia/reperfusion. *Mol. Cell. Biochem.* **437**, 163–175 (2018).

65. Hung, N. D., Kim, M. R. & Sok, D.-E. Mechanisms for anti-inflammatory effects of 1-[15(S)-hydroxyeicosapentaenoyl] lysophosphatidylcholine, administered intraperitoneally, in zymosan A-induced peritonitis. *Br. J. Pharmacol.* **162**, 1119–35 (2011).

66. Akerele, O. A. & Cheema, S. K. Fatty acyl composition of lysophosphatidylcholine is important in atherosclerosis. *Med. Hypotheses* **85**, 754–760 (2015).

67. Fitzpatrick, F. A. & Soberman, R. Regulated formation of eicosanoids. *J. Clin. Invest.* **107**, 1347–51 (2001).

68. Lesnefsky, E. J., Slabe, T. J., Stoll, M. S. K., Minkler, P. E. & Hoppel, C. L. Myocardial ischemia selectively depletes cardiolipin in rabbit heart subsarcolemmal mitochondria. *Am. J. Physiol. Circ. Physiol.* **280**, H2770–H2778 (2001).

69. Chen, Q. & Lesnefsky, E. J. Depletion of cardiolipin and cytochrome c during ischemia increases hydrogen peroxide production from the electron transport chain. *Free Radic. Biol. Med.* **40**, 976–982 (2006).

70. Iverson, S. L. & Orrenius, S. The cardiolipin-cytochrome c interaction and the mitochondrial regulation of apoptosis. *Arch. Biochem. Biophys.* **423**, 37–46 (2004).

71. Shen, Z., Ye, C., McCain, K. & Greenberg, M. L. The Role of Cardiolipin in Cardiovascular Health. *Biomed Res. Int.* **2015**, 891707 (2015).

72. Maguire, J. J. *et al.* Known unknowns of cardiolipin signaling: The best is yet to come. *Biochim. Biophys. Acta - Mol. Cell Biol. Lipids* **1862**, 8–24 (2017).

73. Lesnefsky, E. J. & Hoppel, C. L. Ischemia–reperfusion injury in the aged heart: role of mitochondria. *Arch. Biochem. Biophys.* **420**, 287–297 (2003).

74. Chen, Q., Moghaddas, S., Hoppel, C. L. & Lesnefsky, E. J. Ischemic defects in the electron transport chain increase the production of reactive oxygen species from isolated rat heart mitochondria. *Am. J. Physiol. Physiol.* **294**, C460–C466 (2008).

75. Matyash, V., Liebisch, G., Kurzchalia, T. V, Shevchenko, A. & Schwudke, D. Lipid extraction by methyl-tert-butyl ether for high-throughput lipidomics. *J. Lipid Res.* **49**, 1137–46 (2008).

76. Bartlett, E. M. & Lewis, D. H. Spectrophotometric determination of phosphate esters in the presence and absence of orthophosphate. *Anal. Biochem.* **36**, 159–167 (1970).

77. Pluskal, T., Castillo, S., Villar-Briones, A. & Oresic, M. MZmine 2: modular framework for processing, visualizing, and analyzing mass spectrometry-based molecular profile data. *BMC Bioinformatics* **11**, 395 (2010).

78. R Core Team. R: A language and environment for statistical computing.R Foundation for Statistical Computing, Vienna, Austria. (2018).

79. Rstudio Team. RStudio: Integrated Development Environment for R. (2016).

80. Xia, J. & Wishart, D. S. Using MetaboAnalyst 3.0 for Comprehensive Metabolomics Data Analysis. in *Current Protocols in Bioinformatics* **55**, 14.10.1-14.10.91 (John Wiley & Sons, Inc., 2016).

81. Murdoch, D. & Chow, E. Ellipse: Functions for drawing ellipses and ellipse-like confidence regions. R package version 0.4.1. 2018.

82. Benjamini, Y. & Hochberg, Y. Controlling the False Discovery Rate: A Practical and Powerful Approach to Multiple Testing. *Journal of the Royal Statistical Society. Series B (Methodological)* **57**, 289–300 (1995).

83. Kolde, R. Pheatmap: Pretty Heatmaps. R package version 1.0.12.

84. Wickham, H. ggplot2 – Elegant Graphics for Data Analysis. Springer Verlag New York. (2016).

85. Wickham, H. The Split-Apply-Combine Strategy for Data Analysis. *J. Stat. Softw.* **40**, (2011).

86. Wickham, H., François, R., Henry, L. & Müller, K. dplyr: A Grammar of Data Manipulation. R package version 0.7.7. (2018).

87. Wickham, H. & Henry, L. tidyr: Easily Tidy Data with ‘spread()’ and ‘gather()’ Functions. (2018).

88. Slowikowski, K. ggrepel: Automatically Position Non-Overlapping Text Labels with ‘ggplot2’. R package version 0.8.0. (2018).

5.5. Supplementary information

Supplementary Table S 1: Summary of the phospholipid molecular species that were identified and quantified by high-resolution LC-MS and MS/MS analysis. Species are annotated as PL(C:N), where PL is the phospholipid class, C the number of carbons and N the number of double bonds. An asterisk (*) in the fatty acyl column was added when there was no information about the fatty acyl chains (NA), but other reporter ions were observed.

Species assigned	Ion	Exact m/z	Observed m/z	ppm	RT	Most probable fatty acyl chain content according to MS/MS data
CL(68:5)	$[M-2H]^{2-}$	698.4706	698.4706	0.0	1.9	NA
CL(68:6)	$[M-2H]^{2-}$	697.4631	697.4631	0.0	1.9	16:1/16:2/18:1/18:2
CL(70:5)	$[M-2H]^{2-}$	712.4860	712.4849	-1.6	1.9	NA
CL(70:6)	$[M-2H]^{2-}$	711.4780	711.4761	-2.7	1.9	NA
CL(70:7)	$[M-2H]^{2-}$	710.4710	710.4716	0.9	1.9	16:2/18:1/18:2/18:2; 16:1/18:2/18:2/18:2
CL(72:5)	$[M-2H]^{2-}$	726.5020	726.4989	-4.3	1.9	18:0/18:2/18:1/18:2
CL(72:6)	$[M-2H]^{2-}$	725.4940	725.4916	-3.3	1.9	18:0/18:1/18:2/18:3
CL(72:7)	$[M-2H]^{2-}$	724.4860	724.4839	-2.9	1.9	NA
CL(72:8)	$[M-2H]^{2-}$	723.4780	723.4794	2.0	1.9	18:1/18:2/18:2/18:3
CL(72:9)	$[M-2H]^{2-}$	722.4720	722.4720	0.0	1.9	16:0/16:1/20:4/20:4; 18:1/18:2/18:3/18:3
CL(74:10)	$[M-2H]^{2-}$	735.4796	735.4796	0.0	1.9	NA
CL(74:8)	$[M-2H]^{2-}$	737.4948	737.4948	0.0	1.9	18:1/18:2/18:3/20:2; 18:1/18:2/18:2/20:3
CL(74:9)	$[M-2H]^{2-}$	736.4863	736.4863	-0.1	1.9	18:1/18:3/18:3/20:2; 18:2/18:2/18:3/20:2; 18:1/18:3/18:2/20:3; 18:0/18:3/18:3/20:3; 18:2/18:2/18:2/20:3; 16:0/18:2/20:4/20:3; 16:1/18:1/20:4/20:3; 16:0/18:3/20:3/20:3; 16:1/18:2/20:3/20:3; 16:1/18:0/20:4/20:4; 18:0/18:2/18:3/20:4; 18:1/18:1/18:3/20:4; 16:0/18:1/20:4/20:4; 18:1/18:2/18:2/20:4
CL(76:10)	$[M-2H]^{2-}$	749.4919	749.4919	0.0	1.9	18:1/18:2/20:3/20:4; 18:0/18:3/20:3/20:4; 18:1/18:1/20:4/20:4; 18:2/18:2/20:2/20:4; 18:1/18:3/20:2/20:4; 18:0/18:4/20:2/20:4; 18:1/18:4/20:2/20:3; 18:2/18:3/20:2/20:3;

						18:1/18:1/18:2/22:6; 18:0/18:1/18:3/22:6; 18:0/18:2/18:2/22:6; 18:1/18:2/18:2/22:5; 18:0/18:3/18:2/22:5; 18:1/18:2/18:3/22:4; 16:0/18:0/20:4/22:6; 16:1/18:1/20:3/22:6; 16:0/18:2/20:3/22:6; 16:0/18:2/20:2/22:6; 16:1/18:1/20:2/22:6; 16:0/18:1/20:4/22:5; 18:0/18:3/20:1/20:4; 18:1/18:2/20:1/20:4; 18:2/18:2/20:0/20:4; 16:0/20:2/20:4/20:4
CL(76:11)	$[M-2H]^{2-}$	748.4860	748.4860	0.0	1.9	18:1/18:2/20:4/20:4; 18:0/18:3/20:4/20:4; 18:0/18:4/20:3/20:4; 18:2/18:2/20:3/20:4; 18:1/18:3/20:3/20:4; 18:1/18:4/20:2/20:4; 18:2/18:3/20:2/20:4; 18:1/18:2/18:2/22:6; 18:0/18:2/18:3/22:6; 18:2/18:2/18:2/22:5; 18:1/18:3/18:2/22:5; 18:0/18:4/18:2/22:5; 18:2/18:2/18:3/22:4; 16:0/18:2/20:3/22:6; 16:0/18:2/20:4/22:5; 16:0/18:2/20:5/22:4; 16:1/18:1/20:3/22:6; 16:1/18:1/20:4/22:5; 16:1/18:1/20:5/22:4; 16:0/18:1/20:4/22:6; 16:1/18:0/20:4/22:6; 16:0/20:3/20:4/20:4; 16:1/20:2/20:4/20:4; 16:0/18:3/20:4/22:4; 16:1/18:2/20:4/22:4; 16:0/18:4/20:3/22:4; 16:0/18:3/20:2/22:6; 16:1/18:2/20:2/22:6; 16:0/20:2/20:5/20:4; 16:0/18:1/20:5/22:5
CL(76:12)	$[M-2H]^{2-}$	747.4796	747.4796	0.0	1.9	18:1/18:3/20:4/20:4; 18:2/18:2/20:4/20:4; 18:2/18:2/18:2/22:6; 18:1/18:2/18:3/22:6; 18:0/18:3/18:3/22:6; 16:0/18:3/20:3/22:6;

						16:0/18:2/20:4/22:6; 16:0/20:4/20:4/20:4; 18:0/18:4/20:4/20:4; 18:3/18:2/18:2/22:5; 18:2/18:3/20:3/20:4; 16:1/18:1/20:4/22:6
CL(78:11)	$[M-2H]^{2-}$	762.5020	762.5012	-1.1	1.9	18:1/18:2/20:2/22:6; 18:1/18:2/20:3/22:5; 18:1/18:2/20:4/22:4; 18:1/18:2/20:5/22:3;
CL(78:12)	$[M-2H]^{2-}$	761.4940	761.4936	-0.6	1.9	16:0/18:1/22:3/22:6; 16:0/18:1/22:4/22:5;
CL(78:13)	$[M-2H]^{2-}$	760.4867	760.4852	-2.0	1.9	18:1/18:2/20:4/22:6; 18:1/18:2/20:5/22:5; 16:0/18:1/22:6/22:6; 16:0/18:2/22:5/22:6
CL(78:14)	$[M-2H]^{2-}$	759.4780	759.4765	-2.0	1.9	NA
PG(32:0)	$[M-H]^{-}$	721.5020	721.5039	2.6	2.0	NA
PG(32:1)	$[M-H]^{-}$	719.4860	719.4896	5.0	2.0	NA
PG(34:1)	$[M-H]^{-}$	747.5180	747.5183	0.4	2.0	16:0/18:1; 16:1/18:0
PG(34:2)	$[M-H]^{-}$	745.5020	745.5035	2.0	2.0	16:0/18:2; 16:1/18:1
PG(36:1)	$[M-H]^{-}$	775.5490	775.5486	-0.6	2.0	18:0/18:1; 16:0/20:1
PG(36:2)	$[M-H]^{-}$	773.5330	773.5348	2.4	2.0	18:0/18:2; 18:1/18:1; 16:0/20:2
PG(36:3)	$[M-H]^{-}$	771.5180	771.5169	-1.4	2.0	16:0/20:3; 18:1/18:2; 18:0/18:3
PG(36:4)	$[M-H]^{-}$	769.5020	769.5029	1.1	2.0	16:0/20:4; 18:2/18:2; 18:1/18:3
PG(38:4)	$[M-H]^{-}$	797.5330	797.5342	1.6	2.0	18:0/20:4
PG(38:5)	$[M-H]^{-}$	795.5180	795.5162	-2.3	2.0	NA
PG(38:6)	$[M-H]^{-}$	793.5020	793.5033	1.6	2.0	NA*
PI(34:0)	$[M-H]^{-}$	837.5490	837.5451	-4.6	2.0	NA
PI(34:1)	$[M-H]^{-}$	835.5340	835.5350	1.2	2.0	16:0/18:1; 16:1/18:0
PI(34:2)	$[M-H]^{-}$	833.5180	833.5198	2.1	2.0	16:0/18:2; 16:1/18:1
PI(36:1)	$[M-H]^{-}$	863.5650	863.5646	-0.5	2.0	NA
PI(36:2)	$[M-H]^{-}$	861.5490	861.5505	1.7	2.0	18:0/18:2; 18:1/18:1
PI(36:3)	$[M-H]^{-}$	859.5340	859.5344	0.5	2.0	16:0/20:3; 18:1/18:2; 18:0/18:3
PI(36:4)	$[M-H]^{-}$	857.5180	857.5193	1.5	2.0	16:0/20:4; 18:2/18:2; 18:1/18:3
PI(38:3)	$[M-H]^{-}$	887.5650	887.5628	-2.5	2.0	18:0/20:3
PI(38:4)	$[M-H]^{-}$	885.5490	885.5507	1.9	2.0	18:0/20:4
PI(38:5)	$[M-H]^{-}$	883.5340	883.5346	0.6	2.0	18:0/20:5; 18:1/20:4; 18:2/20:3; 16:1/22:5
PI(38:6)	$[M-H]^{-}$	881.5180	881.5189	1.0	2.0	16:0/22:6; 18:2/20:4; 18:0/20:5
PI(40:4)	$[M-H]^{-}$	913.5810	913.5769	-4.5	2.0	NA
PI(40:5)	$[M-H]^{-}$	911.5650	911.5648	-0.2	2.0	18:0/22:5; 18:1/22:4; 20:0/20:5

PI(40:6)	$[M-H]^-$	909.5490	909.5501	1.2	2.0	18:0/22:6; 18:1/22:5; 18:2/22:4; 20:2/20:4; 20:1/20:5
LPI(16:0)	$[M-H]^-$	571.2880	571.2899	3.3	2.1	16:0
LPI(18:0)	$[M-H]^-$	599.3200	599.3208	1.4	2.1	18:0
PA(34:1)	$[M-H]^-$	673.4810	673.4828	2.7	2.7	16:0/18:1
PA(36:2)	$[M-H]^-$	699.4970	699.4986	2.3	2.7	18:0/18:2; 18:1/18:1
PA(36:3)	$[M-H]^-$	697.4810	697.4809	-0.1	2.7	18:1/18:2
PS(36:1)	$[M-H]^-$	788.5440	788.5449	1.1	2.8	18:0/18:1
PS(36:2)	$[M-H]^-$	786.5290	786.5302	1.5	2.7	18:0/18:2
PS(38:3)	$[M-H]^-$	812.5440	812.5423	-2.1	2.3	NA
PS(38:4)	$[M-H]^-$	810.5290	810.5295	0.7	2.3	18:0/20:4; 16:0/22:4
PS(38:5)	$[M-H]^-$	808.5130	808.5128	-0.3	2.3	18:0/20:5; 18:1/20:4
PS(38:6)	$[M-H]^-$	806.4970	806.4971	0.1	2.3	16:0/22:6; 18:2/20:4
PS(40:4)	$[M-H]^-$	838.5600	838.5608	1.0	3.2	18:0/22:4
PS(40:5)	$[M-H]^-$	836.5440	836.5415	-3.0	3.1	18:0/22:5; 18:1/22:4; 18:2/22:3
PS(40:6)	$[M-H]^-$	834.5290	834.5299	1.0	3.1	18:0/22:6; 20:2/20:4
PS(40:7)	$[M-H]^-$	832.5130	832.5133	0.4	3.0	18:1/22:6; 18:2/22:5; 18:3/22:4; 20:4/20:3
PS(42:8)	$[M-H]^-$	858.5290	858.5286	-0.5	2.9	20:4/22:6
PS(42:9)	$[M-H]^-$	856.5130	856.5119	-1.3	3.3	20:5/22:4; 20:4/22:5; 20:3/22:6
Cer(d34:1)	$[M+H]^+$	538.5200	538.5201	0.3	3.2	NA
Cer(d36:1)	$[M+H]^+$	566.5510	566.5517	1.3	2.9	d18:1/18:0
Cer(d38:1)	$[M+H]^+$	594.5830	594.5827	-0.4	2.9	NA
Cer(d38:2)	$[M+H]^+$	592.5670	592.5666	-0.6	2.8	NA
Cer(d40:1)	$[M+H]^+$	622.6140	622.6135	-0.8	3.2	NA
Cer(d42:1)	$[M+H]^+$	650.6450	650.6458	1.2	3.3	NA
Cer(d42:2)	$[M+H]^+$	648.6290	648.6300	1.5	3.4	NA
PE(32:0)	$[M+H]^+$	692.5230	692.5233	0.4	4.8	16:0
PE(32:1)	$[M+H]^+$	690.5070	690.5076	0.9	4.7	16:1
PE(32:2)	$[M+H]^+$	688.4920	688.4924	0.6	4.8	NA
PE(34:0)	$[M+H]^+$	720.5540	720.5522	-2.5	4.7	NA
PE(34:1)	$[M+H]^+$	718.5390	718.5381	-1.2	4.7	16:0/18:1
PE(34:2)	$[M+H]^+$	716.5230	716.5236	0.9	4.7	16:0/18:2; 16:1/18:1
PE(34:3)	$[M+H]^+$	714.5070	714.5088	2.6	4.7	16:0/18:3; 16:1/18:2
PE(36:1)	$[M+H]^+$	746.5690	746.5658	-4.2	4.6	16:0/20:1; 18:0/18:1
PE(36:2)	$[M+H]^+$	744.5540	744.5555	2.0	4.6	16:0/20:2; 18:0/18:2; 18:1/18:1
PE(36:3)	$[M+H]^+$	742.5390	742.5391	0.1	4.6	16:0/20:3; 18:1/18:2
PE(36:4)	$[M+H]^+$	740.5230	740.5234	0.5	4.6	16:0/20:4; 18:1/18:3; 18:2/18:2
PE(36:5)	$[M+H]^+$	738.5070	738.5064	-0.8	4.7	16:0/20:5; 18:1/18:4; 18:2/18:3; 16:1/20:4
PE(38:1)	$[M+H]^+$	774.6010	774.6007	-0.4	4.6	18:0/20:1

PE(38:2)	$[M+H]^+$	772.5860	772.5862	0.2	4.6	18:0/20:2; 18:2/20:2
PE(38:4)	$[M+H]^+$	768.5540	768.5547	1.0	4.4	18:0/20:4; 16:0/22:4
PE(38:5)	$[M+H]^+$	766.5390	766.5371	-2.4	4.5	NA
PE(38:6)	$[M+H]^+$	764.5230	764.5231	0.1	4.5	16:0/22:6; 18:2/20:4
PE(38:7)	$[M+H]^+$	762.5070	762.5057	-1.7	4.6	16:1/22:6; 18:3/20:4
PE(38:8)	$[M+H]^+$	760.4920	760.4884	-4.8	4.7	NA*
PE(40:10)	$[M+H]^+$	784.4920	784.4885	-4.5	4.6	NA*
PE(40:3)	$[M+H]^+$	798.6010	798.5998	-1.5	4.5	18:1/22:2; 18:2/22:1
PE(40:4)	$[M+H]^+$	796.5800	796.5828	3.5	4.4	18:0/ 22:4
PE(40:5)	$[M+H]^+$	794.5700	794.5661	-4.9	4.4	18:0/ 22:5; 20:0/20:5
PE(40:6)	$[M+H]^+$	792.5540	792.5541	0.1	4.4	18:0/22:6; 18:1/22:5; 18:2/22:4; 18:3/22:3
PE(40:7)	$[M+H]^+$	790.5300	790.5315	1.9	4.4	18:2/22:5; 18:1/22:6
PE(40:8)	$[M+H]^+$	788.5230	788.5218	-1.5	4.4	18:2/22:6; 20:4/20:4
PE(40:9)	$[M+H]^+$	786.5070	786.5053	-2.1	4.5	20:4/20:5
PE(42:10)	$[M+H]^+$	812.5230	812.5195	-4.3	4.3	20:4/22:6
PE(42:11)	$[M+H]^+$	810.5070	810.5053	-2.1	4.4	NA*
PE(42:6)	$[M+H]^+$	820.5860	820.5841	-2.3	4.3	20:4/22:2; 22:4/20:2
PE(42:7)	$[M+H]^+$	818.5700	818.5672	-3.4	4.3	20:4/22:3; 20:1/22:6
PE(42:8)	$[M+H]^+$	816.5540	816.5524	-2.0	4.3	20:2/22:6; 20:4/22:4
PE(42:9)	$[M+H]^+$	814.5390	814.5363	-3.3	4.3	NA
PE(O-32:1) PE(P-32:0)	$[M+H]^+$	676.5280	676.5285	0.7	4.7	NA
PE(O-34:1) PE(P-34:0)	$[M+H]^+$	704.5590	704.5586	-0.5	4.7	NA
PE(O-34:2) PE(P-34:1)	$[M+H]^+$	702.5440	702.5408	-4.5	4.7	NA
PE(O-34:3) PE(P-34:2)	$[M+H]^+$	700.5280	700.5289	1.3	4.7	O-16:0:18:3; O-16:1/18:2; P-16:0/18:2; P-18:2/16:0
PE(O-34:4) PE(P-34:3)	$[M+H]^+$	698.5130	698.5134	0.6	4.7	NA
PE(O-36:2)	$[M+H]^+$	730.5750	730.5739	-1.5	4.6	O-18:0/18:2
PE(O-36:3) PE(P-36:2)	$[M+H]^+$	728.5590	728.5600	1.4	4.6	O-18:1/18:2; O-16:1/20:2; P-18:0/18:2; P-16:0/20:2
PE(O-36:4) PE(P-36:3)	$[M+H]^+$	726.5440	726.5420	-2.7	4.5	O-16:1/20:3; O-16:0/20:4; P -16:0/20:3;
PE(O-36:5) PE(P-36:4)	$[M+H]^+$	724.5280	724.5285	0.8	4.5	O-16:1/20:4; P-16:0/20:4
PE(P-36:5)	$[M+H]^+$	722.5130	722.5109	-2.9	4.6	P-16:0/20:5
PE(O-38:2)	$[M+H]^+$	758.6060	758.6055	-0.6	4.6	O-20:0/18:2
PE(O-38:3)	$[M+H]^+$	756.5910	756.5908	-0.3	4.6	NA

PE(P-38:2)						
PE(O-38:4) PE(P-38:3)	$[M+H]^+$	754.5750	754.5720	-3.9	4.4	O-18:0/20:4; O-18:1/20:3; O-16:1/22:3; O-16:0/22:4; P-16:0/22:3; P-18:0/20:3
PE(O-38:5) PE(P-38:4)	$[M+H]^+$	752.5590	752.5599	1.2	4.4	O-18:1/20:4; O-20:4/18:1; O-16:1/22:4; P-16:0/22:4; P-20:3/18:1; P-18:0/20:4
PE(O-38:6) PE(P-38:5)	$[M+H]^+$	750.5440	750.5433	-0.9	4.4	O-18:2/20:4; O-20:4/18:2; O-16:1/22:5; P-18:1/20:4; P-20:3/18:2; P-16:0/22:5
PE(P-38:6)	$[M+H]^+$	748.5280	748.5283	0.4	4.4	P-18:2/20:4; P-16:0/22:6
PE(P-38:7)	$[M+H]^+$	746.5130	746.5106	-3.3	4.5	NA*
PE(P-40:9)	$[M+H]^+$	770.5130	770.5105	-3.3	4.4	NA*
PE(P-40:10)	$[M+H]^+$	768.4970	768.4955	-1.9	4.6	NA*
PE(O-40:5) PE(P-40:4)	$[M+H]^+$	780.5910	780.5909	-0.1	4.4	O-20:1/20:4; O-18:1/22:4; O-18:0/22:5; P-18:0/22:4; P-20:0/20:4
PE(O-40:6) PE(P-40:5)	$[M+H]^+$	778.5750	778.5729	-2.7	4.4	O-20:2/20:4; O-18:2/22:4; O-18:1/22:5; O-18:0/22:6; P-18:1/22:4; P-18:0/22:5; P-20:1/20:4
PE(P-40:6)	$[M+H]^+$	776.5590	776.5587	-0.4	4.3	P-18:0/22:6
PE(P-40:7)	$[M+H]^+$	774.5440	774.5432	-1.1	4.3	NA*
PE(P-40:8)	$[M+H]^+$	772.5280	772.5264	-2.1	4.4	NA*
PE(P-42:9)	$[M+H]^+$	798.5440	798.5433	-0.9	4.3	NA*
PE(P-42:10)	$[M+H]^+$	796.5280	796.5257	-2.9	4.3	NA*
PE(O-42:6) PE(P-42:5)	$[M+H]^+$	806.6060	806.6047	-1.7	4.3	NA*
PE(P-42:6)	$[M+H]^+$	804.5910	804.5906	-0.5	4.2	NA*
PE(P-42:7)	$[M+H]^+$	802.5750	802.5732	-2.3	4.3	NA*
PE(P-42:8)	$[M+H]^+$	800.5590	800.5577	-1.6	4.3	NA*
LPE(16:0)	$[M+H]^+$	454.2928	454.2927	-0.1	6.7	16:0
LPE(18:0)	$[M+H]^+$	482.3241	482.3248	1.6	6.5	18:0
LPE(18:1)	$[M+H]^+$	480.3085	480.3092	1.4	6.5	18:1

LPE(18:2)	$[M+H]^+$	478.2928	478.2940	2.5	6.4	18:2
LPE(20:4)	$[M+H]^+$	502.2928	502.2932	0.7	6.2	20:4
LPE(20:5)	$[M+H]^+$	500.2772	500.2751	-4.2	6.4	NA
LPE(22:4)	$[M+H]^+$	530.3241	530.3250	1.8	6.1	22:4
LPE(22:5)	$[M+H]^+$	528.3085	528.3099	2.6	6.2	NA
LPE(22:6)	$[M+H]^+$	526.2928	526.2928	0.0	6.1	22:6
LPE(O-16:0)	$[M+H]^+$	438.2979	438.2981	0.5	6.4	NA*
LPE(O-18:0)	$[M+H]^+$	466.3292	466.3298	1.3	6.2	NA*
PC(32:0)	$[M+H]^+$	734.5700	734.5705	0.7	19.5	16:0/16:0
PC(32:1)	$[M+H]^+$	732.5540	732.5547	1.0	19.2	16:0/16:1
PC(32:2)	$[M+H]^+$	730.5390	730.5394	0.5	19.3	14:2/18:0; 14:1/18:1; 14:0/18:2
PC(34:0)	$[M+H]^+$	762.6010	762.5978	-4.2	18.8	16:0/18:0
PC(34:1)	$[M+H]^+$	760.5860	760.5855	-0.6	18.8	16:0/18:1
PC(34:2)	$[M+H]^+$	758.5700	758.5707	1.0	18.8	16:0/18:2; 16:1/18:1
PC(34:3)	$[M+H]^+$	756.5540	756.5536	-0.5	19.4	16:0/18:3; 16:1/18:2; 16:2/18:1
PC(34:4)	$[M+H]^+$	754.5390	754.5378	-1.6	18.1	14:0/20:4; 16:2/18:2
PC(34:5)	$[M+H]^+$	752.5230	752.5216	-1.8	19.3	14:1/20:4
PC(36:1)	$[M+H]^+$	788.6170	788.6151	-2.5	18.2	16:0/20:1; 18:0/18:1
PC(36:2)	$[M+H]^+$	786.6010	786.6019	1.1	18.1	16:0/20:2; 18:1/18:1; 18:0/18:2
PC(36:3)	$[M+H]^+$	784.5860	784.5846	-1.8	18.2	16:0/20:3; 18:1/18:2; 18:0/18:3
PC(36:4)	$[M+H]^+$	782.5700	782.5705	0.6	17.3	16:0/20:4; 18:1/18:3; 18:2/18:2
PC(36:5)	$[M+H]^+$	780.5540	780.5534	-0.8	18.8	16:0/20:5; 16:1/20:4; 16:2/20:3; 18:1/18:4; 18:2/18:3
PC(36:6)	$[M+H]^+$	778.5390	778.5374	-2.0	18.3	NA*
PC(36:7)	$[M+H]^+$	776.5230	776.5217	-1.7	17.9	NA*
PC(38:1)	$[M+H]^+$	816.6480	816.6475	-0.7	17.7	16:0/22:1; 18:0/20:1; 20:0/18:1
PC(38:2)	$[M+H]^+$	814.6330	814.6294	-4.4	17.7	16:0/22:2; 18:0/20:2; 18:1/20:1; 20:0/18:2
PC(38:3)	$[M+H]^+$	812.6170	812.6156	-1.7	16.7	16:0/22:3; 18:0/20:3; 18:1/20:2; 18:0/20:1
PC(38:4)	$[M+H]^+$	810.6010	810.6015	0.7	16.7	16:0/22:4; 18:0/20:4; 18:1/20:3
PC(38:5)	$[M+H]^+$	808.5860	808.5844	-2.0	17.1	16:0/22:5; 18:1/20:4; 18:2/20:3
PC(38:6)	$[M+H]^+$	806.5700	806.5700	0.1	16.9	16:0/22:6; 18:2/20:4
PC(38:7)	$[M+H]^+$	804.5540	804.5524	-2.0	17.3	16:2/22:5; 16:1/22:6; 18:2/20:5; 18:3/20:4
PC(38:8)	$[M+H]^+$	802.5390	802.5363	-3.4	17.3	NA*
PC(40:3)	$[M+H]^+$	840.6480	840.6469	-1.4	16.8	18:2/22:1; 18:0/22:3
PC(40:4)	$[M+H]^+$	838.6330	838.6306	-2.9	16.8	18:0/22:4; 18:2:22:2; 20:0/20:4

PC(40:5)	$[M+H]^+$	836.6170	836.6158	-1.4	16.7	18:0: 22:5; 18:1/22:4; 20:1/20:4
PC(40:6)	$[M+H]^+$	834.6010	834.6007	-0.3	16.3	18:0/22:6
PC(40:7)	$[M+H]^+$	832.5860	832.5835	-3.0	16.6	18:1/22:6; 18:2/22:5
PC(40:8)	$[M+H]^+$	830.5700	830.5685	-1.8	16.6	18:2/22:6; 20:4/20:4
PC(40:9)	$[M+H]^+$	828.5540	828.5519	-2.5	16.8	NA*
PC(42:10)	$[M+H]^+$	854.5700	854.5676	-2.8	16.0	20:4/22:6; 20:5/22:5
PC(42:11)	$[M+H]^+$	852.5540	852.5518	-2.6	16.4	NA*
PC(42:5)	$[M+H]^+$	864.6480	864.6481	0.1	16.2	22:1/20:4; 20:0/22:5
PC(42:6)	$[M+H]^+$	862.6330	862.6314	-1.8	16.2	20:0/22:6; 22:2/20:4
PC(42:7)	$[M+H]^+$	860.6170	860.6147	-2.6	16.6	20:1/22:6
PC(42:8)	$[M+H]^+$	858.6010	858.5971	-4.5	16.6	20:4/22:4; 20:2/22:6
PC(42:9)	$[M+H]^+$	856.5860	856.5831	-3.4	16.2	20:4/22:5
PC(44:10)	$[M+H]^+$	882.6010	882.6003	-0.8	15.8	22:4/22:6
PC(44:11)	$[M+H]^+$	880.5860	880.5832	-3.2	15.5	NA*
PC(44:12)	$[M+H]^+$	878.5700	878.5689	-1.3	15.3	NA*
PC(O-32:1) PC(P-32:0)	$[M+H]^+$	718.5750	718.5754	0.6	20.4	O-16:0/16:1; O-16:1/16:0; P-16:0/16:0
PC(O-32:0)	$[M+H]^+$	720.5910	720.5901	-1.2	19.2	O-16:0/16:0
PC(O-34:0)	$[M+H]^+$	748.6220	748.6184	-4.9	19.8	O-18:0/16:0
PC(O-34:1) PC(P-34:0)	$[M+H]^+$	746.6060	746.6062	0.2	19.6	O-16:1/18:0; O-16:0/18:1; O-18:1/16:0; P-16:0/18:0; P-18:0/16:0
PC(O-34:2) PC(O-34:1)	$[M+H]^+$	744.5910	744.5904	-0.9	18.6	O-16:1/18:1; O-16:0/18:2; O-18:2/16:0; P-16:0/18:1; P-18:1/16:0
PC(O-34:3) PC(P-34:2)	$[M+H]^+$	742.5750	742.5756	0.8	18.5	O-16:1/18:2; P-16:0/18:2
PC(O-36:3) PC(P-36:2)	$[M+H]^+$	770.6060	770.6035	-3.2	18.0	O-18:1/18:2; O-16:0/20:3; P-18:0/18:2
PC(O-36:4) PC(P-36:3)	$[M+H]^+$	768.5910	768.5891	-2.4	17.3	O-18:2/18:2; O-16:0/20:4; O-20:4/16:0; P-18:1/18:2
PC(O-36:5) PC(P-36:4)	$[M+H]^+$	766.5750	766.5753	0.4	17.0	O-16:1/20:4; P-16:0/20:4
PC(O-36:6) PC(P-36:5)	$[M+H]^+$	764.5590	764.5586	-0.5	17.7	NA*
PC(O-38:4) PC(P-38:3)	$[M+H]^+$	796.6220	796.6207	-1.6	17.6	O-18:1/20:3; O-18:0/20:4; O-16:0/22:4; P-18:0/20:3
PC(O-38:5)	$[M+H]^+$	794.6060	794.6054	-0.7	16.5	O-18:1/20:3;

PC(P-38:4)						O-18:0/20:4; O-18:0/20:4; P-18:0/20:3
PC(O-38:6) PC(P-38:5)	$[M+H]^+$	792.5910	792.5905	-0.6	16.6	O-16:1/22:5; O-16:0/22:6; P-16:0/22:5
PC(O-38:7) PC(P-38:6)	$[M+H]^+$	790.5750	790.5751	0.1	16.6	P-18:2/20:4; P-16:0/22:6
PC(O-40:7) PC(P-40:6)	$[M+H]^+$	818.6060	818.6039	-2.5	16.2	P-18:0/22:6
SM(d34:1)	$[M+H]^+$	703.5750	703.5755	0.7	24.6	d18:1/16:0
SM(d34:2)	$[M+H]^+$	701.5600	701.5584	-2.3	24.6	NA*
SM(d36:0)	$[M+H]^+$	733.6220	733.6206	-1.9	24.1	NA
SM(d36:1)	$[M+H]^+$	731.6070	731.6070	0.0	24.2	d18:1/18:0
SM(d36:2)	$[M+H]^+$	729.5910	729.5914	0.5	24.1	NA*
SM(d38:1)	$[M+H]^+$	759.6380	759.6383	0.3	23.6	d18:1/20:0
SM(d38:2)	$[M+H]^+$	757.6220	757.6217	-0.4	23.6	NA*
SM(d40:1)	$[M+H]^+$	787.6690	787.6698	1.0	23.1	d18:1/22:0
SM(d40:2)	$[M+H]^+$	785.6540	785.6544	0.5	23.0	NA*
SM(d40:3)	$[M+H]^+$	783.6380	783.6381	0.2	23.3	NA*
SM(d42:1)	$[M+H]^+$	815.7010	815.7009	-0.2	22.5	d18:1/24:0
SM(d42:2)	$[M+H]^+$	813.6850	813.6855	0.7	22.6	d18:1/24:1
SM(d42:3)	$[M+H]^+$	811.6690	811.6697	0.8	22.8	NA*
LPC(16:0)	$[M+H]^+$	496.3400	496.3404	0.8	27.7	16:0
LPC(18:0)	$[M+H]^+$	524.3720	524.3720	0.0	27.2	18:0
LPC(18:1)	$[M+H]^+$	522.3560	522.3565	1.0	27.2	NA
LPC(18:2)	$[M+H]^+$	520.3400	520.3396	-0.8	27.3	18:2
LPC(20:3)	$[M+H]^+$	546.3560	546.3545	-2.7	27.2	NA
LPC(20:4)	$[M+H]^+$	544.3390	544.3395	0.9	26.9	20:4
LPC(22:6)	$[M+H]^+$	568.3400	568.3386	-2.5	26.0	22:6

Supplementary Table S 2: List of the most important phospholipids species, based on their contributions (in percentage) to the first (>1%)(A) and third (>2%) (B) principal components of the PCA model.

A)

	contrib.Dim.1
PC 36:3	1.28
PC 36:1	1.26
PC 32:1	1.22
PC 34:1	1.21
PC 32:2	1.18
PC 34:4	1.18
PC 36:5	1.17
PG 34:2	1.13
PC 34:2	1.13
PS 36:2	1.13
PC 36:2	1.09
PG 36:2	1.05
PC O-34:3	1.03
PI 38:3	1.03
PC 36:6	1.01

B)

	contrib.Dim.3
LPE 20:4	3.07
LPE 22:6	2.74
LPE 22:4	2.70
SM d40:2	2.58
PE 42:8	2.53
LPE 22:5	2.46
LPE 18:2	2.26
PE 40:5	2.25
LPE 20:5	2.17
LPE O-18:0	2.15
LPE O-16:0	2.13
SM d40:1	2.07

Supplementary Table S 3: Kruskal-Wallis H test results for statistically significant differences of phospholipid species between two or more groups.

Label	K.W	sig	FDR
PC 36:7	19.13922	6.98E-05	0.004175
PC 38:5	19.06173	7.26E-05	0.004175
PC 34:4	18.99345	7.51E-05	0.004175
LPI 18:0	18.96296	7.63E-05	0.004175
PC 36:6	18.4192	0.0001	0.004383
LPE 16:0	17.38631	0.000168	0.004524
PE O-34:2	17.36863	0.000169	0.004524
PC 34:5	17.36332	0.00017	0.004524
PE 38:7	17.1145	0.000192	0.004524
LPC 20:4	16.61728	0.000246	0.004524
PE 40:10	16.51651	0.000259	0.004524
PA 34:1	16.33694	0.000283	0.004524
PC 38:7	16.30064	0.000289	0.004524
PC 36:5	16.29566	0.000289	0.004524
PE O-38:8	16.15889	0.00031	0.004524
PC 38:8	15.585	0.000413	0.0056
PE 42:8	15.4818	0.000435	0.0056
PE O-36:6	15.08141	0.000531	0.006461
PE O-42:8	14.81416	0.000607	0.006996
PE 36:5	14.28473	0.000791	0.008273
PE O-42:11	14.27851	0.000793	0.008273
PE O-40:9	14.0819	0.000875	0.008713
PE O-40:10	13.78836	0.001014	0.009652
CL 68:5	13.67966	0.00107	0.009766
PE 36:4	13.02207	0.001487	0.012776
PE 38:8	12.98234	0.001517	0.012776
PE O-408	12.86981	0.001605	0.012792
LPC 22:6	12.80803	0.001655	0.012792
PA 36:3	12.76135	0.001694	0.012792
PE 42:10	12.51852	0.001913	0.013747
PC 34:3	12.48406	0.001946	0.013747
PA 36:2	12.38906	0.002041	0.013965
PC 38:2	12.12469	0.002329	0.015456
CL 78:12	11.23297	0.003637	0.023429
Cer 40:1	11.15773	0.003777	0.023446
PG 384	11.07937	0.003928	0.023446
CL 707	11.06246	0.003961	0.023446
PE O-36:4	10.88889	0.00432	0.024898
PG 32:1	10.71477	0.004713	0.026204

PE O-38:6	10.68404	0.004786	0.026204
PE O-36:5	10.5923	0.005011	0.026765
PE 40:5	10.23777	0.005983	0.031195
PC 32:2	10.16931	0.006191	0.031531
CL 70:6	10.11288	0.006368	0.031696
PE 38:5	9.99335	0.00676	0.032781
PE 36:2	9.956696	0.006885	0.032781
PC 36:4	9.836	0.007314	0.034079
LPE 20:5	9.65374	0.008012	0.036553
PE 38:4	9.180208	0.010152	0.045372

Supplementary Table S 4: post hoc Dunn's multiple comparisons test. Statistically significant phospholipid differences between the groups (control (CT), ischemia (ISC) and reperfusion (I/R)) are marked with * (FDR p < 0.05), and ** (FDR p<0.01).

Label	id	chi2	Z	P	P.adjusted	comparisons
CL685	1	13.67966	3.593727	0.000326	0.000977942	CT - I/R
CL685	1	13.67966	-2.55422	0.010643	0.015963921	I/R - ISC
CL706	4	10.11288	-3.13385	0.001725	0.005175828	I/R - ISC
CL707	5	11.06246	-3.28188	0.001031	0.003093578	I/R - ISC
CL728	9	8.333707	-2.88268	0.003943	0.011829122	I/R - ISC
CL748	12	7.261047	2.539757	0.011093	0.033278837	CT - ISC
CL7811	17	7.052174	2.611013	0.009027	0.027082302	CT - ISC
CL7812	18	11.23297	3.232103	0.001229	0.003686477	CT - ISC
CL7812	18	11.23297	2.384076	0.017122	0.025683079	I/R - ISC
CL7813	19	8.395169	2.766431	0.005667	0.017002077	CT - ISC
CL7813	19	8.395169	2.129219	0.033236	0.04985418	I/R - ISC
PG321	22	10.71477	3.143766	0.001668	0.005003656	CT - I/R
PG321	22	10.71477	-2.36159	0.018197	0.027295479	I/R - ISC
PG341	23	6.772212	2.599167	0.009345	0.028035114	CT - I/R
PG384	29	11.07937	3.296222	0.00098	0.002939837	CT - ISC
PG386	31	7.079365	2.494438	0.012616	0.037847002	CT - ISC
PI340	32	6.026531	2.435419	0.014875	0.044623712	CT - I/R
PI341	33	7.474427	2.732004	0.006295	0.018885124	CT - I/R
PI342	34	6.989788	2.64332	0.00821	0.024629207	CT - I/R
PI361	35	6.242646	-2.45027	0.014275	0.042824891	I/R - ISC
PI363	37	6.054045	2.421308	0.015465	0.046394312	CT - I/R
PI364	38	7.142857	2.672612	0.007526	0.022578945	CT - I/R
PI385	41	8.918297	2.986241	0.002824	0.008472903	CT - I/R
LPI180	47	18.96296	2.850787	0.004361	0.006541685	CT - I/R
LPI180	47	18.96296	4.27618	1.90E-05	5.70E-05	CT - ISC
Cerd401	52	11.15773	-2.56907	0.010197	0.015295795	CT - I/R
Cerd401	52	11.15773	3.133374	0.001728	0.005184274	I/R - ISC
PA341	55	16.33694	4.037674	5.40E-05	0.000161951	CT - I/R
PA341	55	16.33694	2.178821	0.029345	0.044017507	CT - ISC
PA362	56	12.38906	3.502695	0.000461	0.001381727	CT - I/R
PA363	57	12.76135	3.534431	0.000409	0.001225963	CT - I/R
PA363	57	12.76135	2.216507	0.026657	0.039985148	CT - ISC
PS361	58	7.272061	2.58392	0.009768	0.029305357	CT - I/R
PS362	59	6	2.405351	0.016157	0.048470794	CT - I/R
PE321	71	8.666667	2.405351	0.016157	0.024235397	CT - I/R
PE321	71	8.666667	-2.67261	0.007526	0.022578945	I/R - ISC
PE340	73	6	2.405351	0.016157	0.048470794	CT - I/R
PE343	76	7.168855	-2.53937	0.011105	0.03331575	I/R - ISC

PE361	77	8.27866	2.821091	0.004786	0.014358192	CT - I/R
PE362	78	9.956696	2.55461	0.010631	0.015946045	CT - I/R
PE362	78	9.956696	-2.88136	0.00396	0.01187882	I/R - ISC
PE363	79	7.402446	-2.63048	0.008526	0.025579403	I/R - ISC
PE364	80	13.02207	3.015955	0.002562	0.003842573	CT - I/R
PE364	80	13.02207	-3.22395	0.001264	0.003793043	I/R - ISC
PE365	81	14.28473	3.534867	0.000408	0.001223943	CT - I/R
PE365	81	14.28473	-2.92592	0.003434	0.005151604	I/R - ISC
PE381	82	7.373503	-2.19782	0.027962	0.041943247	CT - I/R
PE381	82	7.373503	2.479969	0.013139	0.039418148	I/R - ISC
PE384	84	9.180208	3.029886	0.002446	0.007339388	CT - I/R
PE385	85	9.99335	3.014573	0.002573	0.007720237	CT - I/R
PE385	85	9.99335	2.331468	0.019729	0.029593058	CT - ISC
PE387	87	17.1145	3.772505	0.000162	0.000484851	CT - I/R
PE387	87	17.1145	-3.35664	0.000789	0.001183444	I/R - ISC
PE388	88	12.98234	3.149667	0.001635	0.0049037	CT - I/R
PE388	88	12.98234	-3.09024	0.002	0.002999929	I/R - ISC
PE4010	89	16.51651	3.97983	6.90E-05	0.000206893	CT - I/R
PE4010	89	16.51651	-2.70272	0.006877	0.010316178	I/R - ISC
PE405	92	10.23777	3.149186	0.001637	0.004911782	CT - I/R
PE408	95	8.018411	2.422048	0.015433	0.023149964	CT - I/R
PE408	95	8.018411	-2.48148	0.013084	0.039250885	I/R - ISC
PE409	96	7.278236	2.61362	0.008959	0.026876588	CT - I/R
PE4210	97	12.51852	3.385309	0.000711	0.002132945	CT - I/R
PE4210	97	12.51852	-2.58353	0.00978	0.014669442	I/R - ISC
PE4211	98	7.716641	2.405718	0.016141	0.024211053	CT - I/R
PE4211	98	7.716641	-2.40572	0.016141	0.048422106	I/R - ISC
PE426	99	8.497303	2.62847	0.008577	0.02573097	CT - ISC
PE426	99	8.497303	2.405718	0.016141	0.024211053	I/R - ISC
PE428	101	15.4818	3.727378	0.000193	0.000580445	CT - I/R
PE428	101	15.4818	-2.95517	0.003125	0.004687413	I/R - ISC
PEO.342	105	17.36863	3.237819	0.001204	0.001806707	CT - I/R
PEO.342	105	17.36863	-3.89132	9.97E-05	0.000299096	I/R - ISC
PEO.343	106	8.146067	-2.73284	0.006279	0.018837355	I/R - ISC
PEO.362	108	8.736353	2.910622	0.003607	0.010821295	CT - I/R
PEO.364	110	10.88889	-3.29622	0.00098	0.002939837	I/R - ISC
PEO.365	111	10.5923	-3.25367	0.001139	0.003417791	I/R - ISC
PEO.366	112	15.08141	3.55189	0.000382	0.001147426	CT - I/R
PEO.366	112	15.08141	-3.13577	0.001714	0.002571066	I/R - ISC
PEO.384	115	6.228808	-2.15392	0.031246	0.046869171	I/R - ISC
PEO.386	117	10.68404	-3.26702	0.001087	0.003260523	I/R - ISC
PEO.387	118	8.019203	-2.39087	0.016809	0.025212874	CT - ISC
PEO.387	118	8.019203	-2.50967	0.012084	0.036253295	I/R - ISC

PEO.388	119	16.15889	3.000181	0.002698	0.004047288	CT - I/R
PEO.388	119	16.15889	-3.81706	0.000135	0.000405151	I/R - ISC
PEO.4010	120	13.78836	2.405351	0.016157	0.024235397	CT - I/R
PEO.4010	120	13.78836	-3.65257	0.00026	0.000778885	I/R - ISC
PEO.408	125	12.86981	-2.95608	0.003116	0.004673715	CT - ISC
PEO.408	125	12.86981	-3.23831	0.001202	0.003607156	I/R - ISC
PEO.409	126	14.0819	2.465119	0.013697	0.020545173	CT - I/R
PEO.409	126	14.0819	-3.68283	0.000231	0.000691982	I/R - ISC
PEO.4211	128	14.27851	-3.77308	0.000161	0.000483732	I/R - ISC
PEO.428	131	14.81416	3.579424	0.000344	0.001033058	CT - I/R
PEO.428	131	14.81416	-3.01503	0.00257	0.003854265	I/R - ISC
LPE160	133	17.38631	3.565661	0.000363	0.000544411	CT - I/R
LPE160	133	17.38631	3.654802	0.000257	0.000772141	CT - ISC
LPE180	134	6.994709	2.583525	0.00978	0.029338885	CT - I/R
LPE181	135	7.534046	2.58392	0.009768	0.029305357	CT - I/R
LPE182	136	7.836607	2.791821	0.005241	0.015723687	CT - I/R
LPE204	137	6.991923	2.643724	0.0082	0.024599858	CT - I/R
LPE205	138	9.65374	2.851222	0.004355	0.013065474	CT - I/R
LPE205	138	9.65374	2.494819	0.012602	0.018903206	CT - ISC
LPE224	139	8.804233	2.850787	0.004361	0.013083369	CT - I/R
LPE224	139	8.804233	-2.13809	0.032509	0.048764167	I/R - ISC
PC321	145	8.185773	2.747691	0.006002	0.018004989	CT - I/R
PC322	146	10.16931	2.761699	0.00575	0.008625206	CT - I/R
PC322	146	10.16931	-2.7617	0.00575	0.017250412	I/R - ISC
PC340	147	7.896355	2.8071	0.004999	0.014996914	CT - I/R
PC343	150	12.48406	3.328968	0.000872	0.002615057	CT - I/R
PC343	150	12.48406	-2.68992	0.007147	0.010720222	I/R - ISC
PC344	151	18.99345	4.247132	2.17E-05	6.50E-05	CT - I/R
PC344	151	18.99345	-2.97002	0.002978	0.004466666	I/R - ISC
PC345	152	17.36332	4.128332	3.65E-05	0.000109622	CT - I/R
PC345	152	17.36332	-2.55422	0.010643	0.015963921	I/R - ISC
PC363	155	7.865717	2.59877	0.009356	0.028067543	CT - I/R
PC363	155	7.865717	-2.21267	0.026921	0.040380928	I/R - ISC
PC364	156	9.836	3.105571	0.001899	0.005697364	CT - I/R
PC365	157	16.29566	4.010143	6.07E-05	0.000182046	CT - I/R
PC365	157	16.29566	-2.40609	0.016124	0.024186719	I/R - ISC
PC366	158	18.4192	4.172882	3.01E-05	9.02E-05	CT - I/R
PC366	158	18.4192	-2.95517	0.003125	0.004687413	I/R - ISC
PC367	159	19.13922	4.357741	1.31E-05	3.94E-05	CT - I/R
PC367	159	19.13922	-2.51351	0.011954	0.017930482	I/R - ISC
PC382	161	12.12469	3.460605	0.000539	0.00161689	CT - I/R
PC385	164	19.06173	4.335571	1.45E-05	4.36E-05	CT - I/R
PC385	164	19.06173	2.613221	0.008969	0.013453991	CT - ISC

PC387	166	16.30064	4.010755	6.05E-05	0.000181574	CT - I/R
PC387	166	16.30064	-2.40645	0.016108	0.024162396	I/R - ISC
PC388	167	15.585	3.89073	9.99E-05	0.00029983	CT - I/R
PC388	167	15.585	-2.52452	0.011586	0.017378497	I/R - ISC
PC403	168	8.402036	-2.89577	0.003782	0.011346808	CT - ISC
PC409	174	7.650794	2.761699	0.00575	0.017250412	CT - I/R
PC425	177	6.227925	2.495581	0.012575	0.037725293	I/R - ISC
PCO.364	192	7.581016	2.406453	0.016108	0.048324792	CT - I/R
PCO.364	192	7.581016	-2.36189	0.018182	0.027273103	I/R - ISC
LPC181	215	6.194004	2.435047	0.01489	0.044669583	CT - I/R
LPC182	216	8.859847	2.940322	0.003279	0.009836125	CT - I/R
LPC204	218	16.61728	3.682266	0.000231	0.00069351	CT - I/R
LPC204	218	16.61728	3.355613	0.000792	0.001187838	CT - ISC
LPC226	219	12.80803	3.520552	0.000431	0.001291948	CT - I/R
LPC226	219	12.80803	2.317325	0.020486	0.03072902	CT - ISC

CHAPTER 6. General concluding remarks

Reactive nitrogen species (RNS) are formed in physiological and pathological processes, and can react with different biomolecules, including lipids. Nitrated fatty acids (NO_2FAs) are well-studied, and have been characterized and reported *in vitro* and *in vivo.* Their biological functions were generally described as anti-inflammatory, antioxidant, vasculoprotective, antihyperglycemic, antitumoral and cytoprotective. Mass spectrometry is a key tool in metabolomic studies, allowing to identify and quantify these modified lipid species. The possibility of nitroxidative modifications in FAs being esterified in phospholipids is plausible, but this subject is in an early stage of investigation, although some reports have already described its natural occurrence and biological significance. The covalent adduction of these modified phospholipids to proteins, an important biological mechanism demonstrated for NO_2FAs, also remains unaddressed. Thus, the main aim of this thesis was to deepen our knowledge on the formation, nature and relevance of nitrated and nitroxidized phospholipids and possible adducts with proteins by using MS approaches.

To achieve the proposed aim, part of the work of this thesis was based on *in vitro* models to study species that remained uncharacterized. Previous work reported the formation of nitrated, nitrosated and nitroxidized phospholipids, namely phosphatidylcholines, phosphatidylethanolamines and phospatidylserines, using MS approaches. In this work we studied nitroxidative modifications in cardiolipin, that have not been reported so far. CLs are usually esterified to unsaturated fatty acids, and thus are prone to chemical modification by reactive nitrogen species, similarly to other phospholipids. Cardiolipins are an important phospholipid class present in mitochondria, associated to bioenergetics and cell signalling, and susceptible to get involved in situations of nitroxidative stress. We used a state-of-the-art LC-MS and MS/MS platform and developed new methods for the detection and characterization of nitroxidized cardiolipins. In this study, we reported ten different nitroxidative modifications and different positional isomers. The chromatographic behavior using a C30 reversed phase column was detailed, and the fragmentation pathways in MS/MS were deciphered for the first time. By identifying in the MS/MS spectra some reporter fragment ions, namely modified fatty acids, lysophosphatidic acids, and phosphatidic acids, we unequivocally identified the different nitroxidative modifications, including isomeric species.

Also, *in vitro*, the formation of adducts between nitro-PLs and nucleophilic peptide glutathione was demonstrated for the first time. The MS/MS information revealed structural information and provided valuable reporter ions to pinpoint this adducts, such as *b*, *y* or immonium ions of the peptide containing the modification. This finding suggests that

nitroxidized phospholipid also interacts with proteins, including their hydrophilic domains, and may be involved in processes related to ubiquitous cellular membrane bilayers. The biological significance of these findings needs to be further explored since these compounds may have an added significance when compared to NO_2FAs, due to their different physical and chemical properties. The analytical data obtained in these studies, both for cardiolipin and the nitro-PLs adducts with peptides, is a base for their detection *in vivo*, that should be addressed as the next step in future works.

To understand the impact of nitroxidative stress in the lipidome, we performed an analysis of biological samples of clinical interest by LC-MS, and MS/MS approaches. A model of cachexia in gastrocnemius muscle induced by urothelial cancer in mice, and the therapeutic effect of exercise, was also studied. The lipidome profiling included 12 lipid classes and 211 species. The statistical analysis demonstrated that cachexia is also driven by changes in the lipidome profile, and that exercise reverts partially these changes, restoring a healthy profile. It also established cardiolipins and phosphatidylserines as the main phospholipid species involved in the pathophysiological process. A model of acute myocardial infarction, based on an *ex vivo* experiment in the heart of rats undergoing ischemia and ischemia-reperfusion, was used. The lipidome profile included 12 lipids classes and a total of 219 species. A GC-MS profiling of esterified fatty acids was complementarily performed in this case. The statistical analysis demonstrated that the lipidome is responsive to the onset and progress of the disease, with a different profile in ischemia and after subsequent reperfusion, versus the healthy control. It also allowed to pinpoint species affected, importantly plasmalogens, PUFA-containing phospholipids, cardiolipins, esterified linoleic acid and esterified palmitic acid. In both studies, however, nitroxidized species were not detected.

The findings achieved in this thesis provided an advance in the development of MS approaches to detect nitroxidized phospholipids, including species hitherto uncharacterized as cardiolipin or adducts between nitro-phospholipids and peptides, that can be now searched in biological samples. On the other hand, studies undertaken *in vivo* revealed the importance of nitroxidative stress and the associated lipidic chemophenotype remodelling in diseases, as acute myocardial infarction, and cancer cachexia with exercise treatment. This has allowed us to hypothesize about underlying biological processes and the presence of diagnostic or therapeutic targets, and in general, expand our knowledge on the lipidome modification in pathological conditions and the analytical capabilities of current mass spectrometry techniques for these studies.